UNIVERSITY OF SOUTHAMPTON

FACULTY OF SCIENCE, ENGINEERING AND MATHEMATICS

School of Ocean & Earth Sciences

Constraining Variability of the Atlantic Meridional Overturning Circulation at 25ºN from Historical Observations, 1980 to 2005.

by

Hannah Rachel Longworth

Thesis for the degree of Doctor of Philosophy

May 2007

UNIVERSITY OF SOUTHAMPTON

ABSTRACT

FACULTY OF ENGINEERING, SCIENCE AND MATHEMATICS
SCHOOL OF OCEAN & EARTH SCIENCES

Doctor of Philosophy

CONSTRAINING VARIABILITY OF THE ATLANTIC MERIDIONAL OVERTURNING CIRCULATION AT 25ºN FROM HISTORICAL OBSERVATIONS, 1980 TO 2005

Hannah Rachel Longworth

The Atlantic Meridional Overturning Circulation (MOC) plays an important role in maintaining western Europe's moderate climate. Although expected to weaken under increasing greenhouse gas concentrations, the magnitude of the response remains uncertain. Monitoring of the Atlantic MOC strength at 25ºN commenced in 2004 as part of the UK Rapid Climate Change programme. Prior to this, detection of such a slowing of the MOC and its associated meridional heat transport was inhibited by the temporally sparse observations of its strength. This thesis aims to extend the time series of Atlantic MOC at 25ºN back to 1980 using historical observations, thus constraining the magnitude of its recent interannual variability.

Analysis of transatlantic hydrographic sections at 25ºN show the annual average MOC to have varied in strength by approximately 25% over the last 50 years, with weaker overturning in 2004 than previously computed. Temporal resolution of the dataset is increased through decomposition of the Atlantic MOC at this latitude into its Ekman component computed from wind stress climatology, transport of the Florida Current from cable observations and mid-ocean geostrophic transport from CTD or moored temperature and pressure derived boundary dynamic height profiles. The resulting time series constrain interannual fluctuations of the Ekman, Florida Straits and mid-ocean baroclinic geostrophic transports at ± 1, ± 2, and ± 3 Sv respectively between 1980 and 2005. In addition to interannual fluctuations in strength, evidence is found for a 2 to 3 Sv weakening of the MOC between 1980 and 2005. The underlying changes of increased mid-ocean southward transport of thermocline waters and decreased southward flow of lower North Atlantic Deep Water are consistent in sign, although of reduced magnitude, with the transatlantic hydrographic sections observations. This thesis presents and discusses these findings along with the relative merits of different datasets for detecting such variability.

Contents

CHAPTER 1: **INTRODUCTION** **1**

CHAPTER 2: **A HISTORICAL PERSPECTIVE: DISCOVERY AND QUANTIFICATION OF THE ATLANTIC MOC** **4**

2.1 Introduction 4

2.2 A Qualitative Understanding 6

2.3 Quantification of the Atlantic MOC: A Steady State Picture 9

2.3.1 Early estimates of a weak MOC 9

2.3.2 The Deep Western Boundary Current, Stommel and early indications of a stronger MOC 11

2.3.3 The MOC and its meridional heat transport 15

2.3.4 Today's picture of the Atlantic MOC from the 25ºN section 17

2.3.5 Independent verification for the 16-18 Sv Atlantic MOC 20

2.4 Variability of the Atlantic MOC 23

2.5 Summary 25

CHAPTER 3: **FIVE TRANSATLANTIC HYDROGRAPHIC SECTIONS** **27**

3.1 Introduction 27

3.2 Data and Methods 28

3.2.1 Overview 28

3.2.2 Ekman Transport 29

3.2.3 Florida Straits transport 32

3.2.3.1 Annual mean transports *32*

3.2.3.2 Velocity Profiles *35*

3.2.4 Mid-ocean transport 36

3.2.4.1 The data set *36*

3.2.4.2 The dynamic method *36*

3.2.4.3 Errors *39*

3.3 RESULTS 40

3.3.1 Overview 40

3.3.2 Water Mass Transports 41

3.3.2.1 The upper waters *43*

3.3.2.2 The intermediate waters *46*

3.3.2.3 NADW 47
3.3.2.4 AABW 50
3.3.3 Meridional Heat Transport 51
3.4 Discussion 52
3.5 Summary 57

CHAPTER 4: **METHOD OVERVIEW** **59**
4.1 MOC Components at 26.5ºN 59
4.2 Ekman Transport 60
4.3 Florida Straits Transport 60
4.4 Mid-Ocean Geostrophic Transports 61
4.4.1 Method Overview 61
4.4.2 Preliminary Results 64
4.5 Summary 66

CHAPTER 5: **METHODS AND DATA - END STATIONS** **67**
5.1 Introduction 67
5.2 The Eastern Boundary 67
5.2.1 End Station Selection 67
5.2.1.1 The upper layer 70
5.2.1.2 The intermediate layer 70
5.2.1.3 The middle and deep layers (NADW) 71
5.2.1.4 The selected dataset 73
5.2.2 Salinity Calibration 76
5.2.3 Transport anomaly calculation and errors 78
5.2.3.1 Methods 78
5.2.3.2 Errors 79
5.3 The Western Boundary 80
5.3.1 End Station Selection 80
5.3.1.1 The upper layer 81
5.3.1.2 The intermediate layer 83
5.3.1.3 The middle and deep layers 84
5.3.1.4 The selected dataset 86
5.3.2 Salinity Calibration 89
5.3.3 Transport anomaly calculation and errors 92
5.3.3.1 The reference specific volume anomaly profile 92

5.3.3.2 Appending CTD casts down the slope *93*
5.3.3.3 Transport errors *95*
5.4 Summary 97

CHAPTER 6: **METHODS AND DATA - DYNAMIC HEIGHT MOORINGS** **98**
6.1 Introduction 98
6.2 The Eastern Boundary 98
6.2.1 Introduction 98
6.2.2 Data Inventory 99
6.2.3 Initial data processing – missing pressure estimation 101
6.2.4 Initial data processing – salinity estimation 104
6.2.5 Initial data processing – vertical interpolation 107
6.2.5.1 The $\partial T/\partial p(p)$ climatology *110*
6.2.5.2 The $\partial T/\partial p(T)$ climatology *111*
6.2.5.3 Climatology comparison *112*
6.2.6 Transport anomaly calculation 114
6.2.7 Transport anomaly errors 115
6.2.8 Temperature records at 400 and 1100 dbar 117
6.3 The Western Boundary 119
6.3.1 Introduction 119
6.3.2 Data 119
6.3.3 Initial data processing – pressure 123
6.3.4 Initial data processing – salinity estimation 127
6.3.5 Initial data processing – vertical interpolation 129
6.3.6 Transport anomaly calculation 133
6.3.7 Transport anomaly errors 134
6.3.8 Temperature times series at 400 and 3000 dbar 135
6.4 Summary 137

CHAPTER 7: **RESULTS** **139**
7.1 Introduction 139
7.2 Ekman Transport 139
7.3 Florida Straits Transport 140
7.4 Eastern Boundary Geostrophic Transport 142
7.4.1 Hydrographic End Stations 142

7.4.1.1 Introduction – independence of observations *142*
7.4.1.2 Sub-annual variability *143*
7.4.1.3 Interannual variability *145*
7.4.2 Moorings 147
7.4.2.1 Overview *147*
7.4.2.2 Removal of meddies *148*
7.4.2.3 Seasonal variability *151*
7.4.2.4 Interannual variability *152*
7.5 Western Boundary Geostrophic Transport 157
7.5.1 End Stations 157
7.5.1.1 Overview *157*
7.5.1.2 Sub-annual variability *158*
7.5.1.3 Interannual flow variability *161*
7.5.2 Moorings 164
7.5.2.1 Overview *164*
7.5.2.2 Sub-annual variability *165*
7.5.2.3 Interannual variability *168*
7.6 Summary 173

CHAPTER 8: **DISCUSSION AND CONCLUSIONS** **176**
8.1 Data and Method Evaluation 176
8.2 Interannual Variability 181
8.3 Conclusions 184
8.4 Future Work 186

REFERENCES **188**

Acknowledgements

I would like to thank my PhD advisory panel of Prof. Harry Bryden, Dr. Joel Hirschi and Prof. John Shepherd, and members of the NOC Hydrography team for their guidance during the PhD and time at sea. In particular my supervisor Prof. Harry Bryden has provided a positive perspective and much support throughout.

I gratefully acknowledge data from a number of sources, including that of the RAPID monitoring array's 2004-05 deployment. The 2004 24.5ºN hydrographic section data have been made available by Dr. Stuart Cunningham of NOC. Kiel-276 mooring data and CTD stations in the eastern subtropical North Atlantic were provided by Prof. Gerold Siedler and Dr. Thomas Müeller of IFM-GEOMAR, Kiel, Germany, while the Abaco array mooring datasets come from Prof. William Johns of RSMAS, University of Miami and a number of the CTD casts at the west from Dr. Molly O. Baringer of NOAA/AOML, USA. Florida Current cable transports have been taken from the freely available Atlantic Oceanographic and Meteorological Laboratory web page (www.aoml.noaa.gov/phod/floridacurrent/) and are funded by the NOAA Office of Climate Observations.

CHAPTER 1: **Introduction**

The Meridional Overturning Circulation (MOC) is defined as the zonal integral of the full depth meridional mass or volume transport (Talley et al., 2003). In the Atlantic, although the MOC has a wind driven Ekman component, it is dominated by the northward transport of warm saline upper waters and their southward return flow at depth after cooling induced deep convection and sinking at high latitudes. The latter is termed the thermohaline circulation (THC) and accounts for almost all of the northward heat transport in the Atlantic (Bryden, 1993). It is the northward oceanic heat transport that maintains the mild western European climate relative to that which would result with no MOC (Manabe and Stouffer, 1988; Vellinga and Wood, 2002).

The Atlantic THC (and thus MOC) is predicted to weaken under scenarios of human induced increased atmospheric greenhouse gas concentrations (e.g. Cubasch et al., 2001), possibly cooling western European climate (e.g. Stouffer et al., 2006). Paleoclimatic observations suggest variation in the strength and location of deep water formation to have occurred in the North Atlantic in the geologic past (e.g. Broecker et al., 1985). The present uncertainty is associated not only with whether the THC strength might reduce in the future, but also the rate at which such a change would occur, since this is important for adaptation and mitigation of the effects (e.g. Srokosz, 2003).

Could such a slow down (or shut-down) of the Atlantic THC already be in progress? Until a couple of years ago we were not in a strong position to answer such a question, since the traditional way of measuring the Atlantic MOC strength was through hydrographic sections, repeated at best with decadal frequency. Although these measurements gave a picture of a generally steady state in the overturning strength (e.g. Lavín et al., 1998), the uncertainties were high, largely reflecting unresolved temporal variability. The cost involved with such measurements was also prohibitive, and an alternative monitoring method was required (Marotzke, 2000; Srokosz, 2003). A new observing system resulted, comprising a mooring array across the mid-ocean section

and Florida Straits cable transports at 26.5ºN, as part of the NERC Rapid Climate Change thematic programme (RAPID) (Srokosz, 2003). This system is able to continuously observe the strength and structure of the Atlantic MOC at 26.5ºN (Cunningham et al., 2007, submitted manuscript).

The first deployment of the RAPID monitoring array was in 2004 (Rayner and Cunningham, 2005) and its interpretation is therefore presently limited (by the short duration of the time series) to quantification of high frequency variability of the Atlantic MOC. It would therefore be beneficial if the time series could be extended. In light of the availability of high quality oceanographic observations from the 1950's to present day, with a proliferation in the WOCE era since the 1980's such an extension appears feasible, at least over the last 25 years. This motivates the aim of this thesis; to constrain recent variability of the Atlantic MOC at 26.5ºN through computation of an extension of the RAPID time series back in time to 1980 using historical observations. The focus will be on resolution of interannual variability, to complement the RAPID array results (Cunningham et al., 2007, submitted manuscript).

We start the thesis (Chapter 2) with a historical review of modern understanding of the Atlantic MOC's strength and structure providing valuable context for subsequent work, with regards both the methods employed and the results obtained. It is followed by presentation of our best estimates of Atlantic MOC strength from hydrographic sections at 25ºN (Chapter 3). Although the first four sections (obtained in 1957, 1981, 1992 and 1998) are not new datasets, we include a reanalysis to enable consistent treatment with the repeat section made in 2004 (Bryden et al., 2005b). These sections form the traditional measurement of the Atlantic MOC strength and are arguably the highest quality datasets, providing a reference for the time series developed in the rest of the thesis.

The principal disadvantage of the hydrographic sections for constraining Atlantic MOC variability is their low temporal resolution (5 sections in roughly 50 years). Chapters 4 to 6 detail methods developed to obtain transport estimates with increased temporal resolution. This is achieved by decomposition of the Atlantic MOC at 26.5ºN into the components of Ekman, Florida Straits and mid-ocean geostrophic transports, an overview of which is presented in Chapter 4. Time series of the first two components

are straightforward to obtain using wind stress climatologies and Florida Straits cable time series. For the latter we use dynamic height observations at the western and eastern boundaries of the 25.6ºN section, from both hydrographic end stations (Chapter 5) and moored temperature and pressure time series (Chapter 6). The resultant time series of all components are presented in Chapter 7.

Discussion of these results and those of the transatlantic sections follow in Chapter 8. We aim to answer questions such as; is there evidence of interannual variability in the Atlantic MOC in recent history? And if so, what is its size? Resolution of such issues requires evaluation of the methods developed and the datasets available. This also leads us to consider whether the hydrographic sections are really the best datasets for assessment of changes in the Atlantic MOC strength. A concluding summary of these findings and suggestions for future analyses completes Chapter 8 and the thesis.

CHAPTER 2: **A Historical Perspective: Discovery and Quantification of the Atlantic MOC**

2.1 INTRODUCTION

Here we present a review of the history of modern understanding of the strength of the Atlantic MOC, which arguably originates in 1957. Reflecting the nature of this thesis we focus on resolution of transports, particularly their zonal integral (in which form the MOC is defined), rather than the underlying system dynamics. There is also a bias towards 25ºN. In 1957 a remarkable set of cruises aboard *RRS Discovery II* enabled the first observation of the deep western boundary current in the North Atlantic Ocean to be made and the following transatlantic hydrographic section along 25°N provided data for the first rigorous calculations of the strength and structure of the Atlantic Meridional Overturning Circulation (MOC). Such calculations notably supported Stommel's (1957) original proposition of a 15-25 Sv MOC, the significance of which appeared to have gone unrecognised by the community until the supporting 1957 section analyses. 1957 therefore marks the beginning of modern understanding of the strength of the Atlantic MOC.

In March 1957, Swallow and Worthington (1957, 1961) tracked neutrally buoyant floats deployed between 2000 and 3000m depths over the Blake Plateau southeast of South Carolina on board *Discovery II* and made hydrographic stations on board *Atlantis* to observe the deep western boundary current (DWBC) recently predicted theoretically by Stommel (1957). The floats moved southward at speeds of 9 to 18 cm s^{-1} and these velocities were used to establish a reference level for geostrophic transport estimates that allowed the transport of a deep southward flow of North Atlantic Deep water (NADW) formed in the Labrador and Nordic Seas to be estimated. These were the first direct measurements of the deep western boundary current in the North Atlantic Ocean.

After a brief stop in Woods Hole (Figure 2.1), *Discovery II* headed back towards the English Channel making the first 48°N hydrographic section.

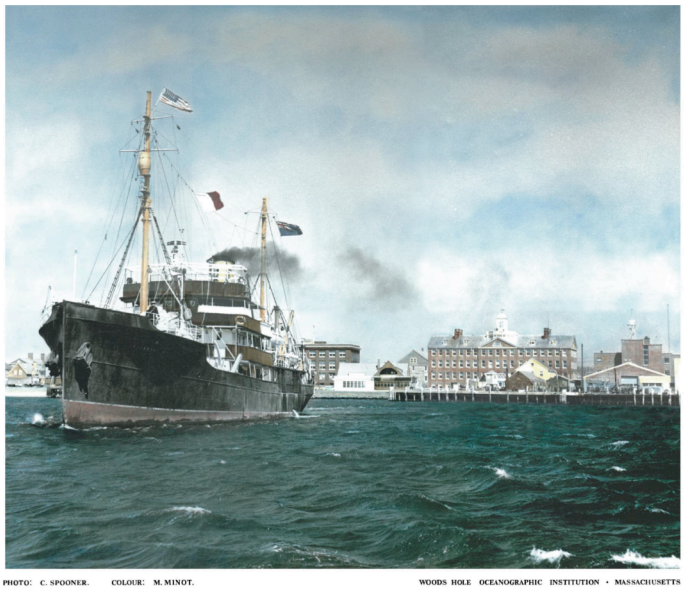

Figure 2.1 *Discovery leaving Woods Hole, Massachusetts in 1957*

In October 1957 *Discovery II* again crossed the Atlantic, making the first transatlantic 24.5°N hydrographic section (Worthington, 1958). This section with later measurements of the Gulf Stream flow through Florida Straits (Niiler and Richardson, 1973) enabled reliable estimates to be made of the size and structure of the Atlantic MOC. In contrast to classic ideas of a small overturning circulation of 7 Sv (Sverdrup et al., 1942), these estimates suggested a substantially larger overturning of 15 to 18 Sv, with a net northward flow of warm, upper waters above 1200 m depth and a compensating southward flow of cold deep waters below 1200 m depth (Roemmich, 1980; Wunsch, 1980; Hall and Bryden, 1982). Given the estimated error of ± 6 Sv associated with hydrographic section layer transports (Ganachaud, 2003) it is perhaps surprising that such consistent MOC strengths of 15-18 Sv have been obtained. Nonetheless, the 1957 *Discovery II* hydrographic section along 24°N led directly to the first modern estimates of the Atlantic MOC strength. *Discovery II* finished 1957 with a hydrographic section from Bermuda to Africa along 32°N.

We start by providing a brief summary of the history of the modern qualitative picture established in 1935 by Wüst (Section 2.2), although development of today's quantitative picture of the Atlantic MOC forms the bulk of this review (Section 2.3). A key

challenge in quantifying the MOC from observations is resolving the underlying variability of the system. To discuss this issue (in Section 2.4) we must depart from the otherwise observationally biased review (reflecting the thesis focus) and touch upon numerical modelling and theoretical studies of the atmosphere and ocean. This area of work is still very much evolving, and we only aim to draw attention to some of the proposed mechanisms of Atlantic MOC variability before interpreting our own observations in subsequent chapters. We conclude with a summary in Section 2.5.

2.2 A QUALITATIVE UNDERSTANDING

The first modern qualitative picture of the Atlantic MOC, arguably Wüst's (1935) scheme, is the culmination of more than a century of deep ocean temperature observations and their interpretation. Here we briefly summarise the key developments that set the scene for the 1957 work aboard *Discovery*, based on the detailed reviews of Deacon (1971), Mills (2005) and Warren (1981). We have not returned to the original source material, and instead refer the interested reader to these key overviews and references therein.

A meridional overturning in the Atlantic reconcilable with today's understanding was first proposed in 1798, by Count Rumford in his essay on the experimental discovery of convection currents in liquids (Deacon, 1971). He cited the cold isothermal layer below 3900 feet observed by Ellis in 1751 at 25ºN, 25ºW (above which the temperature increased toward the surface) as evidence of cooling induced deep water formation near the poles and its subsequent equatorward spreading. Continuity required a poleward surface current and thus the concept of a meridional overturning was established (Deacon, 1971; Warren, 1981). Rumford's was not however the first recognition of density driven circulation. Notably, von Waitz published an explanation for the deep Mediterranean Outflow counter current in 1755 (Deacon, 1985) based on the salinity gradient between the Atlantic and Mediterranean. This was extrapolated to suggest an Atlantic overturning in which salinity dominated the meridional density gradient, causing equatorial sinking, poleward transport at depth and equatorial flow of cold water at the surface. This was in the opposite sense to Rumford's scheme, since von Waitz was seemingly unaware of observations of cold waters at depth despite their documentation as early as 1665 by Boyle (Deacon, 1971).

It was Rumford's scheme which gained acceptance at the time. Detail in the form of two symmetric back to back convection cells was provided by von Lenz in 1840 (Figure 2.2) following his participation in the Russian circumnavigation of the world (1823-1826). Equatorial upwelling of the two cells was invoked to explain observed shoaling of the Atlantic equatorial thermocline. Up until the 1920's the circulation schemes that followed von Lenz's (e.g. those of Schott in 1902 and Brennecke in 1909) retained the two cell and equatorial upwelling structure. Widespread awareness of von Lenz's work only followed Prestwich's supporting paper in 1875, which incorporated all available deep ocean temperature measurements at the time. Meanwhile however, evidence for cross equatorial flows was accumulating from the *Challenger* expeditions (1872-1876). In 1884 and 1895 Buchanan and Buchan each showed both Antarctic Intermediate Water (AAIW) and North Atlantic Deep Water (NADW) north and south of the equator respectively in the hemisphere opposite to that in which they form. Despite this, such findings were not used explicitly to contest the two-cell circulation scheme. Brennecke in 1911 proposed the first cross-equatorial layered circulation scheme comprising southward transport of NADW between the northward moving layers of AAIW and Antarctic Bottom Water (AABW) after the additional observations from *Deutschland*.

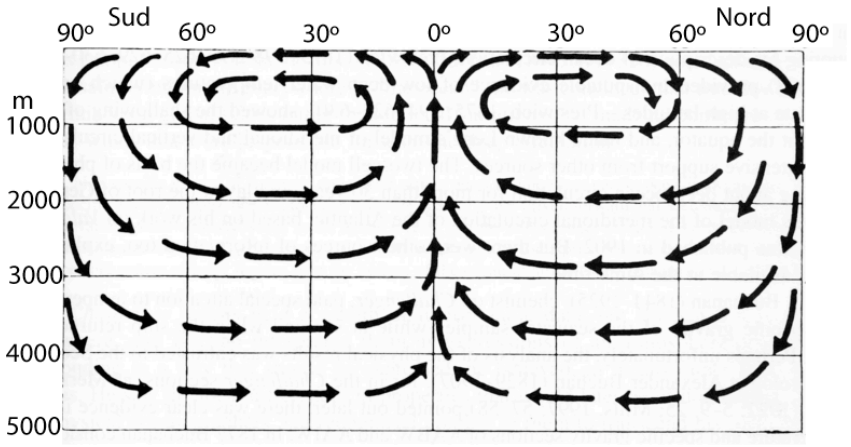

***Figure 2.2** Lenz's two cell circulation scheme proposed in the 1830's and 1840's, reproduced from Mills (2005)*

The 1920's saw a co-ordinated effort by the Germans to resolve questions about the deep ocean circulation starting with systematic re-examination of all deep temperature and salinity observations by Merz. Explicit rejection of Lenz's two-cell scheme resulted from Merz and Wüst's basinwide layered picture of inter-hemispheric exchange,

published in 1922. From the *Meteor* cruise (1925-1927) Wüst published a modified circulation scheme that was to form the classical picture of Atlantic meridional overturning circulation, reproduced in Figure 2.3 (Wüst, 1935). The schematic of hemispheric exchange incorporates spreading layers originating at high latitudes bounded by oxygen minima and temperature inversions. Upper NADW is characterised by a deep salinity maximum while Middle and Lower NADW are identified by oxygen maxima and originate from the Labrador and Greenland seas respectively. The 1922 version's subtropical contribution to deep water formation was rejected following Helland-Hansen and Nansen demonstrating the influence of Mediterranean Water on high salinity, and Wattenberg in 1929 tracing a deep oxygen maximum below the Mediterranean outflow to high latitudes (Warren, 1981).

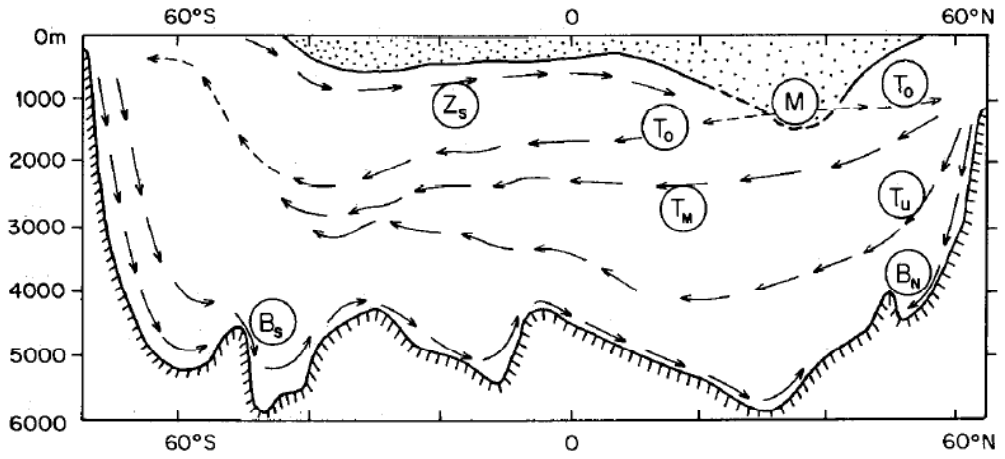

Figure 2.3 *Meridional spreading of water masses in the Atlantic, from Schmitz (1995) - originally from Wüst (1935). Z_S - Subantarctic Intermediate Water; $B_{S(N)}$ – bottom water from south (north); T_O – Upper NADW; T_M – Middle NADW; T_U –Lower NADW; M is the Mediterranean influence. The stippled area is Wüst's warm water sphere.*

It is important to note that even at this time, Wüst recognised that uniform basinwide flows were unrepresentative (Warren, 1981). The 1935 meridional circulation scheme revised the picture of deep circulation filling layers of the ocean as water masses formed to one of organised currents (albeit confined to the west). Previously "spreading layers" had been utilised: meridional current components were deduced from isohalines constructed from arbitrary longitudinal sections of temperature and salinity (Reid, 1981). This approach restricts interpretation to illustration of the consequences of circulation patterns rather than the flow pathway or strength. Wüst examined maxima and minima of salinity and oxygen to identify "core layers" interpreted as primary spreading paths of water from the formation site, under the assumption that beneath a

shallow wind-driven layer, the circulation was almost entirely meridional (Reid, 1981). Vigorous interhemispheric exchange was confined to the western Atlantic, flows in the east comprised zonal spreading or sporadic eddying (Wüst, 1935).

Wüst proposed three sites of deep water formation in the Atlantic, the Antarctic, the Mediterranean outflow and the high northern latitudes. Deep water originating from the latter comprised three layers; upper, middle and lower deep water (collectively known as NADW) that spread southwards above and below the layers of bottom water from the Antarctic (or AABW) and Subantarctic Intermediate water (or AAIW) both moving northwards (Figure 2.3). Bottom water from the Arctic is of secondary importance. Qualitatively at least, the basis of the modern picture of the Atlantic MOC was established with Wüst's 1935 scheme (Figure 2.3), although formation rates and transports had yet to be determined, and the overflow component of the MOC was not adequately emphasised (Warren, 1981).

2.3 Quantification of the Atlantic MOC: A Steady State Picture

2.3.1 Early estimates of a weak MOC

The need to determine transports of Wüst's 1935 circulation scheme did not attract immediate attention from observational oceanographers. Most of the progress of the early to mid 1900's was in application of the dynamic method to regional studies and later, their synthesis into basin circulation schemes concentrating on the upper and intermediate waters. A common feature of the studies is that the MOC deduced is weak, with 6-8 Sv cross equatorial exchange.

The dynamic method for computing ocean circulation, developed from Bjerknes circulation theorem by Sändstrom and Helland-Hansen in 1903, provided methods for calculating vertical shear from a density field by use of the geostrophic approximation. In the early 1900's the direction and relative strength of regional circulation were deduced from studies of the upper ocean. Defant (1941) was the first to apply the geostrophic method to the large scale density field from the *Meteor* expeditions, in his second paper he addressed the problem of computing absolute current magnitude

through employment of a reference level determined by continuity over the Atlantic from 50ºN to 50ºS (reviewed by Reid, 1981). Defant's flow field at 2000m shows a continuous current from the Labrador Sea to 35ºS along the western boundary of the Atlantic, with speeds less than 10 cm s^{-1} in the northern hemisphere. Such maps only covered the upper 3500 dbar at most, determination of interbasin exchange is therefore ambiguous and we turn to Sverdrup et al. (1942)'s oceanographic reference text *"The Oceans"* to gain insight into this period's understanding of the MOC (noting that this book itself references Defant's work). Qualitatively *The Oceans* representation of deep flows is largely based on Wüst's (1935) schematic with three sources for deep water in the North Atlantic; 2 Sv are formed in each of the Labrador Sea, the Greenland-Iceland-Norwegian Sea and at the Mediterranean outflow. The resulting NADW export to the South Atlantic is 9 Sv, supplemented by the assumed water mass conversion of their prescribed northward transports of 2 and 1 Sv of AAIW and AABW respectively, amounting to a 6 Sv MOC.

Support for this weak MOC was provided by the independent study of Riley (1951). Sverdrup et al.'s (1942) 6 Sv NADW formation rate was deduced from comparison of water mass properties between the Sargasso and Caribbean Seas. In their scheme NADW was formed from water sinking in the Labrador Sea (Labrador Sea Water, LSW), in the Nordic seas and from the Mediterranean outflow. The strength of the latter and LSW components were calculated from limited observations of each basin's exchange with the North Atlantic and continuity, but the Nordic sea contribution was merely a residual (Sverdrup et al., 1942). Riley was motivated to understand not the physical circulation but biological productivity and as such, his methods while again based on the geostrophic method, had a number of differences that resulted in an almost independent Atlantic circulation scheme. The assumed level of no motion was selected to conserve mass in a grid of 10º x 10º boxes covering the Atlantic from 60ºN to 60ºS using data from *Dana, Atlantis* and *Discovery* expeditions with additional consideration given to the conservative properties of oxygen and nutrients in the deep ocean. A circulation scheme in remarkably good agreement with Sverdrup et al. (1942) resulted, with 5 Sv of NADW formed and 8.3 Sv of cross equatorial exchange.

Supporting evidence for an Atlantic MOC weaker than 10 Sv was presented as late as 1976 by Worthington (1976). He attempted to synthesise a self-consistent circulation

scheme for the North Atlantic from numerous studies of regional features made during the mid 1900's, concentrating on deep water formation at high latitudes and the Gulf Stream system. A 7 Sv MOC resulted (Figures 2.4(i) and (ii)); 10 Sv of NADW formation but with 4 Sv recirculating north of 40ºN, and 1 Sv of Mediterranean Water southward flow. The NADW involved in interhemispheric exchange originated entirely from the Nordic seas and was partitioned equally between overflows from the Denmark Straits and the Iceland-Scotland Ridge (Denmark Straits Overflow water, DSOW, and Iceland-Scotland Ridge Overflow Water, ISOW respectively). LSW is formed in the scheme (2 Sv) but circulates only locally.

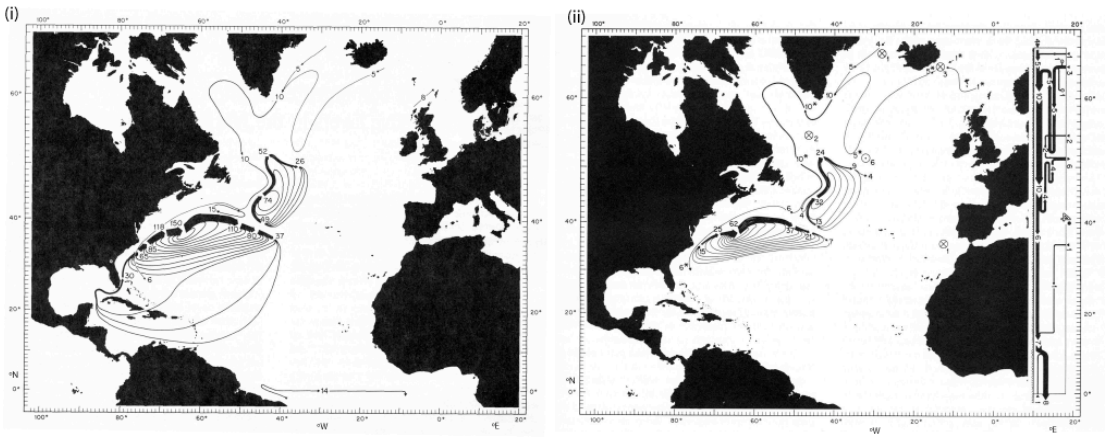

Figure 2.4 *The North Atlantic circulation according to Worthington (1976) of the total water column (i) and the deep waters (colder than 4ºC) only (ii). (i) does not show the 1 Sv of Mediterranean Water formation. The side insert of (ii) is a meridional box model showing exchanges with layers above and across the equator, with 7 Sv net export to the southern Atlantic in this layer.*

Despite discrepancies between the different source water contributions of deep cross equatorial flow suggested by different authors, the above studies present a consistent picture of an Atlantic MOC with strength of 6-8 Sv. Wüst's (1935) schematic was retained in structure, and a quantitative element introduced.

2.3.2 The Deep Western Boundary Current, Stommel and early indications of a stronger MOC

Although Worthington's (1976) calculations of North Atlantic circulation showed an MOC consistent in size with those of 20 and 30 years previously, contrasting work had been produced in the intervening period, notably that reported in Stommel's book "*The Gulf Stream*" (1958). Stommel's (1957) prediction of a DWBC was expanded through

theoretical and laboratory studies of stationary planetary flow driven by source-sink distribution patterns in a cylindrical tank (Stommel et al., 1958), under similar circumstances on a rotating sphere (Stommel and Arons, 1960a), and then extended to a highly idealised model of the world's abyssal ocean circulation (Stommel and Arons, 1960b). Versions of our Figure 2.5 are present in Stommel's 1957 and 1960b papers, showing a cross equatorial exchange of deep waters between 15 and 25 Sv (each line represents approximately 10 Sv). Even the lower limit of this, 15 Sv, would indicate an Atlantic MOC twice as strong as those discussed in the preceding section.

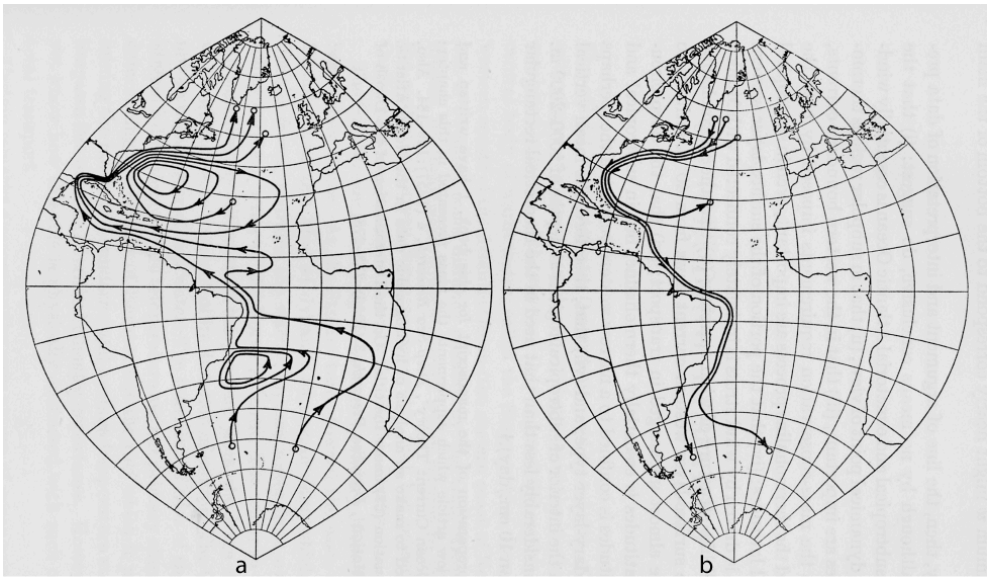

Figure 2.5 *Stommel's (1958) schematic of transport in the upper layers (a) and lower layers (b) of the Atlantic, inferred from data in Figure 2.6. Each transport line represents 10 Sv. Reproduced from Stommel (1958)*

Stommel (1958) presents and explains the observational data behind Figure 2.5 in *"The Gulf Stream",* although the manuscript was completed in 1955. Zonally integrated meridional transport across hydrographic sections of the Atlantic mid ocean and western boundary regions from 30ºS to 50ºN, was computed to identify different flow regimes (Figure 2.6). Transports were referenced to a level between 1200 and 2600m to satisfy mass conservation using the known 26 Sv northward transport through the Florida Straits from cable measurements (discussed in further detail in Section 2.3.4) as a starting point. A deep southward flowing western boundary current below approximately 1500m can be traced into the southern hemisphere from 40ºN (Figure 2.6), while deep transports in the interior are negligible (further north, deep transport is spread across the basin). In the upper waters of the western boundary sections Stommel (1958) demonstrated how flow was northward in the northern hemisphere and

southward in the southern hemisphere due to the combination of anticyclonic subtropical gyre transport with the thermohaline return flow that is northward in both hemispheres. In the mid-ocean sections, transport computed is that of the subtropical gyre return flow. Figure 2.5 is the two-layer summary of these section transports (Stommel, 1958).

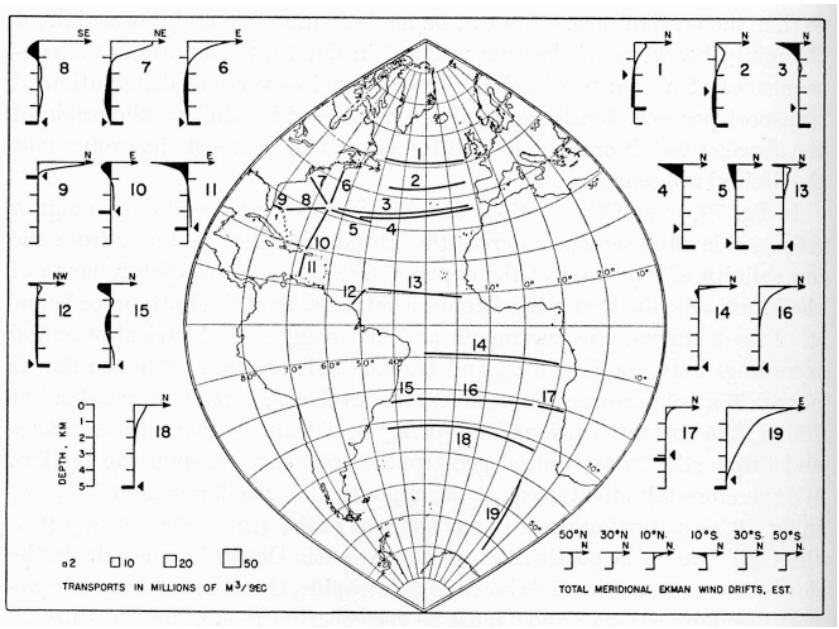

Figure 2.6 *Geostrophic transport per unit depth across sections of the Atlantic Ocean, reproduced from Stommel (1958). The Ekman transports are shown in the lower right corner. For each section, the arrow points to the maximum depth of the data and the solid bar the bottom of the ocean.*

The differences between Stommel's (1958) Atlantic circulation scheme (Figure 2.5) and that of Worthington (1976) (Figure 2.4), are striking, particularly in the overturning circulation strength (15-25 Sv and 7 Sv respectively). Worthington was aware of Stommel's (1958) work but did not favour its implied heat loss to the atmosphere related to the strong formation of deep water associated with the northward transport above the mid depth reference level, which itself Worthington also judged unsuitable for Gulf Stream geostrophic transports following float observations (Worthington, 1976, and references therein).

It is interesting that the mid-depth reference level used by Stommel (1958) was later judged preferable to that of Worthington (1976) for representation of the DWBC transports by Wunsch (1978), work that had itself been motivated by Worthington's (1976) study. In attempting to produce an overall circulation scheme for the North

Atlantic through application of the dynamic method with flows satisfying layer conservation of mass and salt, Worthington (1976) found that he had to invoke non-geostrophic flows. Following this, Wunsch (1977) developed a method of determining the level of no motion as a classical geophysical inverse problem. The inverse method of computing geostrophic circulation from hydrographic sections has gone on to yield many estimates of the Atlantic MOC strength (see Sections 2.3.3 and 2.3.5), but in the late 1970's the interesting study was application of the inverse method to determine transports across two sections crossing the Gulf Stream at the western boundary of the North Atlantic (Wunsch, 1978). Wunsch (1978) explicitly stated his interest in comparison of the flow solution which resulted when an initial reference level of the sea-floor was used e.g. as done by Worthington (1976), compared to a mid-depth reference level that had been favoured earlier, e.g. by Stommel (1958). His personal preference was for the mid-depth reference level, which not only gave a stronger southward Western Boundary Undercurrent of waters colder than 4ºC through the box formed by the sections, but also found the undercurrent waters to originate from further north than the recirculations offshore of Bermuda as in the scheme with the sea-bed reference level (Wunsch, 1978). Additional support for a reference level between 1500 and 2000m came from Swallow and Worthington's (1957, 1961) float observations of isobar slopes (Stommel, 1958). One may wonder whether, if Worthington (1976) had referenced transports to a mid-depth level, the net export of deep waters from the North Atlantic would have been stronger, i.e. he may have found a MOC strength in line with Stommel's (1958) earlier work, and whether he would have had to resort to permitting deviations from geostrophy, which Wunsch (1977) attributes to his "arbitrary selection of a level of no motion".

We suggest that the "reliable circulation diagrams for the North Atlantic" sought by Worthington had a number of shortcomings that impacted upon the MOC proposed, while Stommel as early as 1958 through the use of full zonal hydrographic sections and a mid depth reference level in the western boundary was able to gain significant insight into the nature of the meridional, thermohaline transports. Stommel's work at the end of the 1950's presented a strong case for the thermohaline (overturning) circulation in the Atlantic comprising a DWBC transporting NADW from formation sites in the high latitude northern hemisphere, fed by a return flow in the upper waters of the western boundary, with 15-25 Sv net meridional transport in each layer. Stommel was not

however the first to suggest stronger DWBC transport than the authors of Section 2.3.1 As early as 1955, Wüst's calculations of top to bottom flow speeds from the South Atlantic *Meteor* expedition sections show a DWBC with average speed of 9.2 cm s^{-1} between 10º and 30ºS (Wüst, 1955), broadly consistent with the DWBC strength of 22 Sv later computed by Amos et al. (1971) off the Blake Bahamas Outer Ridge, or 24 Sv near 35ºN (Richardson, 1977). The advantage of Stommel's (1958) study was the computation of section wide zonally integrated transports. These permit direct inference of the MOC strength, unlike DWBC transports alone which were not always interpreted in the wider context of interbasin exchange, and which we now know are sensitive to offshore recirculation gyres (e.g. Lee et al., 1996). We suggest that it is most unfortunate that Stommel's early insights, bearing many similarities with the definitive papers of MOC strength of the 1980s (e.g. Roemmich, 1980; Hall and Bryden 1982), took so many years to be followed up.

2.3.3 The MOC and its meridional heat transport

It took almost 20 years from the publication of Wüst's (1935) Atlantic MOC schematic for its potential role in ocean heat transport to be recognised (Jung, 1952). Having noted that "closed mean vertical circulations in meridional planes might transport large amounts of energy, even though the average velocities are extremely small", Jung (1952) set about quantifying this for the Atlantic. Firstly he constructed a hypothetical model of closed vertical circulation in a meridional plane near 30ºN with northward surface flow above 950m and return flow satisfying continuity to the bottom (4250m) and realistic temperature profiles from the western basin. Oceanic poleward heat transport was approximately a third of that of the global ocean heat transport estimated from radiation data with the residual method (Jung, 1952). A direct calculation using Sverdrup et al. (1942) and Riley's (1951) meridional velocity profiles at 27ºN and temperature data from the *Meteor* was consistent with the model calculation, but uncertainties about mass balance were large and southward transport was confined to depths above 2400m. Although Jung overestimated the global significance of the total meridional heat transport, being seemingly unaware of the absence of a similar overturning circulation in the Pacific and at least weaker deep water formation in the Indian (Sverdrup et al., 1942), the importance of the MOC in energy balance calculations was identified, necessitating determination of its magnitude.

Jung (1955) did follow up his 1952 paper with publication (in an obscure technical report) of mass transport maps of the North Atlantic circulation in three layers and identified exchanges between layers. This was the first analysis of its kind based on a comprehensive data set, but total deepwater transport across 27ºN in the Atlantic of 8.3 Sv is consistent with the other computations of that time (e.g. Sverdrup et al., 1942). Bryan (1962), provided further support for Jung's assessment of the importance of an overturning circulation for meridional heat transport and simultaneously suggested a stronger overturning circulation. Again Bryan used the direct method to estimate heat transport and computed circulation according to Sverdrup transport, thus avoiding selection of a contentious reference level. Specifically the 36ºN section showed significantly stronger meridional heat transport by the overturning circulation than the more vigorous horizontal circulation by virtue of vertical temperature gradients. Notable is the 15 Sv overturn at this latitude, although this was not the focus of Bryan's paper and seemingly not expanded upon.

Bryan (1962) did not include the 1957 *Discovery II* 24ºN section in his heat flux calculations and it was not until the early 1980's that interest was renewed in the problem. A number of authors (e.g. Bryden and Hall 1980; Roemmich 1980), made use of the ideally placed 24ºN section in conjunction with the well constrained transport of the Gulf Stream through the Florida Straits at this latitude (Niiler and Richardson, 1973) as had been first done by Stommel in 1958 (Figure 2.6), although he had used different, non-synoptic sections. Roemmich (1980) applied the inverse methods for ocean circulation developed by Wunsch (1977; 1978) to these observations and computed a 1.2 PW meridional oceanic heat transport, 0.7 PW of which was attributed to the MOC. Of the 30 Sv northward transport through the Florida Straits, 14 Sv retuned south after conversion to deep water at high latitudes while the remaining 16 Sv returned south in the mid ocean at densities less than the maximum in the Florida Current associated with the subtropical gyre. The latter carried only 0.1 PW northward supporting Jung (1952) and Bryan (1962)'s analyses. The remaining 0.4 PW of meridional heat transport was driven by northward Ekman transport at this latitude and its barotropic southward compensation. That Roemmich (1980) obtained a 16 Sv MOC from this study is noteworthy.

Roemmich's work in fact was done at the same time as that of Bryden and Hall (1980) who used the same 1957 24ºN hydrographic section to compute a meridional oceanic heat transport of 1.1 PW. Roemmich regarded the use of inverse methods a progression in that they permitted description of the heat flux mechanisms and resolution of velocity on broad scales (Roemmich, 1980). Hall and Bryden (1982) however, through presentation of transport in the mid ocean and Florida Straits in depth and temperature classes, supported Roemmich's findings showing that of the 28.5 Sv Florida Current transport warmer than 7ºC, 18 Sv were converted to deep water before their southward return across the section, with the remaining 10.5 Sv recirculating in the upper waters of the mid-ocean section (see Table 2.1 in the following section). Furthermore, Wunsch (1980), using model circulations and the inverse method on a dataset of meridional and zonal hydrographic sections in the North Atlantic between 10º and 60ºN found a conversion of 16 Sv of the 31 Sv Florida Straits transport to waters colder than 4.6ºC in the return flow.

We see that from the drive to quantify the meridional heat transport associated with the MOC, initiated by Jung (1952), a new picture of the Atlantic MOC strength emerged around 1980, with most progress originating from the use of the 1957 *Discovery* 24ºN hydrographic section. The 16-18 Sv overturn, notably stronger than Worthington's (1976) 7 Sv and the calculations preceding this, is consistent in structure with Stommel's (1958) model while the principal development in our understanding was associated with better constraint on the strength and associated heat transport.

2.3.4 Today's picture of the Atlantic MOC from the 25ºN section

The new consensus of a 16-18 Sv Atlantic overturning (Roemmich, 1980; Hall and Bryden, 1982; Wunsch, 1980) was accompanied by significant advancement in our understanding as discussed by Hall and Bryden (1982) relative to the key North Atlantic circulation text of the 1970's (Worthington, 1976) (Table 2.1 and Figure 2.7).

Hall and Bryden (1982)'s zonally integrated mid-ocean layer transports (Figure 2.7) clearly show the Wüst (1935) components of meridional exchange. In the mid ocean (Figure 2.7 (ii)) southward return flow of the subtropical gyre is seen above 550m (apart from the upper 25m northward wind driven transport), with the northward core of

AAIW sitting below this to 1150m. From 1150 to 4500m NADW flows southward, then AABW moving north is seen beneath 4500m. Combining this with the northward transport through the Florida Straits, from the surface to 850m (Figure 2.7(i)) we see net northward and southward flows above and below 1150m respectively comprising the meridional overturn (Figure 2.7(iii)). Also included is the wind driven surface Ekman transport of 5 Sv.

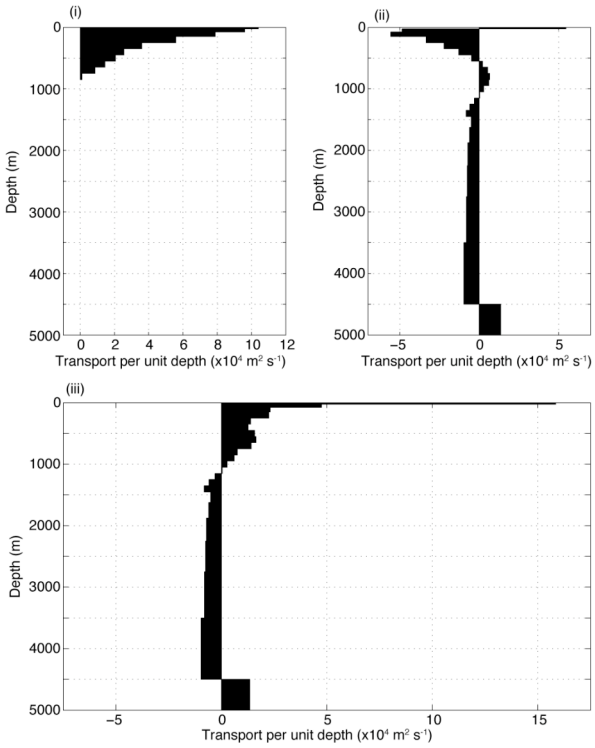

Figure 2.7 *Meridional zonally integrated volume transport per unit depth at 24ºN across the Florida Straits (i), the mid-ocean (ii) and combined Florida Straits plus mid-ocean (iii). Figure produced from Table 5 of Hall and Bryden (1982).*

Hall and Bryden discussed computed meridional flow strengths in the context of Worthingon (1976), which was arguably the key reference text for the North Atlantic circulation at that time. Their main finding in this respect was an increase in the southward transport of waters colder than 4ºC from 7 Sv to 15.6 Sv, and an additional 3 Sv in the 4-7ºC waters (Table 2.1) corresponding to NADW transport. Hall and Bryden (1982) also quantified the northward flow of AAIW as 7-12ºC waters that had not featured in Worthington's (1976) calculations at approximately 2 Sv. Hall and Bryden (1982) showed that the required southward transport in the mid-ocean to satisfy mass balance with northward Florida Straits transport of 29.5 Sv, occurs predominantly in the lower waters colder than 4ºC, rather than in the upper layers at temperatures warmer than 17ºC (Worthington, 1976). This reflects the importance of the meridional

transport's thermohaline component obtained by Hall and Bryden (1982) which was comparable to Stommel's (1958) circulation scheme, but more rigorously computed.

Temperature Class	Transport (Sv)			
	Hall and Bryden (1982)			Worthington (1976)
	Total	Florida Straits	Mid-ocean	Mid-ocean
$\theta > 17^{o}C$	8.9	18.4	-9.5	-15
$12^{o}C < \theta < 17^{o}C$	2.5	5.4	-2.9	-5
$7^{o}C < \theta < 12^{o}C$	6.6	4.7	1.9	-4
$4^{o}C < \theta < 7^{o}C$	-2.3	1.0	-3.3	0
$\theta < 4^{o}C$	-15.6	-	-15.6	-7

Table 2.1 *Meridional volume transports across 25ºN in the Atlantic by temperature class, from Hall and Bryden (1982). Northward Ekman transport of 5 Sv is included in the warmest class of the mid- ocean. Worthington (1976)'s scheme is based on 30 Sv northward transport through the Florida Straits.*

The principles of the method developed by Bryden and Hall (1980) have been broadly employed to determine overturning strength on subsequent occasions at 24ºN, this being arguably best latitude to quantify the meridional cell (Roemmich, 1980). Close to the boundary between ocean heat gain from the atmosphere in the tropics and loss to the atmosphere in the high latitudes, 24ºN is near the latitude of maximum oceanic heat transport (Bryden, 1993). Errors in geostrophic velocity are reduced relative to the equatorial regions while further north increased topography of the Mid-Atlantic Ridge increases noise and reduced vertical density gradients reduce the number of layers and thus the information content of the data in inverse calculations. From knowledge of Florida Current transport from years of monitoring by submarine cable and calibration cruises (Niiler and Richardson, 1973; Larsen, 1992; Baringer and Larsen, 2001) and assuming the Atlantic north of this latitude to be an essentially closed basin, northward transport through the Florida Straits and in the Ekman layer (computed from wind stress climatologies) must be compensated for by southward flow across the mid ocean (Bahamas to Africa). Mass balance may therefore be achieved through imposition of a uniform barotropic compensation velocity. Alternatively a reference level may be identified with the inverse method and additional constraints, for example as done by Roemmich and Wunsch (1985). The subjectivity associated with selection of absolute levels of no motion is thus removed giving confidence in the zonally integrated transports obtained relative to the earlier transport estimates.

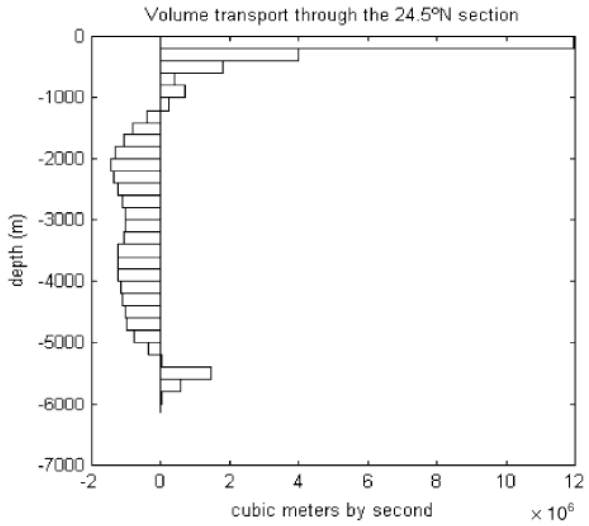

Figure 2.8 *Total volume transport through the 24° N 1992 section by depth classes of 200 m, including Florida Straits, Ekman layer and mid-ocean section. From Lavín et al., (2003).*

Subsequent sections across 24ºN were made in 1981, 1992 1998 and 2004 (Roemmich and Wunsch, 1985; Parilla et al., 1994; Baringer and Molinari, 1999; Bryden et al., 2005b), from which the main addition to our understanding of the MOC has resulted from increased vertical resolution due to replacement of bottle samples and reversing thermometers with continuous recording CTD systems; in particular the two-lobe structure of NADW can be better delineated (Roemmich and Wunsch, 1985). The upper lobe centred around 2100m (Figure 2.8) originates in the Labrador Sea and the lower around 3800m in the Nordic seas. Aside from this, despite employment of a hierarchy of geostrophic models (Roemmich and Wunsch, 1985) and incorporation of silica constraints (Lavín et al., 2003) the zonally integrated profile of meridional velocities proposed by Hall and Bryden (1982), associated with an overturning circulation of 16-18 Sv at 25ºN has provided a robust description of transports in the subsequent sections. The recently reported slowed overturning reported by Bryden et al. (2005) from observations at 24ºN in 1998 and 2004 remains contested (e.g. Levi, 2006) and is returned to in Section 2.4 and Chapter 3.

2.3.5 Independent verification for the 16-18 Sv Atlantic MOC

The identification of water masses constituting the DWBC transport (Roemmich and Wunsch, 1985) permitted quantitative links to be made with high latitude studies.

McCartney and Talley's (1984) box model study of warm to cold water conversion in the high latitude North Atlantic provided independent support for the 16-18 Sv strength subtropical Atlantic MOC. They considered the 11.1 Sv DWBC, consisting of 8.5 Sv LSW and 2.5 Sv from the Norwegian Seas, to be in agreement with Hall and Bryden's (1982) deep southward transport of 15.6 Sv below 4.0ºC Sv with entrainment as the boundary current moves southward.

Additionally an analysis of water mass properties in the Florida Straits and Caribbean passages reinforced the new overturn strength further, through consideration of the rate of replacement of South Atlantic origin waters that feed NADW formation (Schmitz and Richardson, 1991). With a 29 Sv Florida Current, Schmitz and Richardson (1991) showed that the subtropical gyre circulation contributed 16 Sv while the remaining 13 Sv was part of the thermohaline circulation originating in the South Atlantic (identified by virtue of its low salinity with 7.1 Sv warmer than 24ºC and the rest between 7 and 12ºC). A 13 Sv northward interbasin exchange in the upper water column is also consistent with a net southward deep transport of 13 Sv at 32ºS with flows of 17 Sv NADW and 4 Sv AABW northward (Rintoul, 1991).

Global circulation schemes are a natural progression from the calculation of single section zonally integrated flows, which were so important in determining the strength of the MOC. Wunsch (1978) stated that the inverse solution to circulation west of 50ºW in the subtropical north Atlantic was in fact a first step towards the production of a circulation budget for the entire Atlantic and ultimately the world oceans. The completed global inversions of WOCE hydrographic sections found 16 ± 5 Sv of net southward transport below 3.5ºC across 24ºN (Macdonald and Wunsch, 1996), a value confirmed by Ganachaud and Wunsch's (2000) update but with errors decreased to ± 2 Sv. The global inversion arguably provides a better representation of the mean state of the overturning circulation than a single section through forced consistency between section transports separated both temporally and spatially, and is thus less susceptible to anomalous conditions. The notably good agreement between this global inversion and MOC strength as estimated from the 24ºN section (e.g. Lavín et al., 1998) suggests that the 24ºN section and Florida Straits transport are strong constraints in the large scale inversions.

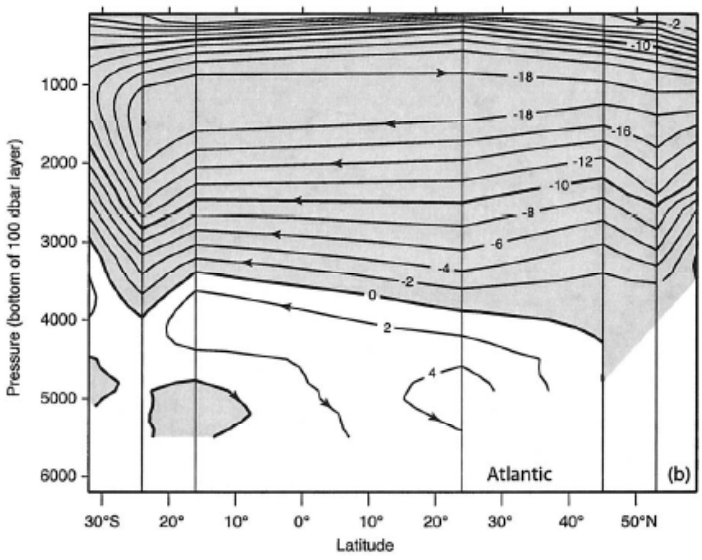

Figure 2.9 *Atlantic meridional overturning streamfunction including Ekman transport, based on observational data. From Talley et al., (2003).*

A complementary approach, and result, was provided by construction of the first Atlantic MOC streamfunction (a diagnostic commonly used in modelling the MOC) from in situ data (Talley et al., 2003). Argued to be no more subjective than the inverse method, meridional geostrophic velocities computed from observations spanning 1957 to the WOCE sections with adjustments based on observed property distributions are integrated from bottom to top (Figure 2.9). As expected, the zonally integrated Atlantic MOC is dominated by NADW, including LSW, and AABW cells, transport of the former is 18 Sv with an error of 3-5Sv at most latitudes. It is expected that future determinations of the streamfunction with global inversions or data assimilation will have an improved accuracy (Talley et al., 2003).

The zonal mean representation (e.g. Figure 2.9) is useful for an overview of the MOC but conceals the fact that meridional exchange is concentrated in western boundary currents of the upper and deep waters. To complement this we therefore present an update of Worthington's (1976) circulation maps (Figure 2.10), derived from synthesis of many of the aforementioned studies and more, by Schmitz and McCartney (1993). The similarity with Stommel's (1958) schematic is notable, but complexity has increased. Recirculation gyres complicate the picture, and their exact offshore extent is unknown at 24ºN and likely to be temporally variable (Bryden et al., 2005a). The construction of streamlines as in earlier works (e.g. Worthington 1976) is therefore not possible, however desirable.

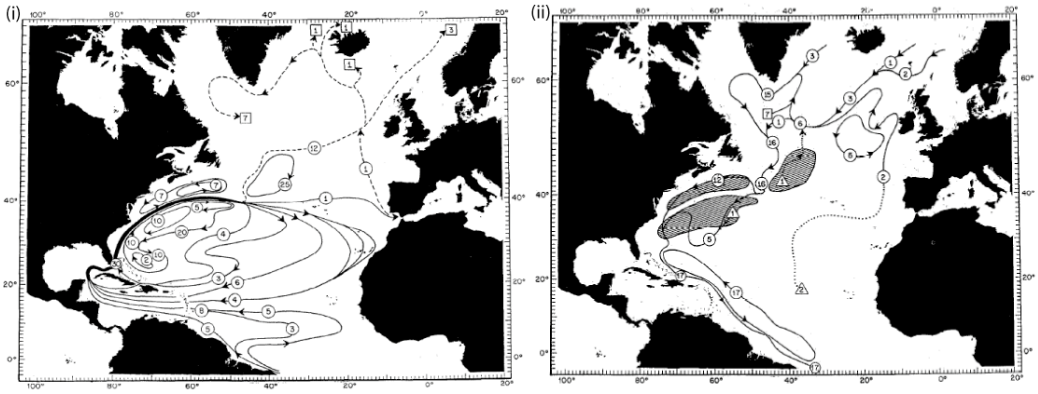

Figure 2.10 *Circulation cartoons for waters warmer than 7ºC (i) and 1.8-4ºC (ii). Transports are in Sv, triangles denote upwelling and squares sinking in or out of the respective layer. In (ii) detail of recirculation gyres is omitted and their general position shaded. Additional cartoons for AAIW and AABW are available in Schmitz and McCartney (1993) from which we take this figure.*

Finally we note that the strength of the Atlantic MOC has been constrained not only by the traditional water properties of temperature and salinity but also radiocarbon observations (Broecker, 1991). The flux of NADW to the deep North Atlantic is calculated from the division of water volume by a radiodecay based residence time with correction for atmospheric carbon ratio changes and the proportion of AABW (estimated from phosphate concentration). Broecker (1991) found a NADW flux of 20 Sv, not inconsistent with hydrographic based transports when the error of order 25% is allowed.

2.4 VARIABILITY OF THE ATLANTIC MOC

Section 2.3 reviewed the support for a steady state Atlantic MOC of 16-18 Sv as all observations since that of the 1957 24ºN section have been consistent within their estimated errors. The system's inherent variability is however a contribution to the large error estimates and remains predominantly unquantified at present. Potential sources of this variability are numerous, and while it is beyond the scope of this review to evaluate all literature on this topic (in particular the many relevant numerical modelling studies upon which a whole review itself could be written), we outline below some of the diverse mechanisms that have been suggested to underlie variability of the Atlantic MOC.

The dominant mode of atmospheric variability in the North Atlantic, the North Atlantic Oscillation (NAO) can affect the strength and character of the Atlantic thermohaline circulation through altered air sea exchange of heat and freshwater (Hurrell et al., 2001). Florida Straits transports are suggested to lag the NAO by approximately 18 months (Baringer and Larsen, 2001) and its extension, the North Atlantic Current, which supplies the high latitude NADW sinking sites, also varies following the NAO (Curry and McCartney, 2001).

Lower limb MOC changes have also been related to the NAO. Freshening of the Nordic Sea overflows since 1965 (Dickson et al., 2002) is anticipated to be accompanied by changes in the overturning strength and has been linked to an increasingly positive state of the NAO (Dickson et al., 2003). Observations in the Faroe Bank Channel have indeed shown that the overflow has not been constant over the last 50 years (Hansen et al., 2001). Latif et al. (2006) argue conversely that such changes in LNADW are insignificant for MOC variability in the near future when compared with LSW formation changes forced by the NAO on multidecadal timescales. That LSW formation is believed to be influenced by the NAO (e.g. Eden and Willebrand, 2001) is interesting in light of the feedback mechanisms between LSW formation and the strength of the MOC through the North Atlantic suggested in an observational study by Koltermann et al. (1999).

In the South Atlantic it is likely that the temporally variable Agulhas leakage in part feeds NADW return flow (Macdonald and Wunsch, 1996; Gordon et al., 1992). Agulhas leakage contributes to the salty thermocline of the Atlantic and thus to NADW formation (Gordon et al., 1992) and may influence the MOC through the effect of the lateral buoyancy flux on the available potential energy (Weijer et al., 1999).

Focus on the density driven sinking component of the MOC to determine its strength may not be the most appropriate if instead the rate limiting factor is the upwelling of deep waters, set by mechanical mixing. This proposal, put forward by Wunsch (2000; 2002) and Wunsch and Ferrari (2004), suggests that the MOC strength is determined not by buoyancy forcing but by wind and tidal mixing. In accordance with this, modelling results have found that stronger winds in the south can increase deep water formation in the north Atlantic since northward transport of water upwelled around

Antarctica by Ekman divergence effectively ventilates deep water from the ocean interior (Toggweiler and Samuels, 1995). In this context the recent trend in the Southern Annular Mode associated with stronger westerly winds around Antarctica (Thompson and Solomon, 2002) may lead to a stronger MOC.

With complex variability mechanisms such as these potentially influencing the Atlantic MOC, it would appear prudent to employ caution when interpreting Bryden et al., (2005b)'s trend towards weakened overturning strength since 1950. The 30% reduction in overturning reported was based on 5 circulation snapshots with unquantified variability at intervening times (Kerr, 2005). This reflects the challenge we currently face in estimating the strength of the Atlantic MOC since presently the variability mechanisms introduced above need to be quantified and await conclusive study.

2.5 SUMMARY

The discovery and quantification of the Atlantic MOC has a long and interesting history. The initial proposition was intuitive; high latitude sinking in both hemispheres with equatorial upwelling produced two equatorially symmetric cells forced by the meridional heat flux gradient. This was later contested following observation of cross equatorial flows and Wüst's classical picture of interhemispheric exchange evolved (Wüst, 1935). High latitude sinking is found in both hemispheres but NADW formation dominates interhemispheric exchange. This exchange shows a layered structure; schematically northward in the surface waters and southward at depth with small northward AABW and AAIW flow in southern and low northern latitudes. Obtained through water mass analysis and the definition of core layers that identified the spreading path of waters from their formation site, Wüst's circulation scheme was broadly confirmed through analysis of later hydrographic sections with geostrophic velocities expressed as a zonally integrated flow (e.g. Stommel, 1958; Hall and Bryden, 1982; Lavín et al., 1998).

A strength of 16-18 Sv (definitions vary between sources but can be broadly regarded as the net meridional deep water transport) is supported by observational studies with data encompassing single hydrographic sections (e.g. Lavín et al., 1998), regional and global inversions (e.g. Macdonald and Wunsch, 1996; Ganachaud and Wunsch, 2000), water

mass property analysis (Schmitz and Richardson, 1991) and radiocarbon observations (Broecker, 1991). This current strength estimate has held since the early 1980's and replaces the previous 6-8 Sv cross equatorial deep water transport. Early work was largely inhibited by controversial choice of reference level velocities in geostrophic calculations, later avoided through employment of mass balance starting with Stommel (1958) and later by the many authors working with the 1957 24ºN section.

Now that the steady state Atlantic MOC strength has been observationally established, resolution of its variability is a timely problem. Since the Atlantic MOC forms part of a complex global system, work to attribute variability of the presently sparse observational datasets to underlying causes has thus far proved inconclusive. This is certainly where the present and future challenges remain, to which the work of this thesis will contribute.

CHAPTER 3: **Five Transatlantic Hydrographic Sections**

3.1 INTRODUCTION

As discussed in Chapter 2, modern understanding of the Atlantic MOC strength and structure originated with analysis of the 1957 24.5ºN transatlantic hydrographic section (Fuglister, 1957). Subsequent reoccupations of this section in 1981, 1992, 1998 and 2004 (Roemmich and Wunsch, 1981; Parilla et al., 1994; Baringer and Molinari, 1999; Bryden et al. 2005b) provide an ideal starting point to assess the changes in the Atlantic MOC over the last 50 years. An overview of this work has been presented already in Bryden et al. (2005b). Here we expand upon that study, again examining the sections in the context of their representation of the annual mean MOC of each year, but addressing Bryden et al. (2005b)'s simplification of constant Florida Straits and Ekman transports over the 50 years. Additionally more detailed studies of the observed changes in water mass and meridional heat transports are presented.

Although the error in transports from one-time hydrographic sections has been suggested to be ± 6 Sv (Ganachaud, 2003), inclusion of property observations (e.g. salinity, temperature) across the 24.5ºN section increases the confidence with which variability may be identified and explained. This is in contrast to the methods developed in subsequent chapters, which are restricted to the section boundaries. Accordingly the annual average MOC for 1957, 1981, 1992, 1998 and 2004 presented in this chapter will form the reference states for subsequent variability estimates.

3.2 DATA AND METHODS

3.2.1 Overview

The annual mean Atlantic MOC is estimated for each 25ºN transatlantic hydrographic section (Figure 3.1) using broadly the same method as that developed for the 1957 section (Hall and Bryden, 1982) incorporating annual average transports of the Ekman component from wind stress climatology and the Florida Straits component from cable observations. This assumes the mid-ocean geostrophic flow field computed with mass balance constraints from each one-time hydrographic section to be representative of annual mean conditions, as supported by both theoretical and modelling studies which show that baroclinic flow structure in the subtropics does not respond to wind or thermal forcing on sub-annual timescales (Gill and Niiler, 1973; Jayne and Marotzke, 1999).

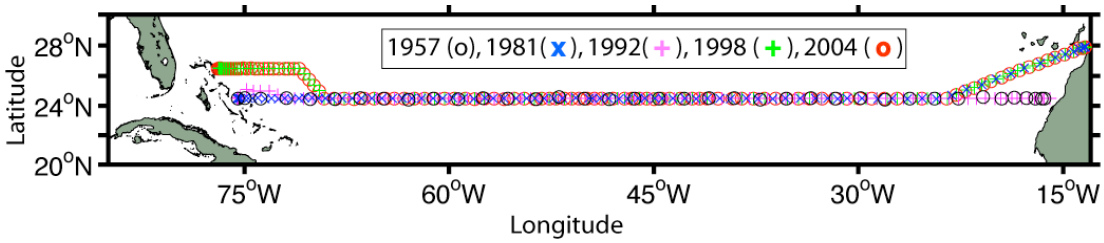

Figure 3.1 *Station positions for the transatlantic hydrographic sections of 1957, 1981, 1992, 1998 and 2004.*

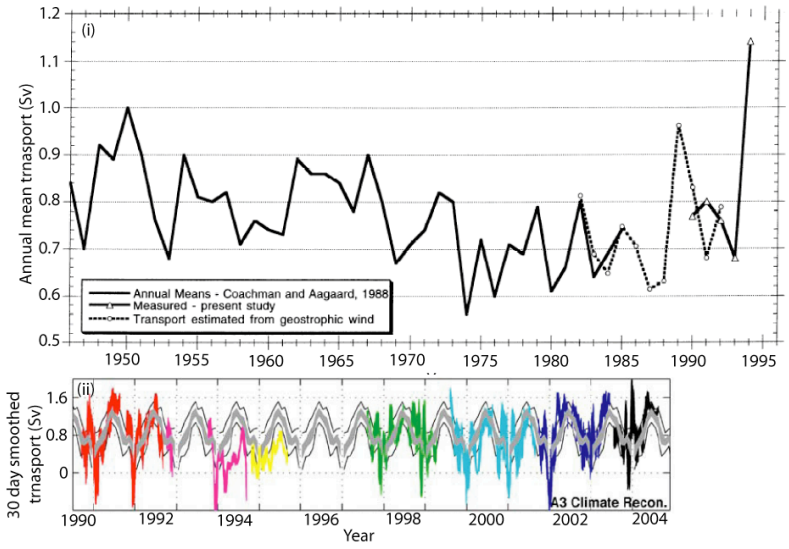

Figure 3.2 *Interannual variability in Bering Straits transport reproduced from Roach et al. (1995) (i), and Woodgate et al. (2005) (ii).*

Traditionally authors have assumed the Atlantic to be a closed basin north of 25ºN (e.g. Hall and Bryden, 1982; Reommich and Wunsch, 1985; Lavín et al., 1998). In fact net inflow from the Pacific to Atlantic via the Bering Straits is well constrained and we see no reason not to incorporate this into the 25ºN section transports. The long term annual mean Bering Strait transport of 0.8 Sv has maximum uncertainty of 30% (Coachman and Aagaard, 1988; Roach et al., 1995; Woodgate et al., 2005), we find no support for any long term trend in this (Figure 3.2) and the weakened transport of 1969 to 1985 noted by Coachman and Aagaard (1988) does not appear to continue though 2004 (Figure 3.2). Although interannual variability of the inflow may in extreme cases be 0.5 Sv (Roach et al., 1995), its standard deviation from 1946 to 1982 is only 0.1 Sv (Coachman and Aagaard, 1988). From this, net transport across each 25ºN section is set to be 0.8 Sv.

3.2.2 Ekman Transport

The annual mean meridional Ekman transport across each repeat of the 25ºN hydrographic section is computed in 1º longitude bins from the NOC global monthly mean wind stress climatology (Josey et al., 1998; 2002):

$$\text{Ekman transport} = -\tau_x L_x / \rho f \qquad (3.1)$$

(e.g. Gill, 1982) where τ_x is the zonal component of wind stress, ρ seawater density, L_x the width of each 1º longitude bin, and f the Coriolis parameter. The NOC climatology is the only one computed from ship observations corrected for biases in observing procedure and is thus expected to be the most accurate of such available products (Josey et al., 2002). Its long term mean (1980 to 2004) Ekman transport across the Atlantic at 25.5ºN of 3.8 Sv is in good agreement with 3.6 Sv from the atmospheric model reanalysis product of National Centre for Environmental Prediction (NCEP) across 25.7ºN. Variability of the two climatologies is also consistent, each having a standard deviation of 1.9 Sv between 1980 and 2004.

Since Ekman transport (long term mean between 1980 and 2005) at 26.5ºN is 30% lower than that at 24.5ºN it is important to follow the ship's cruise track of each transatlantic hydrographic section as closely as possible when computing Ekman transport. The 1957 and 1992 sections therefore use wind stress at 24.5ºN across the whole section, while others use values at 25.5, 26.5 and 27.5ºN towards the eastern

boundary, and the last two use 26.5ºN in the western boundary (Figure 3.3). This is also important to account for the different section widths (Figure 3.1) and an additional reason that the NOC climatology is preferable to NCEP which has 1.9º zonal resolution compared to the 1º of the NOC climatology.

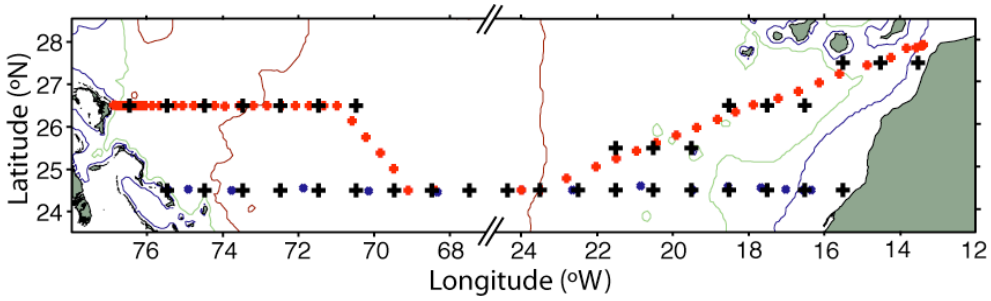

Figure 3.3 *Grid points of the NOC wind stress climatology used for calculation of Ekman transport (+) (1ºx 1º resolution) with the 1998 (+) and 1957 (•) station positions for reference. Note that the mid-ocean between 67.5 and 23.5ºW is omitted where all sections follow the 24.5ºN line. Depth contours of 1000, 3000 and 5000m are included for reference and land is shaded.*

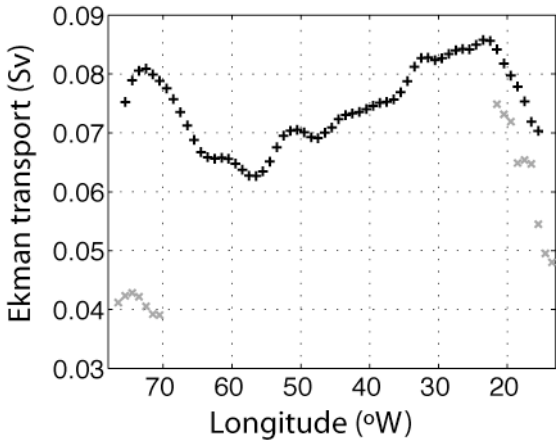

Figure 3.4 *Ekman transport in 1º longitude bins computed from wind stress at the locations of Figure 3.3. The 24.5ºN transports are shown in +, while those angling northward to the eastern and western boundaries are in x.*

The resulting long term mean Ekman transport as a function of longitude is shown in Figure 3.4 with the difference due to cruise track changes only amounting to 0.2 Sv between the long term annual means; 4.5, 4.6 and 4.4 Sv for the 1957/1992, 1981 and 1998/2004 tracks respectively. For calculation of the Ekman component of meridional heat transport (Section 3.3.3) the temperature of the Ekman transport at each 1º point in longitude is the mean 10 dbar temperature of the CTD stations within 1º longitude of this point. This follows Wijffels et al. (1994) who found that 80% of the Ekman transport occurs within 0.1ºC of the 5 dbar temperature and all within 0.2ºC of this.

With a 20 dbar vertical resolution dataset (Section 3.2.4), the 10 dbar temperature is therefore the most appropriate for the Ekman transport.

The annual mean Ekman transports (Figure 3.5, Table 3.1) of 1981, 1992, 1998 and 2004 computed from the monthly resolution climatological NOC wind stress (incorporating the different cruise tracks) have a range of 1.5 Sv from 3.7 Sv in 1981 to 5.2 Sv in 1998, with 10% error (Josey et al. 2002) based on comparison of the NOC monthly mean wind stresses with WHOI meteorological buoy wind observations.

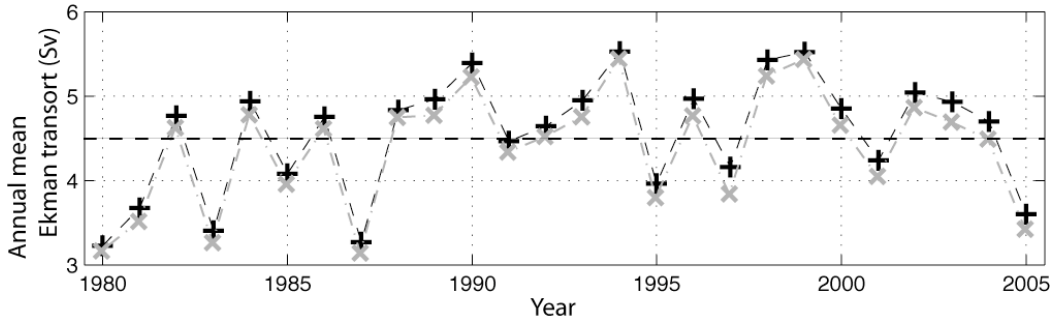

Figure 3.5 *Annual mean Ekman transport from the NOC wind stress climatology at 24.5ºN (75.5ºW to 15.5ºW) (+) and following the 1998 cruise track (x). The 1981 cruise track transports agree with those plotted to within 0.1 Sv. The long term mean transport of 4.5 Sv is also plotted (black dashed line).*

Year	1957	1981	1992	1998	2004
Ekman transport ± error (Sv)	4.5 ± 0.8	3.7 ± 0.4	4.6 ± 0.5	5.2 ± 0.5	4.5 ± 0.5

Table 3.1 *Annual mean Ekman transports for use in mass balance of mid-ocean geostrophic flow. Years 1981-2004 correspond to plotted values of Figure 3.5. The error is 10% of the annual mean transport reflecting the uncertainty in wind stress (Josey et al., 2002) while that of 1957 incorporates the additional uncertainty associated with using the long term mean transport.*

The NOC climatology only extends back to 1980, and for the 1957 section we use the long term mean at 24.5ºN of 4.5 Sv. This is justified since although linear regression shows a trend towards increased transport over time (0.3 Sv per 10 years) this is not significant at the 95% level and is likely due to increase of the winds with the predominantly positive state of the North Atlantic Oscillation (NAO) over the latter part of the record (Josey et al., 2002). The mean annual station based NAO index from 1980 to 2002 inclusive is 0.6, with standard deviation 2.0, which encompasses the 1957 index of –0.5 (Figure 3.6). There is therefore no justification for assuming the 1957 annual average Ekman transport to be any different from the 1980-2005 mean of 4.5 Sv at

24.5ºN but uncertainty is increased to 0.8 Sv (combining the 10% climatology error with the standard deviation of annual mean Ekman transports from 1980 to 2005 of 0.7 Sv, Table 3.1). Although the NCEP wind stress climatology extends back to 1948, we do not use this to estimate the 1957 Ekman transport since there are uncertainties associated with the poorer longitudinal and latitudinal resolution of the NCEP reanalysis product relative to the NOC climatology.

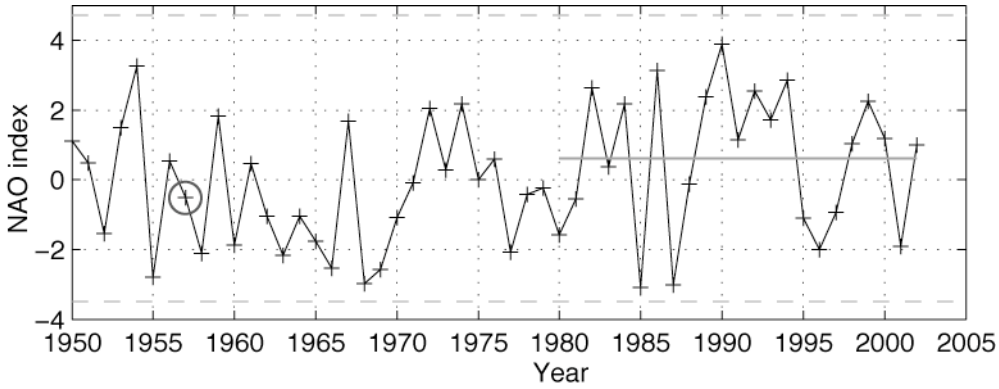

Figure 3.6 *NAO index based on the annual average normalised sea level pressure difference between Ponta Delgada, Azores and Stykkisholmur/ Keykjavik, Iceland (http://www.cgd.ucar.edu/cas/jhurrell/indices.html) in black. The 1957 value is circled and the limits of the 1980-2002 mean (solid grey line) ± one standard deviation over this period are extended back to 1950 with grey dashed lines.*

3.2.3 Florida Straits transport

3.2.3.1 Annual mean transports

There have been a number of projects to monitor transport of the Florida Current by measurement of the potential difference across either end of a submarine electromagnetic cable spanning the Florida Straits, induced by the movement of seawater's charged ions through the Earth's magnetic field. The earliest such observations were by Stommel in 1952 using a telephone cable between Key West and Havana (Larsen, 1992). Larsen (1992) reviews details of both the method and its history. Calibration cruises using dropsondes or LADCP are vital as is knowledge of the magnetic field variations (Larsen, 1992). The transport measured is the total Florida Current, which includes Ekman transport through the Straits and also the wind driven subtropical gyre and thermohaline components. The latter are collectively known as the Gulf Stream on exiting the Straits to the north.

To estimate the annual mean Florida Straits transport for the 1992, 1998 and 2004 sections we make use of the transport time series from cables at 27ºN between West Palm Beach, Florida and Eight Mile Rock, Grand Bahamas (used from 1982 to October 1998) and that between Vero Beach, Florida and Eight Mile Rock which has been operational from March 2000 to the present (Baringer and Larsen, 2001), Figure 3.7. The daily transport time series after removal of the tidal signal and corrected for magnetic variations (http://www.aoml.noaa.gov/phod/floridacurrent) is plotted in Figure 3.8 along with the one-year running mean. Annual mean Florida Strait's transports for 2004, 1998 and 1992 are obtained from this running mean (Table 3.2) although that for 1998 is actually based on the last 12 months of cable transport before the 17 month data gap between October 1998 and March 2000 caused by instrumental problems and cable difficulties during the cable swap from West Palm Beach to Vero Beach.

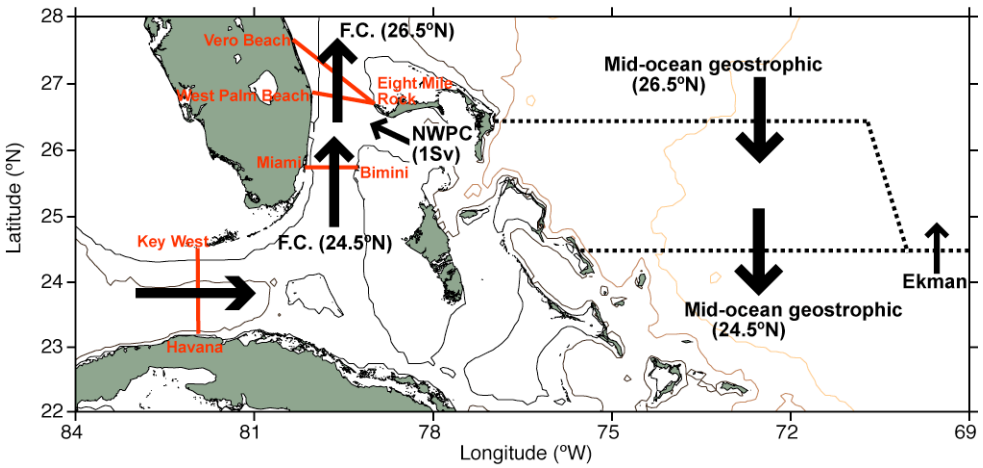

Figure 3.7 *A schematic illustrating the dependence of flow components (arrows) across the 24.5 and 26.5ºN sections on latitude. Mid-ocean components are zonally integrated transports. Land is shaded and depth contours of 200m, 1000m, 3000m and 5000m are plotted. Black dotted lines represent the hydrographic section cruise tracks and red solid lines the location of Florida Current (F.C.) transport monitoring cables. NWPC is the transport through the North West Providence Channel that feeds the Florida Current as measured at 27ºN from the mid-ocean.*

For the 1992 transport, the North West Providence Channel (NWPC) contribution to the Florida Current cable transport at 27ºN must be subtracted since the mid-ocean hydrographic section meets the western boundary south of this (explained in Figure 3.7). Current meter measurements (Hamilton et al., 2005) and dropsonde sections (Leaman et al., 1995) have shown transport through the NWPC to be approximately 1 Sv from the mid-ocean to the Florida Straits (1990-1991). This is a little higher than the 1.5-2.5 Sv estimates from Richardson and Finlen (1967)'s hydrographic sections but

they were spread over only 2 days. 1 Sv is therefore subtracted from the 27ºN 1992 annual mean cable transport to give 30.3 Sv at 24.5ºN (Table 3.2).

Year	1957	1981	1992	1998	2004
Transport ± error (Sv)	31.1 ± 1.8	31.1 ± 1.8	30.3 ± 1.3	34.0 ± 0.8	31.8 ± 0.8

Table 3.2 *Estimated annual mean Florida Straits transport for use in mass balance constraint of mid-ocean geostrophic flow. Refer to text for details of estimation, the years 1957, 1981 and 1992 include the 1 Sv subtracted from measurements at 27ºN to account for the 1 Sv flow through the North West Providence Channel. Justification of errors is provided in text.*

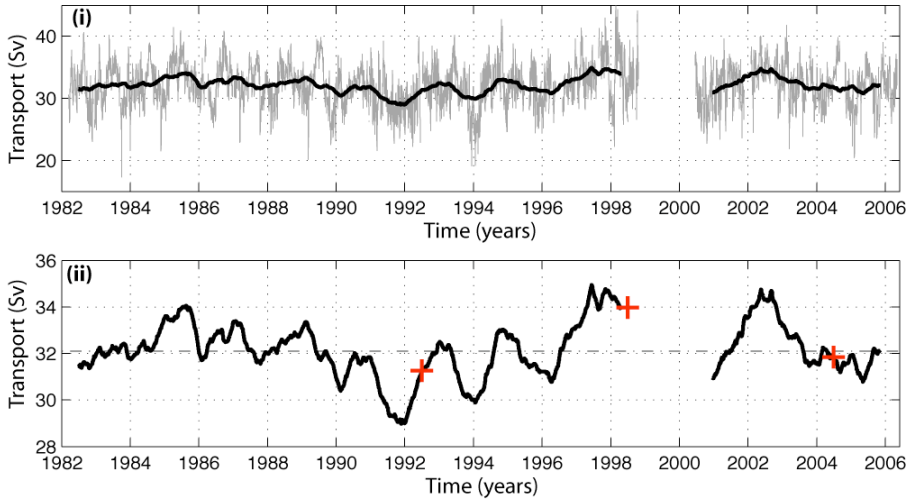

Figure 3.8 *Time series of Florida Current transport at 27ºN from cable measurements. (i) shows the daily mean transports (light grey) with a one-year running mean overlaid (heavy black line). The same one-year running mean transports are plotted in (ii) on an expanded scale with the annual means of 1992, 1998 and 2004 in red crosses, plotted for the 1st July of each year (that of 1998 is based on October 1997-October 1998). The long-term mean of 32.1 Sv is added for reference (dash-dot line). Data are obtained from* http://www.aoml.noaa.gov/phod/floridacurrent *up to 12/5/2006.*

The 27ºN cable was not operational in 1981 or 1957, and for these annual mean Florida Straits transports we use the long term mean 27ºN cable derived flow of 32.1 Sv minus the 1 Sv NWPC contribution (Table 3.2) since Larsen's (1992) reanalysis of all cable transports showed any long term trend for each of the time series 1952 to 1961, 1969 to 1974 and 1981 to 1990 to be less than 0.5 Sv. Also his mean transport of 32.2 Sv at 27ºN is in excellent agreement with both our mean of 32.1 Sv for 1982 to 2006 (Figure 3.8), and Baringer and Larsen's (2001) mean of 32.2 from 1982 to 1998. While the Key West – Havana cable was operational between 1952 and 1961, yielding 491 daily mean estimates of Florida Current, these are not used here for the 1957 annual average transport since meanders are believed to introduce ± 8 Sv uncertainty in transport from

this cable (Larsen, 1992) and inflows through the Santaren and Nicholas Channels (between 23ºN and 24ºN) are unquantified for this period.

The error estimates of Table 3.2 have a number of sources. For 1998 and 2004, 0.8 Sv is the error associated with inference of transport from cable voltages (Larsen, 1992). To this, 1 Sv is added in an r.m.s. sense for the 1992 estimate to incorporate the uncertainty of the NWPC contribution, based on Larsen's (1992) suggestion that the Miami-Bimini cable transport (Figure 3.7) is a few Sv lower than at 27ºN where we use only 1 Sv for the NWPC flow. Finally for the 1981 and 1957 transport errors, these sources are combined with that due to using the long term mean, the standard deviation of which is 1.2 Sv from 1982 to 2005 (Figure 3.8).

3.2.3.2 Velocity Profiles

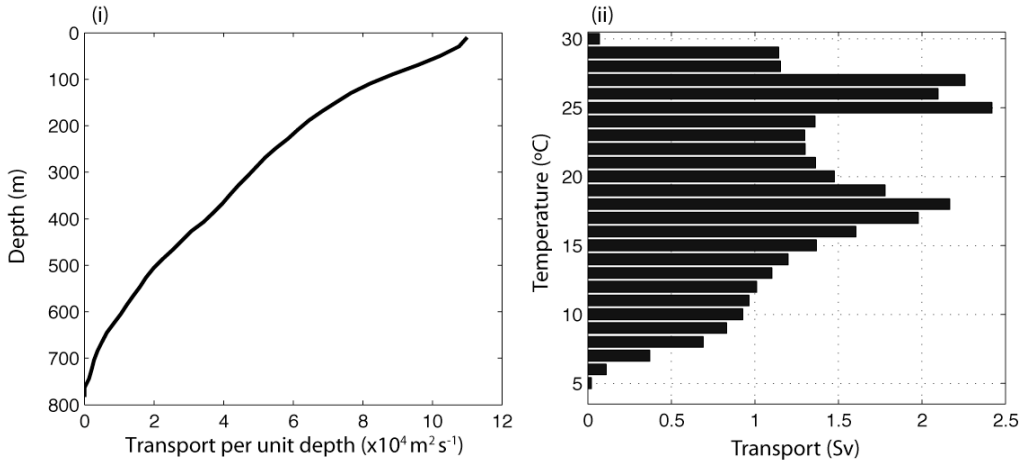

Figure 3.9 *Florida Current transport per unit depth profile (i), and temperature transport in 1ºC temperature layers (ii), for total transport of 32.1 Sv. Both are modelled according to* $Tr_i = A_i * Tr_{total} + B_i$ *where i is either the temperature layer (4.5-5.5, 5.5-6.5… 29.5-30.5ºC) or depth layer (0-5, 5-15, 15-25 … 795-805 m) and A and B are coefficients determined from linear regression of PEGASUS Florida Straits transport to temperature or depth (Baringer and Bryden, personal communication 2006).*

Ultimately it is not just the total transport through the Florida Straits which is required for examination of the MOC structure but also the distribution of this transport with depth and temperature. Although geostrophic transport could be computed from CTD sections across the Florida Straits that accompanied the later four hydrographic sections, referencing this to the sea-bed requires a large barotropic northward flow to be added to achieve consistency with the cable measured transports. This is especially true in 1992 when CTD stations were relatively shallow, thus not resolving the deeper, colder

transport in the Straits with implications for heat transport computed. To avoid such uncertainties we make use of the 65 PEGASUS sections from 16 cruises between April 1982 and July 1984 during which the free-falling instrument measured absolute velocity and temperature (Leaman et al., 1987; Shoosmith et al. 2005). Linear regression of Florida Current transport to depth in 10m bins yields coefficients from which a vertical transport profile of the Florida Current (Figure 3.9(i)) can be estimated given any total transport. Temperature transport is estimated in the same way with regression of transport to temperature in bins of width 1ºC (Figure 3.9(ii)) (Baringer and Bryden personal communication, 2006).

3.2.4 Mid-ocean transport

3.2.4.1 The data set

Repeat occupations of the 24.5ºN transatlantic hydrographic section following the cruise tracks of Figure 3.1 were made during October 1957, August-September 1981, July-August 1992, January-February 1998 and April-May 2004. All are eddy resolving except 1957, an estimate of the effects of which is presented in Section 3.2.4.3 below. 1957 and 1992 follow 24.5ºN across the full section, as do the other sections in the mid-ocean but they were forced to deviate to 28ºN approaching the African coast due to diplomatic clearance issues at the east; and in 1998 and 2004 sections meet the Bahamas at 26.5 rather than 24.5ºN so the section transports could be directly closed with the Florida Straits cable measurements. The hydrographic sections consist of between 38 and 121 vertical temperature, salinity and oxygen profiles obtained from continuously profiling CTD observations (1981 through 2004) or from bottle salinities and reversing thermometers in 1957 with each data set interpolated onto 20 dbar levels. For the CTD sections, dynamic heights are computed directly from the 2 dbar CTD downcast (to retain fine scale variability) then subsampled at 20 dbar intervals which is the working vertical resolution of all other variables.

3.2.4.2 The dynamic method

Velocity shear is computed following the geostrophic method for each station pair across the mid-ocean section at 20 dbar vertical resolution down to the deepest common pressure:

$$(v - v_R) = \frac{1}{f\Delta x}\left(\int_{p_R}^{p} \delta_1 dp - \int_{p_R}^{p} \delta_2 dp\right) \tag{3.2}$$

where v is the average geostrophic velocity between two hydrographic stations 1 and 2 at pressure p relative to pressure p_R, and the specific volume anomaly (δ in $m^3\ kg^{-1}$) is integrated with respect to pressure in Pascals between pressure levels p and p_R (e.g. Pond and Pickard 1983). Below the deepest common pressure of the station pair, velocity is decreased linearly to zero through the bottom triangle (Slater, 2003) if the deepest common pressure is deeper than the reference level. Otherwise, transports are referenced to the sea-bed (deepest common pressure) and transport in the bottom triangle is zero.

A reference level of 3200 dbar is used from the eastern boundary to the start of the deep western boundary current, the position of which is identified from the position of the oxygen front below 1000 m between the highly oxygenated waters of the southward flowing DWBC and the less oxygenated water of the interior flowing northward (Lavín et al., 1998; Figure 3.10). Within the western boundary, a reference level of 1000 db (Olson et al., 1984; Leaman and Harris, 1990) is used corresponding to the transition between northward transport of the Antilles Current in the upper waters and southward deep transport below. Although there may be patches of water with high oxygen concentrations offshore of the identified transition, these are attributed to northward recirculations of the DWBC. The 3200 dbar choice for the ocean interior is justified by Saunders (1982) who found that in the Eastern North Atlantic, a deep level of no motion at 3200 dbar is indistinguishable from shallower levels. This is supported by the analysis of Lavín et al., (1998) who used this reference level and achieved good consistency for the net transports of the 1957 and 1981 sections with the analysis of Roemmich and Wunsch (1985) who employed a reference level of 1000 m across the full section (representative of the flow reversal between the northward moving AAIW and southward UNADW layers) and followed it up with inverse methods enforcing mass and potential vorticity conservation in specified layers. Lavín et al. (1998) argued that the 3200 dbar choice is preferable since it avoids the unrealistically strong deep southward transport in the eastern basin that results with a shallower level.

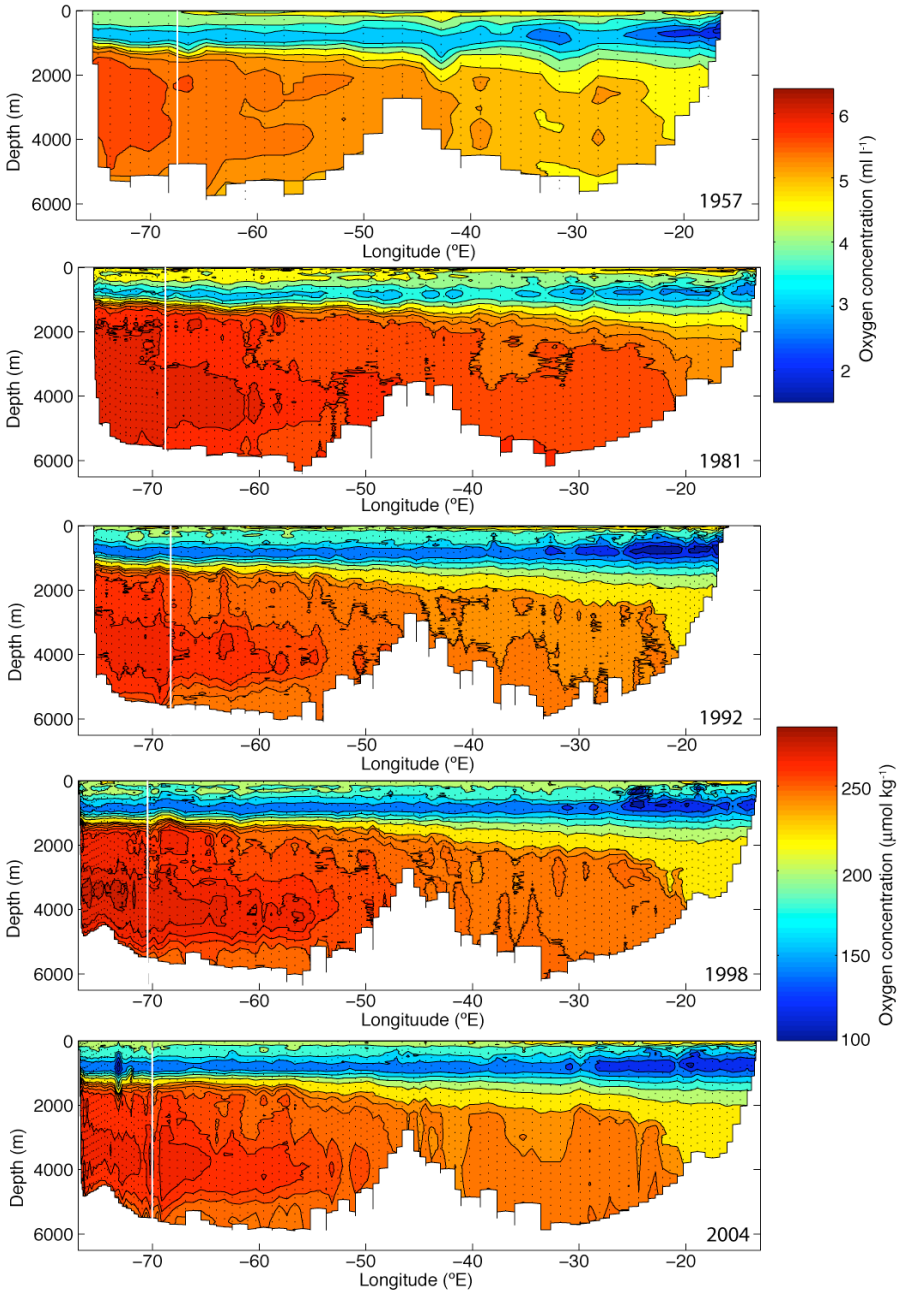

Figure 3.10 *Zonal sections of oxygen from each of the 1957, 1981, 1992, 1998 and 2004 24ºN hydrographic sections. For 1957 and 1981 contours are at 0.5 ml l^{-1} intervals from 1.5 to 5.0 ml l^{-1} and 0.2 intervals to 6.4 ml l^{-1} (both with the same colour scale). The latter three years have contours at 20 µmol kg^{-1} from 100 to 240 µmol kg^{-1}, and then 5 µmol kg^{-1} up to 285 µmol kg^{-1} (again with the same colour scale). Gradients are more important than absolute values for identification of the transition between the western boundary and mid-ocean flow regimes, indicated by a white line. Station positions are shown with dotted lines.*

Year	Stations	Section area (x10^4 km^2)	Reference level velocity (cm s^{-1})	Transport (Sv)		
				Mid-ocean	Florida Straits	Ekman
1957	38	2.99	-0.13	-36.4	31.1	4.5

1981	90	3.26	-0.04	-35.6	31.1	3.7
1992	101	3.02	-0.10	-35.7	30.3	4.6
1998	121	3.30	-0.05	-40.0	34.0	5.2
2004	113	3.29	-0.01	-37.1	31.8	4.5

Table 3.3 *Summary of flow compensation components for the five transatlantic hydrographic sections. Stations are the number of temperature/salinity profiles made across the mid-ocean section, amounting to the area of column 3 (not including the Florida Straits). Ekman and Florida Straits transports are from Tables 3.1 and 3.2, the mid-ocean transport balances these with the net 0.8 Sv of southward flow due to the Bering Straits inflow. The reference level velocity refers to the mid-ocean geostrophic transport, satisfying mass balance.*

Finally a uniform mid-ocean section wide reference level velocity is determined so as to satisfy mass balance of each section, with a net southward flow of 0.8 Sv due to the Bering Straits inflow (Table 3.3).

3.2.4.3 Errors

We do not revisit the question of the uncertainty of transports computed from one-time hydrographic sections since Ganachaud (2003) has already addressed this in a comprehensive manner, finding the net rms transport error across a section to be ± 6 Sv dominated by contributions from eddy variability and internal waves. This was supported by study of the Indian Ocean subtropical gyre at 32ºS, which suggested the error due to the internal wave field to be ± 5-7 Sv (Palmer et al., 2004). The effect of the non-eddy resolving station spacing of the 1957 section has been found to introduce a rms error of ± 1 Sv in the net transports above or below 800m (from subsampling the later sections at comparable longitudinal resolution) although errors in deep water mass layer transports (e.g. LNADW) may reach 3-4 Sv. This results from increased transport in the bottom triangles, for which the method is more uncertain. The 1957 section will therefore be interpreted in this context, the net transport of the upper layer (as used to define the MOC here, Section 3.3.1) is useful, but the individual layer transports are treated with caution.

3.3 RESULTS

3.3.1 Overview

From the definitions of MOC strength reviewed in Chapter 2 we proceed with that of the net northward transport above a given depth level (equal to the deep southward transport of waters after transformation at high latitudes) across the ocean section at 25ºN. 800m is used as the division, corresponding to the maximum depth of the Florida Straits through which the upper northward limb of the MOC is constrained to flow at 25ºN.

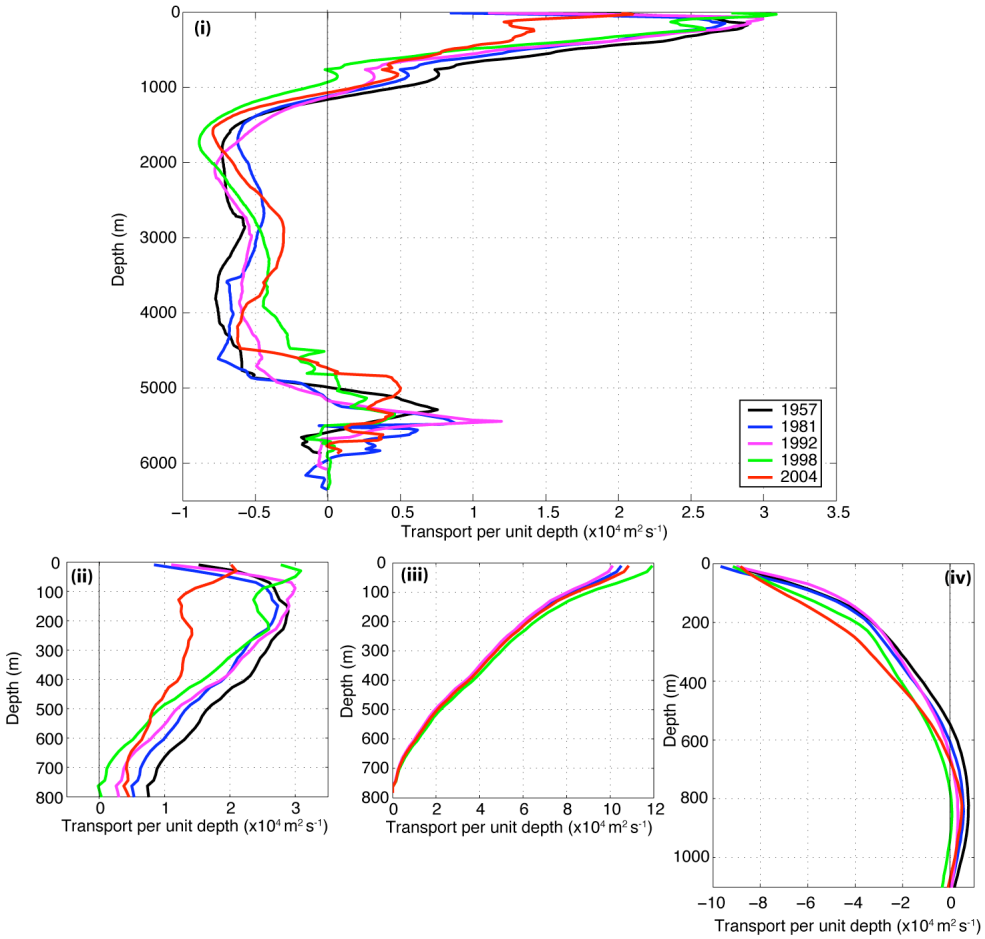

Figure 3.11 *Zonally integrated meridional geostrophic transport per unit depth profiles for the total Florida Straits and mid-ocean geostrophic transports of 1957, 1981, 1992, 1998 and 2004 (i) (excluding Ekman transport). The upper 800m of the combined transport is expanded in (ii), while the Florida Straits and mid-ocean geostrophic components are expanded separately in (iii) and (iv) respectively.*

The zonally integrated meridional transport across the 25ºN section (Figure 3.11) shows northward transport above approximately 1100m. In fact, this is the net result of northward transport in the Florida Straits down to approximately 800m (Figure 3.11(iii)) and southward recirculation of the wind driven subtropical gyre in the mid-

ocean above roughly 700m (Figure 3.11(iv)). The net northward transport above 800m is therefore the thermohaline component of the Florida Current and the upper branch of the MOC at 25ºN. The mid-ocean geostrophic northward flow between 700 and 1100m is that of AAIW and is included in the lower limb of the MOC. The main component of the MOC's lower limb giving net southward transport is the two lobed structure of NADW (Figure 3.11(i)). Upper NADW is seen between 1100 and 3000m, with lower NADW down to approximately 5000m. The northward flow of the bottom waters is AABW.

		1957	1981	1992	1998	2004
Upper	Ekman	4.5	3.7	4.6	5.2	4.5
	Florida Straits	31.1	31.1	30.3	34.0	31.8
	Mid Ocean	-15.6	-18.0	-17.1	-22.1	-23.4
	Total	**20.0**	**16.8**	**17.8**	**17.1**	**12.9**
Lower	Intermediate	1.7	1.1	0.7	-0.2	0.8
	UNADW	-11.4	-9.2	-10.8	-12.8	-10.3
	LNADW	-13.1	-12.2	-10.5	-6.0	-6.8
	AABW	2.0	2.6	2.0	1.2	2.5
	Total	**-20.8**	**-17.6**	**-18.6**	**-17.9**	**-13.7**

Table 3.4 *Total water mass transports across 25ºN in depth classes in the Ekman layer, Florida Straits and mid-ocean above 800m (Upper) and the mid-ocean only below (Lower). Definitions for the lower layer components are as in the text and column 2 of Table 3.5. The net imbalance between upper and lower layers is due to the Bering Straits –0.8 Sv net transport across the section.*

The MOC strength computed from the zonally integrated meridional transports of Figure 3.11 (Table 3.4) ranges from 20 Sv in 1957, 17-18 Sv between 1981 and 1998 to 13 Sv in 2004. A 4-5 Sv weaker overturning in 2004 is a reduction of approximately 25% relative that of the 1980's and 1990's, or a 35% reduction relative to 1957. We examine the water mass transport changes underlying this result in Section 3.3.2 and the effect on meridional heat transport (Section 3.3.3).

3.3.2 Water Mass Transports

Calculation of water mass transports in depth classes (Table 3.4) is open to criticism, since there is no requirement for these layer depths to be invariant over time, as illustrated by the shallower transition from southward LNADW transport to northward AABW flow in the later sections (Figure 3.11). We also therefore compute transports of the MOC's constituent water masses in the potential temperature classes of Table 3.5.

Layer name	Depth limits (m)	Components	Potential Temperature range (ºC)
		Surface	> 24.5
Upper	z ≤ 800	Thermocline	12.5 < θ ≤ 24.5
		Lower thermocline	9.5 < θ ≤ 12.5
Intermediate	800 < z ≤ 1100	AAIW and MW	5 < θ ≤ 9.5
		SLSW	4 < θ ≤ 5
UNADW	1100 < z ≤ 3000	LSW	3.2 < θ ≤ 4
		NAIW and ISOW	2.5 < θ ≤ 3.2
LNADW	3000 < z ≤ 5000	DSOW	1.8* < θ ≤ 2.5
AABW	z > 5000	AABW	θ ≤ 1.8*

Table 3.5 *Water mass definitions in depth or potential temperature layers. Apart from AABW and LNADW, layers are groups of water masses, which we identify in temperature classes but not depth. The lower potential temperature limit of LNADW (1.8*) corresponds to the zero crossing of the zonally integrated meridional temperature profile in 0.05 ºC intervals and is 1.85, 1.70, 1.80, 1.85 and 1.70ºC for the 1957, 1981, 1992, 1998 and 2004 sections respectively. Abbreviations are: AAIW – Antarctic Intermediate Water, MW – Mediterranean Water, (S)LSW – (Shallow) Labrador Sea Water, NAIW - North Atlantic Interior Water, ISOW – Iceland Scotland Ridge Overflow Water, DSOW- Denmark Straits Overflow Water and AABW -Antarctic Bottom Water.*

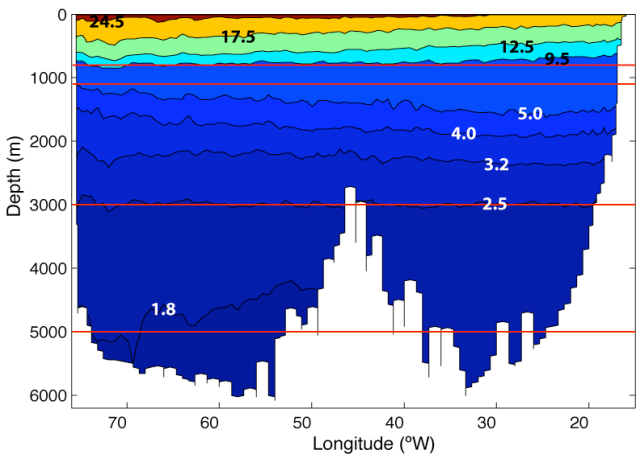

Figure 3.12 *25ºN 1992 mid ocean potential temperature section as a function of depth. Temperature contours are at 1.8, 2.5, 3.2, 4, 5, 9.5, 12.5, 17.5 and 24.5 ºC with depth levels of 800, 1100, 3000 and 5000m overlaid.*

800m corresponds closely to 9.5ºC across the mid-ocean section (Figure 3.12) and therefore this is taken as the upper/lower layer transition. The upper waters are subdivided into the lower and main thermocline (below and above 12.5ºC) with surface waters warmer than 24.5ºC, based on Schmitz and McCartney's (1993) study. In the MOC's lower limb, transport in temperature classes identifies northward flow between approximately 5 and 9.5ºC – thus defining the intermediate waters. Below this we follow Fine's (1995) definitions with UNADW divided into Shallow and Classical LSW (3.2 to 4 and 4 to 5ºC) as well as the mixture of ISOW and North Atlantic Interior

Water (NAIW) between 2.5 and 3.2ºC. The 2.5ºC isotherm lies close to 3000m (Figure 3.12), the upper limit of LNADW (DSOW) while the lower limit is section dependent to maximise transport of AABW (see Table 3.5).

The water mass transports of Table 3.6 including all components (Florida Straits, mid-ocean geostrophic and Ekman) in temperature classes are considered layer by layer through the following sections. Temperature class transports of the mid-ocean result from summation of geostrophic transports as a function of the mean temperature of the station pair at each 20 dbar depth level for which velocities are computed. The MOC computed in temperature classes as net northward transport above 9.5ºC is approximately 2 Sv weaker than that from depth classes due to 2 Sv of the Florida Straits transport being cooler than 9.5ºC (Table 3.6).

	1957	1981	1992	1998	2004
Surface					
MO	-4.0	-3.0	-2.0	3.4	1.2
FS	8.8	8.8	8.6	9.8	9.1
Ek	4.0	2.5	3.4	0.5	1.4
Total	8.8	8.4	10.0	13.7	11.7
Thermocline					
MO	-13.1	-15.4	-14.2	-25.3	-24.1
FS	17.5	17.5	17.1	18.9	17.9
Ek	0.5	1.2	1.2	4.7	3.1
Total	5.0	3.3	4.2	-1.7	-3.2
Lower Thermocline					
MO	0.0	-0.4	-1.3	-1.1	-1.0
FS	2.8	2.8	2.6	3.2	2.9
Total	2.8	2.4	1.3	2.1	1.9
Upper layer total	**16.6**	**14.1**	**15.5**	**14.1**	**10.4**

	1957	1981	1992	1998	2004
Intermediate					
MO	3.3	2.1	0.0	-0.7	1.9
FS	2.0	2.0	2.0	2.1	2.0
Total	5.3	4.1	2.0	1.4	3.9
UNADW					
SLSW	-1.9	-2.1	-1.3	-2.8	-2.1
LSW	-4.9	-3.3	-4.1	-5.0	-5.8
ISOW	-6.0	-3.5	-4.1	-3.8	-2.6
Total	-12.8	-8.9	-9.5	-11.6	-10.5
LNADW	-13.4	-13.6	-9.9	-6.7	-6.2
AABW	3.5	3.6	1.1	2.1	1.6
Lower layer total	**-17.4**	**-14.8**	**-16.3**	**-14.8**	**-11.2**

Table 3.6 *Water mass transports in the potential temperature classes defined in Table 3.6. Totals for layer groups are also given. Note that LNADW and DSOW are the same.*

3.3.2.1 The upper waters

The key observation to explain for this layer is the decreased net northward transport from 17-18 Sv (depth classes) or 14-15 Sv (temperature classes) in 1981-1998 to 13 or 10 Sv in 2004 (Table 3.6). This is identifiable in the drastically different profile of the upper layer MOC at 25ºN in 2004 particularly between 400 and 100m (Figure 3.11(ii)). Table 3.4 shows this to be due to a 5-6 Sv increase in the strength of the upper layer southward mid-ocean geostrophic transport, exceeding 23 Sv in 2004 compared to 16-18 Sv in the three early sections. It is similarly strong in 1998 (22 Sv) but transport of the Florida Straits and Ekman components are also strongly northward (contributing an extra 3 and 1 Sv respectively), and thus largely balance this. The MOC of 1998 therefore appears consistent in strength with the earlier sections.

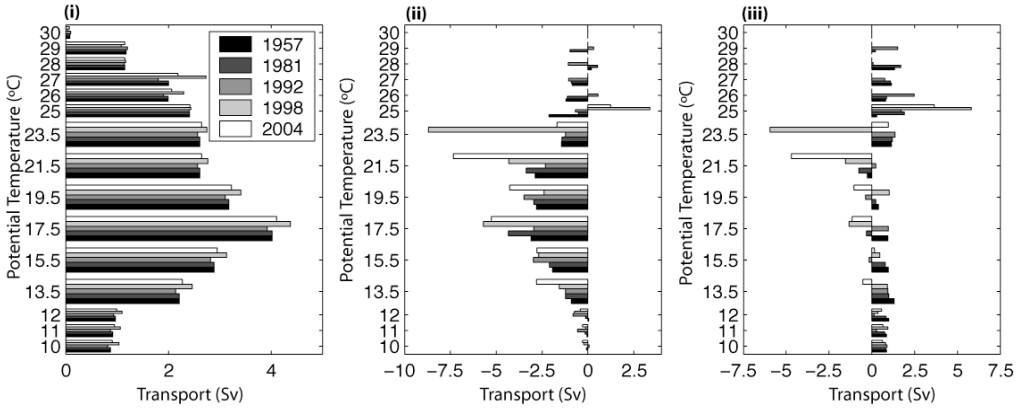

Figure 3.13 *Meridional transport of the upper waters (9.5 to 30.5°C) in the Florida Current (i), the mid-ocean geostrophic flow (ii) and their sum (iii). Layer transport widths are 1°C above 24.5°C and below 12.5°C and 2°C in between, all plotted at the layer mid-point. Legend of (i) applies to all.*

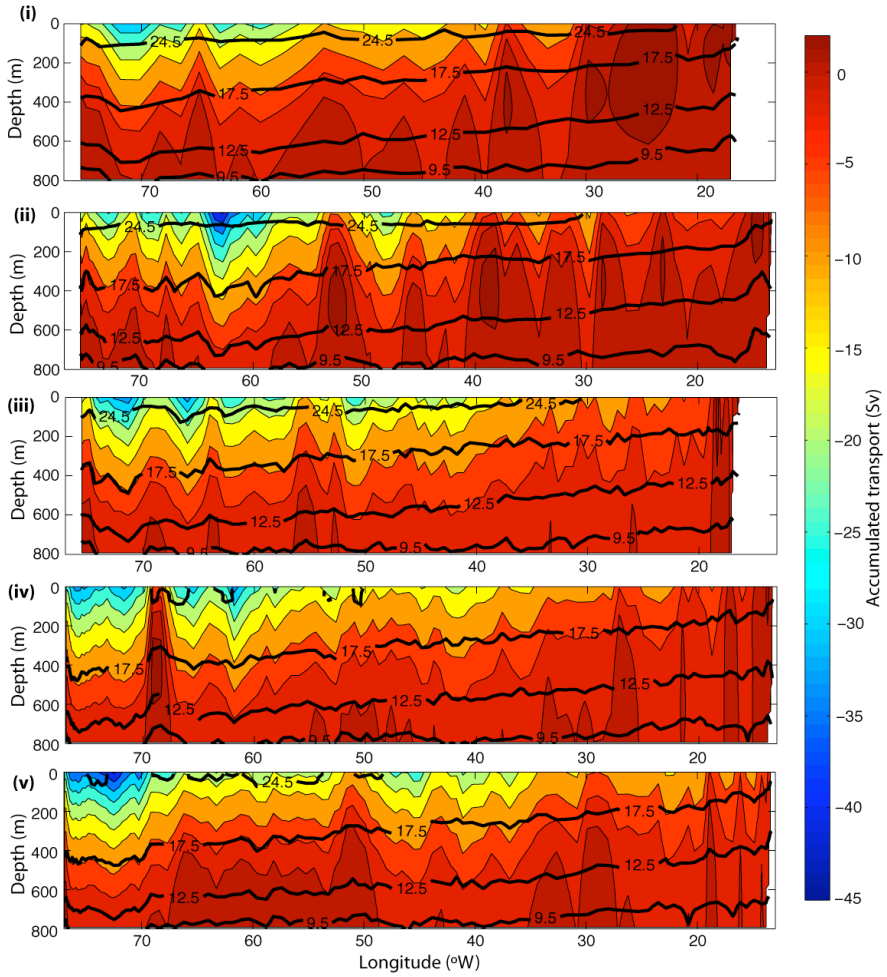

Figure 3.14 *Mid-ocean geostrophic transport accumulated both from east to west and upwards from zero at 800m in 20 dbar levels, such that the total 0-800m transport equals the value in the upper left hand corner of each plot for the 1957 (i), 1981 (ii), 1992 (iii), 1998 (iv) and 2004 (v) sections. Contours are at +2, 0, -2, -5, -10, -15 … -45 Sv intervals all with the same colour scale. Overlaid are the 9.5, 12.5, 17.5 and 24.5°C isotherm depths.*

Table 3.6 and Figure 3.13 show little change in the lower thermocline waters (9.5-12.5ºC) over the years and the surface water changes are due to seasonal variability (Figure 3.14). In the first three sections (summer and autumn months) waters warmer than 24.5ºC extend into the eastern basin as well as the west, the 1998 section has only small patches of water exceeding this temperature consistent with the observations being made in winter, and the spring section of 2004 shows little more (Figure 3.14). This explains why the Ekman transports in 1998 and 2004 are classed as predominantly occurring in the thermocline waters (Table 3.6).

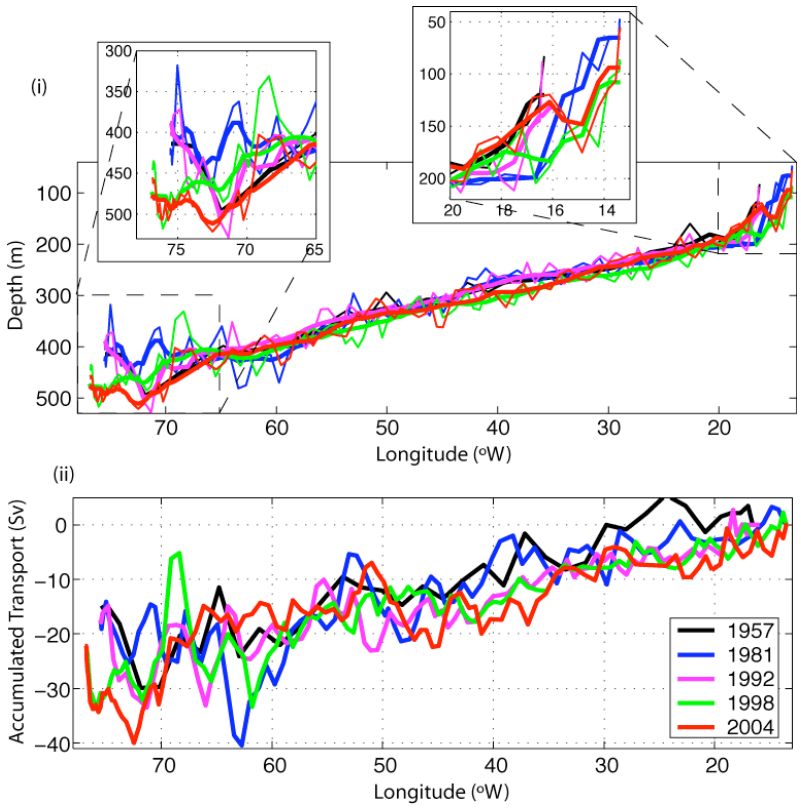

Figure 3.15 *(i) Depth of the 17ºC isotherm across the mid-ocean section (thin lines) and after smoothing with a ± 4º longitude running mean between 70 and 20ºW and a ± 1º window west and east of this (heavy lines). (ii) shows the upper layer (0-800m) transport accumulated from the east to west of each hydrographic section without smoothing. The legend of (ii) applies to all.*

The striking 10 Sv increase in mid-ocean southward transport in 1998 and 2004 occurs in the main thermocline waters (Table 3.6), especially those between 16.5 and 22.5ºC (Figure 3.13(ii)) resulting in net southward transport in certain layers across 25ºN when combined with the Florida Straits temperature transport (Figure 3.13(iii)). Accumulating upper layer transports across the mid-ocean section (Figures 3.14 and 3.15(ii)) identifies

stronger southward transport across much of the 2004 section but particularly in the upper 400m near the western boundary in 1998 and 2004. Notable in the later sections is the warming of mid-thermocline waters at the western boundary as shown by the depth of the 17ºC isotherm (Figure 3.15(i)). In 2004 and 1998 it is 40-60 dbar deeper at the western boundary than in the earlier three years, also expressed in a warming from 17.1 to 17.5ºC at 400 m in the early sections, to 17.8-17.9 in 1998 and 2004. Although there also appears to be warming at the eastern boundary in the later two sections, with deepening of the 17ºC isotherm relative to 1981 (Figure 3.15(i)), the different easternmost longitudes of sections makes direct comparison difficult.

To summarise, in 2004 and 1998 southward transport of waters above 800 m in the mid-ocean compensate more than 70% and 65% of the northward transport of Gulf Stream waters, compared to only 50, 58 and 57% in 1957, 1981 and 1992 respectively. A robust feature of the 1998 and 2004 sections is warming in the thermocline at the western boundary, the net effect of which is to increase the basinwide (Bahamas to Africa) thermocline slope. Details of how this affects the circulation are discussed further in Section 3.4.

3.3.2.2 The intermediate waters

Strictly the approximately 2 Sv of Florida Straits transport in the 5 to 9.5ºC temperature class (Table 3.6) should be included in the upper layer for definition of the MOC strength. Since it varies by less than 0.1 Sv between all sections, it does not contaminate intermediate layer transport variability presently discussed. The mid-ocean intermediate waters comprise AAIW and MW, although Figure 3.16(ii) shows no significant northward transport of MW (more than a Sverdrup) in the eastern basin. There is a general accumulation of transport between 45 and 55ºW where Bryden et al. (1996) found the dominant signal of AAIW properties but overall the signal appears eddy dominated (Figure 3.16(ii)). Total transport of this layer ranges from to –1 to 3 Sv in temperature classes (Table 3.6) or 0 to 2 Sv in depth classes (Table 3.4), with most in 1957 and least in 1998. In 1998 this is due to a reduced depth and temperature range of the northward transport as well as a reduction in strength (Figures 3.11 and 3.16(i)). This layer is not important for defining MOC strength however, and variability between the years is small.

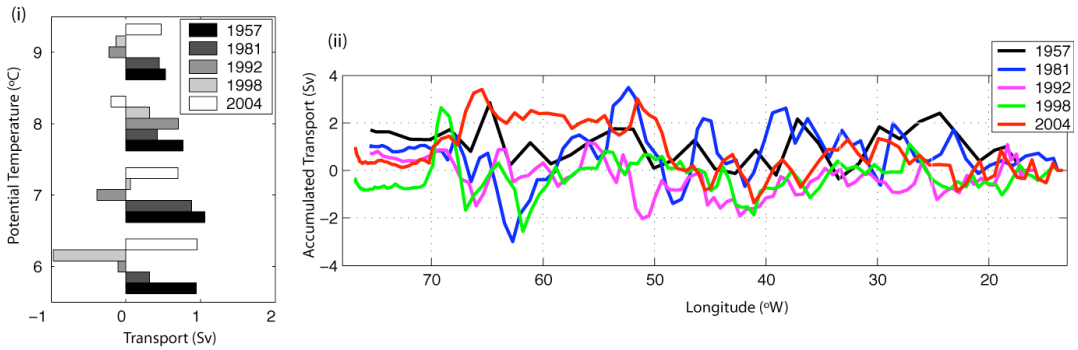

Figure 3.16 *(i) Zonally integrated meridional transport of mid-ocean geostrophic intermediate waters in potential temperature layers (all 1°C width apart from the lowest which is 5 to 6.5°C) and (ii) the accumulated transport of the 800-1100m layer from east to west.*

3.3.2.3 NADW

Southward transport of NADW in the DWBC is the dominant component of the deep limb of the MOC. To discuss the variability of this layer, we consider separately the waters originating from the Labrador Sea and the Nordic Seas. The former includes the Shallow and Classical LSW components, and the latter DSOW and ISOW. ISOW at 25°N, however, is mixed with NAIW and lies at depths of 2300 to 3000m (Vaughan and Molinari, 1997), thus above the traditional definition for LNADW at this latitude of 3000m (e.g. Lavin et al., 1998) and justifying its inclusion in the UNADW layer of Table 3.6. For the purposes of the following discussion (and Figure 3.17) however, we include it as a LNADW component due to its source region. As discussed in Section 3.2.4.3 individual layer transports of the 1957 section are not reliable to within a couple of Sv and are therefore omitted from the following discussion.

Consider first the upper NADW (SLSW and LSW). Southward transport increases from 5 Sv in both 1981 and 1992 to almost 8 Sv in 1998 and 2004 (with approximately 7 Sv in 1957) (Table 3.6). During this time the classical LSW component increases steadily from 3.3 Sv in 1981 to 5.8 Sv in 2004 (Table 3.6) and is particularly notable over temperature ranges of 3.4 to 3.8°C (Figure 3.17(iii)). The contribution of SLSW is smaller, but reaches almost 3 Sv in 1998 as seen clearly by stronger southward flow between 1200 and 1600m (Figure 3.11(i)) - its depth range at 25°N (Vaughan and Molinari, 1997). The deeper core of UNADW transport in 1992 (Figure 3.11(i)) can now be explained by the small SLSW transport (1.3 Sv, Table 3.6) during that year.

Transport of UNADW is concentrated in the DWBC (Figures 3.17(i) and 3.18), which appears narrower in the 1998 and 2004 sections.

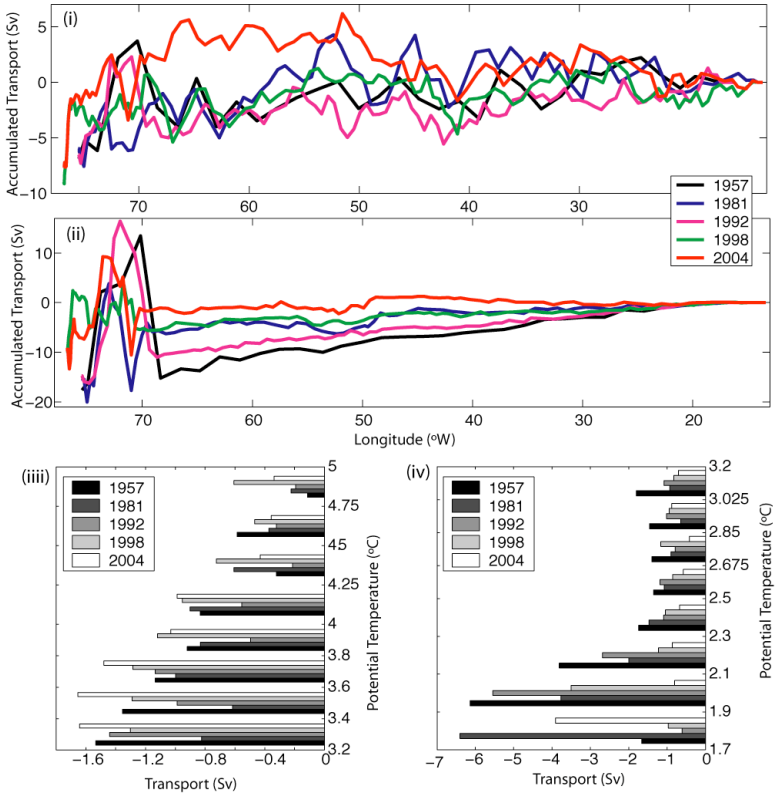

Figure 3.17 *Accumulated meridional geostrophic transport of classical and shallow LSW in depth range 1100 to 2300m (i), and of 2300 to 5000m in (ii) including ISOW, DSOW and NAIW. (iii) and (iv) show the temperature transports for waters of (i) and (ii) with layer intervals denoted by y-axis tick marks. Layer thicknesses are 0.2°C in DSOW (except the coldest which is from 1.85, 1.70, 1.80, 1.85 or 1.70 to 1.9°C - therefore fluctuations in this layer likely reflect the layer width), 0.175°C in ISOW (2.5 to 3.2°C), 0.2°C in LSW (3.2 to 4°C) and 0.25°C in SLSW (4 to 5°C). Using 2300 m to define the base of LSW is applicable to the western boundary region (Vaughan and Molinari, 1997).*

While southward transport of UNADW (LSW and SLSW) shows a trend towards strengthening transport over time, the opposite is true of the lower deep water component with combined transport of the DSOW and ISOW/NAIW layers totalling approximately 17, 14, 11 and 9 Sv in 1981, 1992, 1998 and 2004 respectively. This is primarily due to a striking decrease in the DSOW component from almost 14 Sv in 1981 to just over 6 Sv in 2004, a reduction of more than half its former strength (Table 3.6). This reduction has occurred roughly equally over the temperature range of this layer in the 2004 section, and although transport is similarly weak in 1998 the change is less uniformly distributed (Figure 3.17(iv)). Almost all transport of LNADW is found in the western boundary region (Figure 3.17(ii)) and its weak LNADW component is

particularly apparent in Figure 3.17(iv). The upper LANDW component (2300-3000m) containing the ISOW/NAIW mixture is approximately constant at 4 Sv over these years, but in 2004 it had reduced to 2.6 Sv (Table 3.6). While this is a small change, it is a clear signal in the colder waters of this layer between 2.5 and 2.85ºC (Figure 3.17(iv)). Attributing this change to ISOW or NAIW is not possible but given the striking decrease in DSOW over this period, with both originating from the Nordic seas, ISOW is the logical choice. Of course varying amounts of its NAIW component may have obscured any decrease in ISOW transport in the 1998 section.

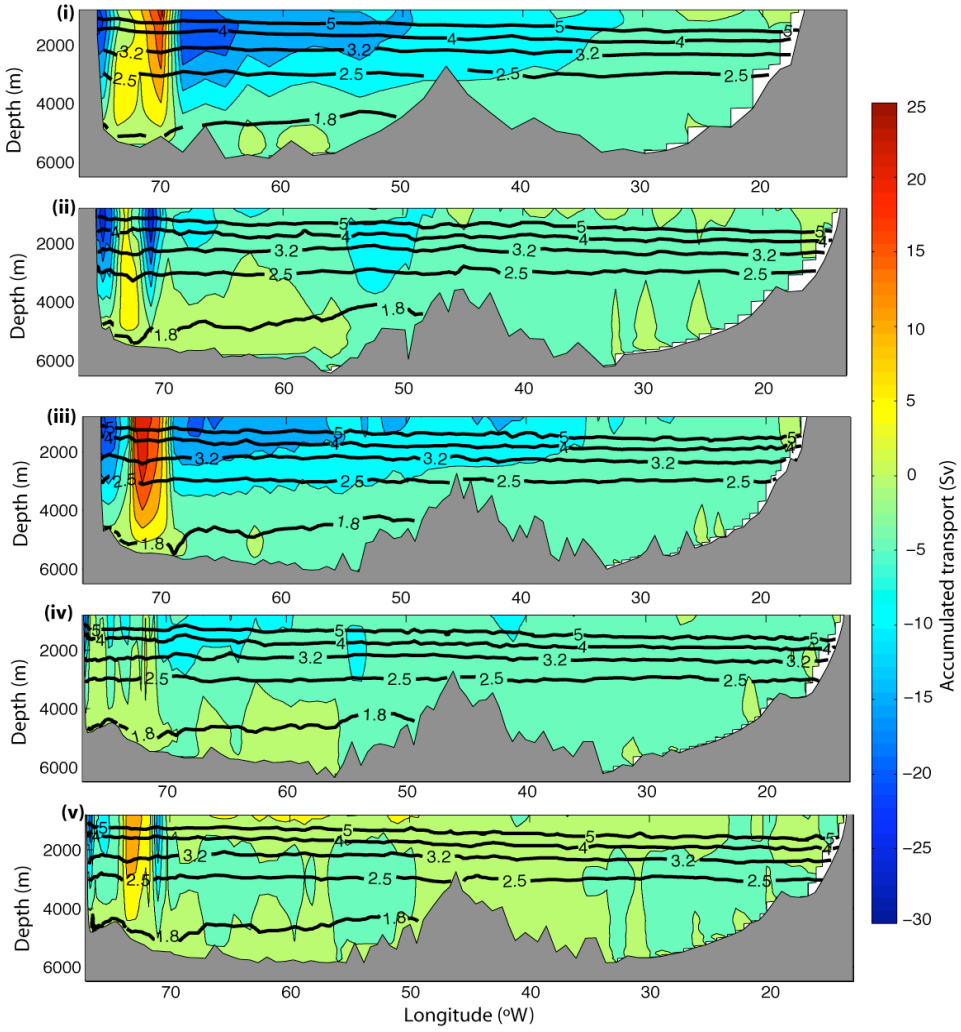

Figure 3.18 *Mid-ocean geostrophic transport accumulated from the eastern boundary and sea floor upwards to 800m (as Figure 3.14) such that the total transport below 800m for each section equals that at the upper left hand corner. Transport contours are at 5 Sv intervals of –30, -25 … 20, 25, all with the same colour scale. Subplots (i) to (v) are years 1957, 1981, 1992, 1998 and 2004 respectively. The 1.8, 2.5, 3.2, 4.0 and 5.0ºC potential temperature isotherms are also plotted and the land mask is overlaid in grey. Gaps at the eastern boundary are because the accumulated transport is plotted at the westernmost longitude of each station pair.*

Transport changes of NADW are dominated by the reduction of southward transport of DSOW, halving between 1981 and 2004, and although there is a slight strengthening of LSW flow in the DWBC this is not enough to compensate. The changes between sections are all concentrated in the DWBC region which is seen to be notably weaker and narrower in 1998 and 2004 than in the earlier sections, with comparably weak offshore recirculation gyres (Figure 3.18).

3.3.2.4 AABW

Like the intermediate waters, total transport of the AABW layer is small and does not form an important component of the MOC at 25ºN, hence we do not pursue the observed variability. AABW is found banked up against the western flank of the Mid-Atlantic Ridge (Figure 3.18), and its transport ranges from 3-4 Sv in 1957 and 1981, to 1-2 Sv in 1992, 1998 and 2004 (Table 3.6). No significance is attributed to the lower transport in the later sections since transport of this layer is strongly dependent on that in bottom triangles, the treatment of which is subjective (Fomin, 1964). The variability of transport with temperature is notable between the sections, although we, like Bryden et al. (1996), find no relation between warmer or colder temperatures and the total volume transport.

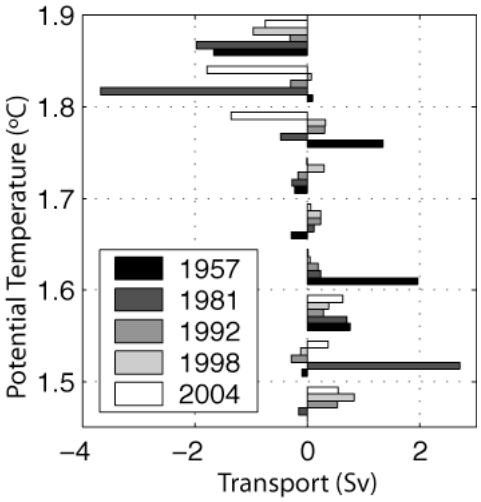

Figure 3.19 *Meridional mid-ocean geostrophic transport of AABW in 0.05ºC potential temperature layers. It is from this figure that the upper limits of AABW transport of 1.8, 1.7, 1.8, 1.85 and 1.7ºC (see Table 3.5) are set, corresponding to the temperature up to which transport in 0.05ºC layers is northward.*

3.3.3 Meridional Heat Transport

Firstly we note that the heat flux divergence across the 25ºN section due to the net -0.8 Sv Bering Straits transport is negligible at 0.02 PW as estimated by multiplication of transport with the difference between the Bering Strait temperature of 0ºC (Coachman and Aagaard, 1988) and the section averaged barotropic temperature at 25ºN of 5.2ºC. The contribution is therefore neglected in the following calculation since the meridional heat transport across this section is of the order 1.5 PW (Lavín et al., 2003).

Meridional heat transports of Table 3.7a are computed following equation (3.3)

$$Heat = \rho C_p \theta_{FS} V_{FS} + \rho C_p \theta_{Ekman} V_{Ekman} + \rho C_p \theta_{mid-ocean} V_{mid-ocean} \quad (3.3)$$

where ρ is density, C_p specific heat capacity, FS denotes the Florida Straits, mid-ocean the geostrophic component of the mid-ocean flow, and V is volume transport of each component with θ its transport weighted temperature (Table 3.7b) following Lavín et al. (1998).

	1957	1981	1992	1998	2004
Florida Straits	2.47	2.47	2.41	2.70	2.53
Ekman	0.48	0.40	0.51	0.50	0.43
Mid-Ocean geostrophic	-1.59	-1.67	-1.54	-2.00	-1.90
Total	1.37	1.20	1.38	1.20	1.06

Table 3.7a *Meridional heat flux components across 25ºN according to equation (3.3), all in PW (1 PW = 1x10^{15} W). Northward fluxes are positive, negative southward.*

	1957	1981	1992	1998	2004
θ_{FS}	19.50	19.50	19.51	19.47	19.47
θ_{Ek}	26.09	26.19	26.47	23.24	23.20
θ_{Mo}	10.72	11.52	10.61	12.27	12.55
Tr_{FS}	31.1	31.1	30.3	34.0	31.8
Tr_{Ek}	4.5	3.7	4.6	5.2	4.5
Tr_{Mo}	-36.4	-35.6	-35.7	-40.0	-37.1

Table 3.7b *Volume transports and transport weighted temperature of 25ºN meridional heat flux components, following definitions of equation (3.3).*

Northward heat transport at 25ºN computed from the 1957, 1981, 1992 and 1998 sections all lie between 1.2 and 1.4 PW, consistent with Lavín et al. (1998)'s calculations, while that of 2004 is notably weaker and only just exceeds 1 PW (Table 3.7a). It should be noted however that the meridional heat transport range of 0.32 PW lies at the detection limits of the method (Lavín et al., 1998). The weak northward heat

transport in 2004 is due to the weak overturning circulation that year. Strong southward mid-ocean geostrophic heat transport (almost 0.4 PW more than in 1992, Table 3.7a) results since more of the section's southward flow occurs in the warm upper waters rather than the cold DWBC, accompanying the weak overturning. This is seen in the 1.9ºC higher transport weighted temperature of this component in 2004 than 1992 (Table 3.7b). With little change in the Ekman or Florida Straits heat fluxes relative to the earlier sections, this results in the relatively small net northward heat transport of 2004. Although 1998 has a mid-ocean geostrophic southward heat transport stronger than 2004 (Table 3.7a), a corresponding increase in the northward Florida Straits heat flux compensates this and the total meridional heat transport that year is consistent with earlier years (Table 3.7a). The high Florida Straits heat flux is due to the increased annual mean volume transport of 1998, rather than a change to its transport weighted temperature (Table 3.7b). This is consistent with Shoosmith et al. (2005)'s findings that the Florida Current's transport weighted temperature does not have a dependence on volume transport.

There is little change in the Ekman heat flux from year to year, with a range of only 0.1 PW. The expected seasonal dependence, due to transport weighted temperature changes (Table 3.7b), is evident in the 0.05 PW smaller northward Ekman heat transport of 2004 than 1957 (Table 3.7a). Transport fluctuations are however equally important, resulting in the second strongest Ekman heat transport occurring in the winter section of 1998.

In summary, annual averaged meridional heat transport by the Ekman, Florida Straits and mid-ocean geostrophic flows have shown variability of 0.1, 0.3 and almost 0.5 PW respectively between the 1957, 1981, 1992, 1998 and 2004 25ºN sections, although the net meridional heat flux variability is smaller at 0.3 PW and is dominated by the latter two components.

3.4 DISCUSSION

Each of the 1981, 1992 and 1998 transport calculations show 17-18 Sv of net northward transport above 800 m across 25ºN, providing a robust baseline estimate of the MOC strength at this latitude. The 1957 20 Sv overturning strength is not inconsistent with this, given the larger errors associated with the early hydrographic section's non-eddy

resolving station spacing, discrete vertical sampling and the long term mean Ekman and Florida Straits transports employed in mass balance. Direct comparison of our results with previous analysis of the 1957, 1981 and 1992 hydrographic sections by Lavín et al. (1998) is complicated by their layer definitions, but we do note that their 1981 and 1992 net mid-ocean southward transports below 600 m of 16 and 17 Sv are consistent with our estimated 17-18 Sv MOC. This is expected since our methods are based on those of Lavín et al. (1998), although as in Bryden et al. (2005b) constant Ekman and Florida Straits transports were used. Confidence in our results is increased by Lavín et al. (2003)'s finding that re-analysis of the 1992 section through an inversion with silica transport constraints changed the MOC strength by less than 1 Sv. We therefore conclude that the Atlantic MOC at 25ºN of 1957, 1981, 1992 and 1998 was 17 to 18 Sv in strength. The weaker 2004 overturn is discussed presently.

The 2004 overturning strength of 13 Sv is approximately 25% weaker than the baseline state, with little change in the Ekman or Florida Straits transports but a 5-6 Sv increase in southward flow of mid-ocean thermocline waters relative to the 1981 and 1992 sections. A change of this magnitude is within the error estimates for hydrographic section transports of ± 6 Sv (Ganachaud, 2003) but close to the detection limit suggested by recent analysis of intra-annual variability of mid-ocean thermocline transport at this latitude with standard deviation 2.7 Sv (Cunningham et al., 2007, submitted manuscript). Similarly strong southward mid-ocean upper layer transport is seen in 1998, but is compensated by unusually strong annual mean Florida Straits and Ekman transports that year resulting in a MOC strength in line with earlier observations. This emphasises the importance of accounting for interannual variability in all components of the MOC at 25ºN and suggests that Bryden et al. (2005b)'s weak 1998 MOC was due to their assumption of constant Ekman and Florida Straits transports, though their changes in the mid-ocean circulation appear robust. The 1998 strengthened upper layer southward flow in the mid-ocean is also consistent with Macdonald et al. (2003)'s analysis of the section that found southward transport of surface waters (above 432 dbar) to be 5.4 Sv stronger in 1998 than 1992 (their Table 3). That was larger than the uncertainty of their layer transport calculations (± 1.7 Sv), and in good agreement with our findings of 5 Sv more southward thermocline transport than in 1992 above 800 m.

The mechanisms underlying the thermocline circulation changes are dependent on changes in wind stress curl (de Boer and Johnson, 2007) since our methods to compute the mid-ocean transports (Ekman dynamics and geostrophic balance with a fixed depth, small, uniform reference level velocity) lead to Sverdrup balance in the linear region of the mid-ocean (de Boer and Johnson, 2007). Whether or not Sverdrup transport across the 25ºN section has been constant since 1980 is dependent on the wind stress climatology employed to compute it (Figure 3.20). Linear regression of Sverdrup transport from the NOC climatology to time shows a 5 Sv increase in southward transport between 1980 and 2004 (Figure 3.20). This increase is in remarkably good agreement with our computed upper layer mid-ocean transport change from 18 Sv in 1981 to 23 Sv in 2004 (Table 3.4). In this case the observed western boundary warming in the later hydrographic sections is interpreted as representative of an increase in the basinwide thermocline slope and thus mid-ocean southward recirculation of the Gulf Stream waters.

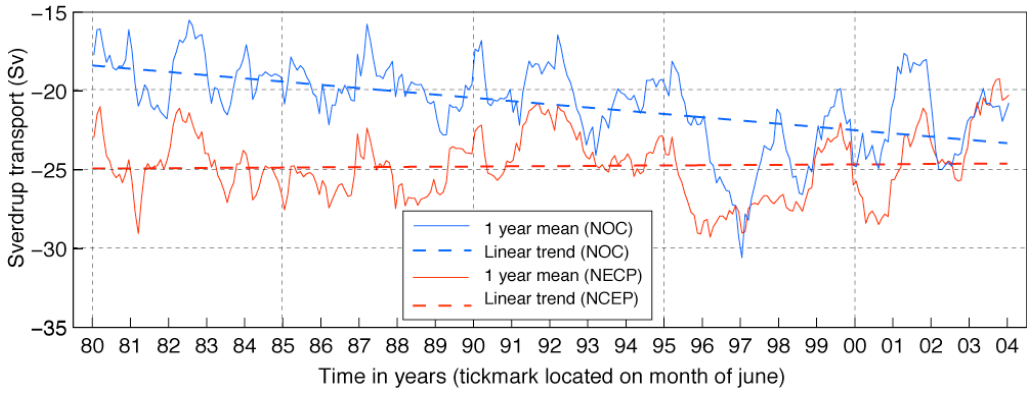

Figure 3.20 *Sverdrup transport across 25.5ºN from the NOC and NCEP monthly wind stress climatologies. Both the one year running mean and a linear trend of this to time are plotted (from Louise Duncan, 2005, personal communication).*

Clearly the NCEP wind stress climatology does not support the above explanation since the trend in Sverdrup transport amounts to less than 0.5 Sv between 1980 and 2004, with weaker southward flow in 2004 than 1981 (Figure 3.20). Following de Boer and Johnson's (2007) argument this requires any change in the mid-ocean transports above the reference level to occur in the non-linear western boundary regime where mesoscale eddy activity is important. Under this scenario the western boundary warming is interpreted as decreasing the slope of the thermocline adjacent to the western boundary (where it descends offshore, Figure 3.15), with a weaker northwards flowing Antilles Current. The net effect of this, with no change in the rest of the mid-ocean upper layer

southward flow, is a stronger southward transport across the whole section as observed in 1998 and 2004. This interpretation is consistent with Fraile-Nuez and Hernández-Guerra (2006)'s Argo float study of eastern basin subtropical recirculation that reported no difference between the April 2002 to March 2003 mean thermocline circulation compared to transports of the 1957, 1981 and 1992 hydrographic sections. We do however point out the absence of boundary observations in their study, essential in setting the section wide mass balance (their dataset contains no observations within 300km of the eastern boundary, east of approximately 18ºW at 24.5ºN, their Figure 1). In summary, we consider our computed strengthened mid-ocean transport of thermocline waters to be a robust feature of the 1998 and 2004 sections, although a weaker MOC results only in the latter. The western boundary warming is a key feature of these changes, regardless of whether or not a long term change in wind stress curl has occurred.

With more of the northward flow (Ekman and Florida Straits transports) returning south across the mid-ocean section in the thermocline waters of the 1998 and 2004 sections than previously, a decrease in strength of the DWBC's southward transport is correspondingly observed. We suggest that ISOW transport in 2004 was less than in previous sections (Table 3.6), which, although uncertain due to the contamination of NAIW in this layer (Fine, 1995), is consistent with Hansen et al. (2001)'s reported 20% reduction in the strength of the Faroe Bank Channel overflow since 1950. The observed decreased DWBC transport at 25ºN is dominated by the 50% reduction of DSOW flow since 1981. Resolution of this with high latitude changes is not straightforward, indeed there is a suggestion that the overflow was 30% stronger in 1999-2003 than previously (Macrander et al., 2005). There is also no evidence for weakening of the Denmark Straits overflow since the 1970's (Girton et al., 2001), although Macrander et al. (2005) pointed out the dataset limitationsfor this. Longer timescale data sets were analysed by Bacon (1998) and Kieke and Rhein (2001) to compute combined baroclinic transport of LNADW (Gibbs Fracture Zone Water or ISOW, and DSOW) around Cape Farewell and in the Irminger Sea. They concurred that flows were weak in the 1950/1960's and the 1990's but high through the 1980's. Stramma et al. (2004) suggest a spreading time for DSOW of 4 years from the Denmark Straits to the Grand Banks which would suggest a travel time of approximately 6-7 years from Cape Farewell to 25ºN. Perhaps the weak LNADW transport at 25ºN in 1998 and 2004 is a signal of the weakened 1990's

transport around Cape Farewell. This explanation would however suggest similarly weak DSOW transport in 1981 following the 1960's/1970's Cape Farewell weak transport, although we note the absence of high latitude observations between 1970 and 1975 (Bacon, 1998; Kieke and Rhein, 2006). In summary, there are unexplained differences between our subtropical observations of reduced LNADW transport in 1998 and 2004 and the transports of this water mass computed either at the overflows or around Cape Farewell. Interpretation of such transport changes is admittedly speculative due to the uncertainties in computed layer transports with intra-annual variability of LNADW flow at this latitude of 3.5 Sv (Cunningham et al., 2007, submitted manuscript). Such observations cannot be resolved with the five hydrographic sections and illustrate their key limitation: a lack of temporal resolution that will be addressed in subsequent chapters of this thesis.

The fluctuating UNADW transports of Table 3.4 belie the steady increase in LSW transport through the latter four sections. Although smaller than the intra-annual variability of 3.1 Sv (Cunningham et al., 2007, submitted manuscript), this amounts to a 44% strengthening of this DWBC component between 1981 and 2004 (Table 3.6). A new colder, fresher version of LSW has been observed in the DWBC at 26.5ºN since 1994 (Molinari et al., 1998) resulting from deepening of convection in the Labrador Sea since the 1970's (Dickson et al., 1996). Even though deducing MOC strength changes from convection changes is complicated (e.g. Marotzke and Scott, 1999) and is likely influenced by the location of convection (Spall and Pickart, 2001), our observed strengthening LSW transport in the subtropics over time seems consistent with the LSW formation changes inferred by Dickson et al. (1996) from the increased convective activity. The trend towards strengthened classical LSW transport in the DWBC over time amounts to less than 3 Sv between 1981 and 2004 and is therefore not sufficient to compensate the concurrent weakening of LNADW transport at 25ºN.

Although the later sections (1998 and 2004) joined the western boundary 2 degrees further north than those made in previous years, we do not believe this to be an important factor in the changes in transport observed. We acknowledge that the DWBC appears narrower in the 1998 and 2004 sections, with weaker recirculation gyres (Figures 3.17(i) and 3.18). This is likely to be an anomaly in time rather than in space, given that a strong DWBC recirculation regime has also been seen at 26.5ºN in moored

current meter observations (e.g. Lee et al., 1996; Bryden et al., 2005a). We have also accounted for changes in the Florida Straits transport with latitude and know of no other factor that should bias the 26.5ºN DWBC transports low relative to those of 24.5ºN.

Lastly we justify our interpretation of transports as annual averages even though mid-ocean hydrographic sections were made in different months of the year. The mid-latitude first mode baroclinic adjustment timescale is on the order of a decade (Gill, 1982), and theoretical arguments have shown the deep ocean's response to seasonally varying winds to be primarily barotropic north of 15ºN (Gill and Niiler, 1973). Therefore providing that the annual mean Ekman and Florida Straits transports are employed for mass balance (as done here), the overturning computed is that of the annual average also. Accordingly even though the mid-ocean meridional geostrophic heat transports have equal range with, and follow the phase of, the baroclinic heat flux seasonal cycle at 26ºN proposed by Molinari et al. (1990) and reiterated by Baringer and Molinari (1999), we do not believe that the variability is due to a seasonal cycle. Indeed Wacongne and Crosnier (2002) have found the baroclinic heat flux annual cycle's phase and amplitude in the Levitus 1982 climatology (Baringer and Molinari, 1999), not to be robust compared with other climatologies. Instead they argued that it most likely results from non-synoptic sampling of the western boundary regions as these have significant sub-basin scale variability in space and time (Wacongne and Crosnier, 2002). It follows that our heat and water mass transports are best interpreted as representative of the annual average conditions, with meridional heat transport at 25ºN 0.3 PW weaker in 2004 than 1992, accompanying the reduced overturning strength.

3.5 SUMMARY

Analysis of five repeats of the 25ºN transatlantic hydrographic section with mass balance constraints have shown an MOC of 17-18 Sv to be stable from the 1950's to 1990's but with a weaker 13 Sv overturn in 2004, accompanied by a reduction in northward meridional heat transport of 0.3 PW from 1992 to 2004. Although the net reduction in upper layer transport of 5-6 Sv is at the detection limits of one-time hydrographic sections analysed with mass balance constraints (Ganachaud, 2003), mid-ocean thermocline transport is up to 10 Sv stronger in 1998 and 2004 than in 1957, 1981

and 1992 consistent with observed warming in the thermocline warming at the western boundary. Lower layer changes that compensate are concentrated in DWBC transports of DSOW, with a 50% reduction in southward transport between 1981 and 2004. Reconciling the deep water transport changes with high latitude processes remains unresolved and requires longer time series of deep water transports.

That such variability in the Atlantic MOC exists in 5 high quality transatlantic hydrographic sections provides strong motivation for further study of the problem. Clearly we wish to know whether the 2004 section is representative of a new state towards which the MOC is evolving or whether such weak overturning states have occurred frequently over the last 25 years but our hydrographic sections have been during periods that miss them. The data available to assess this question and its interpretation constitute the remainder of this thesis.

CHAPTER 4: **Method Overview**

4.1 MOC COMPONENTS AT 26.5ºN

We showed in Chapter 3 that the Atlantic MOC can undergo fluctuations of order 25% in strength on interannual timescales, but in doing so exhausted the traditional data set of transatlantic hydrographic sections with which to further constrain the nature of the observed variability. In this chapter, we outline methods to increase the temporal resolution of the Atlantic MOC time series between 1980 and 2005 through its decomposition into the three components of Figure 4.1. Time series of each component may then be determined separately as outlined below for the wind driven Ekman transport (Section 4.2), Gulf Stream flow through the Florida Straits (Section 4.3), and the mid-ocean geostrophic transport (Section 4.4). We work at the latitude of 26.5ºN since this corresponds to the position of the Florida Straits cable, and as will be shown (Chapters 5 and 6) historical data at the western boundary is concentrated at this latitude.

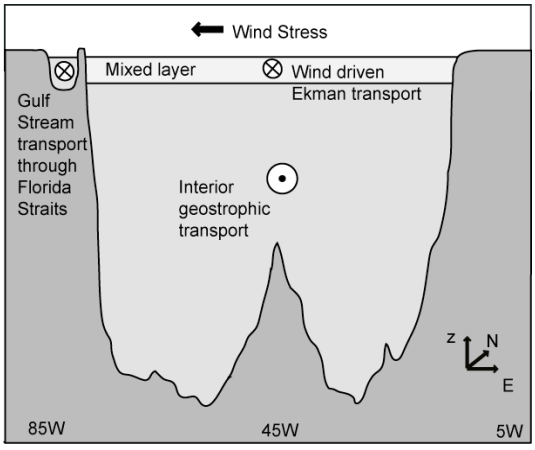

Figure 4.1 *Schematic of decomposition of the Atlantic MOC at 26.5ºN into the three components of Gulf Stream flow through the Florida Straits, Ekman flow and mid-ocean (interior) geostrophic transport.*

There are two complementary aims to this analysis. One is to determine the interannual variability of the Atlantic MOC between 1980 and 2005, for which we require annual

averages of the Florida Straits and Ekman components and assume that the interior geostrophic transport does not vary on sub-annual timescales. The other is to estimate the error associated with using a single observation of the mid-ocean geostrophic transport to represent annual average conditions. For this component of the MOC we therefore must compute its variability both at high frequencies and on interannual timescales. The decomposition of the MOC into the three components at 26.5ºN is an approach analogous to that employed in analysis of the transatlantic hydrographic sections, and in modelling studies of Atlantic MOC variability at this latitude (Hirschi et al., 2003). The difference is that we can compute only the baroclinic component of the interior geostrophic flow. If interannual time series of each component can be obtained then the barotropic component of the mid-ocean transport could be found by application of a mass balance constraint (as in Chapter 3), but data limitations will suggest that this is not possible (Chapter 8).

4.2 EKMAN TRANSPORT

Ekman transport across the mid-ocean section is computed from the NOC climatology monthly mean wind stresses (Josey et al., 1998; 2002) as in Section 3.2.2 but at the constant latitude of at 26.5ºN. Figure 3.5 showed this component to benefit from a complete record of annual mean transports between 1980 and 2005. These are presented, with examination of variability in Section 7.2.

4.3 FLORIDA STRAITS TRANSPORT

As in Section 3.2.3 variability in Florida Straits transport from 1982 to 2005 is assessed from cable derived transports at 26.5ºN. These are free to download (http://www.aoml.noaa.gov/phod/floridacurrent), and all except the last 6 years have already been analysed in Baringer and Larsen (2001). The required annual mean transport time series from 1980 to 2005, presented in Section 7.3 is, with the exceptions of 1980-1981 and 1998 to 2000, complete.

4.4 MID-OCEAN GEOSTROPHIC TRANSPORTS

4.4.1 Method Overview

As previously discussed (Chapter 3) this component is traditionally estimated from transatlantic hydrographic sections. In order to obtain flow estimates with increased temporal resolution, some simplifications are required. In the absence of intervening topography and wind forcing, the zonal average of the mid-ocean meridional baroclinic geostrophic velocity profile may be estimated from a pair of deep hydrographic stations selected from either end of the mid-ocean section (Hall and Bryden, 1982; Marotzke et al., 1999; Lynch-Stieglitz, 2001). Consider two hydrographic stations, W and E at the western and eastern boundaries respectively of the 26.5ºN section (referred to subsequently as end stations) separated by distance Δx. At a given pressure (p) the average geostrophic velocity (v) between W and E relative to a reference pressure (p = p_R) with reference velocity (v = v_R), is computed from

$$(v - v_R) = \frac{1}{f\Delta x}\left(\int_{p_R}^{p} \delta_E dp - \int_{p_R}^{p} \delta_W dp \right) \tag{4.1a}$$

where f is the Coriolis parameter, δ is the specific volume anomaly (in $m^3\ kg^{-1}$) and pressure is in Pascals (Pond and Pickard, 1983). Or in mixed units as a function of dynamic height (ΔD) relative to pressure p_R (in dbar), with δ in $cm^3\ g^{-1}$

$$(v - v_R) = \frac{10}{f\Delta x}(\Delta D_E - \Delta D_W) \quad \text{where} \quad \Delta D = \int_{p_R}^{p} \delta dp \tag{4.1b}$$

(Pond and Pickard, 1983). Application of (4.1b) over full depth can therefore be used to estimate the zonally integrated MOC at 26.5ºN under the assumption that a uniform reference level across the section is a workable simplification though it is formally only valid above the depth of the Mid-Atlantic Ridge.

The method of (4.1) also permits consideration of the contribution to MOC variability made independently by changes at each boundary. This is done by assuming the density structure of one boundary to be constant and computing changes in transport relative to a pre-determined reference profile at the other boundary. Formally, suppose we have two end station pairs at different times such that W_r and E_r provide an estimate of the MOC at an arbitrary reference time t_r and W_1 and E_1 that at time t_1. We would like to know the change in the mean velocity profile between the end stations at the different

times, to compute the change in flow strength at time t_1 relative to time t_r. First we note that the transport per unit depth across the section relative to pressure p_R between the end stations is given from (4.1b) by

$$\Delta x(v - v_R) = 10(\Delta D_E - \Delta D_W) / f \tag{4.2}$$

If the velocity at time t_r is v_r and that at time t_1 is v_1 the transport anomaly per unit depth at t_1 relative to t_r is given by

$$\Delta x(v_1 - v_R) - \Delta x(v_r - v_R) = 10(\Delta D_{E_1} - \Delta D_{W_1}) / f - 10(\Delta D_{E_r} - \Delta D_{W_r}) / f \tag{4.3}$$

Assuming that the dynamic height structure at the east is constant then the transport anomaly (change in zonally integrated meridional transport) per unit depth referenced to time t_r, relative to pressure p_R resulting from changes at the western boundary is proportional to the dynamic height change at this boundary

$$\Delta x(v_1 - v_R) - \Delta x(v_r - v_R) = 10(\Delta D_{W_r} - \Delta D_{W_1}) / f \tag{4.4}$$

and the equivalent transport anomaly assuming no change at the western boundary is obtained from

$$\Delta x(v_1 - v_R) - \Delta x(v_r - v_R) = 10(\Delta D_{E_1} - \Delta D_{E_r}) / f \tag{4.5}$$

The sign reversal between (4.4) and (4.5) is intuitive. Consider the upper layer mid-ocean southward transport referenced to 800 dbar. Increased southward flow results from an increase in the dynamic height (relative to 800 dbar) at the western boundary but a decrease at the eastern boundary. Given dynamic height profiles at either boundary, baroclinic transport anomalies in depth layers (representative of specified water masses) may then be computed relative to some reference state using (4.4) and (4.5).

There are two possible sources of data for use with equations (4.4) and (4.5). The conventional approach is to use hydrographic stations taken from either boundary at 26.5ºN (e.g. Hall and Bryden, 1982). The number of stations for this purpose is however limited, particularly at the eastern boundary where there are only between 7 and 11 suitable stations for all water mass layers considered. Data is more abundant at the west with 39 stations for all layers except that of LNADW for which there are 29. Chapter 5 details methods of end station selection and processing.

We also consider derivation of dynamic height from moored temperature and pressure records in the boundary regions (Chapter 6). While this data source improves temporal resolution compared to the end stations since moorings are often deployed for periods exceeding a year with sampling intervals of a day or less, the vertical resolution is significantly less than the 2 dbar of CTD casts. Use of mooring time series therefore presents us with the challenges of vertical interpolation as well as salinity estimation for construction of dynamic height profiles and temperature anomalies.

The use of temperature and pressure observations to compute dynamic height was originally motivated by Stommel's (1947) recognition that the increasingly popular use of the (expendable) bathythermogram, (X)BT, provided a potentially valuable resource for geostrophic velocity computations if density could be derived from the directly measured temperature and pressure. He showed that if a water mass's known T-S correlation were employed, then the errors in dynamic height were small enough to permit meaningful current computations in certain cases. Emery (1975) along with Emery and Wert (1976) developed Stommel's (1947) idea systematically, culminating in reference T-S curves for 10º by 10º boxes in the Pacific from 20ºS to 40ºN for computation of dynamic height from XBT temperature and pressure records. Siedler and Stramma's (1983) study extended the method to the Northeast Atlantic, giving consideration to the relative merits of alternative estimators of density from temperature and pressure with final errors in geostrophic velocities as low as 5%. Concurrently, an equivalent study was under way in the western Atlantic at 26.5ºN but using moored temperature sensors rather than XBT casts for the estimation of dynamic height. Again the error arising from the approximation in salinity was smaller than the natural variability of the mesoscale field (Zantopp and Leaman, 1984).

The use of moored temperature and pressure time series in particular for dynamic height derivation can be traced back to the Mid Ocean Dynamics Experiment (MODE). Bryden (1974) evaluated the geostrophic approximation through comparison of direct current meter measurements with flow speeds computed geostrophically from mooring temperature and pressure sensors. As such the moorings were viewed as acting as "continuously operative hydrographic stations" (Bryden, 1974). A number of subsequent studies to estimate geostrophic transports from moored temperature and pressure time series have been made of the Antarctic Circumpolar Current (Whitworth,

1983), Kuroshio (Johns et al., 2001) and Atlantic DWBC both at 16ºN (Kanzow et al., 2006) and 26.5ºN (Johns et al., 2005). They have largely concurred that with certain caveats (discussed subsequently in our application of the method) monitoring of large scale baroclinic ocean circulation can be achieved with errors smaller than the variability (Kanzow et al., 2006; Johns et al., 2005). We therefore aim to apply this method to construct continuously operative hydrographic stations from historical mooring data sets at each boundary to complement the traditional hydrographic end stations to monitor the mid-ocean geostrophic transport component of the MOC at 26.5ºN (Chapter 6).

4.4.2 Preliminary Results

Before considering new hydrographic end stations (Chapter 5) we present an application of the above method to stations taken from the transatlantic hydrographic sections (Chapter 3). At the west and east we select the CTD cast closest to the boundary but deeper than 4000m (Figure 4.2 and Table 4.1), and use a reference specific volume anomaly profile equal to the mean of the 5 stations at each boundary. Transports are referenced to 800 dbar at the west and 3200 dbar at the east (consistent with Sections 5.2.3 and 6.3.6) and the 0-800m, 800-1100 and 1100-3000m layer transport anomalies are computed (Table 4.1) to be representative of the upper, intermediate and upper NADW water masses (layer definitions were justified in Section 3.3.2).

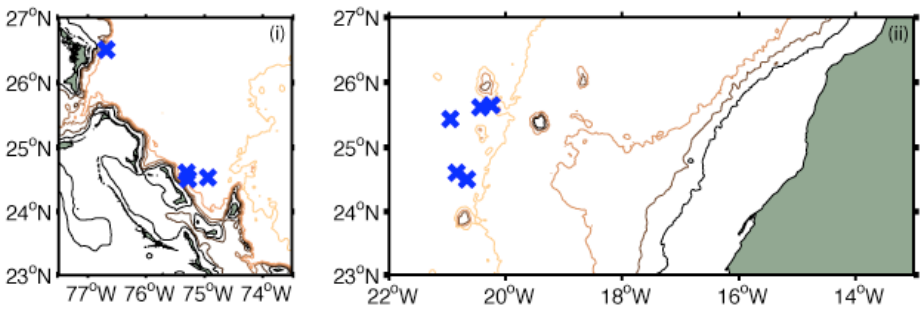

Figure 4.2 *Location of end stations selected from transatlantic hydrographic sections at the west (i) and east (ii). Depth contours are at 1000, 2000, 3000 and 4000m, land is shaded.*

Standard deviation of the 0-800m layer transport anomalies at the west is almost twice that at the east (2.8 and 1.5 Sv respectively, Table 4.1) suggesting that the contribution to upper layer meridional transport variability made by the western boundary is larger

than that from the east. This is despite the end stations selected being significantly closer to the boundary at the west than east (Figure 4.2) from which we would expect the eastern boundary variability contribution to be an overestimate. While AAIW shows similar variability at the west and east, variability of UNADW (the middle layer) is significantly greater at the west than east, with standard deviations in layer transport anomalies of 5.6 and 1.0 Sv respectively.

Western Boundary						
Year	Lon (ºW)	Lat (ºN)	Depth (m)	Layer transport anomalies (Sv)		
				0-800m	800-1100m	1100-3000m
1957	74.94	24.53	4862	1.1	-0.1	-3.8
1981	75.29	24.50	4038	1.9	-0.2	-1.1
1992	75.30	24.61	4713	2.6	-0.2	-4.4
1998	76.68	26.50	4576	-1.1	0.1	9.4
2004	76.68	26.51	4425	-4.2	0.4	-0.7
Transport standard deviation (Sv)				2.8	0.3	5.6

Eastern Boundary						
Year	Lon (ºW)	Lat (ºN)	Depth (m)	Layer transport anomalies (Sv)		
				0-800m	800-1100m	1100-3000m
1957	20.84	24.60	4162	-1.3	-0.6	-1.2
1981	20.95	25.43	4454	-0.2	0.2	0.3
1992	20.66	24.50	4108	-0.6	-0.2	-0.8
1998	20.43	26.62	4290	-0.5	0.1	0.7
2004	20.24	26.65	4190	2.6	0.4	1.0
Transport standard deviation (Sv)				1.5	0.4	1.0

Table 4.1 *Transport anomalies computed from CTD stations of the transatlantic hydrographic cruises of Chapter 3, used here as end stations at the western and eastern boundaries. Station location and depths also given. The upper part of the table presents transport anomalies of the 0-800m, 800-1100 and 800-3000m layers at the east and the lower part those at the west.*

These preliminary calculations also illustrate the validity of the end station method. The combined eastern boundary plus western boundary upper layer transport anomalies of years 1957 through 2004 are -0.2, +1.7, +2.0, -1.6 and -1.6 Sv about the long term mean. That the 1981 and 1992 net transport anomalies of the upper layer are positive while those of 1998 and 2004 are negative is consistent in sign with strengthened mid-ocean southward transport of thermocline waters in later years, as found in Section 3.2.2 (remembering that a positive transport anomaly is indicative of northward flow).

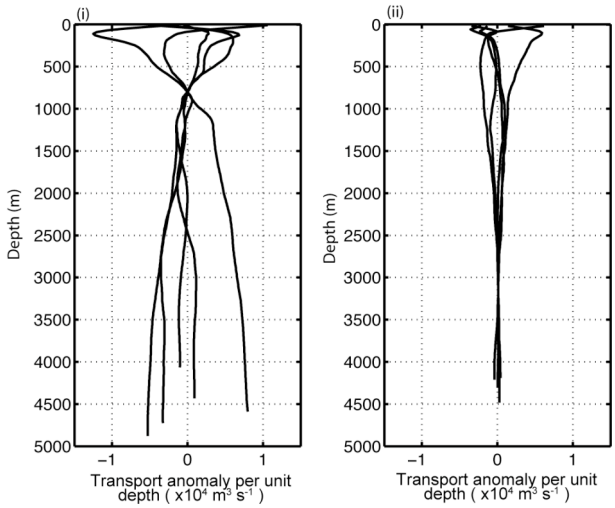

Figure 4.3 *Transport anomaly per unit depth profiles of end stations of Table 4.1, relative to the group mean and referenced to 800dbar or 3200dbar at the west and east respectively.*

4.5 SUMMARY

In this brief chapter we have outlined how the variability of the Atlantic MOC at 26.5ºN can be decomposed into the three components of wind driven Ekman transport, Gulf Stream flow through the Florida Straits and mid-ocean geostrophic transport (baroclinic part only). Data sets of the Ekman and Florida Straits components are essentially complete from 1980 to 2005 for the purpose of computing annual mean transports, and thus assessing their contribution to MOC variability on interannual timescales.

There is not such a convenient dataset available with which to assess the mid-ocean geostrophic transport's contribution. The next two chapters are devoted to construction of such a dataset and its subsequent analysis. Preliminary application of the end station method (Section 4.4.2), shows the method to resolve the trend in upper layer flows computed from the hydrographic sections of Chapter 3 and suggests that the contribution of the western boundary will be dominant over that of the east. The results of application of the methods developed will be presented in Chapter 7.

CHAPTER 5: **Methods and Data - End Stations**

5.1 INTRODUCTION

This chapter details the procedures employed in selection and processing of CTD casts at the eastern and western boundaries of the 26.5ºN Atlantic section for use as end stations, following the methods of Section 4.4. Particular attention is paid to definition of the study region at each boundary from which casts are selected since this determines the magnitude of method errors due to flows inshore of the end stations. Any inshore flows are excluded from the basin-wide mid-ocean geostrophic transport anomalies that the method aims to assess. We aim to minimise the meridional transport anomaly error of the upper (0-800m), intermediate (800-1100m), middle (1100-3000m) and deep (3000-4700m) layers. The transport anomaly calculation procedure outlined in Section 4.4 is also expanded upon for each boundary - first the east (Section 5.2), then the west (Section 5.3), with a summary in Section 5.4.

5.2 THE EASTERN BOUNDARY

5.2.1 End Station Selection

To define a study region for selection of such end stations, two questions must be answered: how far offshore can an end station lie such that meridional transports inshore of it are not so large as to prevent detection of a signal, and what is the meridional scale along the boundary over which we expect the computed dynamic height profile to be representative of that at 26.5ºN? The answers lie in the hydrography and circulation of the region reviewed below; first to set the north-south extent of the study region, then to determine offshore limits of each layer.

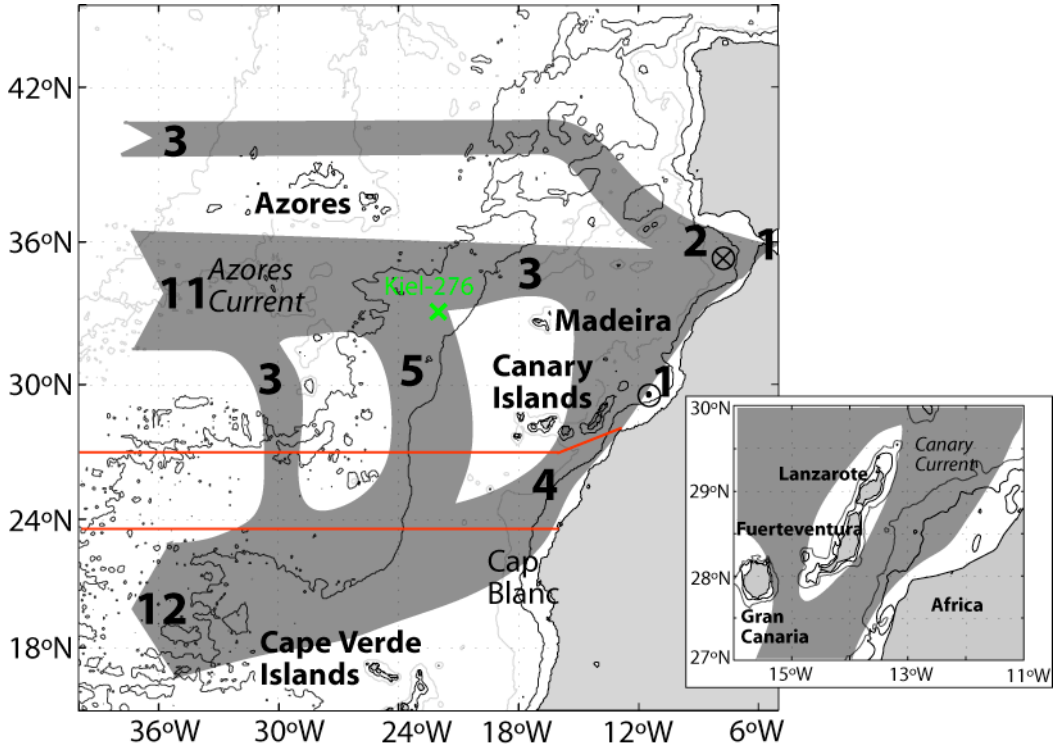

Figure 5.1 *Schematic of upper layer circulation in the eastern North Atlantic, modified from Figure 11.6 of Siedler and Onken (1996), itself a synthesis of regional hydrographic studies made in the 1980's and early 1990's. Transports are in Sv, with upwelling denoted by dotted circle and downwelling denoted crossed circle. The pathway of flow through the Canary Islands has been modified to include probable transport between Gran Canaria and Fuerteventura as well as through the Lanzarote passage (insert), as observed during CANIGO (Canary Islands Azores Gibraltar Observations) (Hernández-Guerra et al., 2002). Depth contours are at 1000, 3000 and 5000m, land above sea level is shaded. In the insert the 200m isobath is added. The defined study region (see text) is indicated in red, and the location of mooring Kiel-276 shown for reference (Section 6.2).*

Eastern basin end stations must be positioned east of the subtropical gyre recirculation, so that transport anomalies computed represent the full zonal integral of transport across the mid-ocean section. As the Gulf Stream flows eastward of the Grand Banks off Newfoundland, near 50ºW it separates into the North Atlantic Current which flows northeast constituting the thermohaline (overturning) component while the rest continues eastward as the Azores Current. The Azores Current is therefore the eastern basin Gulf Stream recirculation (Käse and Krauss, 1996; Klein and Siedler, 1989; Figure 5.1). While a significant part of the recirculation may occur in the western basin (e.g. Schmitz and McCartney, 1993), eastern basin flows are notable with southward transport in three branches (Figure 5.1). The easternmost of these, the Canary Current, originates at the intersection between the Azores Current and the African coast, the most southerly position of which occurs in summer at 31-32ºN (Klein and Siedler,

1989). In the absence of the Canary Islands, this would set 31ºN as the northern limit for end stations. Dynamic height profiles near the Canary Islands however are undesirable since inshore of the islands they do not represent mid-ocean transports due to intervening topography, while those offshore miss the transport signal between the islands. Multi-year current meter and hydrographic estimates suggest 1 to 3 Sv of transport between Gran Canaria and Fuerteventura or Fuerteventura and Africa (Hernández-Guerra et al., 2005; Hernández-Guerra et al., 2003; Hernández-Guerra et al., 2002). Introducing a 3 Sv transport anomaly error due to position alone is not acceptable, and we therefore define the northern limit of the study region by the cruise track of the 1981, 1998 and 2004 hydrographic sections as a line 0.1º north of the section path into the African coast (Figures 5.1 and 5.6).

To determine the southern limit for end station selection, water mass distribution is considered. The Canary Current comprises southward flow of North Atlantic Central Water (NACW) along the eastern Atlantic boundary to 20-22ºN where the Cape Verde Frontal Zone marks its convergence with South Atlantic Central Water (SACW) (Arhan et al., 1994). Here it leaves the coast (Figure 5.1) and flows westward as the subtropical gyre return flow feeding the North Equatorial Current (Arhan et al., 1994; Siedler and Onken, 1996). The 1988 Bord-Est hydrographic section running from 20-60ºN approximately 200 nm from the continental slope, showed some leakage from the Canary Current into the interior further north, with steady accumulation of westward flow totalling 4 Sv between 25ºN and 20ºN, but less than ±1 Sv north of 25ºN (Arhan et al., 1994). To limit meridional changes in strength of the Canary Current to the order of 1 Sv along the north-south extent of the study region, we set the southern limit at 23.8ºN (based on an accumulation of 1 Sv westward transport over 1.2º latitude from Figures 13 and 14 of Arhan et al., 1994). The southward limit is also required to exclude the region south of Cape Blanc which has a strong seasonal upwelling cycle; north of this, upwelling occurs year round (Hernández-Guerra and Nykjaer, 1997; Mittelstaedt, 1991). Strong seasonality in the observations would complicate interpretation so 23.8ºN represents a satisfactory boundary.

The offshore limit of the end station selection region is dependent on flow of each water mass, discussed for each layer in turn. From this point forwards, all offshore distances are defined as relative to the location of the nearest 800 m isobath.

5.2.1.1 The upper layer

Meridional transport of the upper 1000m accumulated from the African coast across 25ºN agrees well with that predicted by the Sverdrup balance, being approximately linear for the easternmost 4000km of the section (Roemmich and Wunsch, 1985). Similarly transport of the 0-800m layer for the five transatlantic hydrographic sections of Chapter 3 accumulates approximately linearly at a rate between 3 and 5 Sv per 1000km for the first 4500km from the first station of each section (Figure 5.2). Regression coefficients, when adjusted for the distance from the 800m isobath, predict 1 Sv of accumulated southward transport 160 km offshore in 2004 or 300km offshore in 1957 with all other years lying in between (Figure 5.2). Because linear regression does not account for eddies a couple of Sverdrups transport may result even with an inshore station, but since Gulf Stream recirculation is the signal we are concerned with capturing, based on Figure 5.2 we select an offshore limit of 160km for upper layer end stations.

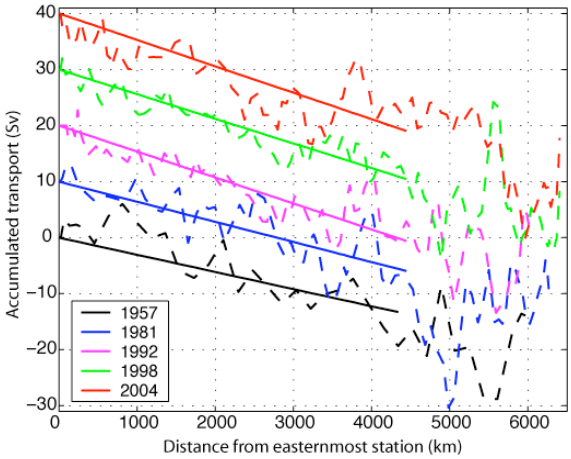

Figure 5.2 *(i) Accumulated meridional 0-800m transport for the 25ºN hydrographic sections (Section 3.3.2.1) as a function of zonal distance from the easternmost station (dashed lines) and the least squares linear regression passing through zero at the first station, of accumulated transport versus distance out to 4500km from the origin (solid lines). The linear regressions have slopes (± 95% confidence interval) of -3.1(± 0.4), -3.6(± 0.3), -4.6(± 0.2), -4.4(± 0.1) and -4.7(± 0.3) Sv per 1000 km in 1957, 1981, 1992, 1998 and 2004, and accumulate 1 Sv of southward transport at distances of 322, 278, 217, 227 and 213 km from the 800m isobath.*

5.2.1.2 The intermediate layer

Firstly we note that the meridional extent of the study region (23.8 to 28ºN) is sufficiently small to prevent a latitudinal bias in the water masses contributing to intermediate layer dynamic height profiles. Diluted Mediterranean Water dominates this

layer although Arhan et al., (1994) observed a northward flowing along-slope undercurrent of diluted AAIW as far north as the Canary Islands and we therefore expect both water masses to contribute to the properties of this layer. Transport between 800 and 1100 m, accumulated from the eastern boundary of the five transatlantic hydrographic sections of Figure 5.3, shows an eddy dominated signal with net transport in the eastern basin less than ± 2.5 Sv. This is consistent with the results of Macdonald (1998) and Schmitz and McCartney's (1993) circulation syntheses, the latter of which shows in the intermediate water cartoon a possible 2 Sv recirculation of AAIW north of the Cape Verde Islands and 1-2 Sv circulation of Mediterranean Outflow Water confined north of the Canary Islands. From this we set the offshore limit for intermediate water end stations at the eastern boundary as 500km from the 800m isobath, and anticipate the transport error inshore of this being less than ± 1 Sv (Figure 5.3) although there may be an eddy signal.

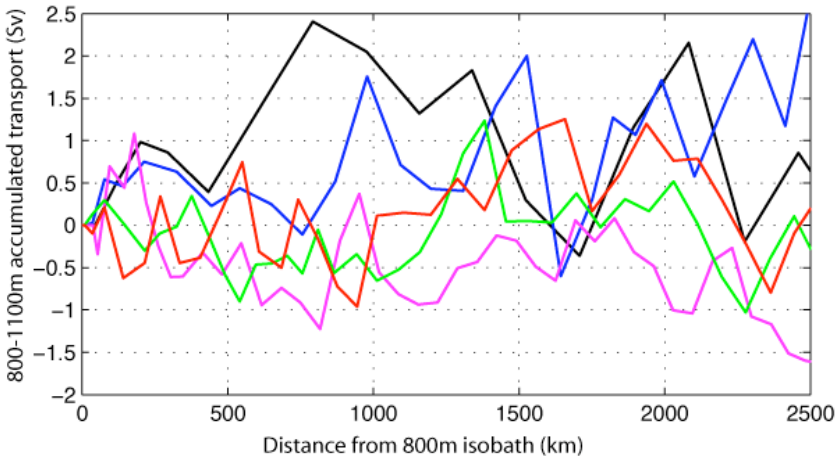

Figure 5.3 *Transport of the 800-1100m layer, accumulated from the location of the eastern boundary 800m isobath for the 1957 (black), 1981 (blue), 1992 (pink), 1998 (green) and 2004 (red) hydrographic sections out to the Mid Atlantic Ridge.*

5.2.1.3 The middle and deep layers (NADW)

While 4-6 Sv of southward transport in the 1100 - 3000 m layer (UNADW) accumulates across the eastern basin in the 1957 and 1992 hydrographic sections (Figure 5.4), net transport in 1981, 1998 and 2004 amounted to less than ± 2 Sv. In order to resolve the full extent of this layer, stations must be taken at least 50 km or 230 km from the 800 m isobath at 26ºN and 24.5ºN respectively, corresponding to the location of the 3000 m isobath (Figure 5.1). Transport (Figure 5.4) appears eddy dominated within 500km of the 800m isobath (amounting to at most 2 Sv in 1998) and

we select this as the offshore limit since it permits a reasonable number of end stations (Section 5.2.1.4). We take confidence from Schmitz and McCartney (1993) who suggested only 2 Sv northward transport of NADW (1.8 to 4ºC) in the Canary Basin, due primarily to upwelling of AABW from below, and thus predominantly in the LNADW layer. With such a small transport in the UNADW layer, it follows that the location of the eastern boundary UNADW end station is not of great importance for limiting the transport error of this layer.

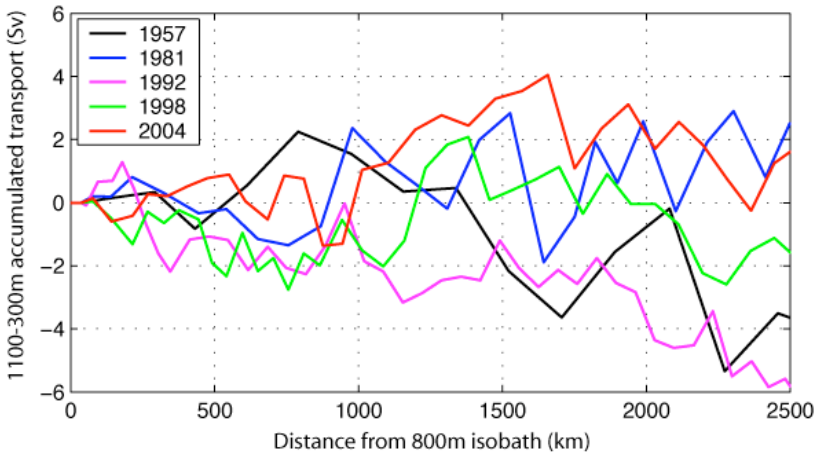

Figure 5.4 *Transport in the 1100-3000m layer accumulated from the eastern boundary 800m isobath for the 1957, 1981, 1992, 1998 and 2004 hydrographic sections out to the Mid Atlantic Ridge.*

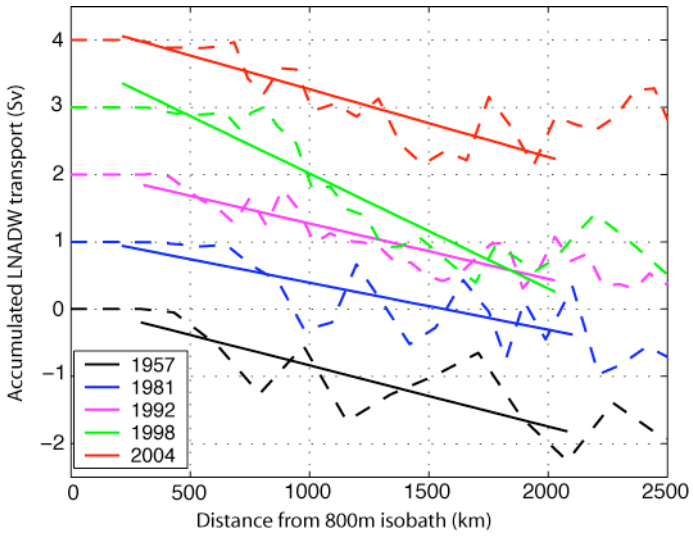

Figure 5.5 *Transport of LNADW (3000-5000m) accumulated from the eastern location of the 800m isobath for the 25ºN hydrographic sections in 1957, 1981, 1992, 1998 and 2004 (dashed lines). Least squares linear fit of transport from where water depth exceeds 3000m on the section to 2000km offshore – the eastern side of the Mid Atlantic Ridge (solid lines). Rate of accumulation of LNADW (with 95% confidence interval) in Sv per 1000km is -0.9 ± 0.6, -0.7 ± 0.3, -0.8 ± 0.2, -1.7 ± 0.2 and -1.0 ± 0.3 in 1957, 1981, 1992, 1998 and 2004 respectively.*

Accumulation of LNADW transport is, to a first approximation, linear from the eastern boundary to the mid Atlantic Ridge in the five 25ºN hydrographic sections (Figure 5.5). The best fit line shows 1 Sv of southward transport accumulated at 1560, 1180, 1330, 1010 and 1260 km from the 800m isobath in 1957 through 2004 (although we have less confidence in the 1981 and 1957 values due to large station spacing and the importance of bottom triangle transport, Section 3.2.4). Due to the limited data set we take the conservative choice of 1000 km as the maximum distance offshore for the LNADW end stations, noting that the 5000m isobath sits approximately 640 km offshore from the 800 m isobath between 22 to 26ºN increasing to 740 km between 27 and 30ºN.

5.2.1.4 The selected dataset

Review of circulation and hydrography in the eastern north Atlantic between the Canary Islands and the Cape Verde Frontal Zone have led to definition of our eastern boundary study region as in Figure 5.6 with a southern limit of 23.8ºN and a northern extent dependent on longitude: 27ºN east of 16.5ºW and approximately north-east into the African Coast from there. The offshore limits are water mass dependent at 160km, 500km, 500km and 1000km for the upper, intermediate, middle and deep layer transport anomalies respectively. CTD casts are taken from one of the transatlantic hydrographic section datasets, NOC/RAPID mooring cruises (Cunningham, Rayner et al., 2005) the World Ocean Database 2001, directly from IFM-Kiel or Hydrobase (2003) at 20 dbar resolution after simple quality control. Stations with pressure jumps or from cruises with data of dubious quality (including Kiel cruises M53, M56/1 and M57 in 1980 and 1990, T. J. Müller personal communication, 2004) are excluded. From the dataset obtained, we select for each time separated by more than two days, the CTD casts closest to the boundary for each layer where data coverage permits. If a station is present in multiple sources the order quoted above is used to remove duplicates - Hydrobase receives the lowest preference due to reduced vertical resolution - 10 dbar compared with 2 dbar from the other sources. In total, 10, 11, 9 and 7 end stations are identified for the upper, intermediate, middle and deep layers respectively (Table 5.1 and Figure 5.6).

	Aug-81	Jul-83	Nov-84	Nov-87	Jun-88	Aug-88	Oct-91	Jun-92	Jul-92	Dec-92	Sep-94	Jan-98	Apr-98	Jul-03	May-04	Apr-05
UPPER LAYER																
Day	12th		11th				22nd	12th	21st	9th	30th	24th			9th	5th
Origin	S		W				W	W	S	W	K	S			S	M
Lon (°E)	-13.55		-16.77				-14.42	-17.10	-16.93	-17.57	-14.81	-13.55			-13.55	-16.15
Lat (°N)	27.85		25.38				27.50	23.94	24.50	24.39	27.54	27.85			27.85	26.92
Dist (km)	6		45				68	12	32	79	98	6			6	111
Depth (m)	972		2793				1001	981	1403	1929	2498	1070			1081	3483
dSal																0.0044
INTERMEDIATE LAYER																
Day	13th		11th	15th	4th				22nd	9th	30th	25th	28th		8th	5th
Origin	S		W	W	W				S	W	K	S	H		S	M
Lon (°E)	-15.58		-16.77	-20.00	-21.05				-16.93	-17.57	-14.81	-16.11	-21.34		-15.59	-16.15
Lat (°N)	-27.23		25.38	25.00	24.70				24.50	24.39	27.54	27.03	24.00		27.23	26.92
Dist (km)	117		45	322	409				32	79	98	119	424		118	111
Depth (m)	3095		2793	3927	4298				1403	1929	2498	3470	4426		3131	3483
dSal	0.0066			0.0057	0.0015							0.0058	0.001		0.0054	0.0044
MIDDLE LAYER																
Day	13th		11th	15th	4th				22nd			25th	28th		8th	5th
Origin	S		W	W	W				S			S	H		S	M
Lon (°E)	-15.58		-17.06	-20.00	-21.05				-19.58			-16.11	-21.34		-15.59	-16.15
Lat (°N)	-27.23		25.51	25.00	24.70				24.51			27.03	24.00		27.23	26.92
Dist (km)	117		76	322	409				261			119	424		118	111
Depth (m)	3095		3204	3927	4298				3323			3470	4426		3131	3483
dSal	0.0066		0.0027	0.0057	0.0015				0.0055			0.0058	0.001		0.0054	0.0044
DEEP LAYER																
Day	15th	28th				14th			25th			28th		18th	5th	
Origin	S	W				W			S			S		H	S	
Lon (°E)	-24.29	-24.00				-25.83			-24.67			-24.22		-25.06	-23.50	
Lat (°N)	24.47	24.00				26.04			24.50			24.50		27.00	24.51	
Dist (km)	727	690				912			765			720		876	648	
Depth (m)	5114	5056				5269			5110			5124		5230	5003	
dSal	-0.0003	0.0007				0.0040			-0.0004			0.0015		0.0008	0.0011	

Table 5.1 *Selected Eastern Boundary End Stations. Day is the date of the month, Origin is data source; S-transatlantic hydrographic section, W-World Ocean Database 2001, M-NOC mooring cruise, K-IFM Kiel, H-Hydrobase 2003, Dist is distance from 800m isobath, Depth is station depth and dSal the salinity calibration offset applied (Section 5.2.2).*

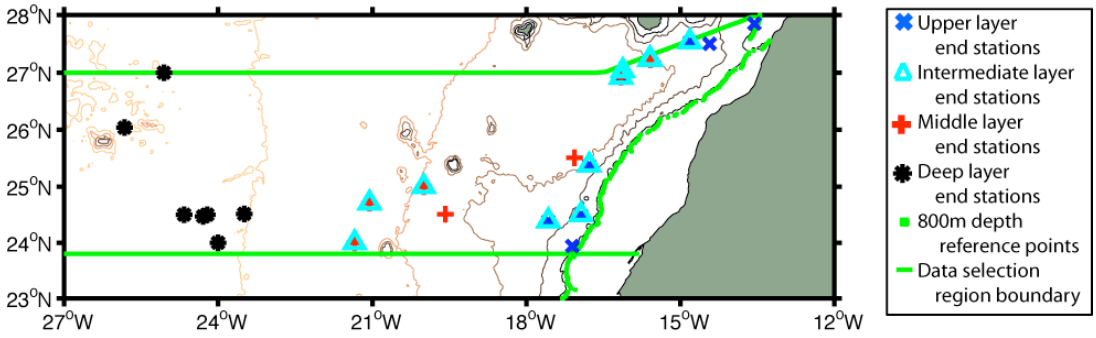

Figure 5.6 *Location of selected eastern boundary end stations for each layer, based on distance from 800m isobath within the defined region, as plotted in green. Depth contours are indicated at 1000m intervals to 6000m with land shaded.*

Screening of the selected end stations for meddies (anticyclonically rotating lenses of Mediterranean Water found in the Canary Basin e.g. Fiekas et al., 1992; Richardson and Tychensky, 1998) is performed and any stations showing such characteristics are rejected since they are not representative of boundary conditions. Observed as positive salinity and temperature anomalies with depth of influence between 800 and 1200m we see the resulting positive anomaly in dynamic height for one of the 1992 Hésperides stations in Figure 5.7. Station 24 (see legend for station details) sampled a meddy as identified by the anomalous θ-S relationship at 6-7ºC (Figure 5.7(i)), with resulting difference in the 0-800m layer transports between this and the adjacent station avoiding the meddy of 2.7 Sv.

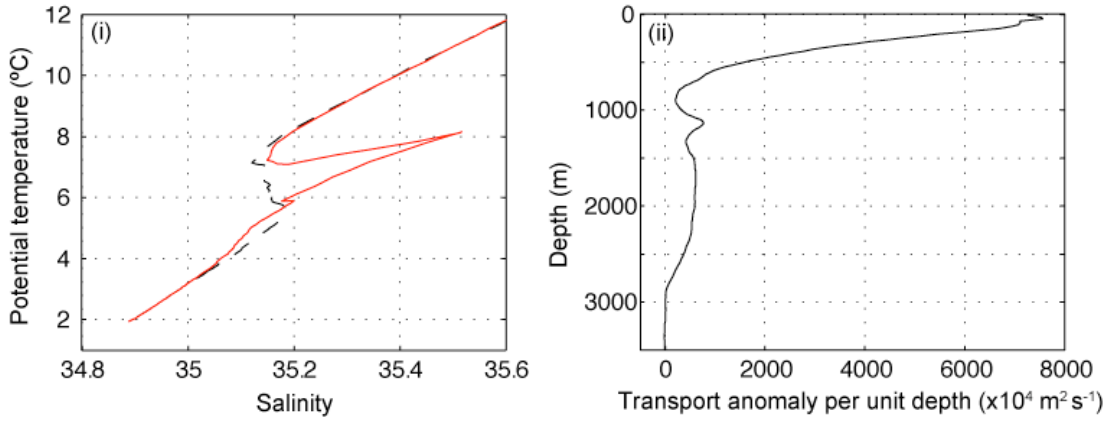

Figure 5.7 *(i) T-S diagram for Hésperides 1992 25ºN stations 23 (black dashed line) and 24 (red solid line), where 24 sampled a meddy. Station 24 was at 28.0ºW, 24.5ºN with a depth of 5554m, while 23 was 68 km away at 27.3ºW, 24.5 ºN depth 5480m, both taken on 27th July 1992. (ii) shows the transport anomaly per unit depth profile of station 24 relative to station 23.*

5.2.2 Salinity Calibration

Since order 0.005 salinity differences in deep water (2.0 to 2.8ºC) can induce order 2 Sv transports (Slater, 2003), we must consider whether a salinity range up to 0.008 on potential temperature surfaces in the deep water observed in the selected boundary end stations (Figure 5.8) is the result of measurement error or real variability. We expect all CTD salinities in this dataset to have been calibrated to bottle salinities measured with a salinometer, itself calibrated with International Association for the Physical Sciences of the Ocean standard seawater (SSW) - common practice since the early 1980's (Mantyla, 1994). This type of salinometer has sensitivity better than 0.001 (Mantyla, 1994), and incorporating the accuracy of routine best practice at sea (0.0007 to 0.0010) gives a lower limit on salinity measurement accuracy of 0.001 (Bacon et al., 2000). Possible changes in sampling equipment or methods, evaporation between sample collection and analysis or salinometer discontinuities at 35.0 however, may contribute additional errors during bottle salt measurement and while discrepancies between tested SSW conductivity ratio and the labelled value have been smaller than 0.0015 since 1980 (Mantyla, 1994) long term storage of the SSW can result in salinity errors up to 0.003 (Bacon et al., 2000). Also errors may be increased during the calibration procedure in the presence of hysteresis in CTD pressure or temperature between the down and upcasts since traditionally the upcast is calibrated and the calibration applied to the downcast (e.g. Bryden et al., 2003). We therefore argue that variability up to 0.008 in salinity is not outside the bounds of experimental error given that calibrated salinity of modern CTD systems has a nominal accuracy of 0.005 (Emery and Thomson, 2001).

The uniformity of properties of LNADW in the northeast Atlantic basin (e.g. Tsuchiya et al., 1992), a consequence of its topographic isolation was noted by Saunders (1986) who suggested that the constancy of the θ-S relationship over 2.0-2.5ºC in the region 15-30ºW, 20-46ºN between 1977 to 1986 provided a suitable environmental standard for salinity measurement accuracy. Mantyla (1994) reviewed and developed this, finding a latitudinal dependence in the slope of the θ-S line, although this amounts to a change in salinity of only 0.0002 at 2.0ºC between 23.8ºN and 28ºN and 0.0006 at 2.5ºC (using Table 2 of Mantyla, 1994). This is significantly smaller than detection limits for our eastern boundary study region and is therefore neglected. Mantyla (1994) also suggested constancy of the relationship back to 1927, consistent with a multi-decadal age of these waters (Doney and Bullister, 1992).

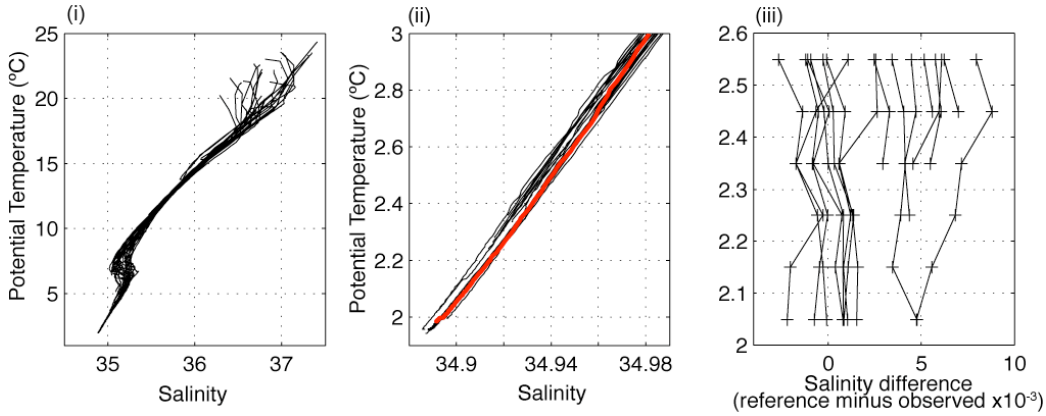

Figure 5.8 *Potential temperature – salinity plots of the 25 selected eastern boundary end stations before calibration (i). The deep waters are expanded in (ii) with the reference relationship overlaid in red. Anomalies of this reference station minus measured end-station salinity on 0.1°C potential temperature layers are in (iii). The reference station is station 15 from the Hesperides 1992 transatlantic section, with a minimum potential temperature of 1.98°C this is the easternmost CTD cast to reach waters colder than 2.0°C, with a depth of 4566m at 21.97°W, 24.51°N taken on 24th July 1992.*

We make use of the invariance of the LNADW θ-S relationship in the eastern boundary region and calibrate the selected end station salinities to remove the variability assumed to be due to measurement error. Calibration is performed relative to a reference station from the 1992 Hésperides cruise (Figure 5.8) by addition of an offset such that the calibrated salinities have zero mean offset relative to the reference station on the deepest four 0.1°C potential temperature levels (from 2.05°C) if the station resolves 2.2°C, or otherwise on all 0.1° levels below 2.5°C. This procedure gives preference to the deeper waters where variability is smaller (Figure 5.8(ii)), while the method of using the mean over this temperature range is supported by the linear relationship between θ and S found by Mantyla (1994) and Saunders (1986). We also exclude waters below 2.05° since the 2 degree discontinuity observed at 2.08°C (Broecker et al., 1976) marks the transition between LNADW and diluted AABW below (Tsuchiya et al., 1992) which can be seen in the reference curve (Figure 5.8(ii)).

The calibrations applied to end stations are all smaller than 0.008, with mean and standard deviation of 0.003 and 0.003 for the 16 stations deep enough to be calibrated (Figure 5.9). While there is a positive bias to the calibrations this is not of concern since we aim to compute a self consistent set of transport anomalies within the data set rather than absolute transports.

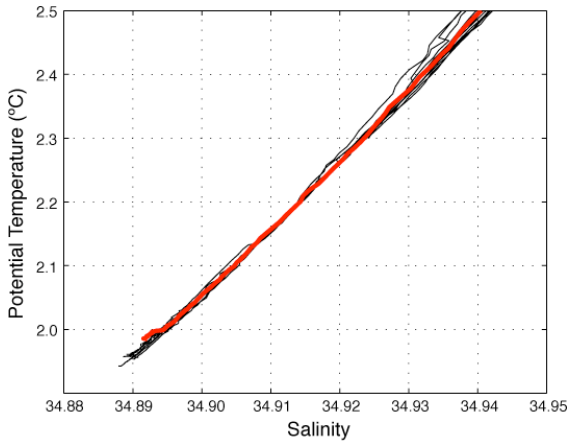

Figure 5.9 *Calibrated θ-S relationship for eastern boundary end stations, with the reference station in red.*

5.2.3 Transport anomaly calculation and errors

5.2.3.1 Methods

Transport anomalies are computed using equation (4.5) relative to a reference dynamic height profile which itself is the mean specific volume anomaly of the selected end stations in the 0-800m, 800-3000 and deeper than 3000m layers (Figure 5.10).

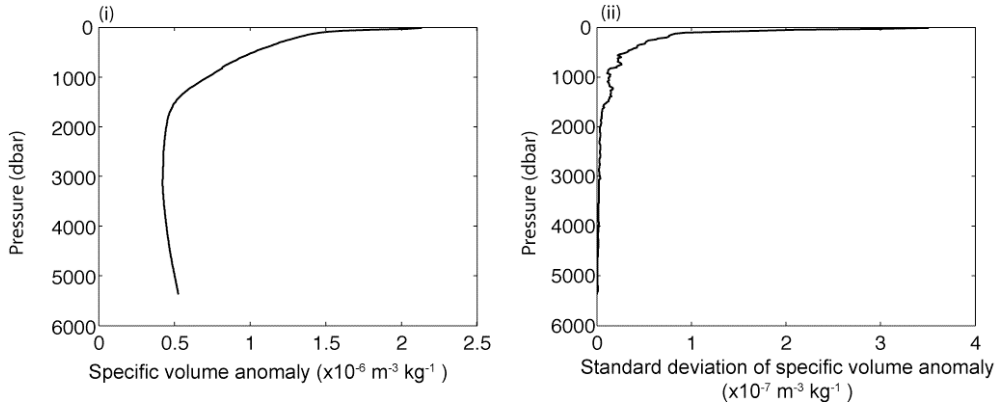

Figure 5.10 *The eastern boundary specific volume anomaly reference curve (i) constructed from the selected end stations, the standard deviation of which is shown in (ii) on pressure levels.*

Dynamic heights are referenced to 3200 dbar, following Section 3.2.4, and consistent with Arhan et al. (1994) who used 2.5ºC (approximately equal to 3200 dbar) for calculation of the zonal circulation across the Bord-Est line. An alternative reference level of 1320 dbar was suggested by Fiekas et al. (1992), specifically to examine the Canary Basin thermocline circulation. We do not adopt the shallower level here since

the 3000-5000m layer transport anomalies that result are judged artificial: the 7 deep end stations produce rms transport anomalies of 2.6 Sv or 0.4 Sv when referenced to 1320 or 3200 dbar respectively. The deeper reference level resolves the upper layer transport variability sufficiently well - the standard deviation of 0-800m transport anomalies referenced to 3200 dbar is 2.0 Sv which is significantly larger than the rms difference in upper layer transport anomalies due to use of the two reference levels of 0.4 Sv.

To compute the deep layer transport anomalies we could append CTD casts coincident in time down the continental slope as has been done to construct boundary dynamic height profiles from mooring data (Cunningham et al., 2007, submitted manuscript). We decide against this however since the 3000m isobath is found 40-200km offshore while the 5000 m isobath is 640-700 km offshore, hence end stations that resolve 3000 m and 5000 m could be separated by up to 500km, a distance significantly larger than the characteristic eddy scale at 25ºN of 170km (Stammer and Böning, 1996). We therefore argue that the possible effect of discontinuities introduced in the dynamic height profile by appending casts separated by such distances outweighs the arguments for appending casts in this region where boundary currents are weak and hence a station's offshore distance is not critical.

5.2.3.2 Errors

Although end stations have been carefully selected in order to minimise the boundary transport anomaly error associated with inshore flows, possible errors associated with data accuracy remain. Salinity calibration has the risk of removing natural variability in addition to the measurement error we have sought to eliminate. A uniform salinity offset, ΔS, is added to each end station and the resulting transport anomaly error (relative to that of calibrated salinity without offset) computed (Table 5.2). ΔS of -0.005 is used corresponding to the accuracy of calibrated salinity from modern CTD systems (Emery and Thomson, 2001). Similarly the transport error associated with addition of a uniform temperature offset, ΔT, of 0.002 to CTD casts simulates the transport uncertainty due to CTD temperature sensor accuracy of ±0.002 over –3 to 32ºC (Emery and Thomson, 2001) and a pressure offset, Δp, of 3.5 dbar due to pressure errors. The pressure error is an upper bound, since the SBE 9 CTD in sea trials (Hendry, 1993)

showed less than 0.5 dbar hysteresis and nonlinearity over the full sensor range (Emery and Thomson, 2001); but due to the age of some data we also note a 1978 CTD pressure sensor review which found errors exceeding 3.5 dbar below 3500 dbar (Emery and Thomson, 2001).

In calculating the final error estimate for each layer transport anomaly computed from end stations (column 7 of Table 5.2) we include the effects of distance offshore along with CTD measurement and calibration accuracy. The combined errors are estimated to be less than ± 1.5 Sv for all layers except that of UNADW for which it is ± 2.6 Sv (Table 5.2), being principally due to the location component.

Depth layer (m)	$\Delta T = 0.002$ $\Delta S = 0$ $\Delta p = 0$	$\Delta T = 0$ $\Delta S = -0.005$ $\Delta p = 0$	$\Delta T = 0$ $\Delta S = 0$ $\Delta p = 3.5$	Obs. error	Location error	Total error
0-800	0.1	0.7	0.1	0.7	1.0	1.2
800-1100	0.1	0.3	0.0	0.3	1.0	1.0
1100-3000	0.0	1.6	0.1	1.6	2.0	2.6
3000-5000	0.0	1.0	0.0	1.0	1.0	1.4

Table 5.2 *Estimated end station layer transport anomaly errors all in Sverdrups. Columns 2 to 4 are the root mean square errors resulting from addition of temperature, salinity or pressure offset to eastern boundary CTD casts, with the combined error, due to measurement errors and calibration of the CTD salinity (obs. error) in column 5. The location error of column 6 is that due to end station offshore position (Section 5.2.1) and the Total error (column 7) is the combination of Location and Observational errors.*

5.3 THE WESTERN BOUNDARY

5.3.1 End Station Selection

We review the western boundary circulation (Figure 5.11) with particular attention to its zonal structure, meridional consistency and temporal variability to set the study region for this boundary. As at the east, we define all distances relative to the westernmost 800m isobath, positive in an offshore direction, thus removing the effect of varying shelf width along the western boundary.

The western boundary at 26.5ºN has been extensively monitored with mooring arrays and short CTD sections from 1986 to 1998. Bryden et al. (2005a) synthesised all current meter observations at this location, presenting the time averaged western boundary circulation (Figure 5.11insert). The Antilles Current (AC) is a northward flow in the

upper 1000m between the boundary and 110km offshore, below which is the southward flowing Deep Western Boundary Current (DWBC) centred 55km offshore. Both have implications for end station selection.

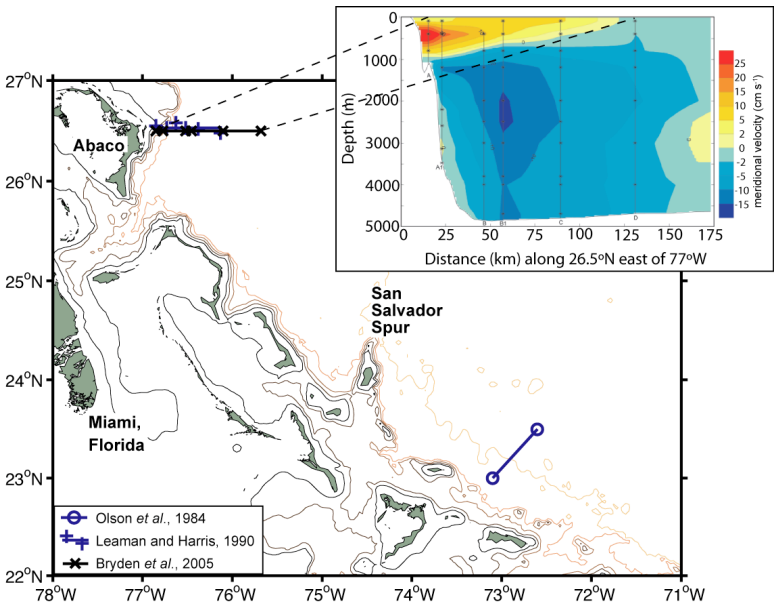

Figure 5.11 *Bathymetry of the western boundary region, depth contours at 1000m intervals, land shaded with a selection of observation locations referred to in text. Structure of the time-averaged western boundary current east of Abaco to 172 km offshore from the Abaco moored current meter arrays in insert (from Figure 3 of Bryden et al., 2005a).*

5.3.1.1 The upper layer

The warm northward flow of the Antilles Current is found on the shelf adjacent to the Bahamas boundary. Olson et al.'s (1984) regional study comprising CTD casts, moored current meters and historical XBT sections, showed the AC to be a weak continuous flow between 300 and 1000m depth along the outer Bahamas north of 22ºN (Figure 5.12) which plays a role in the Gulf Stream recirculation, a view that persists today (Lee et al., 1996). Transport of 4.0 Sv to the northwest through their boundary current meter mooring pair near 73ºW, 23ºN (Figure 5.11) from November 1980 to October 1981 is consistent with the 26.5ºN moored current meter array's long term mean AC transport from September 1984 to June 1997 of 5 Sv (±1.8 Sv error) (Lee et al., 1996; Bryden et al., 2005a). These estimates are in reasonable agreement with Inverted Echo Sounder (IES) and bottom pressure observations overlapping the last 16 months of Bryden et al. (2005a) time period that yielded an AC transport of 6.1 Sv ± 1.7 Sv error (Meinen et al., 2004) and 3.6 Sv mean geostrophic AC transport referenced with PEGASUS velocities

from 11 boundary CTD sections between April 1985 and September 1987 (Leaman and Harris, 1990).

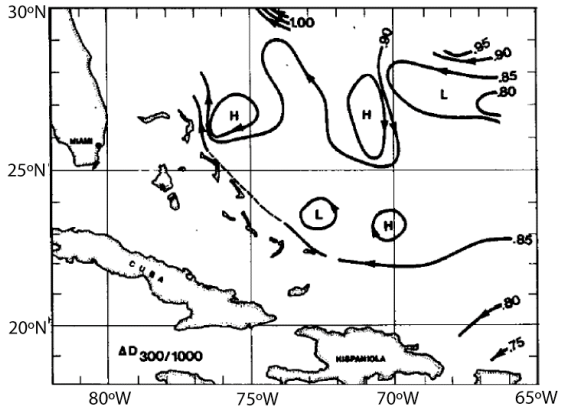

Figure 5.12 *Dynamic topography for 300/1000 dbar from Olson et al. (1984) - their Figure 6(b). Arrowheads on height contours denote direction of shear between layers. Note the suggestion of continuity from inflow around 23°N, 66°W into a boundary current along the Bahamas.*

End stations should ideally be inshore of the AC or at least have error estimates reflecting the anticipated order 5 Sv northward transport within 80-110km of the western boundary (Lee et al. 1996; Bryden et al. 2005a). It is unfortunate for resolution of the zonal structure of the AC that the innermost mooring of the Abaco array, A, 5km from the 800m isobath is found at the current core (Bryden et al. 2005a; Meinen et al., 2004). We therefore examine the full transatlantic hydrographic section 0-800m transports accumulated from the western boundary along with those from Leaman and Harris (1990) (Figure 5.13) and compute the distance at which the accumulated transport exceeds given thresholds (Table 5.3). Most sections show northward transport of the AC out to at least 25 km offshore, with 1 Sv accumulated transport a mean distance of 14 km offshore. We therefore select this as the offshore extent of the upper layer study region with associated error ± 2 Sv (based on the mean plus one standard deviation of accumulated transport 14km offshore, Table 5.3).

Target transport error (Sv)	Distance (km)	σ of transport at Distance (Sv)
1.0	14	1.3
1.5	17	1.6
2.0	21	2.3

Table 5.3 *The distance (column 2) at which the mean of all transports of Figure 5.13 equals the target transport error (column 1). Column 3 is the standard deviation of accumulated transports at the distance of column 2. Distances are relative to the 800m isobath and are based on linear interpolation between station positions.*

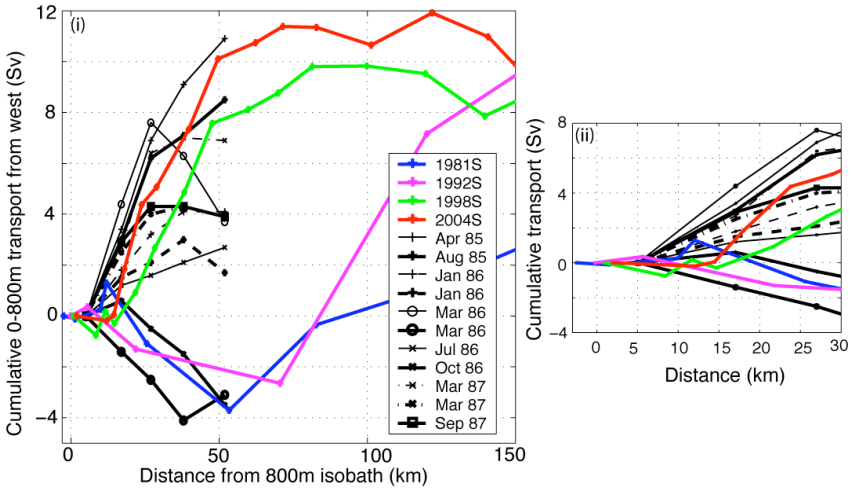

Figure 5.13 *Accumulated transport of the 0-800m layer from the western boundary as a function of distance relative to the position of the 800m isobath (negative distances are inshore of this). Transports are computed from the transatlantic hydrographic sections (Chapter 3) and Leaman and Harris (1990)'s Table 3. All sections are at 26.5ºN except 1992 and 1981 (Figure 3.1) (ii) expands the shoreward 30km.*

5.3.1.2 The intermediate layer

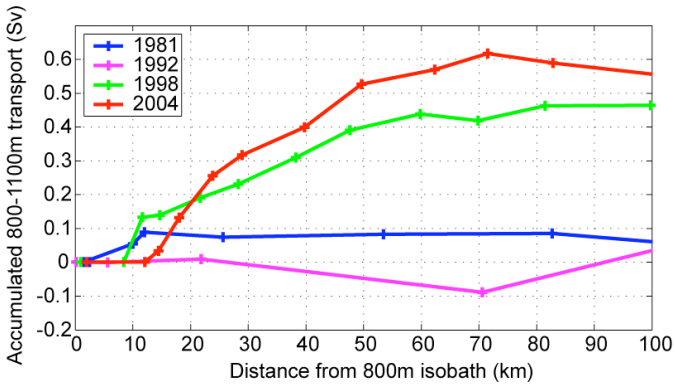

Figure 5.14 *Accumulated transport of the 800-1100m layer from the western boundary as a function of distance relative to the position of the 800m isobath from the transatlantic hydrographic sections (Chapter 3).*

At 25ºN we expect to find AAIW predominantly in the Florida Straits, where it has been traced by virtue of its salinity minimum and silica maximum along the east coast of South America, through the Caribbean Sea and Gulf of Mexico into Florida Straits via the Yucatan Channel and after which it continues northeast as a core in the Gulf Stream past the Grand Banks to 60ºN just south of Iceland (Tsuchiya, 1989). While AAIW is zonally widespread in the mid-ocean south of 20ºN, Bryden et al. (1996) clearly demonstrate its signal over the Mid-Atlantic Ridge at 24.5ºN in the 1981 and 1992 transatlantic hydrographic sections. Northward transport of the 800-1100m layer within 100 km of the western boundary (Figure 5.14) is negligible in the 1981 and 1992 transatlantic sections, and less than a Sverdrup in 1998 and 2004 (although similarity

with Figure 5.13 suggests the latter may be associated with base of the Antilles Current). This supports our conclusion from Tsuchiya's (1989) AAIW circulation pathways that the location of the western boundary end station for this layer is not critical. For convenience we therefore use the same end stations as for the middle layer transport anomalies, all found within 20km of the 800m isobath (Section 5.3.1.3) since the shelf slopes steeply in this region (Figure 5.11). Figure 5.14 estimates the 800-1100m layer transport anomaly error to be less than ± 0.2 Sv due to this distance offshore.

5.3.1.3 The middle and deep layers

The DWBC flows southwards though our study region with its core approximately 55km offshore at 26.5ºN (Bryden et al., 2005a) and follows the shelf edge to 24ºN before an excursion around the San Salvador Spur (at approximately 74.5ºW, 24ºN) and exiting the region as a boundary constrained southward flow but with complicated recirculation gyres (Johns et al., 1997). Our view of the zonal structure of the DWBC is largely derived from data at 26.5ºN where most observations in the subtropical western boundary have been made but we assume the results to hold further south. Before proceeding, a comment must be made about the definition of the layer depths. Thus far the deep layer, comprising LNADW has been defined as 3000-5000m. At the western boundary however, water depth does not exceed 5000m until approximately 74ºW at 26.5ºN (Figure 5.11) which is 252 km from the 800m isobath. Since the core of the DWBC (which we must resolve with end stations) is located approximately 200km inshore of this (Bryden et al., 2005a) 5000m is not appropriate for the base of the deep transport layer and we instead use 4700km at the western boundary being only 16km from the 800m isobath at 26.5ºN.

To examine the zonal structure of the DWBC, a number of datasets are available. It has been common, to compute its total transport (800m or 1000m to the bottom) rather than that of upper and lower NADW separately. Since we are interested in minimising the error for both the middle and deep layers, we estimate the accumulated transport offshore of each separately using Bryden et al. (2005a)'s observations that the cores of upper and lower NADW transport are vertically aligned in the long term mean (Figure 5.11 insert) out to the recirculation regime (172km west of 77ºW) and that the ratio of

upper NADW (800-3000m) to lower NADW (3000-4700m) transport per unit depth is approximately 11:8 (from their Figure 6). The results of this from Leaman and Harris (1990)'s CTD section transports are plotted in Figure 5.15. Note that no allowance is made for the intermediate layer transport in Figure 5.15 since Figure 5.14 shows this contribution to be negligible and authors differ in their selection of the upper limit of UNADW in this region between 800 and 1000m (e.g. Leaman and Harris, 1990; Bryden et al., 2005a).

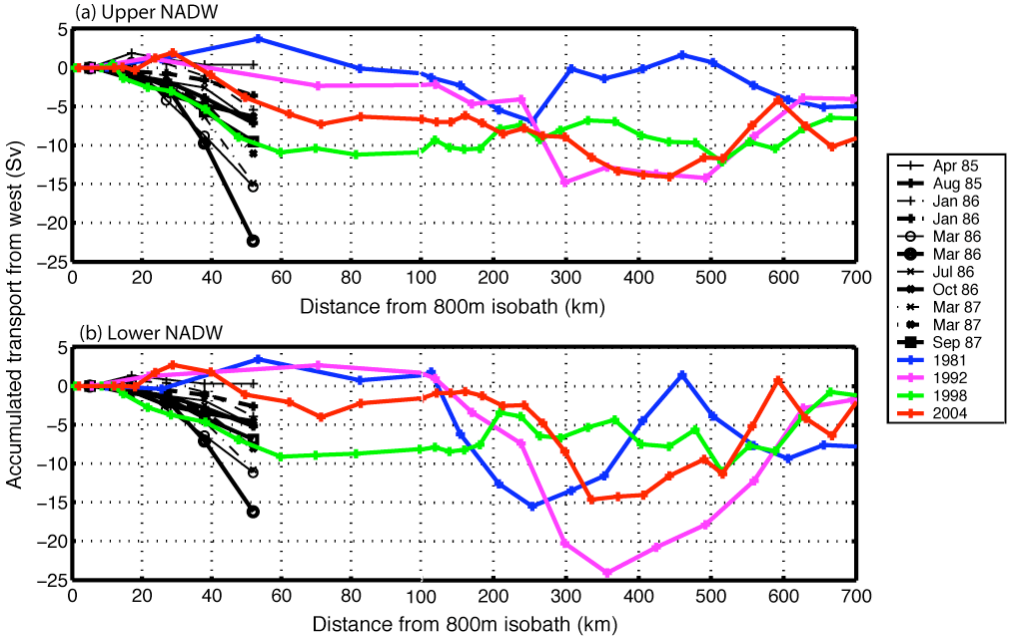

Figure 5.15 *DWBC transport accumulated from the western boundary, relative to distance from the 800m isobath from CTD sections for (a) upper NADW (800-3000m) and (b) lower NADW. Black lines are CTD/PEGASUS derived transports (Leaman and Harris, 1990) splitting their computed total transport below 800m by the ratio 11:8 – see text for details. Transports from the transatlantic sections are represented by coloured lines. Note change of x-axis scale at 100km.*

Target transport error (Sv)	UNADW		LNADW	
	Distance (km)	σ of transport at Distance (Sv)	Distance (km)	σ of transport at Distance (Sv)
1.0	19	1.1	20	0.9
1.5	23	1.4	24	1.2
2.0	26	1.8	28	1.6

Table 5.4 *The distances (columns 2 and 4) at which the mean of all UNADW or LNADW transports of Figure 5.15 equal the target transport errors of column 1. Columns 3 and 5 are the standard deviation of accumulated transports at the distances of columns 2 and 4. Distances are relative to the 800m isobath and are based on linear interpolation between station positions.*

Bryden et al. (2005a) found that in the long term mean 2 Sv of DWBC transport (below 1000m) accumulates approximately 44km from 77°W or 37km offshore (from the 800m

isobath), which we estimate to correspond to 1.1 Sv of UNADW and 0.8Sv of LNADW. The hydrographic sections of Figure 5.15 however, show that in the mean 1.0 Sv of UNADW and LNADW transport both accumulate approximately 20 km from the boundary (Table 5.4). We therefore err on the side of caution, selecting 20 km as the offshore limit for middle layer end stations with associated transport error of ± 2 Sv (mean plus standard deviation of accumulated transports 20 km offshore, Table 5.4). For the deep layer however, there are only 4 CTD casts deeper than 4700m within 20 km of the boundary and we therefore proceed with an offshore limit of 37km for this layer, placing confidence in the mooring derived accumulated transport which better accounts for temporal variability in the region through daily sampling for almost 11 years (Bryden et al., 2005a). The associated deep layer transport anomaly error is estimated to be ± 3 Sv based on the 1 Sv accumulated transport and a standard deviation in Figure 5.15 accumulated transports of 2.5 Sv at 37 km offshore.

5.3.1.4 The selected dataset

Layer	Offshore limit (km relative to the 800m isobath)	Layer transport anomaly error (Sv)
Upper (0 - 800m)	14	± 2
Intermediate (800 – 1100m)	20	± 0.2
Middle (1100 – 3000m)	20	± 2
Deep (3000 – 4700m)	37	± 3

Table 5.5 *Western boundary end station offshore limits and estimated error due to location.*

Our nominal latitude of study is 26.5ºN, but with the transatlantic sections meeting the western boundary between 24.5 and 26.5ºN we define the latitudinal limits of our western boundary region as 24 and 27ºN, over which range we do not expect the structure or strength of the meridional circulation to vary significantly (Sections 5.3.1.1 and 5.3.1.3). CTD casts are taken from one of the transatlantic hydrographic section datasets, the World Ocean Database 2001, AOML/NOAA directly or Hydrobase (Table 5.6) and smoothed to 20 dbar resolution after simple quality control. If a station is present in multiple sources the order quoted above is used to remove duplicates as in Section 5.2.1.4. From the initial data set of 373 stations between 77 and 73ºW, only 5 were rejected due to inconsistent temperature stratification (anomalously deep thermoclines). Of the accepted stations, we select all casts separated by more than 7 days or 1º in latitude within the offshore limits of Table 5.5 for calculation of the upper,

middle (and intermediate) and deep layer transport anomalies. The estimated errors due to station location are also given in Table 5.5. We obtain 39 stations for the upper and middle layers with 29 for the deep layer (Figure 5.16 and Table 5.6).

UPPER LAYER (0-800m)

Date	Source	Distance (km)	Depth (m)	Lat (°N)	Lon (°E)	dSal
4-Sep-81	sectn	4	2837	24.47	-75.44	-0.0001
3-Nov-81	wod01	6	1092	26.72	-76.95	NaN
25-Apr-85	wod01	8	3624	26.56	-76.77	0.0023
11-May-85	wod01	7	3468	26.55	-76.78	0.0012
29-Aug-85	wod01	1	1027	26.55	-76.84	NaN
19-Jan-86	wod01	12	3529	26.55	-76.73	0.0024
5-Feb-86	wod01	10	3460	26.55	-76.75	0.0016
22-Jul-86	wod01	1	1080	26.54	-76.84	NaN
18-Nov-86	wod01	12	3744	26.51	-76.73	0.0015
19-Mar-87	wod01	3	1481	26.59	-76.84	NaN
27-Mar-87	wod01	1	1339	26.56	-76.85	NaN
3-Sep-87	wod01	2	1268	26.56	-76.85	NaN
8-Oct-88	wod01	1	1055	26.54	-76.85	NaN
13-Mar-89	wod01	1	1148	26.54	-76.84	NaN
28-Feb-90	aomlw	2	1343	26.57	-76.85	NaN
18-Jun-90	hybas	7	1412	26.49	-76.82	NaN
28-Jun-90	hybas	2	2277	24.26	-74.45	NaN
29-Jun-90	hybas	14	4522	25.51	-76.35	0.0014
30-Jun-90	hybas	13	1414	26.49	-76.74	NaN
9-Jan-91	hybas	10	3876	26.51	-76.76	0.0004
15-Jun-91	hybas	9	3544	26.53	-76.76	0.0042
22-Sep-91	hybas	10	3554	26.52	-76.76	0.0009
20-Jul-92	hybas	7	3323	24.55	-75.46	-0.0014
4-Aug-92	hybas	2	1335	24.00	-74.40	NaN
11-Aug-92	hybas	2	1399	26.54	-76.83	NaN
14-Aug-92	sectn	7	3321	24.55	-75.46	-0.0016
30-Mar-94	aomlw	6	1017	26.50	-76.85	NaN
10-Jul-96	hybas	4	1282	26.52	-76.83	NaN
31-Jul-96	aomlw	4	1280	26.52	-76.83	NaN
11-Jun-97	hybas	10	3871	26.51	-76.75	-0.0005
22-Feb-98	sectn	6	1370	26.50	-76.82	NaN
28-Apr-01	aomlw	13	3842	26.50	-76.73	-0.0018
26-Jun-02	aomlw	4	1075	26.52	-76.83	NaN
11-Feb-03	aomlw	4	1083	26.52	-76.84	NaN
7-Apr-04	sectn	5	1709	26.53	-76.81	NaN
2-Oct-04	aomlw	10	3551	26.50	-76.77	0.0019
8-May-05	aomlw	4	1083	26.52	-76.83	NaN
23-May-05	aomlw	4	1036	26.52	-76.84	NaN
21-Sep-05	aomlw	3	1092	26.52	-76.83	NaN

INTERMEDIATE AND MIDDLE LAYERS (800-1100m and 1100-3000m)

Date	Source	Distance (km)	Depth (m)	Lat (°N)	Lon (°E)	dSal
4-Sep-81	sectn	6	3483	24.49	-75.42	-0.0019
25-Apr-85	wod01	8	3624	26.56	-76.77	0.0023
11-May-85	wod01	7	3468	26.55	-76.78	0.0012
29-Aug-85	wod01	11	3507	26.53	-76.75	0.0005
19-Jan-86	wod01	12	3529	26.55	-76.73	0.0024
5-Feb-86	wod01	10	3460	26.55	-76.75	0.0016
23-Jul-86	wod01	12	3603	26.53	-76.74	0.0004
18-Nov-86	wod01	12	3744	26.51	-76.73	0.0015
19-Mar-87	wod01	9	3552	26.54	-76.76	0.0015
27-Mar-87	wod01	10	3581	26.55	-76.75	0.0011
3-Sep-87	wod01	8	3617	26.55	-76.77	-0.0016
7-Oct-88	wod01	12	3198	26.53	-76.73	-0.0008
13-Mar-89	wod01	10	3597	26.55	-76.75	-0.0006
28-Feb-90	aomlw	11	3061	26.55	-76.75	0.0001
20-Jun-90	hybas	19	4527	26.50	-76.67	-0.0002
27-Jun-90	hybas	14	4817	24.25	-74.33	0.0007
29-Jun-90	hybas	14	4522	25.51	-76.35	0.0014
9-Jan-91	hybas	10	3876	26.51	-76.76	0.0004
15-Jun-91	hybas	9	3544	26.53	-76.76	0.0042
22-Sep-91	hybas	10	3554	26.52	-76.76	0.0009
20-Jul-92	hybas	7	3323	24.55	-75.46	-0.0014
5-Aug-92	hybas	4	3014	24.00	-74.36	-0.0026
11-Aug-92	hybas	14	3843	26.50	-76.72	-0.0034
14-Aug-92	sectn	7	3321	24.55	-75.46	-0.0016
2-Jun-93	aomlw	17	4334	26.50	-76.68	0.0014
13-Jul-94	aomlw	18	4428	26.50	-76.68	0.0007
8-Mar-96	aomlw	17	4583	26.50	-76.69	0.0031
10-Jul-96	hybas	11	3869	26.50	-76.75	0.0002
31-Jul-96	aomlw	11	3869	26.50	-76.75	0.0005
11-Jun-97	hybas	10	3871	26.51	-76.75	-0.0005
22-Feb-98	sectn	11	3849	26.50	-76.75	0.0003
28-Apr-01	aomlw	13	3842	26.50	-76.73	-0.0018
26-Jun-02	aomlw	11	3759	26.50	-76.76	0.0013
11-Feb-03	aomlw	14	3916	26.50	-76.72	-0.0042
8-Apr-04	sectn	11	3815	26.52	-76.75	-0.0002
2-Oct-04	aomlw	10	3551	26.50	-76.77	0.0019
8-May-05	aomlw	10	3793	26.50	-76.76	-0.0020
23-May-05	aomlw	11	3856	26.50	-76.76	-0.0003
20-Sep-05	aomlw	10	3485	26.50	-76.77	0.0002

Table 5.6a *Selected western boundary upper, intermediate and middle layer end stations. Source is the data source; sectn-transatlantic hydrographic section, wod01-World Ocean Database 2001, aomlw-NOAA/AOML and, hybas-Hydrobase 2003. Distance is distance from the 800m isobath, Depth is station depth and dSal the salinity calibration offset applied (Section 5.3.2).*

DEEP LAYER (3000-4700m)												
M. Date	L. Date	Source	M. Depth (m)	L. Depth (m)	M. Lat (°N)	L. Lat (°N)	M. Lon (°E)	L. Lon (°E)	L. Dist (km)	Separation (km)	M. dSal	L. dSal
4-Sep-81	3-Sep-81	sectn	3483	4826	24.49	24.50	-75.42	-74.41	27	21	-0.0019	-0.0007
5-Feb-86	6-Feb-86	wod01	3460	4799	26.55	26.54	-76.75	-76.52	33	23	0.0016	0.0009
23-Jul-86	22-Jul-86	wod01	3603	4719	26.53	26.54	-76.74	-76.53	32	21	0.0004	-0.0004
18-Nov-86	19-Nov-86	wod01	3744	4741	26.51	26.54	-76.73	-76.52	33	20	0.0015	0.0016
19-Mar-87	19-Mar-87	wod01	3552	4791	26.54	26.53	-76.76	-76.54	31	22	0.0015	0.0021
27-Mar-87	28-Mar-87	wod01	3581	4725	26.55	26.54	-76.75	-76.53	32	23	0.0011	0.0005
3-Sep-87	3-Sep-87	wod01	3617	4813	26.55	26.55	-76.77	-76.54	31	23	-0.0016	-0.0009
13-Mar-89	14-Mar-89	wod01	3597	4712	26.55	26.54	-76.75	-76.54	30	20	-0.0006	-0.0007
28-Feb-90	28-Feb-90	aomlw	3061	4815	26.55	26.54	-76.75	-76.53	32	22	0.0001	-0.0002
20-Jun-90	20-Jun-90	hybas	4527	4813	26.50	26.52	-76.67	-76.53	33	14	-0.0002	-0.0009
27-Jun-90	27-Jun-90	hybas	4817	4817	24.25	24.25	-74.33	-74.33	14	0	0.0007	0.0007
29-Jun-90	29-Jun-90	hybas	4522	4798	25.51	25.49	-76.35	-76.19	19	5	0.0014	0.0005
9-Jan-91	10-Jan-91	hybas	3876	4821	26.51	26.47	-76.76	-76.53	33	23	0.0004	0.0007
20-Jul-92	20-Jul-92	hybas	3323	4715	24.55	24.62	-75.46	-75.32	24	17	-0.0014	-0.0010
5-Aug-92	5-Aug-92	hybas	3014	4748	24.00	24.01	-74.36	-74.28	12	8	-0.0026	-0.0024
11-Aug-92	10-Aug-92	hybas	3843	4777	26.50	26.46	-76.72	-76.61	25	12	-0.0034	-0.0004
14-Aug-92	14-Aug-92	sectn	3321	4713	24.55	24.61	-75.46	-75.30	24	17	-0.0016	-0.0011
8-Mar-96	8-Mar-96	aomlw	4583	4832	26.50	26.50	-76.69	-76.51	35	17	0.0031	0.0037
10-Jul-96	10-Jul-96	hybas	3869	4836	26.50	26.43	-76.75	-76.52	36	25	0.0002	0.0000
31-Jul-96	30-Jul-96	aomlw	3869	4836	26.50	26.43	-76.75	-76.52	36	25	0.0005	0.0015
22-Feb-98	21-Feb-98	sectn	3849	4720	26.50	26.50	-76.75	-76.62	24	13	0.0003	-0.0001
28-Apr-01	28-Apr-01	aomlw	3842	4708	26.50	26.50	-76.73	-76.61	24	11	-0.0018	-0.0029
26-Jun-02	25-Jun-02	aomlw	3759	4734	26.50	26.50	-76.76	-76.61	24	13	0.0013	0.0025
11-Feb-03	11-Feb-03	aomlw	3916	4812	26.50	26.50	-76.72	-76.60	26	11	-0.0042	-0.0043
8-Apr-04	9-Apr-04	sectn	3815	4820	26.52	26.50	-76.75	-76.53	33	22	-0.0002	-0.0003
2-Oct-04	1-Oct-04	aomlw	3551	4810	26.50	26.50	-76.77	-76.57	29	19	0.0019	0.0028
8-May-05	8-May-05	aomlw	3793	4808	26.50	26.50	-76.76	-76.57	28	18	-0.0020	-0.0017
23-May-05	22-May-05	aomlw	3856	4802	26.50	26.50	-76.76	-76.57	28	18	-0.0003	-0.0010
20-Sep-05	19-Sep-05	aomlw	3485	4797	26.50	26.50	-76.77	-76.76	10	1	0.0002	-0.0023

Table 5.6b *Selected western boundary deep layer end stations. Source is the data source; sectn-transatlantic hydrographic section, wod01-World Ocean Database 2001, aomlw-NOAA/AOML and, hybas-Hydrobase 2003. Dist is distance from the 800m isobath, Depth is station depth and dSal the salinity calibration offset applied (Section 5.3.2). The duplicate columns for variables refer to the shallower (prefix M.) and deeper (prefix L.) CTD casts which are appended down the slope.*

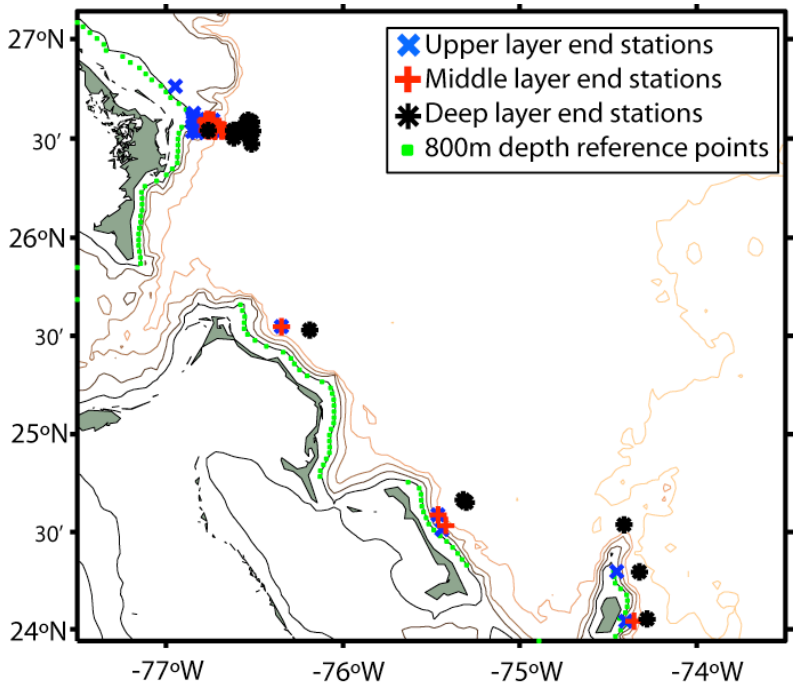

Figure 5.16 *Location of selected end stations for computation of layer transport anomalies. Selection is based on distance from the westernmost 800m isobath in the study region (green dots). Note no stations are taken west of San Salvador Spur due to intervening topography.*

5.3.2 Salinity Calibration

As at the eastern boundary, we must consider whether the salinity range up to 0.01 on potential temperature surfaces in the deep water observed in the selected boundary end stations (Figure 5.17) is the result of measurement error or real variability. We examine salinity anomalies on potential temperature levels relative to a reference station, taken as the 3rd CTD station from the western boundary of the 1992 Hésperides cruise at 75.30°W, 24.61°N with a depth of 4713m (the closest to the boundary that reaches 1.9°C).

The case for variability of order 0.01 in deep salinity being due to measurement error was made for the eastern boundary dataset, but recent observations of freshening in the high latitude North Atlantic deep waters of DSOW and ISOW (e.g. Dickson et al., 2002) necessitate consideration of whether this signal may have reached 25°N before we calibrate away the observed variability. Bryden et al. (1996) showed freshening of 0.005 (at the limits of detection) from 1981 to 1992 in LNADW at the western boundary of 24.5°N but Vaughan and Molinari's (1997) study of temperature and salinity variability

of the DWBC at 26.5ºN from 1984 to 1993 found no evidence for changes in LNADW, other than those due to movement of isopycnals. It is possible that Vaughan and Molinari (1997)'s dataset was too short to detect Dickson et al. (2002)'s long term freshening rates of 0.012 to 0.015 per decade since the early 1970's, traced from the overflows though the Labrador Seas.

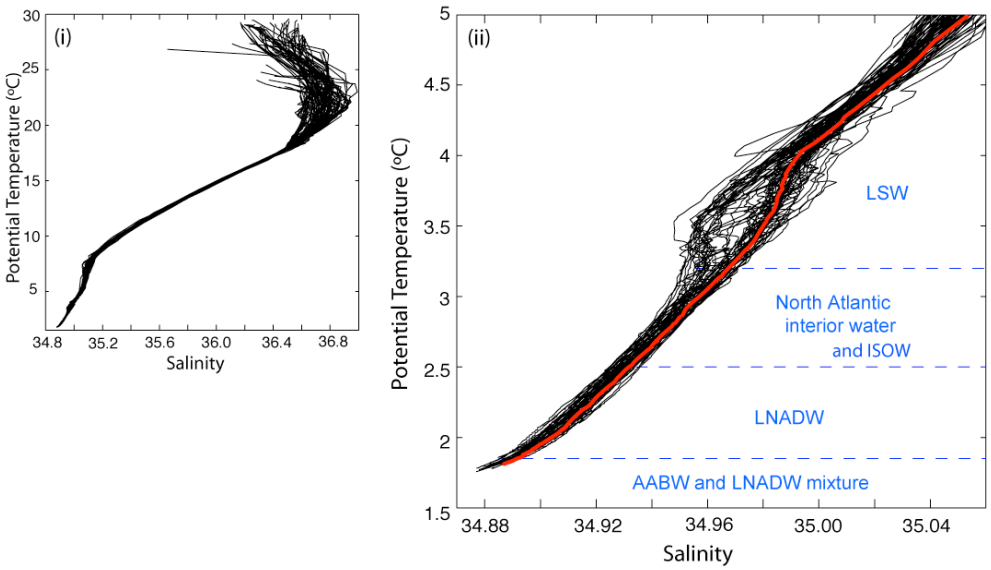

Figure 5.17 *The θ-S relationship of 25ºN western boundary end stations before salinity calibration of the full water column (i) and deep waters only in (ii), with the reference Hésperides station in red (ii). Water mass boundaries (1.85, 2.5 and 3.2ºC) follow Vaughan and Molinari (1997).*

If such a freshening is present in LNADW in our study region then we would like to retain the signal while simultaneously reducing any noise due to measurement error. Here the tightest part of the deep θ-S curve is below 3ºC (Figure 5.17); comprising an AABW/LNADW mixture below 1.8ºC, DSOW between 1.85 and 2.5ºC then ISOW and NAIW between 2.5 and 3.2ºC (Fine and Molinari, 1988; Fine, 1995; Molinari et al., 1998). Calibration of the AABW/LNADW mixture is not feasible since we expect characteristics of this layer to vary with distance from the Mid-Atlantic Ridge against which the AABW typically banks up (Bryden et al., 1996). Salinity anomalies of the DSOW and ISOW/North Atlantic interior waters on 0.1ºC potential temperature surfaces from the 280 CTD stations sampling these layers in the DWBC (defined to be inshore of 150km from the 800m isobath) relative to the 1992 reference station both show freshening over time (Figure 5.18). Linear regression of 5-year mean salinity anomalies for each layer is significant at the 99% confidence level and amounts to freshening of 0.0085 and 0.0077 from 1980 to 2005 for DSOW and ISOW respectively.

Standard deviations of each 5 year mean are less than 0.001 for DSOW and 0.002 for ISOW, both smaller than the anticipated salinity measurement error in the western boundary of 0.003 (Vaughan and Molinari 1997). The trend over the 25 years of this study is therefore judged significant and a suitable calibration procedure is now adopted.

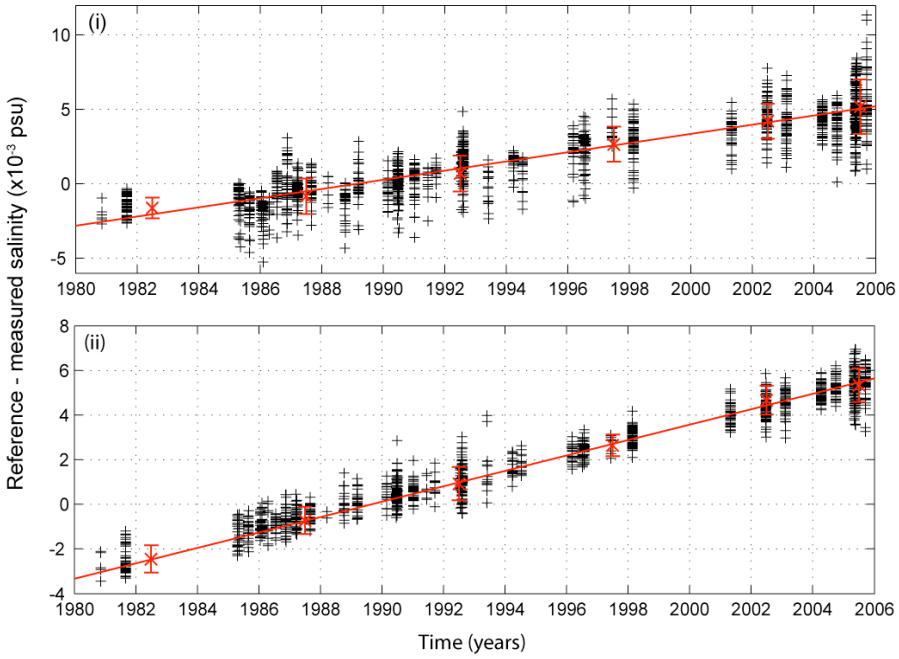

Figure 5.18 *Salinity anomalies (Hésperides reference minus measured) on 0.1°C potential temperature levels between 2.55 to 2.95°C for ISOW (i) and 1.95 and 2.45°C for DSOW (ii) as a function of time. CTD casts are within 150km of the 800m isobath between 24 and 27°N. Linear regression over time of the five year mean salinity anomalies from 1980 to 2005 and 2005-2006 annual mean (x) (with error bars of ± 2σ) after rejection of points outside the mean ±0.003 (—) shows freshening from over the 25 years at approximately 0.0031 and 0.0034 per decade for ISOW and DSOW respectively.*

The salinity of western boundary end stations which reach the temperature range of DSOW are calibrated by applying an offset such that the resulting mean difference between the calibrated salinity and a time varying reference derived from the linear regression of salinity anomaly with time plotted in Figure 5.18(ii) on 0.1°C potential temperature levels of DSOW is zero. The DSOW layer is calibrated in preference to that of ISOW due to larger variability in the latter, presumably reflecting variable amounts of NAIW and the longer transit time from its source region over the Iceland-Scotland Ridge (Dickson et al., 2002). The trend is still resolvable in the ISOW layer however, and therefore if a CTD casts contains measurements in this layer but not DSOW, the

mean ISOW salinity anomaly is used in calibration (using the same procedure as for DSOW).

CTD stations that do not reach the temperatures of LNADW layer are not calibrated. LSW (or upper NADW) is found in the more variable region of the θ-S plot (Figure 5.17(ii)), with classical LSW typically occupying 3.2 to 3.9ºC and Southern LSW above this to approximately 5ºC (Fine, 1995). Vaughan and Molinari (1997) found evidence of cooling and salinification between 1984 and 1993 in classical LSW typified by 2-3 year period oscillations while Molinari et al. (1998) documented a 0.1ºC cooling and 0.02 freshening from 1994 to 1998 of this layer. Although it may be possible to allow for the effects of long term trends in a salinity calibration reference station as discussed for LNADW above, oscillations present greater uncertainties since variability at low latitudes is only expected to be 2% of the subpolar source amplitude for hydrographic tracers of temperature or salinity (Waugh and Hall, 2005). Also LSW properties at low latitudes are influenced by entrainment, recirculation and mixing at the Gulf Stream - DWBC cross over, which may be dependent on Gulf Stream characteristics (Spall, 1996). As such it is unrealistic to extrapolate from variability in the source water properties of LSW to changes in the θ-S relationship at 26ºN.

In summary, we have developed a calibration procedure to account for the observed freshening of LNADW at 26.5ºN in the western boundary, which we apply only to end stations deep enough to reach temperatures of ISOW or lower. Of the 92 CTD casts selected as end stations (there are duplicates between the layers), 65 resolve temperatures of DSOW and are calibrated from this layer, an additional 3 casts resolve ISOW only and are calibrated accordingly. The mean salinity offset applied is less than 0.001 with a standard deviation of 0.0017 (Table 5.6).

5.3.3 Transport anomaly calculation and errors

5.3.3.1 The reference specific volume anomaly profile

Following equation (4.4) all transport anomalies are computed relative to a reference dynamic height profile. The reference specific volume anomaly profile (Figure 5.19) is computed separately for the three layers, 0-800m, 800-3000m and 3000-4700m as the mean on 20 dbar pressure surfaces from calibrated CTD casts selected as end stations.

Dynamic height anomaly profiles are referenced to 1000 dbar, consistent with the computation of geostrophic velocities of the transatlantic hydrographic sections (Section 3.2.4).

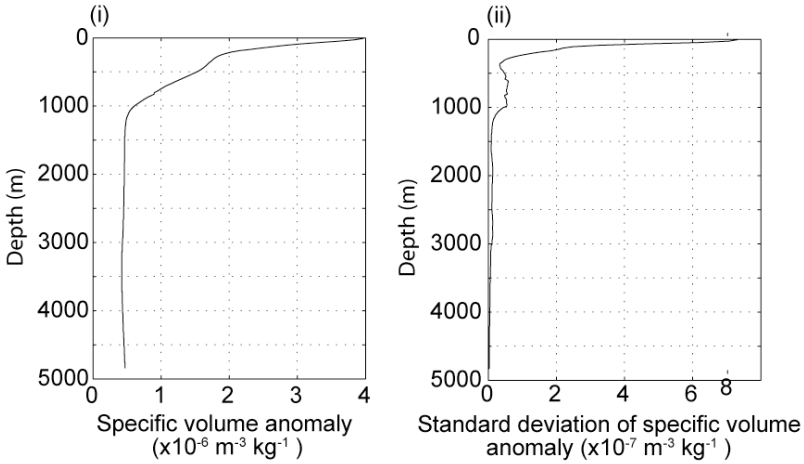

Figure 5.19 *Specific volume anomaly reference profile constructed from CTD casts (i) with the standard deviation of specific volume anomaly between constituent casts (ii).*

5.3.3.2 Appending CTD casts down the slope

Calculation of transport anomalies of the upper, intermediate and middle layers simply follows equation (4.4) with the end stations of Table 5.6 referenced to the dynamic height computed from the specific volume anomaly curve of Figure 5.19. The deep layer however is more complicated since stations deeper than 4700m (the maximum depth of the LNADW layer defined at this boundary) are frequently found more than 30 km from the 800m isobath, with significant transport inshore of this above the LNADW layer (e.g. Figure 5.11 insert). Eddies in the thermocline propagate westwards into the boundary on 70-100 day timescales (Lee et al., 1996), which combined with meandering (Lee et al., 1996) or pulses in strength of the DWBC (Chave et al., 1997) make this a highly variable current regime. Referencing dynamic height to 1000 dbar means that temperature anomalies at mid depth are integrated into the deep layers. We argue that such anomalies 30km offshore resulting from any of the above variability mechanisms result in a deep dynamic height profile not representative of conditions at the boundary.

To compute the deep layer transport anomaly we therefore append, on pressure surfaces, two CTD casts crawling down the slope. The upper part of the profile is taken from the

middle layer end station and below its maximum depth we add the lower part of the CTD cast resolving 4700m, casts being separated in time by at most 1 day. To prevent temperature inversions due to isotherm slopes between the two appended stations, the 20 and 40 dbar properties below the lowest common pressure of the station pair are smoothed with a cubic spline interpolation over the property values 40 dbar above and 60 dbar below the lowest common pressure. This has a negligible effect on transport anomalies.

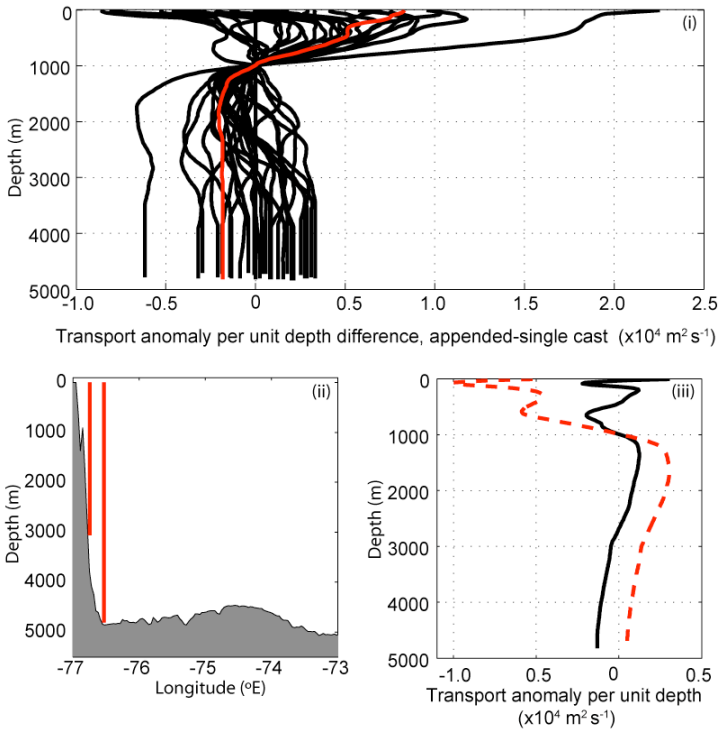

Figure 5.20 *Comparison of transport anomalies resulting from appending CTD casts down the slope with those from a single offshore station. (i) Difference between transport anomaly per unit depth profiles computed using a single end station that resolved 4700m, and a station constructed by appending a middle and deep end station. All transport anomalies are referenced to 1000 dbar and the specific volume anomaly reference curve of Figure 5.19. The red line is the difference for 28th February 1990, using stations at 26.55°N, 76.75°W, 11km offshore with depth 3061m and at 76.53°W, 33km offshore with depth 4815m, locations plotted with topography in (ii). The individual transport anomaly per unit depth profiles for these stations are in (iii), solid line: appended cast, dashed line: single station.*

CTD stations of 28th February 1990 illustrate the error that could result if we did not follow the method of crawling down the slope. Both stations are along the 26.5°N line, 11 and 32 km from the 800m isobath (Figure 5.20(ii)). The discrepancy between the transport anomaly per unit depth profiles from the appended and single CTD stations (Figure 5.20(iii)) is due in large part to a warm anomaly in the offshore profile between

1000 and 1307 dbar of approximately 0.4ºC, resulting in a difference between the deep layer transport anomalies of 3 Sv. We argue that carrying this warming signal in dynamic height into the lower layer anomaly is unrealistic since the majority of shear in the profiles is found above 2000m - note the similarity in shape of the profiles below 1500m despite originating from different casts above 3060m (Figure 5.20(i)). The above cast pair is not an extreme case when compared with the difference between methods for all station pairs (Figure 5.20 (i)) which reaches -10 Sv in one case (appended minus single cast), with group mean and standard deviations of 0.4 Sv and 3.7 Sv respectively.

We believe that transport anomalies computed from CTD casts combined in this way, with that closest to the boundary deeper than 3000 m used to its full depth and the next offshore station to reach 4700m appended to its base, provide the best representation of boundary conditions, as required to resolve basin wide baroclinic flows.

5.3.3.3 Transport errors

As reviewed in Section 5.3.1 end stations are selected so as to minimise the flow inshore of the station. We aimed to limit inshore flows to 1 Sv but the actual error is estimated to be larger due to variability; ± 2, ± 0.2, ± 2 and ± 3 Sv for the upper, intermediate, middle and deep layers respectively (Table 5.5). There remains an error due to accuracy of temperature, pressure and salinity observations used to compute dynamic height. These are estimated as in Section 5.2.3.2 with offsets of temperature, salinity and pressure of 0.02ºC, 0.005 and 3.5 dbar respectively (Table 5.7). For the deep layer there is an additional error due to flows below 4700m which are not resolved by end stations at this boundary since zonally integrated meridional transport profiles for the full section at 25ºN show LNADW transport down to approximately 5000m (Figure 3.11). Transport between 4700m and 5000m for the 1981, 1992, 1998 and 2004 sections is -1.3, -1.2, 0 and 0.8 Sv respectively (omitting the 1957 section due inferior resolution of bottom topography). These give a rms error of 1.0Sv for LNADW transport due to excluding the component below 4700m. The combined errors from all sources are provided in Table 5.7.

There are two 2-3 day periods during which CTD stations were taken at different latitudes of the western boundary but still within our study region at distances offshore

suitable for use as end stations (Table 5.8). The variability in layer transport anomalies from these stations provides support for the estimated errors incurred through application of the end station method (Table 5.7). For each group of stations, the transport range is within two times the expected error, consistent with the actual transport anomaly lying within the bounds set by the mean of the group ± the calculated error. The only exception occurs for the deep layer, June 1990 when a transport range of 8.9 Sv is seen but this is only marginally larger than two times the expected error of 8.4Sv for this group.

Depth layer (m)	$\Delta T = 0.002$ $\Delta S = 0$ $\Delta p = 0$	$\Delta T = 0$ $\Delta S = -0.005$ $\Delta p = 0$	$\Delta T = 0$ $\Delta S = 0$ $\Delta p = 3.5$	Obs. error	Location error	Total error
0-800	0.0	0.3	0.0	0.3	2.0	2.0
800-1100	0.0	0.1	0.0	0.1	0.2	0.2
1100-3000	0.1	1.2	0.1	1.3	2.0	2.4
3000-4700	0.2	2.8	0.2	2.8	3.0	4.2

Table 5.7 *Estimated end station layer transport anomaly errors all in Sverdrups. Columns 2 to 4 are the root mean square errors resulting from addition of temperature, salinity or pressure offset to western boundary CTD casts, with the combined error, due to measurement errors and calibration of the CTD salinity (obs. error) in column 5. The location error of column 6 is that due to end station offshore position (Section 5.3.1) and the Total error (column 7) is the combination of Location and Observational errors, for the 3000-4700m layer this also includes the 1 Sv error due to flows between 4700 and 5000m.*

	Date	Latitude	Distance (km)	Transport anomaly (Sv)	Transport range (Sv)
Upper layer	28-Jun-90	24.26	2	-0.7	3.9
	29-Jun-90	25.51	14	3.2	
	30-Jun-90	26.49	13	0.4	
	11-Aug-92	26.54	2	1.7	0.9
	14-Aug-92	24.55	7	2.6	
Middle layer	27-Jun-90	24.25	14	2.2	4.5
	29-Jun-90	25.51	14	-2.3	
	11-Aug-92	26.50	14	-0.9	0.7
	14-Aug-92	24.55	7	-1.6	
Deep layer	27-Jun-90	24.25	14	5.7	8.9
	29-Jun-90	25.49	19	-3.2	
	11-Aug-92	26.46	25	-2.9	1.9
	14-Aug-92	24.61	24	-4.8	

Table 5.8 *Variability in end station layer transport anomalies for stations taken within 3 days, at different latitudes. Note that for the deep layer distance refers to the offshore, deeper station, of the appended pair.*

In summary we accept that the variability seen at any one time is large within the layer transport anomalies (Table 5.8), but the estimated errors for this method appear to

account for this. The errors are dominated by the location component (with salinity calibration also important for LNADW) and are due predominantly to having to use CTD stations not immediately adjacent to the boundary. This is however necessary if we are to have enough historical end stations at the west to examine variability throughout the 25 years.

5.4 SUMMARY

We have carefully selected CTD casts suitable for use as end stations at both boundaries of 26.5ºN in the Atlantic over the last 25 years. To minimise measurement errors, deep salinities are calibrated to a constant deep θ-S relationship at the east, while the significant freshening trend observed at the west of LNADW (both DSOW and ISOW) at approximately 0.003 per decade on potential temperature surfaces is incorporated in the calibration procedure at the west. Transport anomalies (with errors estimates) are computed relative to the group mean for each of the upper, intermediate, middle and deep layers at each boundary although data coverage is notably better at the west; 29 or more stations for each layer, compared to 9 to 11 at the east.

CHAPTER 6: **Methods and Data - Dynamic Height Moorings**

6.1 INTRODUCTION

Resolution of both interannual changes and possible sub-annual signals from datasets comprising between 9 and 39 observations in 25 years, as is the case for the end station layer transport anomalies (Chapter 5), is anticipated to be difficult. Transport anomalies with higher temporal resolution are required, for which we turn to dynamic height moorings introduced in Section 4.4. This chapter describes the associated methods, including selection of suitable mooring datasets, estimation of salinity and missing pressure records and their subsequent vertical interpolation, before computation of dynamic height for geostrophic transport anomalies. At the west the layers are the same as for end stations (upper, intermediate, middle and deep), but at the east we are only concerned with increasing the dataset for the upper layer since variability of lower limb MOC transports originating at the eastern boundary is negligible (Section 7.4.1). The procedures developed are described in detail first for the eastern boundary (Section 6.2), then with more brevity for the west (Section 6.3), with summarising comments in Section 6.4.

6.2 THE EASTERN BOUNDARY

6.2.1 Introduction

Unfortunately no suitable moored time series of temperature and pressure observations for resolution of upper layer transport anomalies are available within our eastern boundary study region of Figure 5.6. Although there have been RAPID moorings at the east of the 25ºN section since 2004, the first year's deployment lost all data above 500m. Other projects such as ESTOC and CANIGO with moorings deployed around the Canary Islands are also not suitable due to intervening topography between the east and

western boundaries. The only other mooring with long term deployments in the eastern basin of the subtropical north Atlantic is Kiel-276. At a nominal location of 33ºN, 22ºW this mooring has been maintained since 1980 (Armi and Zenk, 1984; Siedler et al., 1985; Zenk and Müller, 1988; Müller and Siedler, 1992; Siedler et al., 2005).

The location of Kiel-276 prevents a transport anomaly time series from being treated analogously to the end station transport anomalies since it sits offshore of the easternmost recirculation branch of the subtropical gyre (see Figure 5.1 in Section 5.2.1). Instead since Kiel-276 is located south of the Azores Front (Siedler et al., 2005) we aim to constrain variability of the Azores Current by assuming no change in dynamic height on its northern boundary in an approach equivalent to Curry and McCartney's (2001) index for NAC transport but without the northern station. The difficulties associated with this approach are two fold. Firstly there is no northern dynamic height station, and secondly the Azores Front is known to meander north-south in the region of Kiel-276 (e.g. Tychensky et al., 1998; Siedler et al., 2005). We recognise the limitations of this approach but it is the best data set we have found to quantify the variability at the east.

In the following we describe processing details of the Kiel-276 temperature and pressure time series with the ultimate aim of quantifying the timescale and magnitude of any changes in subtropical gyre recirculation in the eastern north Atlantic between 1980 and 2000. Transport anomaly computation follows equation (4.5) and thus a positive value represents a strengthening of the gyre - warming in the thermocline waters increases dynamic height relative to 800m which with no change at the (imagined) northern dynamic height profile equates to an increased eastward transport in the upper waters and a stronger subtropical gyre recirculation.

6.2.2 Data Inventory

The Siedler et al. (2005) version of the Kiel-276 mooring dataset from April 1980 to April 2000 has kindly been made available to this project. 21 mooring deployments were made over 20 years at locations between 33 and 34ºN within ± 0.2º of 22ºW with temperature measured at up to 8 points through the water column and with 1 to 3

pressure sensors as shown in Figure 6.1 (except for November 1985 to January 1989 when no pressure records were obtained).

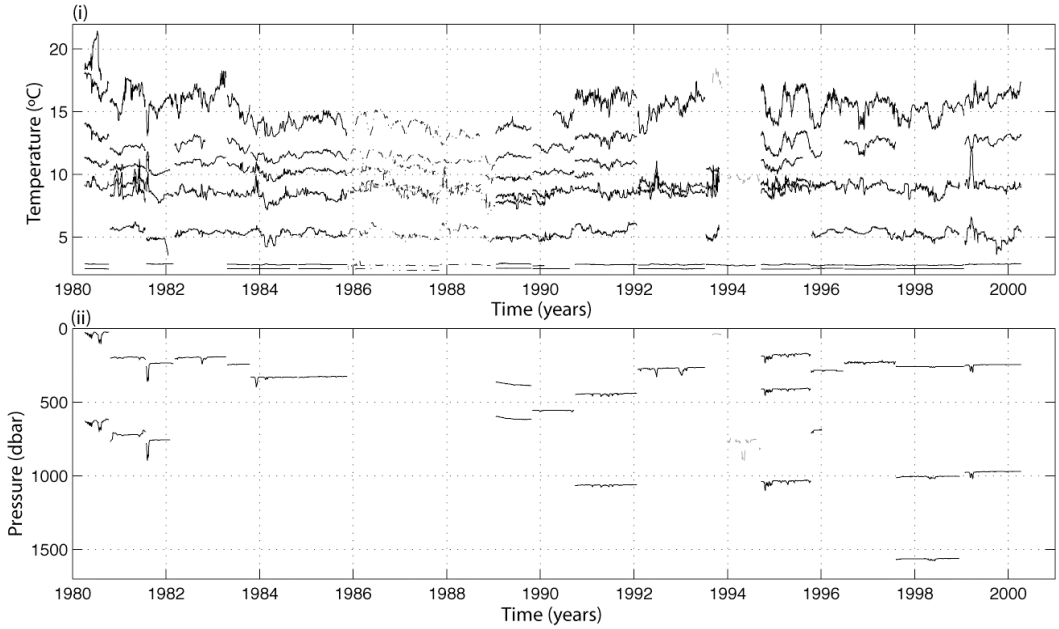

Figure 6.1 *Data coverage of temperature (i) and pressure (ii) from mooring Kiel-276. Dashed-dot lines in temperature correspond to the time when no pressure records were obtained, and dashed lines in temperature and pressure, when upper instrument (including the pressure record) is from a different mooring.*

Deployment	Start Date	End Date	Nominal Instrument Depths (m)							
264010	4-Apr-80	12-Oct-80	24*	124	376	627*	926	2966	4707	
276010	21-Oct-80	23-Jul-81	195*	499	697*	995	1095	1591		
276020	31-Jul-81	25-Feb-82	243*	550	748*	1149	1665	3020		
276030	9-Mar-82	13-Apr-83	194*	428	629	1032	1535			
276040	23-Apr-83	15-Oct-83	243*	475	675	1075	1575	2980	5175	
276050	24-Oct-83	21-Oct-84	327*	560	760	1160	1660	3050		
276060	30-Oct-84	12-Nov-85	327*	562	764	1168	1670	3080	5224	
276100	18-Jan-89	23-Oct-89	367*	595*	800	1100	1200	1700	3050	5185
276110	31-Oct-89	21-Sep-90	320	555*	755	1055	1155	1655	3045	5190
276120	29-Apr-90	23-Jan-92	215	445*	645	965	1065*	1565	3000	
276130	1-Feb-92	7-Jul-93	270*	1000	1100	3000	5185			
276150	20-Sep-94	11-Oct-95	240*	470*	670	970	1120*	3030	5275	
276160	16-Oct-95	22-Jun-96	270*	500*	1000	1600	3000	5185		
276170	30-Jun-96	4-Aug-97	270*	500	1000	1600	3000	5185		
267180	9-Aug-97	21-Jan-99	270*	1000*	1600*	3000	5185			
276190	21-Jan-99	10-Apr-00	270*	500	1000*	1600	3000			

Table 6.1 *Nominal instrument depths and sampling periods of Kiel-276 deployments used in this study. Depth levels with both temperature and pressure sensors are denoted with *, otherwise temperature only is measured. Deployments 276070-276090 inclusive are excluded from this table due to the absence of any pressure records as is 276140.*

Subsequent analysis (Section 6.2.3) shows that mooring motion under strong currents can induce pressure deviations up to 120m. With no way of correcting temperature

records for such possible motion, we do not use data from the time periods without pressure records. Such times include deployment 276140 (September 1993 to September 1994) and, while an additional mooring was deployed 0.8º south of Kiel-276, we do not combine the records to prevent introduction of unquantifiable errors. Aside from these periods, data gaps between deployments are at most 12 days (Figure 6.1 and Table 6.1). Data obtained is in a workable format having undergone quality control and processing in previous studies (Armi and Zenk, 1984; Siedler et al., 1985; Zenk and Müller, 1988 and Müller and Siedler, 1992).

6.2.3 Initial data processing – missing pressure estimation

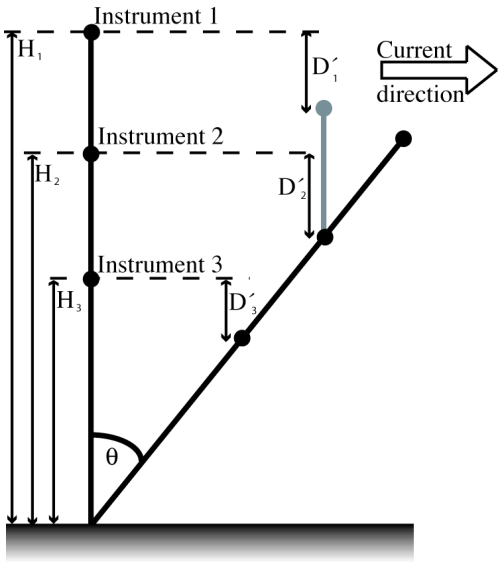

Figure 6.2 *Schematic of alternative pressure estimation models. With a background flow in the direction shown, the pendulum method assumes a uniform inclination of the mooring to the vertical at angle θ, while the pmin method assumes that above a certain pivot depth, the surface flotation is sufficiently strong that the mooring remains vertically aligned. The alternative positions with the pendulum model (black) or the pmin method (grey) are shown for Instrument 1. D' is the vertical displacement of a given instrument from its minimum depth, assumed to occur when the mooring is upright. If D' of one instrument is known, that of the remaining instruments can be estimated according to the preferred model.*

To obtain a dynamic height time series from the Kiel-276 data set a pressure record is required for all measured temperature records. With one good pressure record for each mooring deployment we can estimate the vertical mooring structure through application of either the pendulum or pmin models (explained in Figure 6.2) and thus obtain missing pressure records while incorporating the effects of mooring inclination in background flows. To evaluate alternative models we make use of deployments with

pressure sensors at multiple depths after initial screening for bad data which is rejected. Records are defined as bad if they drift by more than 10 dbar over the deployment duration or are unstable. This results in rejection of the 240 and 1120 m pressure records of deployment 276150, that at 697 m of deployment 276010 and at 500 m of 276160.

To explain the possible pressure models consider a mooring with two pressure records, from which we compute the deviation from the minimum depth of the upper and lower instruments, D_1' and D_2' respectively (in metres). The depth changes of either instrument can then be estimated using both of the methods of Figure 6.2, and their relative performance evaluated. According to the pmin method

$$\hat{D}_1' = D_2' \text{ and } \hat{D}_2' = D_1' \tag{6.1}$$

while the pendulum model (following notation of Figure 6.2) states that

$$\hat{D}_1' = D_2' \frac{H_1}{H_2} \text{ and } \hat{D}_2' = D_1' \frac{H_2}{H_1} \tag{6.2}$$

The standard error of the pmin method is equal for both instruments;

$$s_\varepsilon = \sqrt{\frac{1}{n-1}\left(D_1' - D_2'\right)^2} \tag{6.3}$$

while for the pendulum method the standard error of the fit is dependent on whether we are extrapolating upwards or downwards, (with $s_{\varepsilon(up)}$ the standard error of estimating the upper instrument's pressure from that of the lower instrument and vice-versa);

$$s_{\varepsilon(up)} = \sqrt{\frac{1}{n-1}\left(D_2' \frac{H_1}{H_2} - D_1'\right)^2} \quad s_{\varepsilon(down)} = \sqrt{\frac{1}{n-1}\left(D_1' \frac{H_2}{H_1} - D_2'\right)^2} \tag{6.4}$$

the results of which are summarised in Figure 6.3 and Table 6.2.

In all cases except (ii) of Figure 6.3 the ratio of D_1' to D_2' is significantly greater than 1.0 at the 95% confidence level (Table 6.2). This means that the upper instrument experiences larger depth changes than the lower instrument due to currents overcoming mooring flotation. Thus the pendulum method is more appropriate than the pmin method. Slopes of the least squares regression of D_1' to D_2' are in good agreement with the ratio of H_1 to H_2. Following equation (6.2), the pendulum method sets the y-intercept of Figure 6.3 to zero and the linear regressions all give the intercept to be less

than ± 2 m. A non-zero offset may be due to inaccurate measurement of instrument separation before deployment rather than the pendulum method being inappropriate. 2 m is very small given a mooring cable over 5km long - which we attribute in large part to the careful data processing and nominal depth adjustments made by Siedler et al. (2005). The standard error of $\hat{D}'$ from the pendulum method is marginally smaller than, or equal to, that of the pmin model, supporting preference of the pendulum model. Both are smaller than 6 m for all deployments with multiple good pressure records. We note the validity of the pendulum model over a range of depth intervals from 270-1000m in the case of 272190, and down to 1600m in 276180.

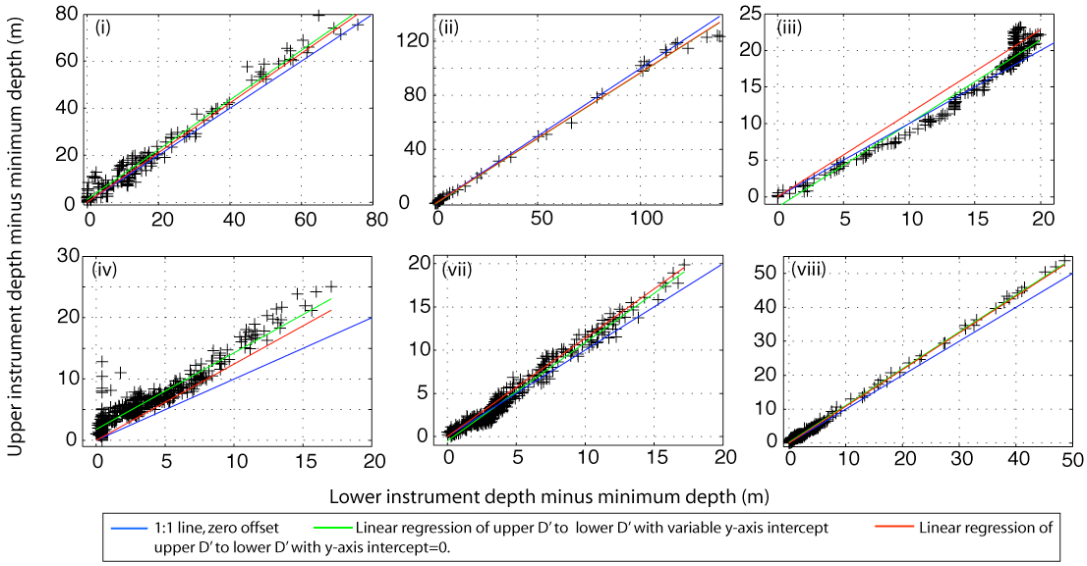

Figure 6.3 *Correlation between upper and lower instrument D', with regression lines overlaid. Data sets in each subplot correspond to those of Table 6.2 which also reports regression coefficients.*

Following the above evaluation, we compute missing pressure records corresponding to each pressure record, and replace those deemed bad on the basis of drift, discontinuities or sticking, using the pendulum method applied to depth changes computed from the most stable pressure record of each deployment (Table 6.3). The estimated error in pressure is less than 6 m (dbar).

Deployment (plot)	N	Nominal instrument depths (m)		H_1/H_2	Slope ± C.I.	y-intercept ± C.I	r^2	$s_{\varepsilon(pmin)}$ (m)	$s_{\varepsilon(pendulum)}$ (m)	
		Upper	Lower						Upper	Lower
(i) 264010	166	24	627	1.1	1.1 ± 0.0	1.2 ± 0.7	0.971	4.1	3.5	3.1
(ii) 276020	184	243	748	1.1	1.0 ± 0.0	-0.2 ± 0.3	0.997	2.0	5.2	4.7
(iii) 276100	279	367	595	1.1	1.1 ± 0.0	-1.4 ± 0.4	0.965	1.7	0.9	1.4
(iv) 276120	482	445	1065	1.2	1.2 ± 0.0	1.8 ± 0.2	0.893	3.1	1.1	2.3
(v) 276180	491	1000	1600	1.2	1.1 ± 0.0	-0.5 ± 0.1	0.971	0.8	0.4	0.7
(vii) 276190	440	270	1000	1.2	1.1 ± 0.0	0.3 ± 0.1	0.996	1.0	0.7	0.7

Table 6.2 *Comparison of pendulum and pmin methods for mooring pressure model. For the selected deployments corresponding to the subplots of Figure 6.3, the instrument height ratio is based on a water depth of 5290m and the notation is from equation (6.2). For the N good data points of the two records, the linear regression of D1' to D2' coefficients, slope and y-intercept with 95% confidence intervals correspond to the green lines of Figure 6.3. The standard error is that resulting from using the pmin or pendulum model to estimate measured pressure records following equations (6.3) and (6.4). The upper error is that obtained using the lower record D' to predict the upper with the pendulum model.*

Deployment	Reference Instrument	Pressures computed
264010	24	124, 376, 926 2966, 4707
276010	195	499, 995, 1095, 1591
276020	243	550, 1149, 1665, 3020
276030	194	428, 629, 1032, 1535
276040	243	475, 675, 1075, 1575, 2980, 5185
276050	327	560, 760, 1160, 1660, 3050, 5240
276060	327	562, 764, 1168, 1670, 3080, 5240
276100	367	800, 1100, 1200, 1700, 3050, 5185
276110	555	320, 755, 1055, 1155, 1655, 3045, 5190
276120	445	215, 645, 965, 1565, 3000
276130	270	1000, 1100, 3000, 5185
276150	470	240, 670, 970, 1120, 3030, 5275
276160	270	500, 1000, 1600, 3000, 5185
276170	270	500, 1000, 1600, 3000, 5185
276180	1000	270, 1600, 3000, 5185
276190	270	500, 1600, 3000

Table 6.3 *Reference instruments and estimated records of Kiel-276 mooring deployments following the pendulum method. Records are replaced if bad.*

6.2.4 Initial data processing – salinity estimation

Computation of dynamic height anomalies requires a vertical density profile as input, we have temperature and pressure but lack salinity. A comprehensive study of the computation of geopotential anomalies from temperature and pressure records in the north east Atlantic (Siedler and Stramma, 1983) found that errors for the 0-1000 dbar layer were minimised at the location of Kiel-276 by estimation of salinity from a climatological T-S relationship (compared to the alternatives of salinity-depth or

density-depth relationships). We follow this method, using an iterative approach with reference T-S and θ-S curves constructed from CTD stations between 32-34ºN and 21 to 23ºW obtained from the World Ocean Database, 2001 and Hydrobase 2003. Of the 62 stations obtained, 5 are rejected due to possibly sampling a meddy. Meddies are transient events at Kiel-276 and the climatology need not account for them since they are rejected from the computed time series (Section 7.4.2.2). Positive meddy identification in the CTD stations is made when a salinity anomaly relative to the mean of all stations is greater than two standard deviations on at least one pressure level between 800 and 1400 dbar. Excluding these stations the remaining 57 CTD casts have good interannual and seasonal coverage from June 1981 to July 2003 (Figure 6.4).

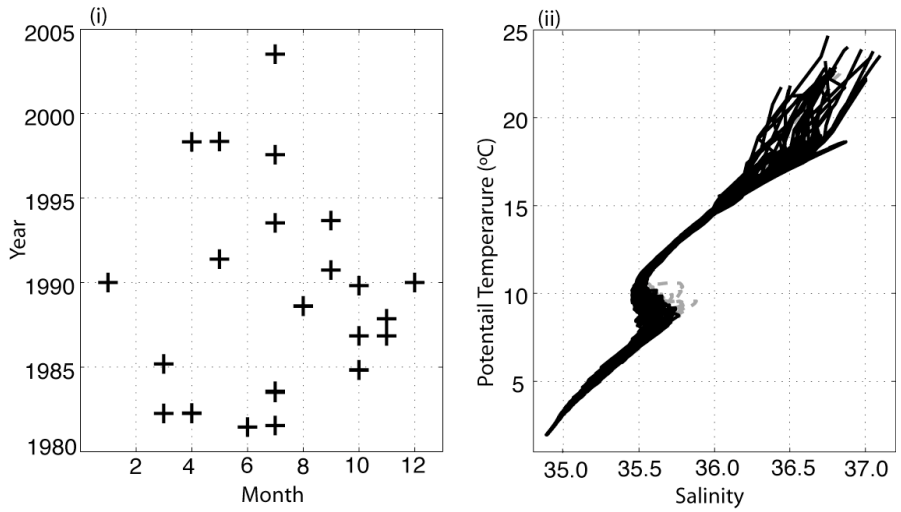

Figure 6.4 *CTD stations near the Kiel-276 mooring (± 1º latitude or longitude) used for construction of the T-S and θ-S reference curves. (i) shows temporal coverage, seasonal vs. interannual and (ii) the θ-S curves. Stations sampling significantly more Mediterranean Water, grey dashed lines in (ii) are probably associated with meddies and are excluded.*

We use the procedure below to construct the T-S and θ-S curves of Figure 6.5, broadly following that developed by Emery and Wert (1976). Average salinity is computed from the 57 20-dbar resolution CTD casts in 0.1ºC temperature intervals up to 18ºC and 0.5ºC levels above this. Points outside the mean ± two standard deviations are rejected. A 9 point running mean is then applied twice to smooth in the vertical. The standard deviation of salinity in Figure 6.5(i) is less than 0.05 below 17ºC (approximately 220m) and smaller than 0.01 below 4ºC (approximately 2000m). The influence of variable concentrations of Mediterranean water between 6 and 11ºC (650 to 1500m) is clearly visible. Construction of the reference curve following the above procedure using

summer stations (April-September inclusive) and winter ones does not provide any justification for employment of a seasonally varying reference curve (Figure 6.5, insert (ii)).

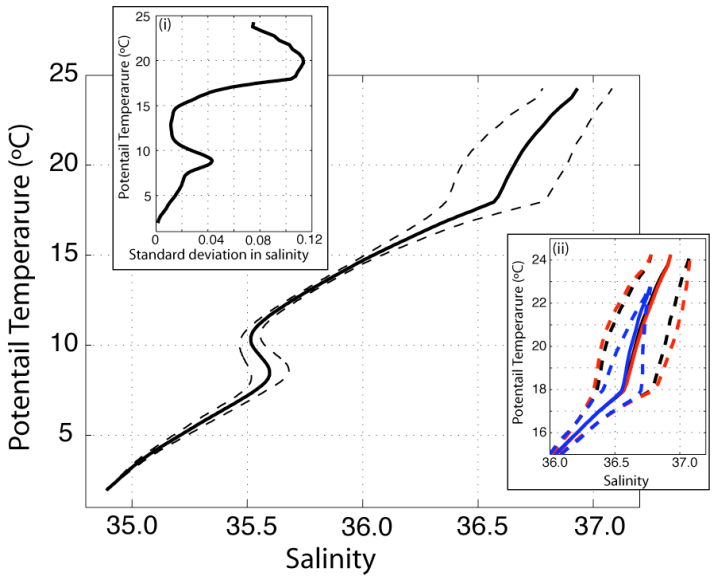

Figure 6.5 *The potential temperature-salinity reference curve (solid line) ± two times the standard deviation (dashed lines). The standard deviation is plotted separately in insert (i) while insert (ii) is also the mean reference curve ± two standard deviations but computed for the summer stations (red) and winter stations (blue) with all stations in black.*

Since both the T-S and θ-S reference curves show a unique salinity for all temperatures, salinity can be estimated for every measured temperature and corresponding measured or estimated pressure using an iterative process. The initial salinity estimate is made from linear interpolation of the reference T-S curve at the measured temperature. The corresponding potential temperature is computed using the seawater routines, and a new salinity estimate made from the reference θ-S curve. While the difference between the salinity estimates is greater than 0.0001, the θ-S estimation loop is repeated using the new salinity, as summarised in Figure 6.6.

The error in salinity associated with employment of the reference T-S and θ-S curves and iteration procedure is estimated by applying the procedure to the reference CTD stations (Figure 6.7). The influence of varying concentrations of Mediterranean Water near 1000 dbar is evident where the salinity error (mean ± one standard deviation) increases to ± 0.05 (Figure 6.7). The error is also large in the upper layer, exceeding 0.1

on pressure levels at the surface due to seasonal changes. The implications of this are discussed in Section 6.2.6.

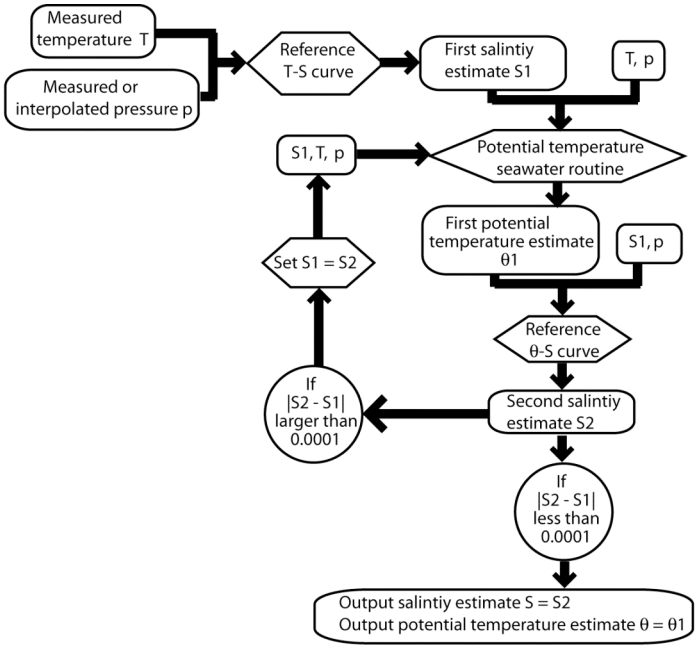

Figure 6.6 *Process of estimation of salinity (S) and potential temperature (θ) from temperature (T) and pressure (p) inputs using reference θ-S and T-S curves.*

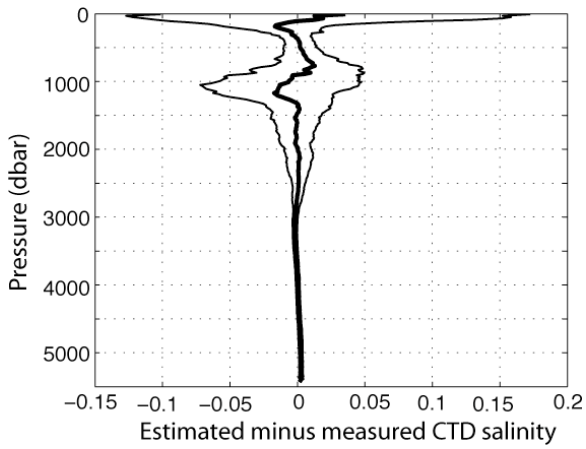

Figure 6.7 *Error in salinity of CTD casts when estimated using T-S and θ-S reference profiles relative to measured salinity. Mean of 57 CTD casts is plotted (heavy line) with ± one standard deviation. The mean is not identically equal to zero due to smoothing employed in calculation of the reference curves.*

6.2.5 Initial data processing – vertical interpolation

With temperature and pressure measured at discrete depths up to 730m apart in the vertical and the means to calculate salinity at these points, specific volume anomaly time series are available at a number of levels on the mooring. How to integrate these

vertically (interpolation between the measurement levels as well as extrapolation above the shallowest instrument) to give dynamic height time series from which we may compute transport anomalies is next addressed.

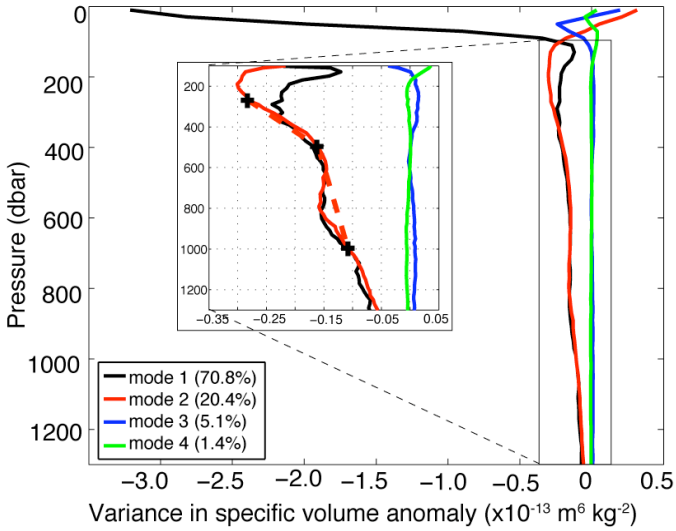

Figure 6.8 *EOF's of specific volume anomaly computed over 0-1300 dbar, after subtraction of the mean profile. In the expanded section between 100 dbar and 1300 dbar nominal instrument depths of 270, 500 and 1000m are overlaid joined by straight dashed lines, representing the profile produced by linear interpolation between the data points.*

Examination of the vertical structure of specific volume anomaly changes as a function of pressure, relative to the mean, from the CTD casts of Section 6.2.4 (Figure 6.8), shows that while the first two EOF's together account for more than 90% of the variance and follow a similar structure below 300 dbar, linear interpolation (the simplest possible model) between measurement levels may not be suitable. The nominal instrument depths plotted on Figure 6.8 of 270, 500 and 1000m represent a typical mooring configuration (Table 6.1) and show that most of the vertical structure would be captured by linear interpolation. The same cannot be said for low resolution cases such as deployment 267180 with no instruments between 270 and 1000m (Table 6.1). An alternative to linear interpolation is therefore sought, such as interpolation with a vertical temperature gradient ($\partial T / \partial p$) climatology according the equation (6.5), where 1 and 2 identify two mooring instrument levels following Johns et al. (2005):

$$T(p) = \sum_{i=1}^{2} w_i \left[T(p_i) + \int_{p_i}^{p} \frac{\partial T}{\partial p}(T)dp \right]$$

$$\text{or} \quad T(p) = \sum_{i=1}^{2} w_i \left[T(p_i) + \int_{p_i}^{p} \frac{\partial T}{\partial p}(p)dp \right] \tag{6.5}$$

$$\text{and } w_i = 1 - \left| \frac{p - p_i}{p_2 - p_1} \right|$$

The alternative forms of (6.5) account for whether the climatology is constructed as a function of pressure or temperature. Previous investigators (e.g. Zantopp and Leaman, 1984; Johns et al., 2005; Kanzow et al., 2006) constructed $\partial T / \partial p$ climatologies in temperature co-ordinates rather than pressure since Zantopp and Leaman (1984) found this better resolved the 18ºC water. Our interest in the upper water column and the idea that seasonal stratification may have a more robust vertical structure with respect to pressure rather than temperature, combined with the expected sensitivity of vertical interpolation employing a lookup procedure in temperature to small scale temperature irregularities, leads us to consider the relative merits of both climatology constructions. Accordingly we construct climatologies both as a function of pressure and temperature (Figure 6.9b) from the CTD casts between 31 and 33ºN, 21 and 23ºW deeper than 1300 dbar (total 52, plotted in Figure 6.9a) and compare the resulting errors in employment of equation (6.5).

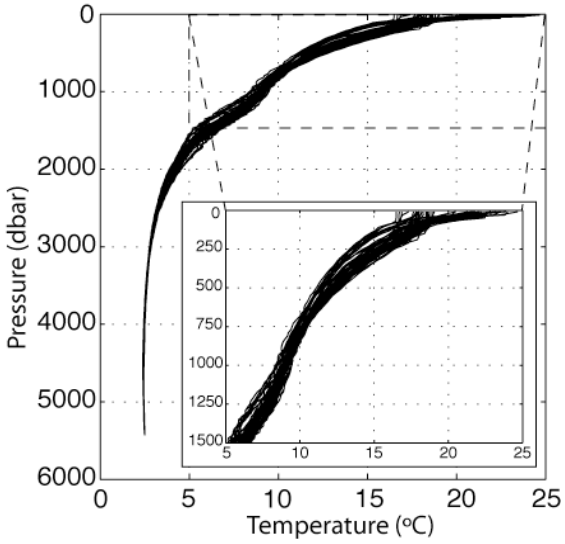

Figure 6.9a *Temperature profiles of the CTD casts used to compute the climatologies of Figure 6.9b.*

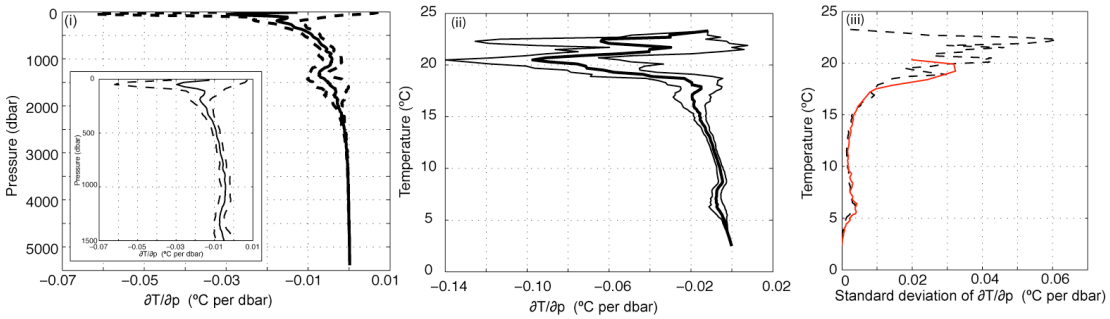

Figure 6.9b *Construction of a ∂T/∂p climatology, as a function of pressure (i) or temperature (ii). For vertical levels and smoothing employed refer to text. The mean (solid lines) with limits of ± 2 standard deviations (dashed or thin lines) are shown. Standard deviations of the climatologies are compared in (iii) with that constructed as a function of pressure plotted at the mean temperature for each pressure level (red solid line), while the black dashed line shows the standard deviation of the temperature co-ordinate reference curves.*

6.2.5.1 The $\partial T/\partial p(p)$ climatology

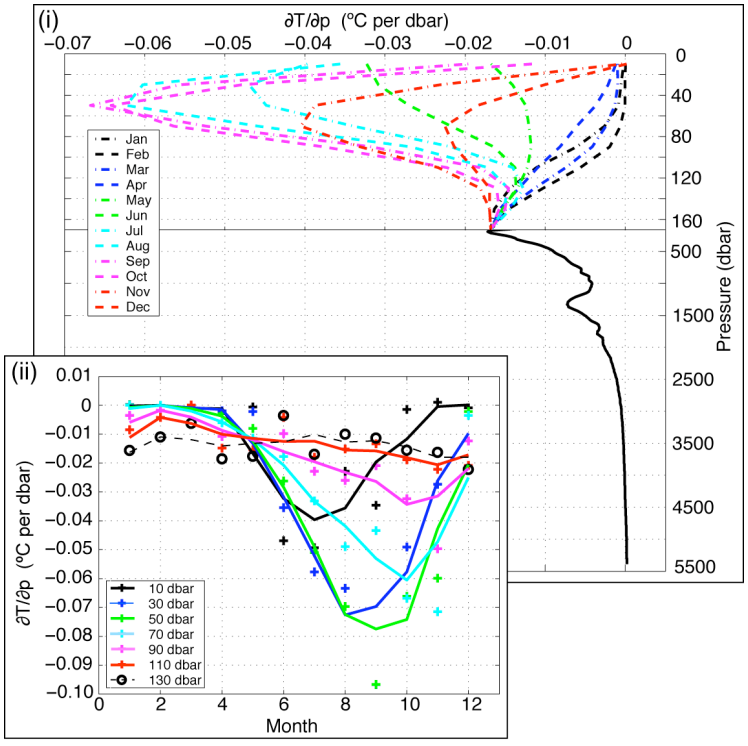

Figure 6.10 *The monthly reference ∂T/∂p climatology constructed as a function of pressure (i). Note the expanded vertical scale above 170 dbar, below which there is no temporal dependence. Construction details (see text) are illustrated in (ii). The* **+** *and* **o** *are the monthly mean ∂T/∂p values at each depth, which are smoothed with a ± one month running mean to give the coloured lines. Resulting monthly values are then smoothed in the vertical to give (i).*

Construction of this climatology entails computation of ΔT for each 20 dbar level of the CTD casts. Points outside the mean ± two standard deviations are rejected and the mean

recomputed and smoothed once with a three point running mean. The resulting profile with variability shown by two times the standard deviation, smoothed as the mean is shown in Figure 6.9b(i). The upper water variability is likely to be seasonal so we also construct monthly mean profiles from the 57 CTD casts deeper than 300 dbar in the same way, although February is the mean of January and March since there are no CTD casts that month. The monthly profiles are temporally smoothed with a ± one month running mean (to reduce the impact of possible interannual variability on the climatology from months where we have few CTD casts) into the seasonally varying $\partial T/\partial p(p)$ climatology of Figure 6.10(i). ∂T/∂p on 20 dbar levels are shown in Figure 6.10(ii) before and after temporal smoothing. The smoothed monthly resolution climatology is used for the upper 150 dbar of the ∂T/∂p reference, and below this the mean $\partial T/\partial p(p)$ of Figure 6.9b(i) is appended. Finally to ensure a smooth profile at the join between the upper variable section and deep constant parts, we apply a ± 20 dbar running mean to all months, resulting in the $\partial T/\partial p(p)$ climatology of Figure 6.10(i).

From Figure 6.10 we see that the $\partial T/\partial p(p)$ climatology captures the expected annual stratification cycle of the upper water column. Waters are vertically well mixed from January through April when we see the onset of summer stratification of the upper 100 dbar, with vertical gradients strongest between 30 and 70 dbar. Stratification peaks towards early autumn and the peak is later deeper in the water column (in July, August, September and October at 10, 30, 50 and 70 dbar respectively) consistent with surface wind mixing eroding stratification downwards. With weakened incoming solar radiation in autumn, rapid vertical homogenisation results through to December (Figure 6.10).

6.2.5.2 The $\partial T/\partial p(T)$ climatology

The $\partial T/\partial p(T)$ reference curve of Figure 6.9b(ii) is obtained by computing temperature changes in 20 dbar levels at the mean temperature of the two levels, points are grouped in 0.2ºC intervals and smoothed vertically with a three point running mean after rejection of points outside the mean ± two standard deviations. Preliminary bi-monthly mean profiles showed no difference between those of December/January,

February/March or April/May. Therefore to construct the climatology of Figure 6.11 we work with a winter mean profile of December to May inclusive and bi-monthly means for the rest of the year. These curves are smoothed twice vertically with a 5 point (1ºC) running mean before appending to the lower ∂T/∂p profile below 17.3ºC. A final smoothing is done with a 1ºC running mean over data points up to 0.4ºC away from 17.3ºC to produce the seasonally dependent reference curves plotted in Figure 6.11.

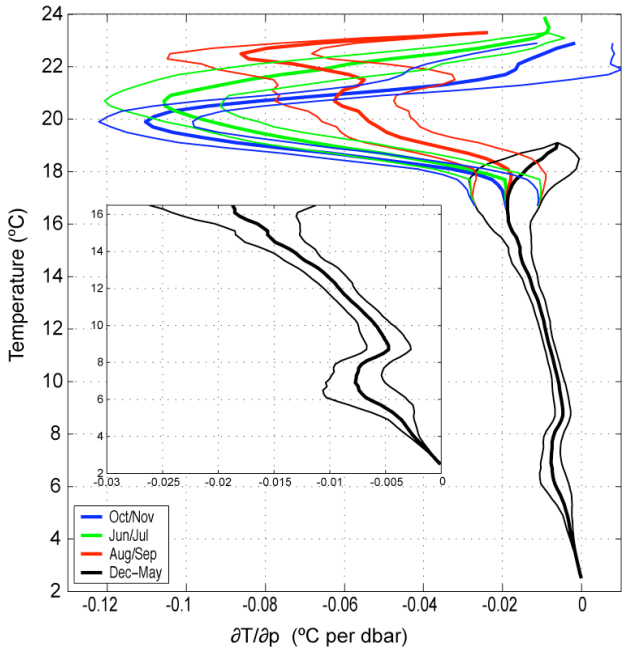

Figure 6.11 *The monthly reference ∂T/∂p climatology constructed as a function of temperature, with limits of ± one standard deviation.*

6.2.5.3 Climatology comparison

The errors associated with vertical interpolation using both climatologies (Figure 6.12) are assessed by subsampling the reference CTD stations at nominal depths sampled by Kiel-276 and recomputing temperatures at 20-dbar resolution according to equation (6.5). Between each instrument pair we interpolate downwards from the upper measurement level in 20 dbar increments keeping the bottom temperature and pressure fixed, best illustrated with the following example. With mooring observations at 270 and 1010 dbar, we first compute temperature at 290 dbar from equation (6.5) with the 270 and 1010 dbar observations as instruments 1 and 2, then temperature at 310 dbar is computed by re-application of equation (6.5) with instrument 1 as the previously estimated 270 dbar observation, and instrument 2 still as 1010 dbar. This process is continued downwards in 20 dbar increments until we reach 990 dbar. Above the depth

of the upper instrument (l in equation 6.6), we must rely on extrapolation upwards using the value of temperature computed a cycle before (20 dbar below), and so on to the surface:

$$T_{l-20} = T_l + \left.\frac{\partial T}{\partial p}\right|_{T=T_l} \Delta p \qquad \text{with } \Delta p = -20 \text{ dbar.} \tag{6.6}$$

The ∂T/∂p climatology constructed as a function of pressure performs better in the upper 100 m (where seasonal effects are important) than that constructed on temperature surfaces, with mean errors of -0.5ºC and -1.9ºC respectively (Figure 6.12). This is consistent with our reasons for investigating the use of the former, and we are reassured that the estimated error range of -2 to 0.5ºC at the surface (mean ± one standard deviation) is still notably smaller than the 7ºC range observed in the 10 dbar constituent CTD temperatures (Figure 6.9a). Below this depth, there is little difference in the errors of the alternative climatologies, although that of temperature performs marginally better around 800 m (Figure 6.12). The actual errors are dependent on mooring resolution with effectively no error at each instrument location and maximum errors roughly halfway between instruments.

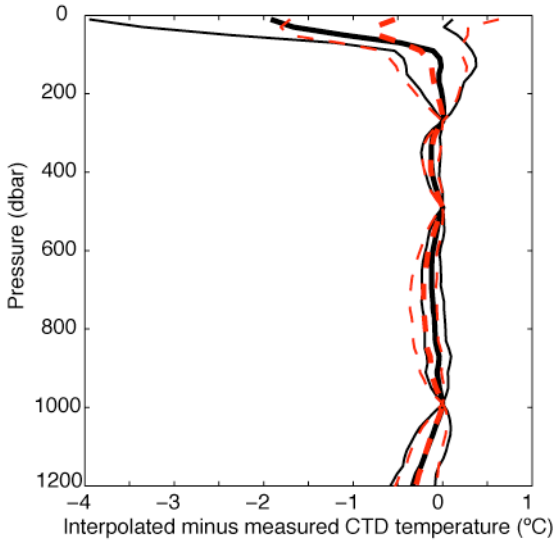

Figure 6.12 *Error in CTD temperature after subsampling temperature and pressure at a typical mooring vertical resolution (270, 490, 990 and 1590 dbar) and recomputing the 20 dbar resolution temperature profile using equation (6.5) with the ∂T/∂p climatology as a function of temperature (black) or pressure (red). The error is the mean of the 44 CTD casts which have depths greater than 1590 dbar (heavy line) with ± one standard deviation (thin lines).*

We adopt the $\partial T/\partial p(p)$ climatology (Figure 6.10) for vertical interpolation of the Kiel-276 mooring data set given the smaller estimated error over the upper 100m (Figure 6.12) and negligible differences in performance with the $\partial T/\partial p(T)$ below this. A formal assessment of the errors associated with the vertical interpolation is presented in Section 6.2.7.

6.2.6 Transport anomaly calculation

Broadly the approach to estimate Kiel-276 transport anomalies follows that applied to the CTD end stations. From the mooring temperature and pressure records, we compute daily dynamic height profiles from 20 dbar interpolated temperatures with salinity estimated from the T-S and θ-S climatologies. Given a dynamic height profile, the 0-800m layer transport anomaly is calculated using equation (4.5) relative to a mean state defined from the CTD stations between 32 and 34ºN, 21 to 23ºW. The upper 800m of this reference specific volume anomaly profile (Figure 6.13) is the mean on 20 dbar pressure levels of the 53 CTD casts deeper than 800 m, and the lower part is the mean of the 33 casts deeper than 5000m. Large variability in the upper 100 dbar is seen due to seasonal effects (Figure 6.13(ii)).

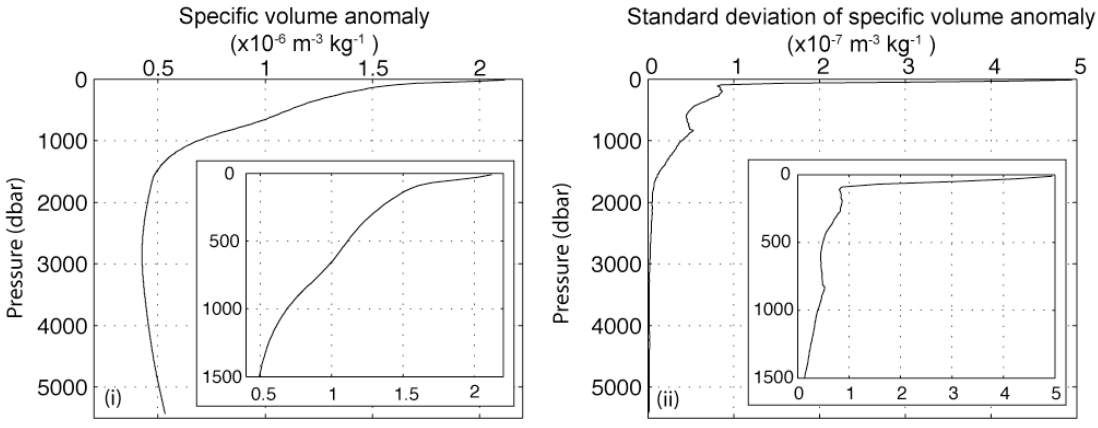

Figure 6.13 *Reference specific volume anomaly profile (i) for Kiel-276 mooring transport anomalies, with upper 1500 dbar expanded in insert. Standard deviation of specific volume anomaly (ii) of constituent CTD casts, again with the upper 1500 dbar expended in the insert.*

Dynamic height profiles are referenced to 1300 dbar for calculation of the transport anomalies. This was the choice of Stramma and Siedler (1988)'s study of seasonal

changes in the subtropical gyre from geostrophic transports, a problem analogous to this one, albeit using CTD stations over a larger region. Their level of no motion followed Stramma (1984)'s earlier search for suitable reference surfaces in the eastern subtropical North Atlantic through combination of the dynamic method and conservation of mass, resulting in 1300 dbar at the location of Kiel-276. Müller and Siedler (1992) found this to be consistent with the first 8.5 years of the Kiel-276 direct current observations, except when meddies pass the mooring (Siedler et al.,1985) but this is not a problem here as such times are excluded from our records (Section 7.4.2.2).

The disadvantage of 1300 dbar as a reference level is that the uncertainty of salinity estimation peaks close to 1100 dbar (Figure 6.7) due to varying concentrations of Mediterranean Water. It is however preferable to the alternative of 800 dbar which would be suitable based on the dynamic method alone, but is not supported by mass conservation according to Stramma (1984). Referencing to the surface is undesirable because seasonal uncertainties in temperature and thus estimated salinity incur a larger error in dynamic height than those of Mediterranean Water and although a reference level of 3200 dbar would be consistent with the end station observations, poor vertical resolution by the Kiel-276 mooring of deep water temperature profiles precludes this. We do however take confidence that the standard error in upper layer transport anomaly of 52 CTD casts referenced to 1300 dbar compared to those referenced to 3200 dbar at Kiel-276 is only 0.9 Sv. Therefore upper layer transport anomalies at Kiel-276 are referenced to 1300 dbar since this reference level gives the smallest uncertainties.

6.2.7 Transport anomaly errors

The various sources of error in calculation of Kiel-276 upper layer transport anomalies are now formally calculated. We follow Johns et al. (2005) in method and compute the error due to temperature measurement accuracy (ε_T), pressure estimation by the pendulum method (ε_p), salinity estimation (ε_S), and vertical interpolation (ε_I). In each case the error is computed as the 0-800m layer transport difference resulting from the error source after calculation of the specific volume anomaly with the following modifications. ε_T equals 0.01ºC which is the assumed temperature sensor accuracy, is added to the CTD measured temperature; ε_p equals 5 dbar and is added to pressure (following Table 6.2) while salinity is recalculated using the T-S and θ-S climatologies

for ε_S. The modifications are made to the smoothed 20 dbar CTD casts except for the vertical interpolation error which is mooring specific. For this, for each deployment temperature and pressure are subsampled at the nominal mooring instrument depths down to the first instrument deeper than 1300 dbar (the reference level), and then interpolated to 20 dbar using the $\partial T/\partial p\,(p)$ climatology, salinity is retained as measured in the original CTD cast and the transport recomputed. This procedure is repeated using all CTD casts at Kiel-276 that resolve the maximum nominal depth of the subsampling with the mean and rms errors of the mooring-independent error sources listed in Table 6.4a and the mooring-specific interpolation error and the combined error in Table 6.4b.

Transport error (Sv)	ε_T	ε_p	ε_S
Mean	0.2	0.1	-0.4
RMS	0.2	0.1	1.6

Table 6.4a *Estimated mean and root mean square transport errors of the upper layer transport anomaly of Kiel-276 mooring records due to measurement accuracy of temperature, pressure and salinity. All values in Sv.*

Mooring	N	ε_I	ε_{Total}	Mooring	N	ε_I	ε_{Total}
264010	36	1.3	2.1	276110	40	0.6	1.7
276010	44	0.9	1.8	276120	44	0.8	1.8
276020	40	1.1	2.0	276130	36	2.5	3.0
276030	44	1.1	2.0	276150	36	0.9	1.8
276040	44	0.9	1.8	276160	43	1.4	2.1
276050	40	0.9	1.8	276170	43	1.4	2.1
276060	40	1.0	1.9	276180	43	2.8	3.2
276100	40	0.6	1.7	276190	43	1.4	2.1

Table 6.4b *As Table 6.4a but the mooring configuration specific interpolation transport error and the total error,* $\varepsilon_{Total} = \sqrt{(\varepsilon_T^2 + \varepsilon_p^2 + \varepsilon_S^2 + \varepsilon_I^2)}$*. N is the number of CTD casts on which the estimate of* ε_I *is based. All values in Sv.*

Based on the calculations of Table 6.4 we estimate the 0-800m layer transport anomaly error of Kiel-276 observations to be approximately ± 2 Sv for all deployments except 276130 and 276180 for which this increases to ± 3 Sv. Although large, these errors are unbiased and result from careful consideration of data quality and development of methods to minimise them. The error contribution from temperature or pressure accuracy is negligible (Table 6.4a) with salinity estimation and vertical interpolation

providing the dominant contributions, 1.6 Sv for the former and between 0.6 and 2.8 Sv for the latter. Transport anomalies will be computed for all available records, and then interpreted within the limitations of the estimated error (Section 7.4.2).

6.2.8 Temperature records at 400 and 1100 dbar

Since the transport anomaly error (Table 6.4) varies significantly over the 20 years due to mooring configuration reaching ± 3 Sv for two deployments, we complement the dynamic height transport anomaly dataset with a time series of temperature at 400 dbar. The temperature record is used both to check transport anomalies and as an interpretive tool to identify shifts in the position of the Azores Front.

Upper layer transport anomalies computed geostrophically from dynamic height anomalies of the 51 reference CTD casts in the region of Kiel-276 deeper than 1300 dbar have strong correlation (significant at the 95% confidence level) with temperature at 400 dbar (Figure 6.14). Linear regression of the transport anomaly to 400 dbar temperature (T_{400}) yields a transport anomaly proxy of

$$\Delta tr_{400} = A*(T_{400} - 12.98) + B \quad (6.7)$$

with A = 6.34 ± 0.52 and B = 0.02 ± 0.30. This fit accounts for 92.5% of the observed variability, and an rms error of 1.0 Sv with no significant trend of the residuals over the temperature range.

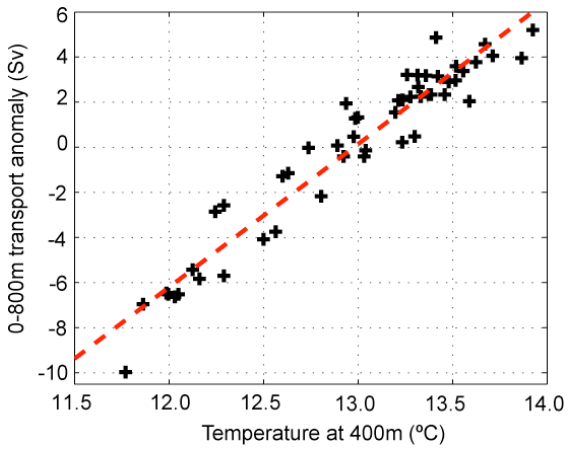

Figure 6.14 *Correlation between CTD temperature at 400 dbar and the measured 0-800m transport anomaly (i) Linear least squares regression of individual data points (+) is shown with red dashed line.*

We compute a T_{400} record from the Kiel-276 dataset by correction of the nearest temperature and pressure measurement in the vertical using $T_{400} = T_p + \int_p^{400} \frac{\partial T}{\partial p}(T_p)dp$ and the $\partial T/\partial p(T)$ climatology of Figure 6.9b(ii). The ∂T/∂p climatology as a function of temperature is used rather than that of pressure since over the depth ranges which we are correcting the measured T(p) to 400 dbar, the estimated error in the $\partial T/\partial p(T)$ climatology is marginally smaller (Figure 6.12) and in all cases the closest instrument to 400 dbar is below the depth where seasonal changes in the climatologies become important and better resolved by $\partial T/\partial p(p)$.

The error in T_{400} resulting from mooring sampling depths (the nearest instrument to 400m may be up to 130m away, Table 6.1) is estimated by subsampling one CTD cast at the mooring measured depths for the entire record and recomputing T_{400}. This gives an rms error for 5581 observations of 0.08ºC, which results in an additional uncertainty of the transport anomaly proxy of 0.5 Sv ($\Delta tr \propto 6.3 * T_{400}$ by equation 6.7). Combining this with the uncertainty of the regression which has an rms error of 1.0 Sv, suggests that the geostrophic transport anomaly should agree with that from the T_{400} proxy to within ± 1.1 Sv.

An error of 1.1 Sv for the 0-800m layer transport anomaly at Kiel-276 calculated from the temperature at 400 dbar is lower than the estimated error for geostrophic transport anomalies computed from all Kiel-276 records after vertical interpolation and salinity estimation (Table 6.4) and compares favourably against a standard deviation in the CTD transport anomalies of 3.8 Sv. The limitation of the T_{400} approach is its lack of information about the vertical structure of variability such as the inability to resolve seasonal signals in the upper 100 m. The 400 dbar temperature record forms a very valuable cross reference for the dynamic height transport anomalies, intended to complement rather than replace the latter dataset.

The method applied to construct a 400 dbar temperature record is also used to obtain a similar temperature time series at 1100 dbar, near the mid-point of the vertical extent of salt lenses/meddies (Armi and Zenk, 1984). This is used as a tool to identify times when

anomalous Mediterranean Water concentrations contaminate the transport anomaly signal. Such a time series is required since meddies render most of the assumptions underlying the construction of this time series invalid and must therefore be excluded (Section 7.4.2.2). The rms error in T_{1100} estimated by subsampling a CTD cast in the different mooring configurations is 0.12ºC (5315 data points).

We will show that the temperature records at fixed depths of 400 and 1100 dbar obtained from the above method provide a useful interpretive tool for analysis of the Kiel-276 transport anomalies (Section 7.4.2).

6.3 THE WESTERN BOUNDARY

6.3.1 Introduction

At the western boundary we are lucky to have one of the longest time series of moored sensors in the deep ocean (Bryden et al., 2005a): repeat deployments between 1986 and 1998 of a moored current meter array fitted also with temperature and pressure sensors east of Abaco, part of NOAA/AOML's Subtropical Atlantic Climate Studies Program (STACS), Western Atlantic Thermohaline Transport Study (WATTS), the Atlantic Climate Change Program (ACCP) and later (2004-2005) the UK RAPID program. Although our methods below are broadly based on those of Johns et al. (2005) who monitored transport of the DWBC using these mooring data sets to reference mooring derived geostrophic velocities with bottom pressure observations, our work has the important distinction that through careful instrument selection, the transport anomalies obtained may be interpreted in the context of end stations.

6.3.2 Data

Current meter mooring arrays deployed across the western boundary current at 26.5ºN east of Abaco provide temperature and pressure time series at discrete depths in seven 1-2 year periods between 1986 and 1997 documented in data reports by Zantopp et al. (1989a; 1989b; 1990; 1993; 1996; 1998a; 1998b). An additional year of mooring data was obtained in 2004/05 when the Abaco array was supplemented with additional moorings from the U.K. RAPID program (Rayner and Cunningham, 2005). Following the selection criteria for end stations at the western boundary (Section 5.3.1), here we

review the available data from moorings in positions A, A_1, B and B_1 of the Abaco arrays and wb1 to wbh2 of the RAPID array (Figure 6.15) with B_1 being the furthest offshore at 41 km from the 800m isobath (summarised in Table 6.5).

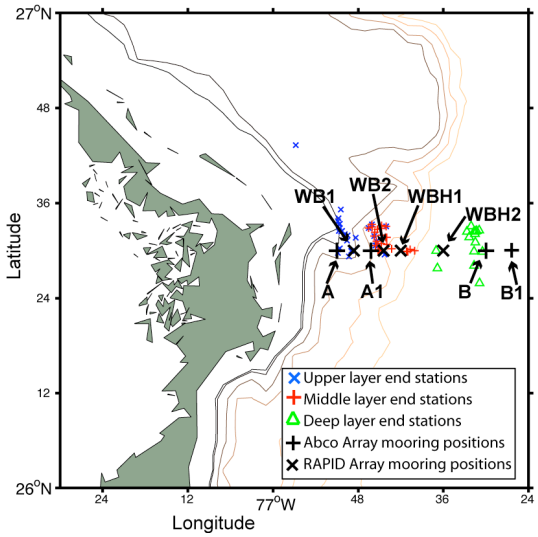

Figure 6.15 *Location of western boundary moorings from the Abaco and RAPID arrays. Selected end stations north of 26ºN are also plotted. Land is shaded with depth contours at 800, 1000, 2000, 3000, 4000 and 4500m.*

Array	Mooring	Position	Start Date	End Date	Water depth (m)	Nominal Instrument Depths (m)								
Stacs-7	224	A_1	28-Mar-86	27-Mar-87	3593	150*	400*	1150*	2593	3093	3493			
	225	B	18-Apr-86	27-Mar-87	4855	1200*	2500	3860	4760					
Stacs-8	230	A_1	30-Mar-87	20-Jun-88	3593	100*	400*	1200	2200	3100	3500			
	231	B	17-Apr-87	20-Jun-88	4829	100*	400*	1200*	2500	3500	4000			
	232	B_1	16-Apr-87	19-Jun-88	4840	100*	400*	1200	2500	3800	4700			
Stacs-10	250	A	09-Oct-88	23-Apr-90	900	100*	400	800						
	251	B_1	08-Oct-88	17-Jun-90	4850	100*	400*	1200	2400	3800				
WATTS	268	A	19-Jun-90	01-Jan-92	900	100	400*	800*						
	269	B_1	20-Jun-90	10-Feb-92	4838	180*	480*	880*	1280*	2080	3080	4080		
ACCP-1	296	A	11-Feb-92	02-Oct-93	824	70*	370*	770						
	297	B	15-Feb-92	28-Dec-93	4849	100*	200	400*	800*	1200*	2000	3000	4000	4840
ACCP-2	310	A	29-Sep-93	24-Dec-95	856	50	350*	650						
	311	B	**LOST**											
ACCP-3	329	A	31-Oct-95	12-Jun-97	1006	100*	400*	700						
	330	B	31-Oct-95	12-Jun-97	4840	1200*	1600	2000	2500	3000	3500	4000	4500	4840*
	BJA	A	29-Mar-04	27-Nov-04	1003	400*	600	800						
Rapid	wb1_1_200420	wb1	27-Mar-04	09-May-05	1382	250*	400	600*	800*	1000*	1200*	1375*	1382*	
	wb2_1_200419	wb2	26-Mar-04	11-May-05	3898	104*	154*	304*	444*	645*	845*	1046*	1246*	1647
							2039*	2541*	3042*	3543	3738*	3898*		
	wbh1_1_200418	wbh1	23-Mar-04	09-May-05	4287	3837*	3937*	4037*	4187*	4237	4287*			
	wbh2_1_200417	wbh2	25-Mar-04	08-May-05	4800	4350*	4450*	4550	4700*	4750*	4800*			

Table 6.5 *Abaco and RAPID array western boundary data availability. Nominal instrument depths are for temperature sensors and also pressure if *. If no useable data was recovered from a given instrument it is not listed, e.g. wb1's 50 and 100m temperature records are bad and therefore omitted from the table. Similarly for the RAPID moorings, all levels had pressure sensors but they are not recorded here if the data is bad. For reference, positions A, wb1, A_1, wb2, wbh1, wbh2, B and B_1 are 5, 6, 9, 12, 16, 25, 35 and 41 km from the 800m isobath. All moorings except wbh1 and wbh2 are full depth. The upper part of mooring 330 was lost before recovery while no data was recovered from 150 or 400m on mooring 225.*

From each of the Abaco array deployments spanning March 1986 to June 1997, either mooring A or A_1 (within 5 or 9 km of the 800m isobath) has at least two instruments in the upper 800m potentially suitable for upper layer transport anomaly calculation. The extent to which this is possible will be examined in subsequent sections noticing the poor vertical resolution with the deepest instrument sitting above 800m on moorings 296, 310 and 329. For the 2004/2005 RAPID array deployment, we consider mooring wb1 for the upper layer transport variability calculations since this is only 1 km offshore of mooring A but with better resolution in the vertical (Table 6.5). Similarly it may be possible to examine intermediate layer flow variability (800-1100m) from the dynamic height records of moorings A_1 and wb1 which both resolve this depth, although A sits in water too shallow to be used in a similar manner. We could use the B moorings in intervening periods since we do not anticipate significant AAIW transport in close proximity to the western boundary but as will be shown, the records of A_1 and wb1 suggest the signal of this layer to be negligible.

For the middle layer representing upper NADW only moorings A, wb1, A_1, wb2 and wbh1 are within the offshore limit for end station selection (20km). Both A_1 moorings and that of wb2 resolve 3000m, and are therefore suitable for investigation of the middle layer transport anomaly between March 1986 and June 1988 and March 2004 to May 2005. For the remainder of the Abaco array deployment period (July 1988 to June 1997) there are no suitable measurements since while the B and B_1 moorings are of the required depth, they are positioned offshore of the 20km limit (Figure 6.15).

The deep layer is more complicated. Mooring B (depth 4800m) lies within the cut off of 37km offshore for the deep layer end stations. As discussed in Section 5.3.3.2 however for end stations, CTD casts are appended such that the upper part of the dynamic height profile is constructed from an inshore shallow station, representative of boundary conditions. It is not appropriate to join dynamic height profiles from mooring A to the lower part of those from B since A sits on the shelf and its maximum depth is above or at the top of the UNADW layer, thus the resultant dynamic height profile could still be contaminated by on/offshore meanders of the DWBC core (Lee et al., 1996). Mooring A_1 on the other hand resolves the UNADW layer and is found in the approximate location of the middle layer CTD end stations inshore of the upper core of the DWBC. We therefore construct dynamic height profiles from all temperature and pressure

records of mooring A_1 with the deep records of mooring B (and B_1 for Stacs-8) appended to the bottom. For the RAPID deployment, we again follow the procedure of crawling down the slope, using the wb2 mooring observations down to 3898m, wbh1 between 3937 to 4287m and wbh2 from 4350 to 4750m (Table 6.5). wb1 is not used due to bad records at 50 and 100m and short records at 1000 and 1200m.

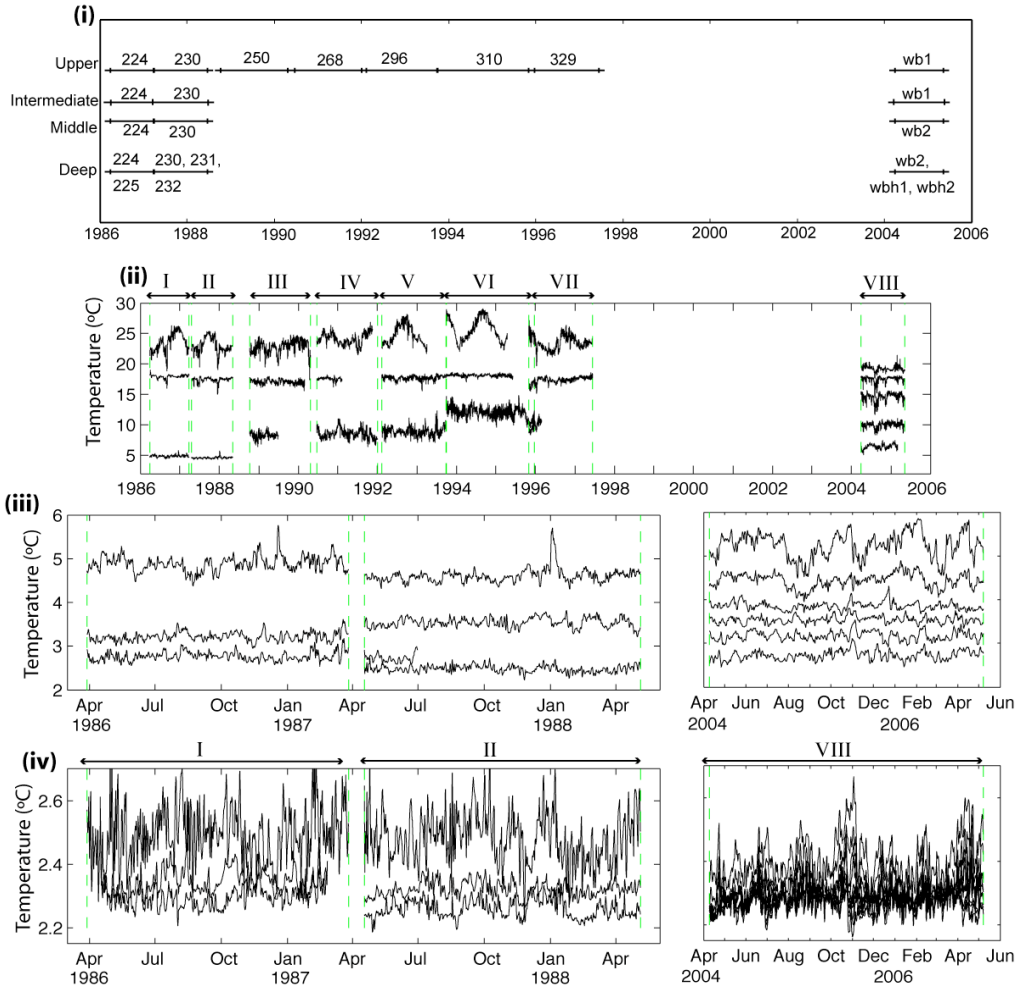

Figure 6.16 *Mooring data availability at the western boundary. (i) is a schematic of the moorings selected for calculation of each layer transport anomaly time series while (ii) to (iv) show the raw mooring temperature records over these times for the upper/intermediate layers, middle and deep layers respectively. Some temperature records are duplicated between plots. Periods I to VIII refer to different mooring deployments for convenience. Note the different time scales for (ii) to (iv).*

Mooring choice and data availability are summarised in Figure 6.16. There are suitable observations in the upper layer almost continuously from 1986 to 1999, although individual instrument failure does have to be allowed for (Figure 6.16) such as the 400m record of Period IV (WATTS) and the 3100m record of Period II. No observations are available for the years 1998 to 2003 between the last recovery of the Abaco array and

the start of RAPID. We use the 40 hour low pass Lanczos-cosine filtered dataset (to remove sub-tidal, tidal and inertial period variability) subsampled at 12 hour intervals (Lee et al., 1996).

Data from the Abaco arrays have been quality controlled at source (see previously referenced Abaco data reports), although some questionable observations are excluded (including the last month of mooring 225's 4760m temperature record which appears to drift by 0.6ºC after having been stable to within 0.03ºC for the first 10 months of the record). A detailed study of pressure sensor performance (Section 6.3.3) is also made since drifts will bias dynamic height anomaly time series. The RAPID mooring observations are taken from the unfinalised data set and we must therefore make judgments about quality. The only temperature records we exclude are those of mooring wb1 at 50 and 100 m depths (sensors pegged out due to having been set with incorrect range). The pressure records at 400m on mooring wb1, 1647 and 3543m on wb2, 4237 on wbh1 and 4550m on wbh2 are also unusable and excluded (Table 6.5). Although some moorings have conductivity sensors we do not use the measured salinity, as discussed in Section 6.3.4.

6.3.3 Initial data processing – pressure

As for Kiel-276, after initial quality control pressures are estimated for each temperature time series without an accompanying pressure record following either the pmin or pendulum method (or a combination of the two) with a minimum requirement of one "good" pressure record per mooring. We assess the validity of the two models at the western boundary using moorings with multiple good pressure sensors from the Abaco array and the instruments above and below each missing record of the RAPID array to compute the correlation between deviations from the upright position, D', (measured depth minus the minimum depth recorded, assumed to be when the mooring is upright) for each instrument pair (upper:lower). A 1:1 relationship is seen if the mooring remains vertical over the depth range spanned by the instrument pair, while a ratio larger than 1 is supportive of the pendulum approximation. Figure 6.17 and Table 6.6 summarise the findings.

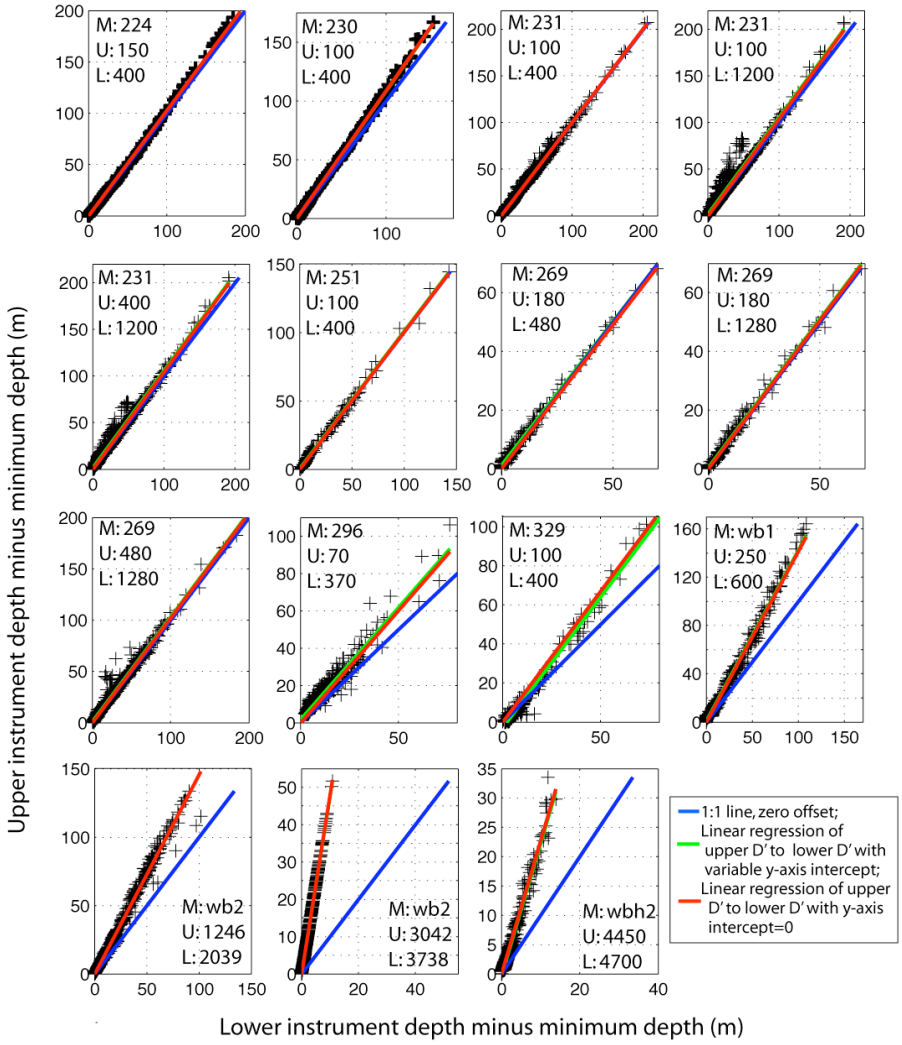

Figure 6.17 *Correlation between upper and lower instrument D', with regression lines overlaid. Data sets in each subplot correspond to those of Table 6.6, which also reports regression coefficients. M is the mooring, with U and D the nominal depths of the upper and lower instruments. The increased variability of mooring 329 400m record for the second half of the deployment (Zantopp et al. 1998b) is excluded.*

The selected pressure model depends on mooring location, since this determines the ambient current strength and thus mooring tilt. Mooring A is positioned on the shelf, in shallow water where transport at all depths is generally northwards due to the Antilles Current (Lee et al., 1996). The ratio of $D'_{upper} : D'_{lower}$ of 1.2 and 1.3 for the upper two instruments of moorings 296 and 329 respectively (Figure 6.17 and Table 6.6), significantly higher than 1.0 is consistent with the mooring behaving as a pendulum, as expected given the strong currents and no instrument being further than 1000m from the sea-bed. Although these ratios are lower than those predicted by instrument heights above the seabed (1.7 and 1.5) this is likely due to incorrect measurement of instrument separation in the original mooring configuration. Similarly, for mooring wb1, on the edge of the shelf break in 1382 m of water, the pressure deviations between 250 and

600m are best modelled by the pendulum method (pressure is bad at the 400m instrument, Table 6.5). For moorings A and wb1 therefore we judge the pendulum method more appropriate than the pmin method for pressure estimation as illustrated by the clear deviation of data points from the 1:1 line of Figure 6.17.

Position / Mooring		N	Nominal instrument depths (m)		H_1/H_2	Slope ± C.I.	y-intercept ± C.I.	r^2	$s_{\varepsilon(pmin)}$	$s_{\varepsilon(pendulum)}$	
			Upper	Lower						Upper	Lower
A	296	835	70	370	1.7	1.2 ± 0.0	1.7 ± 0.2	0.948	4.6	5.2	3.1
	329	683	100	400	1.5	1.3 ± 0.0	-2.8 ± 0.2	0.983	4.0	3.0	1.5
wb1		642	250	600	1.4	1.4 ± 0.0	0.8 ± 0.3	0.988	12.2	7.0	10.7
A_1	224	729	150	400	1.1	1.0 ± 0.0	-0.3 ± 0.9	0.999	1.4	2.1	1.9
	230	898	100	400	1.1	1.1 ± 0.0	-0.4 ± 0.1	0.998	2.5	1.3	1.2
wb2		790	1246	2039	1.4	1.5 ± 0.1	-0.1 ± 0.2	0.991	12.0	6.0	10.2
		775	3042	3738	5.3	4.8 ± 0.0	-0.3 ± 0.0	0.999	9.9	8.1	1.1
wbh2		813	4450	4700	3.1	2.3 ± 0.0	-0.5 ± 0.1	0.978	3.3	1.6	1.1
B and B_1	231	861	100	400	1.1	1.0 ± 0.0	-0.2 ± 0.2	0.994	2.3	3.5	3.3
		861	100	1200	1.3	1.0 ± 0.0	1.5 ± 0.5	0.964	6.3	10.5	8.1
	251	861	400	1200	1.2	1.0 ± 0.0	1.6 ± 0.3	0.983	4.8	6.9	5.7
		123	100	400	1.1	1.0 ± 0.0	0.6 ± 0.5	0.993	2.2	3.0	2.8
	269	140	180	480	1.1	1.0 ± 0.0	1.0 ± 0.3	0.991	1.6	1.7	1.6
		140	180	1280	1.3	1.0 ± 0.0	0.4 ± 0.3	0.988	1.6	5.2	4.0
		572	480	1280	1.2	1.0 ± 0.0	0.9 ± 0.5	0.982	4.2	8.5	6.9

Table 6.6 *Comparison of pendulum and pmin mooring pressure models for records plotted in Figure 6.17. H_1/H_2 is the ratio of upper to lower instrument height above the seabed (Figure 6.2) For the N good data points of the two records, the linear regression of D_1' to D_2' coefficients, slope and y-intercept with 95% confidence intervals correspond to the green lines of Figure 6.17. Standard error is that associated with estimation of measured depth records using the pmin and pendulum models applied to an additional depth record on the same mooring, following equations (6.3) and (6.4); the upper error is that obtained using the lower record of D' to predict the upper, and the lower error is that obtained using the upper record of D' to predict the lower .*

Mooring A_1 is positioned further down the shelf break with 3593 m water depth. The difference between the pendulum and pmin methods for moorings 224 and 230 in this position (instruments at 150/400m and 100/400m) is negligible and the estimated rms error for the two models is only 2 dbar (Table 6.6). The mooring is likely following both the pmin and pendulum models depending on flow characteristics towards the top of the moorings but below these levels we anticipate the pendulum method to become increasingly appropriate towards the sea-bed. In the absence of any strong support for the pmin method (Figure 6.17) we adopt the traditional pendulum method for computing missing pressure records on A_1 moorings in this position, and estimate the associated error to be less than ± 5 dbar (Table 6.6).

For all of the available good multiple pressure record pairs of B or B_1 moorings located between 100 and 1280 m, depth changes at the upper and lower instruments are

approximately equal (lying close to the 1:1 line of Figure 6.17). This suggests that the upper part of the mooring behaves consistently with the pmin model in accordance with the 1 to 4 dbar smaller estimated error for the pmin method than for the pendulum alternative (Table 6.6). The B mooring lies close to the core of the southward DWBC transport with a flow reversal around 1000m and the northward flowing Antilles Current above (Lee et al., 1996), therefore these observations are consistent with surface flotation being sufficient to keep the upper part of the mooring close to vertical (pmin model) in water depths exceeding 4800m. In the deep waters however, flows are stronger and closer to the mooring anchor point the pendulum model is appropriate - supported by the calculations using moorings wbh2 and wb2 (Table 6.6 and Figure 6.17).

Mooring	Position	Reference depth (m)	Instrument depths (m)	Method
224	A	400	1150, 2593, 3093, 3493	Pendulum
225	B	1200	2500, 3860, 4760	Pendulum
230	A_1	400	1200, 2200, 3100, 3500	Pendulum
231	B	1200	2500, 3500, 4000.	Pendulum
232	B_1	400	100	Pmin
			1200, 2500, 3800, 4700	Pendulum
250	A100	100	400, 800	Pendulum
268	A	400	100, 800	Pendulum
296	A	370	770	Pendulum
			70 (where data missing)	Pendulum
310	A	350	50, 650	Pendulum
329	A	100	400, 800	Pendulum
wb1		250	400	Pendulum
wb2		2039	1647	Pendulum
		3543	3738	Pendulum
wbh2		4700	4550	Pendulum

Table 6.7 *Details of pressure calculation following pmin and pendulum methods for western boundary moorings. All pressure sensors of mooring wbh1 appear to drift over the whole time series by an order of magnitude larger than the short term pressure fluctuations around this drift, i.e. those caused by mooring motion, which amount to at most 1 dbar. We therefore conclude mooring motion is insignificant at these depths and we use the nominal instrument depth (assuming no mooring motion with currents) rather than the recorded pressure.*

In summary, we compute missing pressure records (and replace bad ones) with the pendulum method using the closest good pressure record as a reference at all depths for moorings inshore of and including A_1. Further offshore, we use the pmin method down to 1000 dbar (close to the zero crossing of the velocity profiles in the DWBC region) and the pendulum method below this (Table 6.7). Based on Table 6.6 we suggest that an upper bound for the error associated with this estimation of pressures is 10 dbar, although this decreases towards the mooring base where the same angle of mooring tilt

translates to smaller depth changes (following the pendulum model) and most estimated errors are less than 5 dbar (Table 6.6).

6.3.4 Initial data processing – salinity estimation

Although all temperature sensors deployed on the RAPID array have corresponding conductivity sensors, these are uncalibrated in the unfinalised data set used here. To avoid introducing errors of unknown size we do not use these conductivities and instead estimate salinity through an iterative procedure with climatological T-S and θ-S reference curves in the same way as for Kiel-276 (Section 6.2.4). This treatment is consistent with the Abaco array data, for which there are not conductivity measurements for almost all instruments. Reference curves (Figure 6.18) are constructed from CTD casts (see below) following the same methods as described in Section 6.2.4 except that above 18ºC intervals of 0.2ºC are used (rather than 0.5ºC).

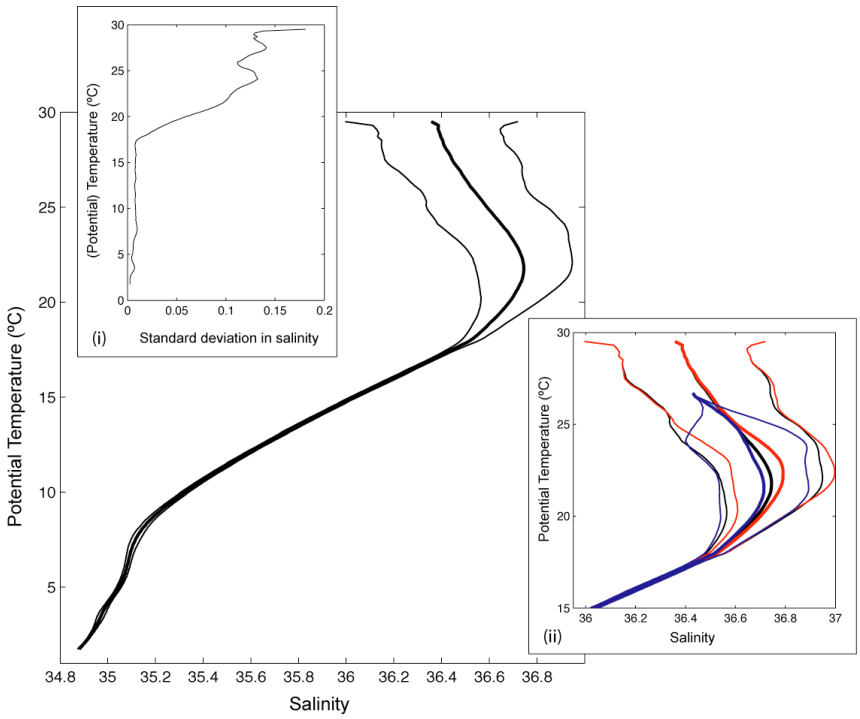

Figure 6.18 *Main: the reference potential temperature-salinity (θ-S) reference curve ± two times the standard deviation of the constituent stations (thin line). The standard deviation is plotted separately in insert (i). (ii) shows the summer (red) and winter (blue) and annual mean (black) reference curves, with the limits of ± 2 standard deviations in thin lines.*

CTD curves used to construct the western boundary reference T-S and θ-S climatologies are formed by crawling down the slope in a similar manner as for the deep layer end stations, primarily because the same CTD casts are used for vertical interpolation between mooring measurement levels (Section 6.3.5) and are therefore required to account for any changes in vertical structure across the boundary region. CTD casts in the reference data set comprise all those within 14 km of the boundary and at times when there is another CTD taken within a day, less than 20 km from the boundary and deeper than 790 dbar, this deeper cast is appended to the base of the inshore station. And if a cast exists still within a day of the first two, but deeper than 3030 dbar and within 37km from the boundary (the offshore limit for deep layer end stations) the deep part of this is added to the base of combined cast. If there is no suitable middle cast, the deep cast is appended to the shallow one directly. To avoid temperature inversions, as described for the deep layer end stations, the 40 dbar below the join is smoothed with a cubic spline interpolation over the 20 dbar above the join to 60 dbar below it. The result is a set of CTD casts for which the upper water column properties are representative of the shelf slope waters while the deeper parts are typical of conditions further offshore. In this reference set are 46 single (inshore) CTD profiles, 14 casts constructed from upper, middle and deep stations and 18 from upper and deep stations. For example on 11th February 2003, there is a CTD profile in the reference dataset made up of the upper 1090 dbar of a cast at 76.84ºW (3.7 km offshore) then a cast at 76.72ºW (14.2 km offshore) down to 3970 dbar with the bottom 920 dbar from a cast at 76.60ºW (25.6 km offshore). All CTD stations are at 26.5ºN.

Note that the CTD casts used to compute the reference climatologies are the calibrated dataset, (described in Section 5.3.2) which account for a steady rate of freshening of LNADW over the 25 years. As a result the CTD casts in the reference dataset have a salinity range of approximately 0.008 on potential temperature levels from 2 to 2.5ºC. The purpose of the deep layer mooring transport anomaly time series is not however, to identify long term trends but to quantify the sub-annual variability – a constraint imposed largely by the data gap from 1988 to 2004. Since UNADW and LNADW transport anomalies computed in periods I/II and VIII are from moorings in different locations and with different instrument configurations (Figure 6.16 and Table 6.5), it is unrealistic to anticipate that the absolute magnitude of transport anomalies can be meaningfully compared for the two time periods. It therefore does not matter that the

deep T-S climatology should ideally be fresher for the RAPID observations than for the early Abaco array deployments. The reference curves constructed (Figure 6.18) are therefore representative of long term average conditions.

Any seasonal variability in the T-S climatology is restricted to temperatures above 19ºC (Figure 6.18). The reference curve constructed only from winter CTD casts (October to March inclusive) is however not significantly different to that from summer casts (Figure 6.18(ii)) and we therefore use the annual mean reference curves at all times. Below the depth of seasonal influence there is little variation in the constituent θ-S curves of the reference profile with standard deviation of salinity less than 0.01 below 17ºC. This is reflected in the small error in salinity resulting when CTD salinities are estimated using our iterative procedure with the T-S and θ-S reference curves (Figure 6.19), remembering that the climatologies do not account for long term trends present in the salinity of these CTD casts.

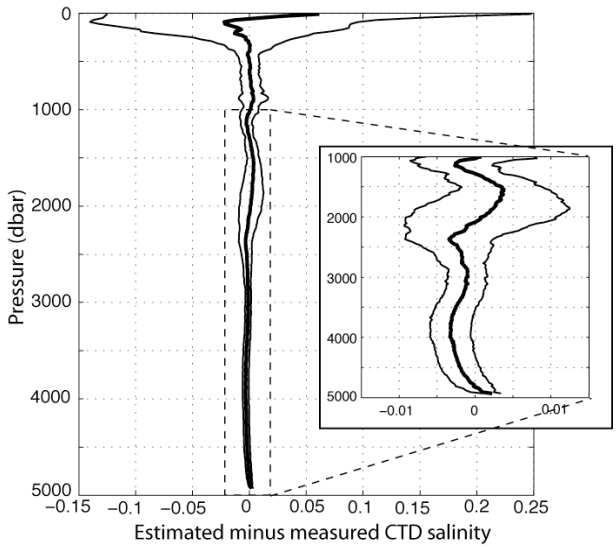

Figure 6.19 *Error in salinity of CTD casts when estimated using T-S and θ-S reference profiles relative to measured salinity. Mean of 78 CTD casts plotted (heavy line) ± one standard deviation. That the mean error is not identically equal to zero reflects the smoothing procedure employed to construct the reference climatologies.*

6.3.5 Initial data processing – vertical interpolation

Vertical resolution of moorings at the western boundary varies significantly over the 25 years, with nominal instrument separations of as much as 1000m in the early Abaco array deployments but not exceeding 500 m in the RAPID moorings (Table 6.5). Comparable dynamic height time series from the differing mooring configurations

therefore requires a vertical interpolation procedure. Linear interpolation between the instrument depths is attractively simple, but would not capture the vertical structure expressed in the EOF's of specific volume anomaly variance as a function of pressure (Figure 6.20). In the upper 400 dbar, linear interpolation between nominal instrument depths of 100 and 400m (typical of mooring A configuration) deviates significantly from the first mode which itself accounts for 75% of the variance (Figure 6.20(i)). Similarly in the UNADW layer, linear interpolation between 1200 and 2200m (mooring A_1) is not a good approximation for the first mode vertical structure which accounts for 70% of the variance below 400m (Figure 6.20(ii)). We therefore follow the approach of vertical interpolation between measurement levels of the Abaco array adopted by previous authors (Zantopp and Leaman, 1984; Johns et al., 2005) and integrate a $\partial T/\partial p$ climatology constrained by the measured temperature and pressures, to obtain 20 dbar resolution temperature profiles. The $\partial T/\partial p$ climatology is constructed in temperature co-ordinates since this better resolves the ∂T/∂p minimum of 18ºC water (Zantopp and Leaman, 1984) compared to pressure co-ordinates employed for Kiel-276 .

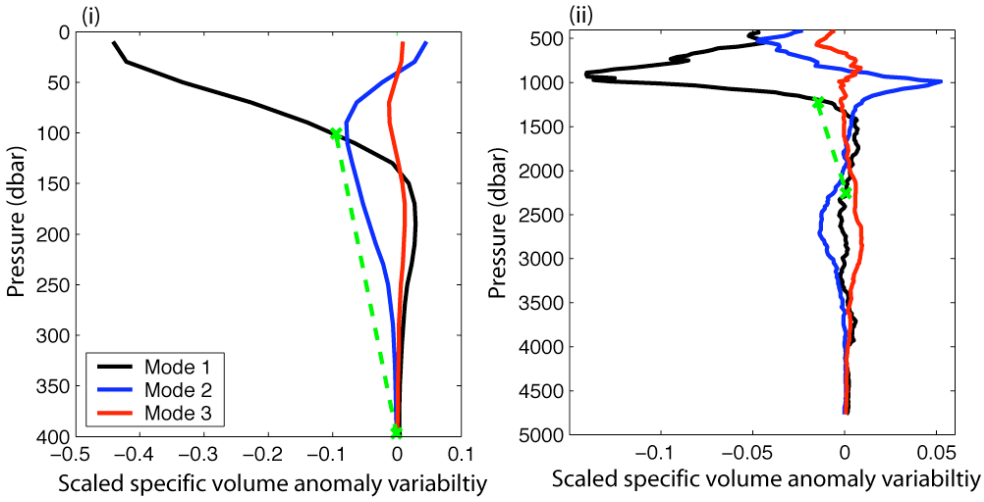

Figure 6.20 *EOF's of specific volume anomaly computed over 0-400 dbar (i) and 400-4700 dbar (ii), after subtraction of mean profile. Nominal instrument depths of 100/400 dbar and 1200/2200 dbar joined by straight lines (dashed green) are added, representing the profile that would be produced by linear interpolation between the data points. Legend of (i) applies to (ii) also.*

The method to construct the seasonally varying ∂T/∂p climatology of Figure 6.21 from the reference CTD casts of Section 6.3.4 broadly follows the methods discussed in Section 6.2.5.2 for Kiel-276. Seasonal variability is restricted to waters warmer than

19ºC. Below this, ∂T/∂p is computed for all CTD casts of the reference dataset in 0.2ºC intervals with points rejected in each interval that lies outside the mean ± two standard deviations. The resulting mean profile is twice smoothed vertically in temperature coordinates with a 1ºC running mean. Above 19ºC the same procedure is followed but for two month periods, also in 0.2ºC intervals but with the 1ºC running mean smoothing applied three times. Any 0.2ºC intervals without observations are filled with linear interpolation. This procedure for the upper waters is found to provide the best compromise between retaining the vertical structure observed but not having the resultant profile distorted by individual casts when only a few CTD profiles are available in for a given 2-month period (there are only 4 profiles for December/January but 20 for February/March). We have investigated use of larger temperature intervals than 0.2ºC and larger smoothing windows than 1.0ºC for constructing the climatology but to no advantage. Finally the upper seasonally varying part of the climatology is joined to the lower single profile at 19ºC then between 18.6 and 19.4ºC the join is smoothed again with a 1ºC mean.

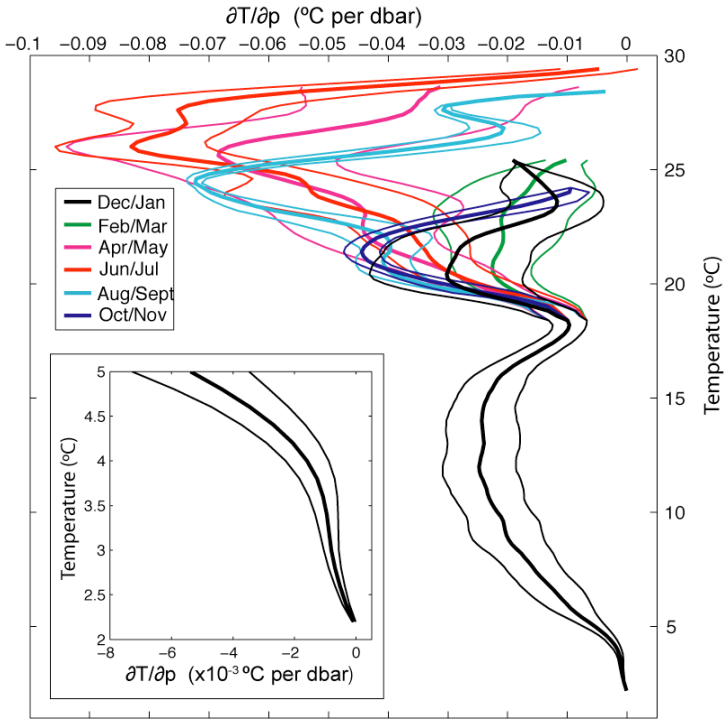

Figure 6.21 *The monthly reference* $\partial T/\partial p(T)$ *climatology, with limits of ± one standard deviation. For construction details refer to text*

Our climatology (Figure 6.21) clearly captures the 18ºC water minimum in vertical temperature gradient. The seasonal cycle shows least stratification of the upper waters

in February-March, with rapid growth of a seasonal thermocline between 20-25ºC from April through July with maximum slope about 5ºC below the surface water. This is evident in August/September and to a lesser extent through to November below the influence of wind mixing which homogenises the surface layer.

The procedure employed to vertically integrate the ∂T/∂p profile has been modified from that of Section 6.2.5 to minimise the resulting error in temperature when instrument separation is large especially through the thermocline. The grey lines of Figure 6.22 show that with the instrument configuration of mooring A_1 interpolation following the Kiel-276 procedure between the 400 and 1200m levels yields temperatures that are likely to be underestimated by 2-3ºC. These are results from subsampling the reference CTD casts and recomputing T(p) at 20 dbar resolution. The three stage interpolation process used here reduces this error in magnitude and removes the bias (Figure 6.22). First we extrapolate downwards from the upper mooring observation (u) to the lower instrument (l):

$$T_{u+20} = T_u + \left.\frac{\partial T}{\partial p}\right|_{T=T_u} \Delta p \quad \text{with } \Delta p = 20 \text{ dbar} \tag{6.7}$$

This is continued downwards in 20 dbar increments with the upper level reference being temperature computed a cycle previously, until the level of the next mooring data point (l). Then we extrapolate upwards in the same manner as was employed above the upper instrument of Kiel-276 (equation 6.6) but from the lower to upper instruments using the value of temperature computed a cycle before 20 dbar below, and so on until the upper mooring observation level is reached. In this way two estimates are obtained for temperature every 20 dbar between the mooring measurement levels. The final temperature estimate is a weighted mean of the two according to distance from the instrument levels. This differs from the Kiel-276 procedure since the upwards interpolated temperature profile is independent of the upper instrument temperature measurement until the weighted mean is computed. For example with instruments at 400 and 800 dbar, the temperature estimated at 500 dbar is equal to 1/4 of the temperature resulting from upward extrapolation from 800 dbar, added to 3/4 of the temperature resulting from downwards extrapolation originating at 400 dbar. Above the uppermost instrument extrapolation is performed in 20 dbar increments using ∂T/∂p of the uppermost temperature as for Kiel-276.

Additionally, for mooring A we have to extrapolate beyond the lowest measurement depth to 800 dbar so that dynamic height can be referenced to this level as discussed in Section 6.3.6. This can result in temperature errors of 3ºC at the base of the profile depending on the distance over which we extrapolate but the error estimates for transport anomaly time series take this problem into account (Section 6.3.7).

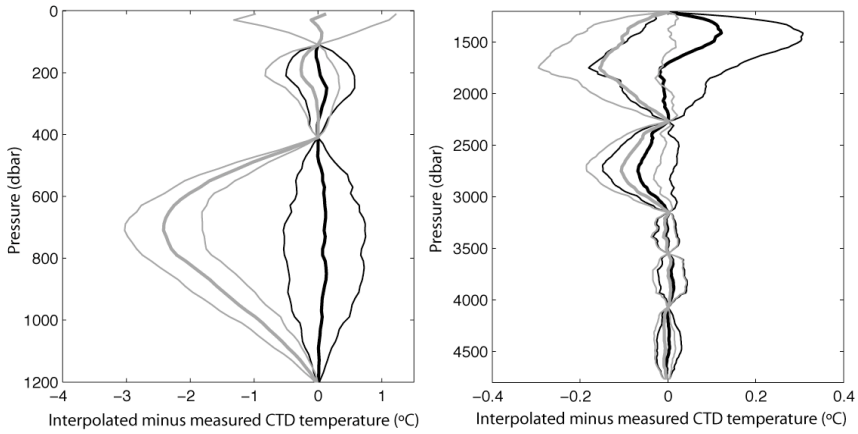

Figure 6.22 *Error in CTD temperature after subsampling temperature and pressure at vertical resolution corresponding to the appended moorings 230, 231 and 232 (100, 400, 1200, 2200, 3100, 3500, 4000 and 4700 m) and recomputing the 20 dbar resolution temperature profile using with different vertical interpolation methods. Grey lines are the interpolation procedure used for Kiel-276 and black that adopted here. The error is the mean of the 78 reference CTD stations of Section 6.3.4.*

6.3.6 Transport anomaly calculation

Measured temperature records with estimated or measured pressure records are used to construct 12 hourly vertical temperature profiles at 20 dbar resolution, after appending the records of different moorings down the slope for the deep layer (Figure 6.16 and Section 6.3.2). Salinity is then estimated from the climatological T-S and θ-S climatologies and the resulting specific volume anomaly used to compute the transport anomalies of the upper, intermediate, middle and deep layers where data permits according to equation (4.4) relative to the same dynamic height reference as for the hydrographic end stations at the western boundary (Section 5.3.3.1).

Rather than the 1000 dbar reference level employed for the end stations however, moored dynamic height profiles are referenced to 800 dbar. This is because on the shelf (mooring A) where the water depth is less than or equal to 1000m the nominal depth of the lowest instrument is between 650 and 800m. The closer the reference level is to the

deepest mooring observations, the smaller the error due to extrapolation of temperature beyond the bottom instrument. Previous studies have used both 1000m (e.g. Olson et al., 1984; Lavín et al., 1998) and 800m as reference levels (Leaman and Harris, 1990) thus mooring transport time series should still be comparable with the end station layer transport anomalies.

6.3.7 Transport anomaly errors

As for Kiel-276 we estimate the error associated with each layer transport anomaly time series following Johns et al. (2005), by calculating the change in transport of the reference CTD casts of Section 6.3.4 that results from uncertainty in temperature (0.01 ºC), pressure (10 dbar, Table 6.6) and salinity (recomputed according to Section 6.3.4), as well as the vertical interpolation procedure. The first three are independent of mooring configuration (Table 6.8a) while that due to vertical interpolation is the result of subsampling CTD casts' temperature and pressure at all mooring resolutions, interpolating these to 20 dbar resolution, extrapolating to the surface and sea-bed as required, then recomputing the transport anomaly with measured salinity, Table 6.8b. Combined transport errors (in a least squares manner) are also included in Table 6.8b.

The upper layer mooring transport anomaly error is estimated to be between 2 and 3 Sv before 1998 but reduced to 0.8 Sv for the RAPID array reflecting the improved vertical resolution which is the main contributor to the uncertainty for all layers. Errors for the intermediate water transport anomaly are only 0.2 to 0.5 Sv due to the thinness of this layer. For the middle and deep layers the errors are larger than 5 Sv for each of the Abaco array deployments but we note that a baroclinic DWBC transport range of approximately 40 Sv has been observed (Johns et al., 2005), in which context the Abaco array mooring observations are still useful. The RAPID array's good vertical resolution through the deep waters pays off with estimated errors less than 2 and 4 Sv for the middle and deep layers respectively. We note that the salinity (and thus the total) error of the lower layers is an over estimate, at 2.4 Sv, since the western boundary freshening of CTD casts is included as an error (refer to Section 5.3.2), and use of calibrated RAPID array salinity would also reduce the error further.

The errors (Table 6.8b) are acknowledged to be large, unfortunately imposed by limited observations in the vertical which interpolation with a $\partial T/\partial p$ climatology can only go so far to resolve. We do note that these errors are unbiased as a result of the data processing methods developed, and we believe them to be as small as possible given the dataset in use.

	ε_T	ε_p	ε_S
Upper layer (0-800m)	0.1	0.1	0.5
Intermediate layer (800-1100m)	0.0	0.0	0.0
Middle layer (1100-3000m)	0.5	0.4	1.0
Deep layer (3000-4700m)	1.2	0.7	2.4

Table 6.8a *Root mean square transport error (in Sv) of reference CTD casts due to simulated uncertainties of 0.01ºC in temperature (ε_T),10 dbar in pressure (ε_p) and salinity (ε_S) from the climatological T-S and θ-S relationships .*

Layer	Mooring	ε_I	N	ε_T
Upper	224	3.2	53	3.2
	230	3.0	50	3.0
	250	1.9	65	2.0
	268	1.9	65	2.0
	296	2.1	65	2.2
	310	3.0	65	3.0
	329	2.4	65	2.5
	Wb1	0.8	50	1.0

Layer	Mooring(s)	ε_I	N	ε_T
Int.	224	0.5	53	0.5
	230	0.5	50	0.5
	Wb1	0.2	50	0.2
Middle	224	8.7	19	8.8
	230	5.4	29	5.5
	Wb2	1.1	37	1.6
Deep	224/225	10.3	19	10.7
	230/231/232	5.4	22	6.1
	Wb2/wbh1/wbh2	2.0	19	3.4

Table 6.8b *As Table 6.8a but the mooring configuration specific interpolation transport error (ε_I) and the total error, $\varepsilon_{Total} = \sqrt{(\varepsilon_T^2 + \varepsilon_p^2 + \varepsilon_S^2 + \varepsilon_I^2)}$. N is the number of CTD casts on which the estimate of ε_I is based.*

6.3.8 Temperature times series at 400 and 3000 dbar

Following the success of estimating the upper layer transport anomaly at Kiel-276 from the temperature at 400 dbar, we consider whether such an approach may also be useful at the western boundary. Linear regression of the 39 upper layer western boundary CTD end station transport anomalies (of Section 7.5.1) to their temperature anomaly at 400 dbar relative to the group mean (Figure 6. 23(i)) accounts for 53% of the variance and is significant at the 95% confidence level:

$$\Delta Tr_{upper} = A*(T_{400} - 17.60) + B \qquad (6.8a)$$

with A = -4.75±1.50 and B = 0.00±0.42. The rms error in transport anomaly resulting from this fit is 1.3 Sv, which compares very favourably with the 2-3 Sv geostrophic upper layer transport error estimated in Section 6.3.7.

Similarly the deep layer transport anomalies of CTD end stations (total 29) are significantly correlated with the temperature anomalies at 3000 dbar (Figure 6.23ii)) according to

$$\Delta Tr_{deep} = A*(T_{3000} - 2.787) + B \qquad (6.8b)$$

with A = 42.63 ± 22.00 and B = 0.9 ± 1.7. The fit accounts for 35% of the observed transport anomaly variance (Figure 6.23(ii)) and has rms error of 4.4 Sv. Although a 4.4 Sv error is large, it is less than the deep layer transport anomaly error of Table 6.8b for the Stacs-7 and Stacs-8 arrays.

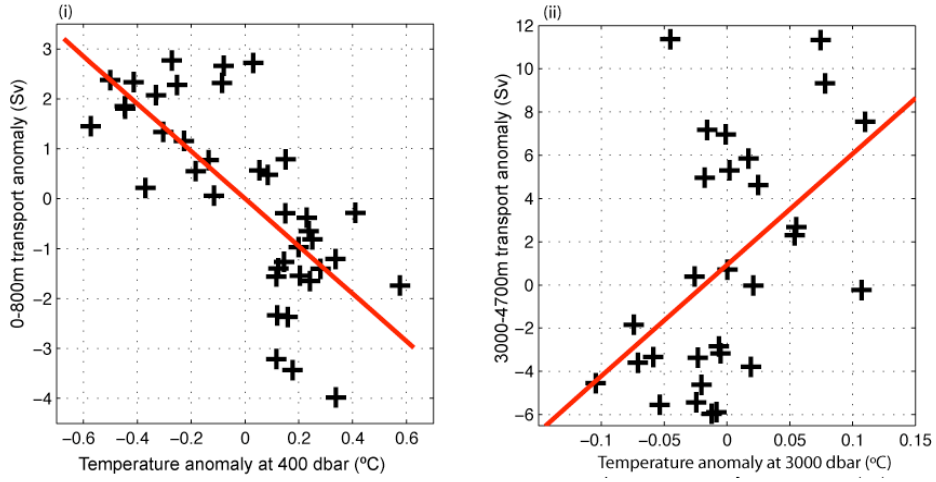

Figure 6.23 *Linear regression of the 0-800m layer transport anomaly to the temperature at 400 dbar minus 17.60ºC (the group mean) (i) or the 3000-4700m transport anomaly to temperature at 3000 dbar minus the group mean of 2.787ºC (ii). Transports are referenced to 800 dbar.*

A T_{400} record is therefore computed from the western boundary moorings by integration of the $\partial T/\partial p\,(T)$ climatology from the closest temperature and pressure observation:

$$T_{400} = T_p + \int_p^{400} \frac{\partial T}{\partial p}(T_p)dp \qquad (6.9)$$

noting that all mooring A deployments have a temperature sensor either at 400m or within 50m of it. The weighted vertical interpolation procedure of Section 6.3.5 is not used since it requires more than one temperature and pressure observation at any one time, and one of the advantages of the T_{400} record is the increased coverage of the

deployment period since it is only limited by instrument failures at 400m, and not those at 100/800m as directly computed transport anomalies are. The uncertainty in T_{400} resulting from this integration is small. Subsampling temperature and pressure of a CTD cast at the pressure measured by the middle instrument of mooring A and estimating the temperature at 400 dbar according to equation (6.9) results in a rms error of 0.07ºC for the 7427 samples.

Calculation of an upper layer transport anomaly proxy from a time series of temperature at 400 dbar according to equation (6.8a) is estimated to have an error of 0.3 Sv (0.07*4.75) due to the accuracy with which T_{400} is estimated, and 1.3 Sv due to the correlation between T_{400} and the transport anomaly, resulting in a combined error of 1.3 Sv. As will be shown, a transport anomaly proxy computed in this way is a valuable tool for cross-referencing the geostrophic transport anomalies (Section 7.5.2).

The same procedure to compute T_{3000} is employed for the times when deep layer transport anomalies are available from moorings, using the 3090m record of mooring 224, 3100m record of 230 and 3042 of wb2. Subsampling CTD casts to estimate the error associated with this at the mooring measured pressures and employment of the vertical interpolation procedure gives an rms error in temperature at 3000 dbar of 0.01ºC from 2184 observations. A deep layer transport anomaly proxy calculated according to equation (6.8b) is therefore estimated to have an rms error of 4.4 Sv (0.42 Sv from the temperature uncertainty and 4.4 Sv from the underlying correlation). Unfortunately although a similar proxy is desirable for the UNADW layer, no significant correlations have been found between temperature at a 1200 or 2500 dbar and the transport anomaly.

6.4 SUMMARY

This chapter has described the methods developed to obtain transport anomaly time series at the western and eastern boundaries to complement end station observations. The western boundary data set of Abaco and RAPID array moorings within our study region allow the continuously operative boundary dynamic height profiles required, to be computed for all transport layers. At the east however, the limitations of a historical project become apparent. The Kiel-276 mooring time series is used, while desirable

from the point of view of its duration (close to 20 years) it is not at the ideal location. Analysis of the transport anomaly time series at Kiel-276 will be used to constrain the magnitude of variability of the eastern basin subtropical gyre recirculation between 1980 and 2000 but we judge that it cannot be interpreted as an end station substitute.

At both boundaries transport anomalies are computed both geostrophically and from a fixed depth temperature transport proxy (at 400 dbar for the upper layer). The latter has two advantages for estimating upper layer transport anomalies. Firstly the 400 dbar temperature record only requires one observation level and therefore provides a more complete time series than the dynamic height derived transport anomalies which require multiple working instruments. Secondly the estimated 400 dbar temperature transport anomaly proxy error is 1.3 Sv, compared to a 2 - 3 Sv error estimated for the Abaco array geostrophic transport anomalies. The reduced error magnitude is largely due to the fixed depth temperature record's low sensitivity to mooring vertical resolution and vertical resolution is the dominant contributor to error in the Abaco array dynamic height transport anomalies. The two records are presented and interpreted together in Chapter 7.

CHAPTER 7: **Results**

7.1 INTRODUCTION

This chapter presents the estimated variability of the Atlantic MOC components at 26.5ºN described in Chapter 4, starting with annual mean Ekman and Florida Straits transports (Sections 7.2 and 7.3). This is followed by results of application of methods developed in the previous two chapters to estimate contributions made by the eastern and western boundaries to the variability of the mid-ocean baroclinic geostrophic flow (Sections 7.4 and 7.5 respectively). The boundary geostrophic transport sections are divided into the results from end stations or moorings, then further into sub-annual or interannual timescale variability. A summary is provided in Section 7.5 before all results are discussed in Chapter 8.

7.2 EKMAN TRANSPORT

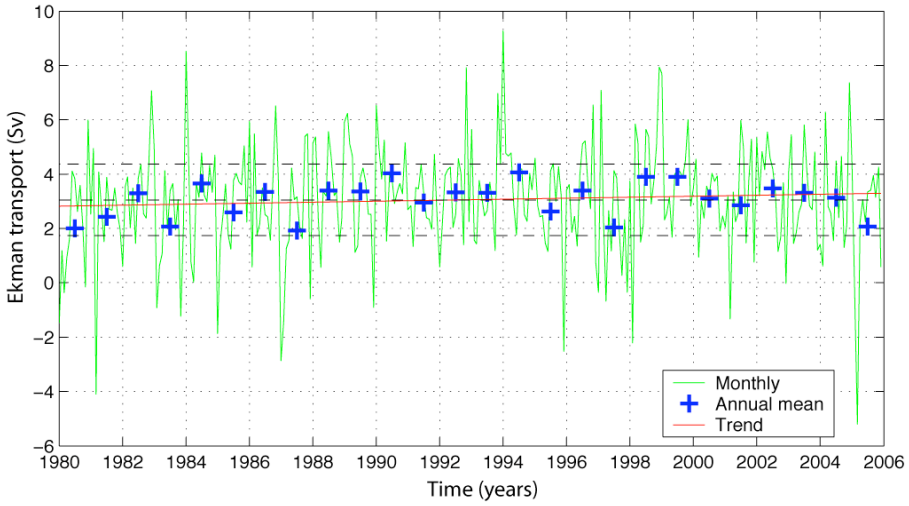

Figure 7.1 *Ekman transport across 26.5ºN from the monthly mean NOC wind stress climatology, 1980 to 2005 inclusive (green), along with the annual mean transports plotted on 1st July of each year (blue +). Linear regression of annual mean Ekman transport to time is indicated by the red line, along with the 1980-2005 mean (black dashed line) and the limits of ± 2 standard deviations of annual mean transports (black dash-dot lines).*

Variability in monthly mean Ekman flow computed from the NOC climatology is large, with transports reaching 9 Sv northwards or 5 Sv southwards (Figure 7.1). The annual means, in which our interest lies, are all within ± 1.2 Sv (one standard deviation equals 0.6 Sv) of the long term mean transport of 3.1Sv. We can therefore say with 95% confidence that no annual average Ekman transport between 1980 and 2005 was significantly different from 3.1 Sv.

Linear regression of the annual average Ekman transports to time (also plotted in Figure 7.1) according to

$$Transport = A(\text{years since } 1980) + B \qquad (7.1)$$

has A of 0.018± 0.035 Sv yr^{-1} and B of 2.83 ± 0.52 Sv (95% confidence limits). Therefore the trend is not statistically significant with a p value (the probability of computing such a fit if not actually present in the data) of 0.31. It amounts to a change of only 0.5 Sv towards stronger northward Ekman flow in 25 years. This analysis leads us to conclude that no annual average Ekman transports between 1980 and 2005 are significantly from the long term mean of 3.1 Sv.

7.3 FLORIDA STRAITS TRANSPORT

The record of daily Florida Straits transport (green lines, Figure 7.2) clearly shows a significant annual cycle, which Baringer and Larsen (2001) found to have a peak to trough range of 3.5 Sv but this is averaged out in the annual means discussed below. Linear regression of annual mean Florida Straits transports to time (again following equation 7.1) shows any long term trend to be even smaller than for the Ekman transports, amounting to only a 0.25 Sv change in 25 years (A = 0.01 Sv yr^{-1} and B = 32.02 ± 1.07 Sv). This trend is not however significant (p = 0.78), and is negligible in comparison with interannual fluctuations in transport (Figure 7.2). Flow through the Florida Straits was strongest in 1985, 1997 and 2002, and weakest in 1991 (Figure 7.2). The range just exceeds ± two standard deviations (with σ = 1.1 Sv). This decadal signal has already been discussed (Baringer and Larsen, 2001) and attributed to an 18 month lagged response of the Florida Current to the NAO, with amplitude of approximately 2 Sv.

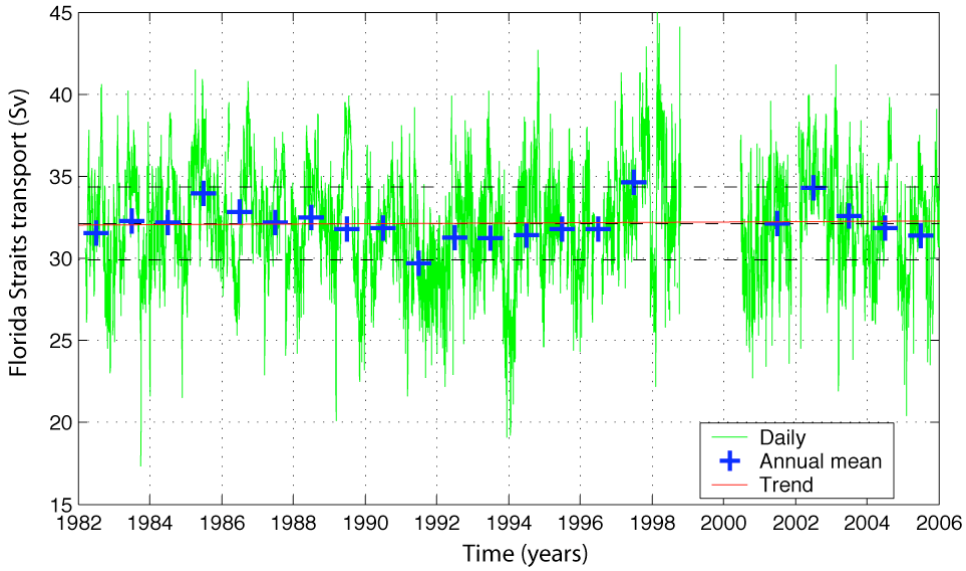

Figure 7.2 *Florida Straits transport at 26.5ºN from cable measurements, 1982 to 2005 inclusive. Daily transports are in green with each year's annual mean plotted on 1st July with a blue +. The linear regression of annual mean transport to time is shown (red line) along with the long term mean (black dashed line) and limits of ± 2 standard deviations (black dash-doted lines).*

In summary, annual mean Florida Straits cable derived transports have a decadal scale oscillation with amplitude ± 2 Sv (Figure 7.2 and Baringer and Larsen, 2001), but no long term trend larger than 0.5 Sv during the period 1982 to 2005. The data gap between 1998 and 2000 can therefore be filled by assuming annual mean Florida Straits transports of 32.1 Sv (the 25 year mean), with introduced error less than ± 2 Sv. Anomalies of the combined northward transport of the Florida Straits and Ekman components of the MOC at 26.5ºN show variability smaller than ± 3 Sv (Figure 7.3) between 1980 and 2005.

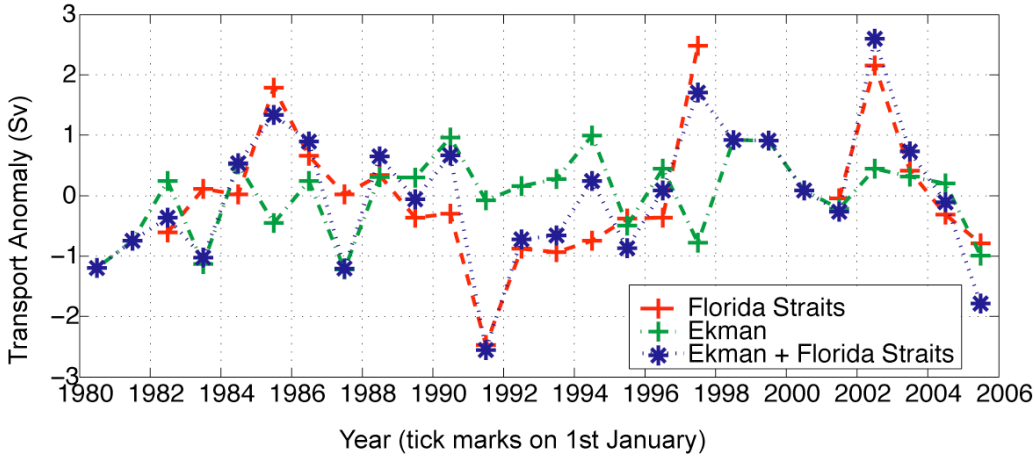

Figure 7.3 *Annual mean Florida Straits and Ekman transports, along with their sum, plotted on 1st July of each year. Years for which Florida Straits transports are not available, the annual mean anomaly is assumed to be zero.*

7.4 EASTERN BOUNDARY GEOSTROPHIC TRANSPORT

7.4.1 Hydrographic End Stations

7.4.1.1 Introduction – independence of observations

In order to interpret end station layer transport anomalies as estimates of water mass transport variability originating at the eastern boundary, we must first address the question of whether these observations are independent. Sampling one anomalous transport event repeatedly would bias the overall variability estimate, but if all observations are independent, the transport anomaly standard deviation can be used. We estimate an independence timescale of 37 days for our eastern boundary study region based on a width of 120 km and Pingree (2002)'s observations of a "*swesty*" (shallow subtropical anticyclonic eddy) propagating at 3.8 cm s^{-1} at 26ºN, 33ºW. He also found similar features within our study region. The minimum temporal separation of end stations selected is 39 days (upper layer, June and July 1992, Table 5.6), but these stations are only 20km apart, which, based on the *swesty* propagation speed requires only 6 days spacing in time for independence. Minimum temporal separation between end stations used for the intermediate, middle and deep layers is 93, 93 and 292 days respectively. All end stations transport anomalies are therefore considered independent.

	Number of observations	Mean Δtr (Sv)	Standard deviation of Δtr (Sv)	Range of Δtr (Sv)	Estimated error in Δtr (Sv)
0-800m	10	-0.6	2.0	6.9	1.2
800-1100m	11	0.2	0.5	1.7	1.0
1100-3000m	9	0.1	1.6	5.0	2.6
3000-5000m	7	0.0	0.6	1.3	1.4

Table 7.1 *Overview of layer transport anomalies (Δtr) at the Eastern boundary. The estimated error is reproduced from Table 5.2 for ease of subsequent reference.*

An overview of variability and the associated errors is summarised in Table 7.1 before the issues of sub-annual and interannual variability are addressed in Sections 7.4.1.2 and 7.4.1.3 (within the obvious limitations of the data available). That the mean layer transport anomalies are not identically equal to zero is not important since variability about the mean is of interest rather than the absolute transports. The non-zero mean results because although dynamic height anomalies are relative to the mean of the

constituent end stations, they are also referenced to either 3200 dbar or the sea-bed and thus include a signal of the structure outside the anomaly depth range.

7.4.1.2 Sub-annual variability

Consideration of whether the seasonally varying upwelling regime of the north east Atlantic subtropical boundary region (e.g. Mittelstaedt, 1991; Hernández-Guerra and Nkyjaer, 1997) may impose a seasonal bias in layer transport anomalies is required before any assessment of interannual variability is made (Section 7.4.1.3). We only examine anomalies of the upper layer in this context since Fraser (2006) showed seasonal variability of Argo float profile geopotential anomalies between 21ºN and 28ºN to be strong above 100m, with no signal below 800m. It is important to do this even though we only have 10 data points for the upper layer since they are spread through all months of the year, except February and March.

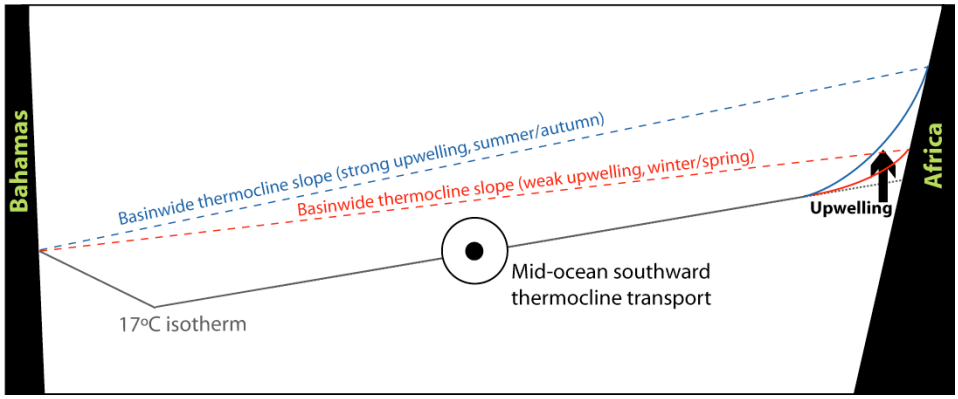

Figure 7.4 *Schematic of the effect of a seasonal cycle in upwelling at the eastern boundary north of 25ºN on the basinwide thermocline slope, and thus net southward transport of thermocline waters in the mid-ocean as estimated from end stations at each boundary. Only the upper water column is represented.*

Between 20ºN and 25ºN upwelling is fairly strong all year round due to steady trade winds: the SST difference between the boundary and open ocean is larger than –3ºC for most of the year, but may exceed –6ºC for a few months in spring and autumn (Mittelstaedt, 1991). North of 25ºN however, upwelling is weaker overall and strongest in summer and autumn when SST differences exceed –3ºC (Mittelstaedt, 1991). If upwelling is weaker in winter/spring north of 25ºN due to the seasonal cycle, we therefore hypothesise that an end station taken in these conditions may be warmer in the thermocline. As illustrated in Figure 7.4 weaker upwelling at the east means warming at

a given depth (relative to the strong upwelling case), which decreases the basinwide thermocline slope (assuming no change at the west) leading to weaker southward transport across the mid-ocean. This is expressed in end station calculations as a positive upper layer transport anomaly at the east. The seasonal dependence assumes that although upwelling is strictly confined to a narrow strip of shelf waters 20-30 km from the coast, the effects may also be felt over the shelf break, where we ideally select upper layer end stations from, due to secondary upwelling (Mittelstaedt, 1991).

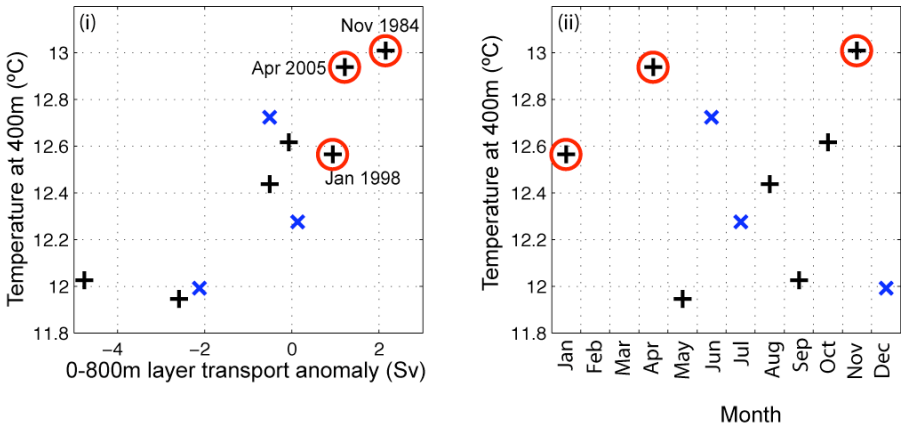

Figure 7.5 *(i): Correlation between upper layer end station transport anomalies and the temperature at 400m. (ii) Temperature at 400m plotted as a function of time through the year. In both, stations north of 25ºN are plotted with (+), those south with (x), with those of November 1984, January 1998 and April 2005 circled red.*

That the three most positive upper layer transport anomalies (2.1, 0.9 and 1.2 Sv) occur in winter/spring end stations north of 25ºN (those circles red in Figure 7.5(i)) is consistent with the above hypothesis (seasonal upwelling influence on computed transport anomalies), and is seen in the stations' high 400m temperatures (Figure 7.5(ii)). Note that we include the November 1984 station in the winter/spring group. The only other end station of winter/spring is that of May 2004 (at 27.85ºN) with an upper layer transport anomaly of –2.6 Sv, suggesting that individual upwelling events (in addition to a seasonal cycle) cannot be ignored. If such a seasonal cycle exists, it is desirable to remove it before trying to extract and interpret interannual changes. This is not possible however with only 6 stations north of 25ºN. The lack of a clear seasonal cycle in the 400m temperatures (Figure 7.5(ii)) of these stations is attributed not to its absence but to insufficient data coverage and possible effects of individual upwelling events. Awareness of the possibility of a positive bias of 1-2 Sv in the upper layer transport anomalies of the November 1984, January 1998 and April 2005 end stations is taken forward to the analysis of interannual variability below.

7.4.1.3 Interannual variability

Figure 7.6 shows the layer transport anomalies for all eastern boundary end stations added to the respective mid-ocean geostrophic layer transport from the 1992 transatlantic hydrographic section. In this way the end station results show the variability of the MOC originating at the eastern boundary around the 1992 section transports, which are assumed to represent the long term mean MOC at 25ºN (Chapter 3). Linear regression of the transport anomalies according to:

$$\Delta tr = A * (\text{year after } 1980) + B \qquad (7.2)$$

is performed with coefficients in Table 7.2, and plotted in Figure 7.6. The observations for each layer are discussed separately in the following sub-sections.

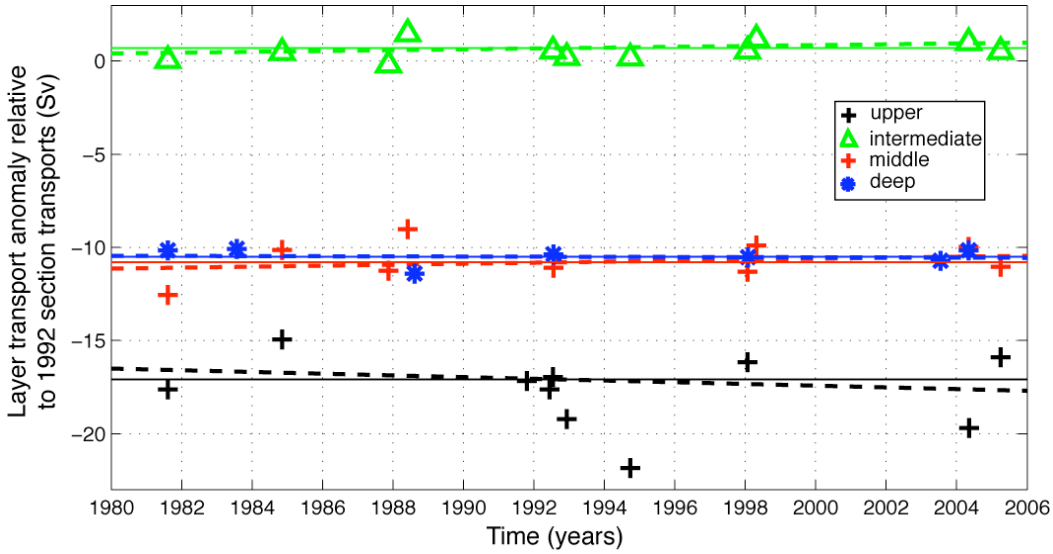

Figure 7.6 *Transport variability of the upper (+, 0-800m), intermediate (Δ, 800-1100m), middle (+, 1100-3000m), and deep (✱, 3000-5000m) layers originating at the eastern boundary. Data points plotted are the end station layer transport anomalies added to the 1992 section transport of the given layer (-17.1, 0.7, -10.8, -10.5 Sv respectively). Thin coloured solid lines show the 1992 layer transport, while the thick dashed lines are the linear regressions of Table 7.2 (colours corresponding to the anomalies).*

Layer	A (Sv yr^{-1})	B (Sv)	R^2 (%)	p value	Δtr in 25 years
Upper (0-800m)	-0.048 ± 0.220	0.1 ± 3.4	3	0.63	-1.2
Intermediate (800-1100m)	0.024 ± 0.047	-0.5 ± 0.7	13	0.28	0.6
Middle (1100-3000m)	0.030 ± 0.106	-0.3 ± 1.7	6	0.53	0.7
Deep (3000-5000m)	-0.005 ± 0.058	0.1 ± 0.9	1	0.83	-0.1

Table 7.2 *Linear regression coefficients with 95% confidence limits of eastern boundary end station layer transport anomalies to time according to equation (7.2). R^2 is the percent of variance of each time series explained by the regression.*

(a) Upper layer

Firstly we note that upper layer transport anomalies originating at the eastern boundary are larger than the estimated error for this layer, with variability ± 4.0 Sv (two times the standard deviation, Table 7.1). Linear regression of these transport anomalies shows a trend towards increasingly negative anomalies over time, indicative of a 1.2 Sv increase in southward geostrophic transport of thermocline waters between 1980 and 2005 (Table 7.2). It is however not surprising that this trend is not significant, even at the 50% level (Table 7.2), given only 10 data points in 25 years and the seasonal and possible spatial influences (discussed in Section 7.4.1.2). We can however say that the trend is not likely to be an artificial effect of the seasonal bias in northern end stations because although the strongest positive transport anomaly occurs near the start of the time series in November 1984, the other two strongly positive anomalies both occur within the last 8 years of the dataset, in the opposite sense to the trend.

Within the limitations of the available dataset for the 0-800m layer, end stations constrain variability originating at the eastern boundary to be ± 4 Sv. This is approximately a quarter of the upper layer's long-term mean transport across 25ºN. Although there may be a trend towards increasing strength of the southward recirculation over time, its magnitude is comparable to the method error of order 1 Sv (Table 7.1).

(b) Intermediate layer

This is the only layer for which a long term trend in the computed transport anomalies approaches significance (seen from Figure 7.6 and the p value of 0.28, Table 7.2). It amounts to a strengthened northward transport of 0.6 Sv over the 25 years but is not larger than the estimated error of ± 1 Sv which itself is larger than the 1992 section mid-ocean intermediate water transport. While this means that we are not able to detect any long term change in meridional transport of this layer originating at the eastern boundary, in part because the transport is so small, this is also the reason that such detection is not important for resolution of MOC variability over the last 25 years. Overall a variability of ± 1 Sv (two times the layer standard deviation) is calculated for intermediate waters at the eastern boundary, of comparable magnitude to the total layer transport (Table 3.4).

(c) Middle layer

This is the layer with the largest estimated error of ± 2.6 Sv (Table 7.1), due predominantly to the noise in transport accumulated from the eastern boundary. The relatively large variability, with standard deviation of 1.7 Sv, is therefore not surprising and indeed all observations lie within the range encompassed by the estimated ± 2.6 Sv error (Table 7.1). In this context, the computed trend towards weakened southward transport of the middle layer by less than 1 Sv in 25 years is insignificant (Table 7.2, Figure 7.6).

(d) Deep layer

The eastern boundary contribution to flow variability of the LNADW layer between 1980 and 2005 is negligible (Figure 7.6). The standard deviation of only 0.6 Sv is well within the estimated layer error (±1.4 Sv, Table 7.1). Notably linear regression shows no long term trend larger than 0.1 Sv during the 25 years (Table 7.2) which is less than 1% of the 10-12 Sv transport of this layer computed from the transatlantic hydrographic sections (Table 3.4).

7.4.2 Moorings

7.4.2.1 Overview

Both the unedited transport anomaly time series of Kiel-276 relative to the mean CTD dynamic-height profile, and the temperature record at 400 dbar (Figure 7.7) are almost continuous for the three periods of 4th April 1980 to 12th November 1985 (2048 days), 18th January 1989 to 7th July 1993 (1631 days) and 20th September 1994 to 10th April 2000 (2029 days). We label these periods I, II and III for convenience. The long term mean transport anomaly is 0.7 Sv and variability is large with a range of 41 Sv, mostly due to the influence of meddies. The mean temperature at 400 dbar is 13.37ºC with standard deviation 0.55ºC. Details of exclusion of the meddies is presented in Section 7.4.2.2, after which the time series are examined for possible existence of a seasonal cycle (Section 7.4.2.3) and to quantify interannual variability in the subtropical gyre recirculation (Section 7.4.2.4).

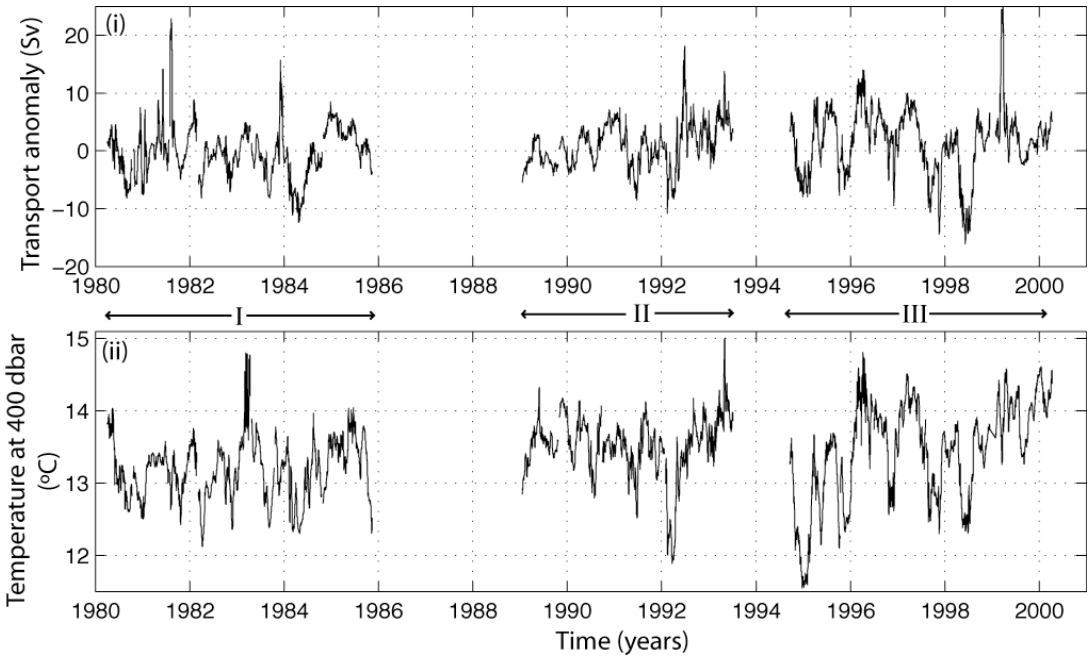

Figure 7.7 *Transport anomaly time series (0-800m) from Kiel-276 mooring derived dynamic height, daily values (i) and the corresponding temperature record at 400 dbar (ii).*

7.4.2.2 Removal of meddies

Siedler et al. (2005) identified 10 meddies at Kiel-276 between April 1980 and 2001 based on anomalies in temperature, current speed and direction. These must be excluded from our transport anomaly time series since the climatological T-S, θ-S and $\partial T/\partial p\,(p)$ relationships used in computation of the dynamic height derived transport anomaly time series are not representative of conditions when meddies are in close proximity to the mooring. Although alternative climatologies could be developed given sufficient suitable CTD casts, meddy events contaminate the transport anomaly record limiting how representative it is of the subtropical gyre recirculation at these times.

We exclude from the time series the meddy periods as identified by Siedler et al. (2005), shown by the grey shaded periods of Figure 7.8, and the additional light blue shaded period which corresponds to a salt lens at the mooring (Armi and Zenk, 1984). Although Siedler et al. (2005) did not class the salt lens as a meddy, the strong positive temperature anomaly at 1100 dbar exceeds two standard deviations of the record mean (Figure 7.8(i)). This is characteristic of, and indistinguishable from, other meddy events justifying its exclusion. Table 7.3 lists the resulting periods of data rejection due to

meddies at or near Kiel-276. Note that no exclusions are made in the 400 dbar temperature record since this does not have a strong meddy signal.

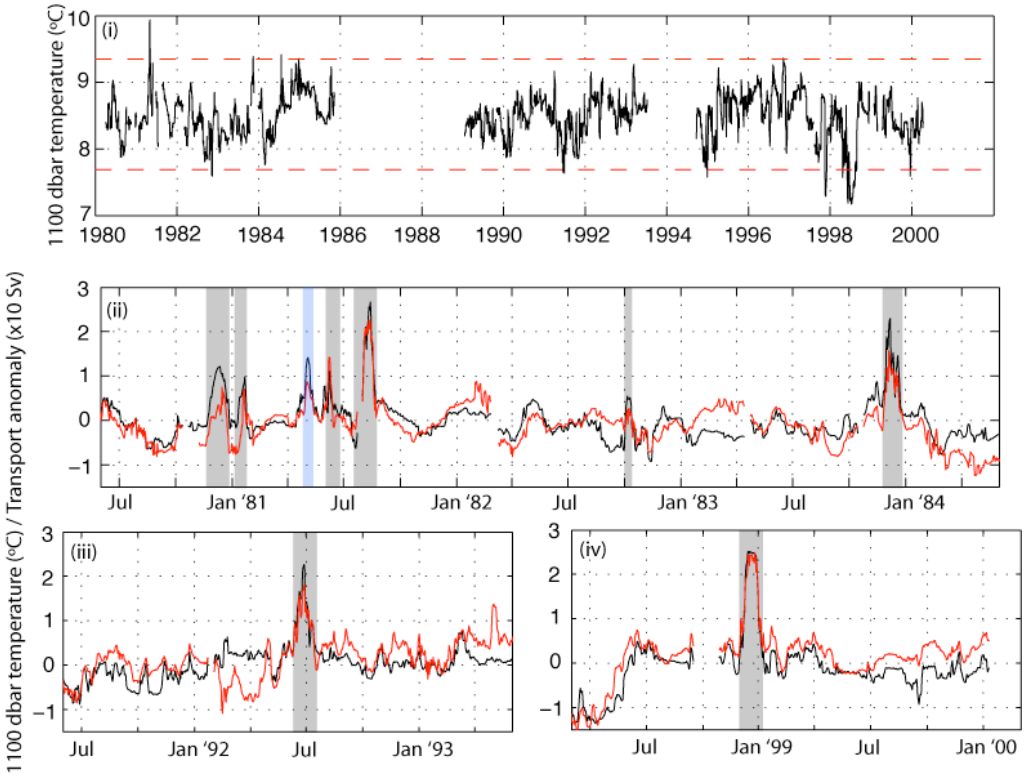

Figure 7.8 *(i) T_{1100} of Kiel-276 (black solid line) and limits of the mean (8.52ºC) ± two times the standard deviation (0.85ºC) (red dashed line). The meddy times identified by Siedler et al. (2005) are not plotted in (i) but are shown in the grey shaded sections of (ii), (iii) and (iv) where T_{1100} is plotted as an anomaly to the mean (black) along with the transport anomaly divided by 10 (red). The blue shaded region is the time when T_{1100} significantly exceeds $\mu \pm 2\sigma$ in (i), corresponding to the salt lens of Armi and Zenk (1984).*

	Start	End	Duration (days)
1	19-Nov-80	25-Dec-80	36
2	4-Jan-81	23-Jan-81	19
3	28-Apr-81	14-May-81	17
3	31-May-81	25-Jun-81	25
5	17-Jul-81	23-Aug-81	37
6	30-Sep-82	12-Oct-82	12
7	22-Nov-83	26-Dec-83	34
8	8-Jun-92	18-Jul-92	24
9	28-Feb-99	10-Apr-99	9

Table 7.3 Times of meddies at Kiel-276, rejected from the transport anomaly record

Removal of meddies and gaps between mooring deployments result in missing data periods of length 5 to 43 days within Periods I, II and III. To facilitate subsequent filtering, since these gaps are shorter than the dominant variability timescale of

approximately 2 months (Table 7.4), the gaps are filled by cubic spline interpolation with a seven day window either side of the data gap. Our estimates of the dominant correlation timescale in the data are obtained from integration of the autocovariance function out to its first zero crossing (Emery and Thomson, 2001).

Figure 7.9 shows that the cubic spline interpolation performs well for all periods between deployments and most of the meddy removal times. The spline interpolated transports of October 1982 and July 1992 however, show an anomaly of comparable magnitude to that of the removed meddy (approximately 10 Sv), but with opposite sign. Such interpolated values may be representative of the actual transport anomaly's evolution in the absence of the meddy - other non-meddy induced transport fluctuations of this size are seen in the record. Or, they may be an artefact of interpolation, influenced by frontal meanders when a meddy is upstream of the mooring (Tychensky et al., 1998). Only for these two periods are the interpolated transports questionable given the errors inherent in computing the transport anomaly record (order 2 to 3 Sv).

Start	Finish	N	T*
4/4/80	12/10/80	192	66
25/8/81	25/2/82	185	56
9/3/82	30/9/82	206	35
14/10/82	13/4/83	182	63
28/12/83	21/10/84	299	68
30/10/84	12/11/85	379	89
18/1/89	23/10/89	279	46
31/10/89	21/1/90	326	43

Start	Finish	N	T*
29/9/90	23/1/92	482	83
20/7/92	7/7/93	353	29
20/9/94	11/10/95	387	65
16/10/95	22/6/96	251	77
1/7/96	4/8/97	400	52
9/8/97	16/12/98	495	63
12/4/99	10/4/00	365	40

Table 7.4 *Integral timescale, T*, of periods of the Kiel-276 dynamic height transport anomaly time series which are continuous for more than 180 days. N is the record length in days.*

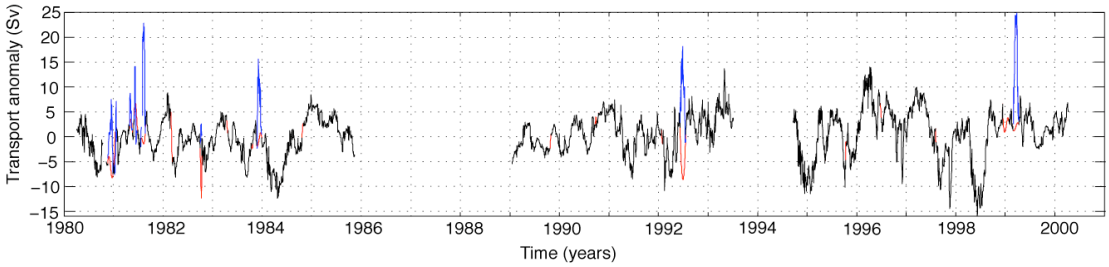

Figure 7.9 *Interpolation across gaps in Kiel-276 transport anomaly time series. The black line is the time series after removal of meddy periods, shown in blue. The red lines are the cubic spline interpolated transport anomalies in the meddy and deployment gaps*

Interpolation is required for subsequent filtering and the possible error introduced is small enough not to be a problem in the interpretation of the high frequency transport anomaly variability discussed next in Section 7.4.2.4. Gaps in the 400 dbar temperature time series are similarly interpolated to give continuous records for each of Periods I, II and III.

7.4.2.3 Seasonal variability

Before the interannual variability is assessed, we make use of Kiel-276 transport anomaly time series to consider Stramma and Siedler's (1988) proposed seasonal cycle in gyre shape. They found summer to be characterised by a southward shift in position of the Azores Current by 2º latitude, and movement of the easternmost branch of the subtropical gyre recirculation towards Africa (refer back to Figure 5.1) while in winter its offshore displacement might be accompanied by northward flow along the slope. Although the gyre recirculation magnitude remains constant, if the signal is real then the suggested changes in Canary Current location have implications for our computed upper layer end station transport anomalies (Section 7.4.1).

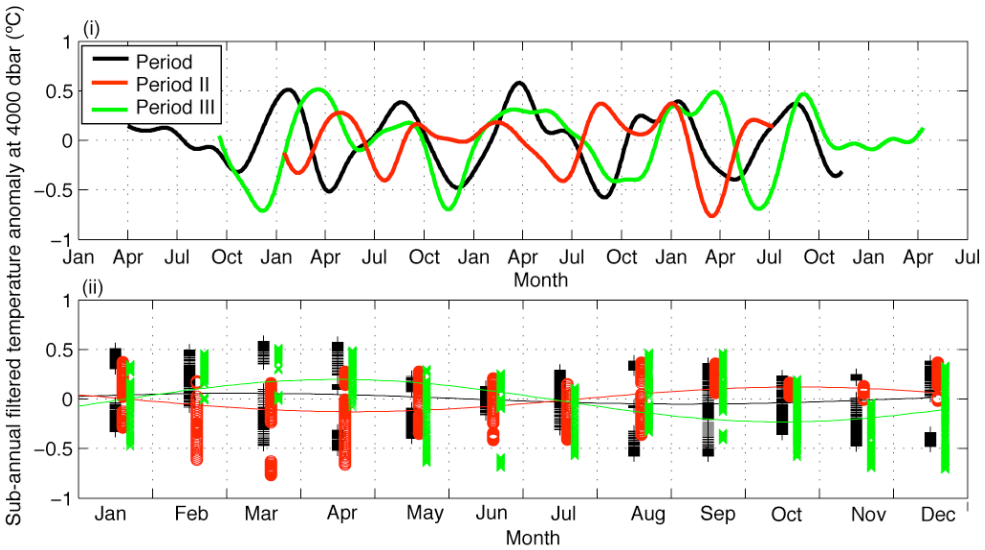

Figure 7.10 *Seasonal variability of Kiel-276 400 dbar temperature anomaly time series, after removal of high frequency variability (low pass Lanczos-cosine filter with time period cut off of 90 days) and of the low frequency signal (removal of a one year running mean). In (i) the time series of each Period, I, II and III, are plotted as a function of month for the period duration. (ii) shows the sinusoidal least squares regression of temperature anomaly to month of year (Table 7.5). Daily transports are plotted at the mid-point of each month, offset slightly between periods I, II and III (colours are the same as in (i)).*

To examine the seasonal signal we filter out both the high and low frequency variability, with a 90-day low pass Lanczos-cosine filter for the former, and a 1 year running mean for the latter. The resulting seasonal component of each period's 400 dbar temperature records is overlaid in Figure 7.10(i). Stramma and Siedler (1988)'s dataset overlaps with only Period I of our records, and they suggested the 200m warming observed every winter to correspond to the northward shift of the Azores Current. While this can be seen in the first two Januarys of Period I in our record, the signal is not robust through the other periods (Figure 7.10(i)). This finding is supported by sinusoidal least squares regression of the temperature anomaly at 400 dbar to $T_{400} = A\cos(\omega t) + B\sin(\omega t) + C$, where $\omega = 2\pi/\tau$ and τ is 12 months, t is time in integer months and A, B, C are coefficients of Table 7.5. Although Periods I and III have peaks in February and April (and thus winter time warming at 400 dbar), Period II shows wintertime cooling. Neither this, nor the very small amplitude of the Period I regression (less than 0.1ºC, Table 7.5) support the existence of a robust seasonal cycle in the position of the Azores Front.

Period	A	B	C	R^2	Amplitude (ºC)	Month of peak
I	0.01 ± 0.02	0.05 ± 0.02	0.00 ± 0.02	2	0.05	February
II	0.07 ± 0.02	-0.10 ± 0.02	-0.00 ± 0.02	11	0.12	October
III	-0.09 ± 0.02	0.20 ± 0.02	-0.02 ± 0.02	21	0.21	April

Table 7.5 *Regression coefficients corresponding to Figure 7.10 (ii). R^2 is the percentage of variance accounted for by the fit.*

From the Kiel-276 time series, we conclude that the seasonal variability in the shape of the subtropical gyre recirculation does not appear to pose a problem for the eastern boundary end station layer transport anomalies, and this is supported by the findings of Le Traon and De May (1994) and Sena Martins et al. (2002). We do note that detection of seasonal timescale variability at Kiel-276 is complicated by the possible interaction of Rossby waves with the Azores Current since Cipollini et al. (1997) found the first baroclinic mode to have a period of the order 200 days in this region. The filtered time series from which Figure 7.10 is plotted therefore may include such a signal.

7.4.2.4 Interannual variability

To determine interannual variability of the subtropical gyre recirculation strength at Kiel-276, we work with a 1 year running mean of the time series (Figure 7.11). This

smoothing is in fact performed on the 90-day low pass Lanczos-Cosine filtered time series to prevent contamination by either of the questionable cubic spline interpolated periods (Section 7.4.2.2) (the 90-day high pass filtered time series is shown in Figure 7.12). It is immediately apparent that there is good agreement between the interannual variability of the 400 dbar temperature and that of the dynamic height transport anomaly records (Figure 7.11). Because a direct proportion relationship has been found between the two (Section 6.2.8), confidence in the directly computed transport anomalies is therefore increased. Comparison of the dynamic height derived transport anomaly with that from the 400 dbar temperature proxy is shown in Figure 7.13.

To interpret the transport anomalies of Figures 7.11 and 7.13 we must distinguish between periods of the record dominated by changes in gyre strength rather than by shifts in the position of the Azores Front. For this we draw on the analyses of Brachet et al. (2004) and Volkov (2005) who inferred fluctuations in the Azores Current strength from altimeter derived sea level anomaly eddy kinetic energy (EKE) observations, and Siedler et al. (2005) who suggested that EKE fluctuations at Kiel-276 were due to changes in the north-south position of the Azores Front. High EKE at Kiel-276 can therefore be interpreted as either stronger transport of the Azores Current, or a southward shift of the Azores Front (Kiel-276 lies to the south of its mean position). Since the Azores Front marks the transition between waters of the subtropical and subpolar gyres, a southward shift should be accompanied by cooling of the thermocline waters at the mooring. Conversely, as explained in Section 6.2.1 strengthened Azores Current transport is associated with a warm anomaly at 400 dbar since this increases the dynamic height relative to the (imagined) reference profile north of the Azores Current. Accordingly, coincident increases (or decreases) in the EKE, transport anomaly and 400 dbar temperature records on interannual timescales, are explained by an increasing (decreasing) Azores Current transport. Alternatively, if the trend in EKE opposes that of the 400 dbar temperature anomaly, frontal shifts are assumed to underlie the observations, preventing detection of fluctuations in the subtropical gyre recirculation strength.

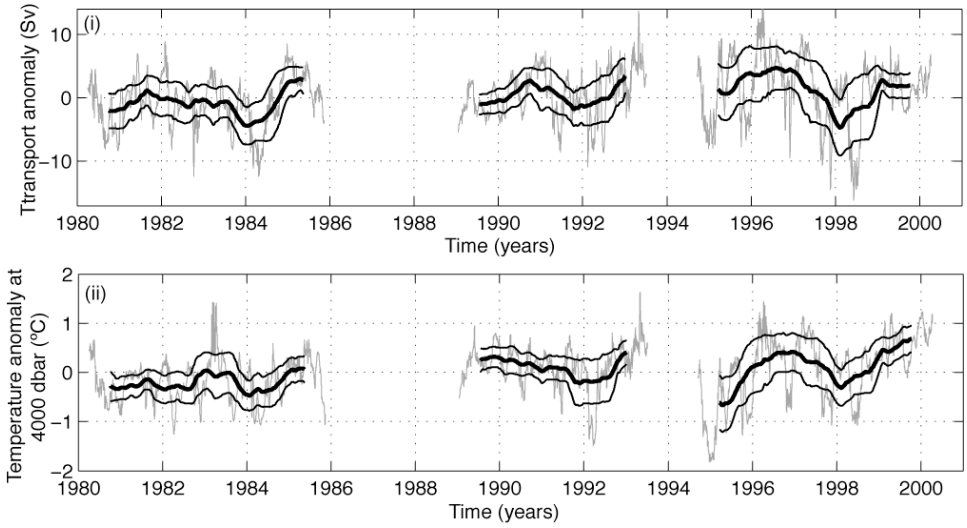

Figure 7.11 *Unfiltered (interpolated) transport (i) and 400 dbar temperature anomaly (ii) time series at Kiel-276 (light grey), with a one year running mean (heavy black). Estimated errors (thin black lines) correspond to the limits of ± 2 standard errors, defined as √(yearly variance/N*) with N*= 6, based on 2 month integral timescale (Table 7.5). Tick marks denote the 1st January.*

We therefore compare the 1 year running mean Kiel-276 transport anomalies (both computed from dynamic height and the 400 dbar temperature anomaly proxy) with annual high frequency dynamic height transport anomaly variance which is taken to represent EKE at the mooring (Figure 7.13). The high frequency transport is that resulting from application of the 90-day high pass Lanczos-cosine filter (Figure 7.12). Although interpolation across some periods where meddies have been removed prevents detailed examination of the high frequency variability, the influence of this on annual high frequency transport variances (as plotted in Figure 7.13), is considered to be negligible.

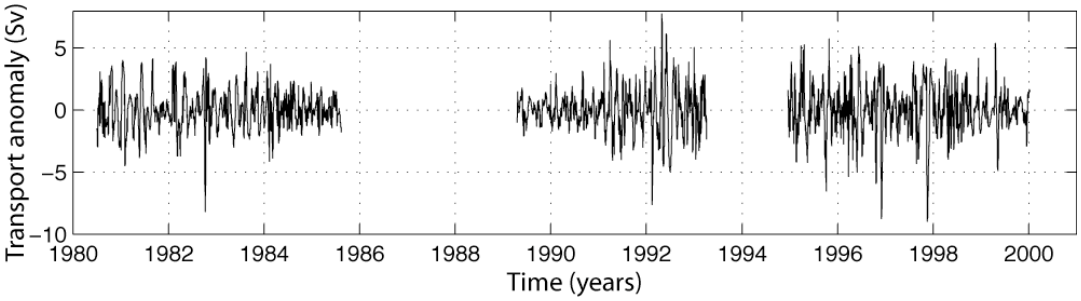

Figure 7.12 *High frequency variability of the Kiel-276 transport anomaly time series (90 day period cut off).*

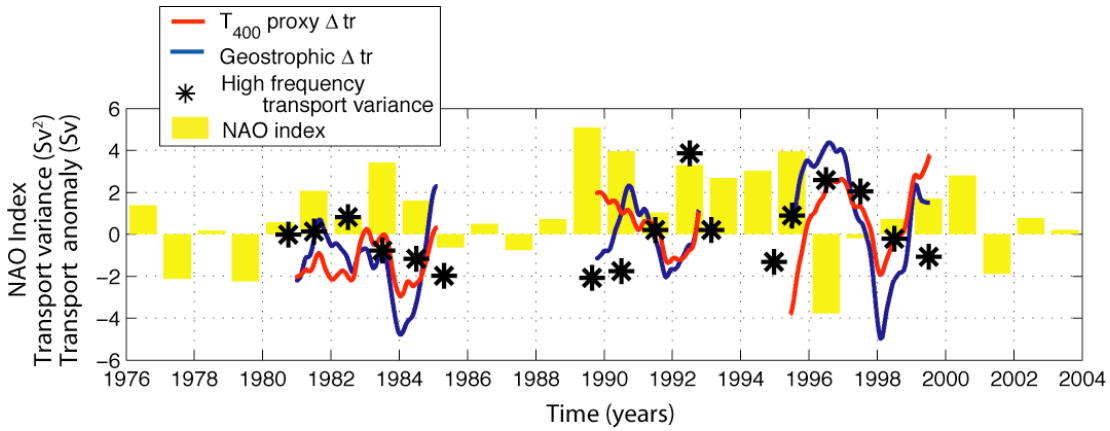

Figure 7.13 *Comparison of interannual filtered transport anomaly time series from Kiel-276 dynamic height and the T_{400} anomaly proxy ($\Delta tr=\Delta T_{400}$*6.3) with the wintertime (December through March) NAO index from Hurrel (http://www.cgd.ucar.edu/cas/jhurrell/indices.html) and 1 year variance of the high frequency transport dynamic height derived transport anomaly of Figure 7.12 plotted as an anomaly relative to the mean. Ticks mark 1st January.*

Between 1995 and 1998 changes in the yearly mean transport anomaly and the high frequency transport variance are of the same sign (Figure 7.13) and can therefore be interpreted as being due to gyre strength changes. Both increase through 1995/96 then decrease to 1998, identifying first a strengthening then a weakening of the eastern basin subtropical gyre recirculation. A decrease of subtropical gyre recirculation strength to 1998 has been suggested qualitatively by Brachet et al., (2004) and Volkov (2005), which Figure 7.13 allows us to quantify at approximately 5 Sv (from the temperature transport anomaly proxy). Brachet et al. (2004) and Volkov (2005) suggested the weakened subtropical gyre to be a response to the strong negative wintertime NAO of 1996 (Figure 7.13) and it is unfortunate that the rest of our transport anomaly record is contaminated by frontal shifts (discussed below), preventing assessment of the validity of this claim with the longer time series. Similarly we cannot comment on whether or not the Azores Current transport recovers into 2000, as proposed by Pingree (2002), although the approximately 6 Sv change observed is as Pingree (2002) recorded.

Aside from the 1995 to 1998 period of the Kiel-276 transport anomaly record discussed above, the remainder is dominated by shifts in the position of the Azores Front. This is seen in the opposing trends of fluctuations in the interannual transport anomalies and high frequency transport anomaly variance. For example after 1998 the transport anomaly increases while EKE decreases (Figure 7.13) consistent with northward movement of the Azores Front away from the mooring signalled by warming in the

thermocline (and a positive transport anomaly) and the decreased mesoscale variability detected at the mooring. This is also true of 1984 to 1986 and possibly 1992 to 1993. The opposite is observed from 1990 to 1992 when EKE increases and the transport anomaly gets less positive, consistent with a southward shift of the Azores Front; increased high frequency at the mooring and cooling in the thermocline. At such times we cannot comment on trends in the strength of the eastern basin subtropical recirculation.

Although even on interannual timescales, north-south shifts in the position of the Azores Front can contaminate the transport anomaly record at Kiel-276 (as discussed in the preceding paragraph) the time series does still provide an upper limit for variability of the eastern basin subtropical gyre recirculation. Although individual transport fluctuations do not necessarily correspond to changes in the gyre strength they do indicate that the eastern basin subtropical recirculation strength has remained constant to within ± 2 Sv for the first half of both the 1980's and the 1990's (Figure 7.13). If any changes in the gyre recirculation strength larger than ± 2 Sv had occurred in the monitoring period we would expect the signal to be apparent above that of shifts in the Azores Front. This constraint is based on the 400 dbar temperature anomaly transport proxy, and although fluctuations of the dynamic height transport record are slightly larger (e.g. in 1984/85 or 1998/2000) we have more confidence in the former since as discussed in Section 6.2.8 the errors are larger for the dynamic height method.

To summarise, although the transport anomalies computed are on the borderline of significance at the 95% level (Figure 7.11), and are largely dominated by changes in the position of the Azores Front rather than changes in the current strength, we have constrained interannual variations of eastern basin subtropical gyre recirculation strength to be less than ±3 Sv, based on the variability of Figure 7.13 and the 1 Sv error of the 400 dbar temperature transport proxy.

7.5 WESTERN BOUNDARY GEOSTROPHIC TRANSPORT

7.5.1 End Stations

7.5.1.1 Overview

As at the eastern boundary, we first consider whether the end station transport anomalies of each layer can be considered independent. For the upper layer, all stations are separated by at least 5 days, or one degree of latitude (Table 5.6). 5 days is the minimum temporal separation required for independence of this layer's transport anomalies, as estimated from a baroclinic Rossby wave propagation speed of 3 to 4 cm s^{-1} at the western boundary (Lee et al., 1996), with our study region width of 14km. Interaction of these Rossby waves with the boundary influences the lower layer circulation (Lee et al., 1996), and study region widths of 20 and 37 km require temporal separation of 8 and 14 days for independence of middle/intermediate and deep layer transport anomalies. These criteria are satisfied by all stations of the middle/intermediate layer that are separated by less than one degree of latitude, and also by all deep layer stations except those of 19th and 28th March 1987, separated by 1 km (Table 5.6). Their transport anomalies however differ by more than 10 Sv and both are included in subsequent analysis.

The overview of western boundary layer transport anomalies (Table 7.6) shows variability to be significantly larger than at the east. Standard deviations of the upper and middle layer transport anomalies are approximately one and a half times those at the east, and that of LNADW is seven times that at the east. This is important since standard deviations larger than the estimated error permit detection of signals above noise that results from method uncertainties. This is not true of the intermediate layer however, for which flow variability is negligible as indicated by the standard deviation of 0.1 Sv, smaller than the estimated error of 0.2 Sv (Table 7.6). As at the eastern boundary, the mean transport anomaly for a layer may not be exactly zero due to referencing to a level outside the layer depth, with the dynamic height reference curve constructed from different stations at different depths. There is the additional affect of appending casts down the slope in the deep layer at the west. The mean value is not important though, since we are concerned with variability about this arbitrary mean state. Finally we note that with more than 25 observations in as many years at this

boundary it may be possible to learn something about both long term changes in water mass transports, as well as those on sub-annual timescales, both are discussed below.

Layer	Number of observations	Mean Δtr (Sv)	Δtr standard deviation (Sv)	Range of Δtr (Sv)	Estimated error in Δtr (Sv)
0-800m	39	0.6	2.8	10.4	2.0
800-1100m	39	0.0	0.1	0.6	0.2
1100-3000m	39	0.0	2.5	10.8	2.4
3000-4700m	29	0.7	4.2	17.3	4.2

Table 7.6 *Overview of layer transport anomalies (∆tr) at the Western boundary. Note that as explained in Section 7.4.1.1 the mean layer transport anomalies are not required to be identically equal to zero.*

7.5.1.2 Sub-annual variability

Current meter observations of western boundary transports at 26.5ºN (Lee et al., 1996) showed seasonal cycles in both the upper layer (Antilles Current) and DWBC transports. We therefore examine the end station layer transport anomalies to see if a similar cycle is found. Although there were both baroclinic and barotropic signals in Lee et al. (1996)'s seasonal cycles, only the former would show up in our observations. Any baroclinic seasonal cycle should be ideally removed before addressing interannual variability (Section 7.5.1.3). To assess this we compute the least squares regression of the observed transport anomalies as a function of month to a sinusoidal curve with periods of both 6 months and 1 year, and variable phase shift according to

$$\Delta tr_{seas} = A\cos(\omega t) + B\sin(\omega t) + C \qquad (7.3)$$

where $\omega = 2\pi/\tau$ and τ is either 12 or 6 months, t is time in integer months and A, B, C are coefficients to be determined (Figure 7.14 and Table 7.7).

Sub-annual regressions of end station upper layer transport anomalies, although not statistically significant, show summer peaks in northward flow (Figure 7.14(i)) in phase with Lee et al. (1996)'s findings, but of reduced amplitude. That both the July and August peaks of the 6 month and 1 year period regressions are consistent with the July maximum of Lee et al. (1996), increases confidence in the end station observations. The regression amplitudes are however less than 1 Sv compared to approximately 7 Sv from the moorings (Lee et al. 1996), although the sinusoidal fits do smooth the July peak for which the monthly anomalies range from 2.5 to 4.5 Sv (Figure 7.14 (i)). It is not surprising that the full magnitude of the July peak in transport is not captured by the end

stations, nor that the fits are not significant even at the 20% confidence level (Table 7.7), given the limited observations and their uneven distribution through the months. June has the most CTD casts with 7, while there are none in December and only two in each of November and January (Table 5.6). The moored dynamic height time series (Section 7.5.2) will be used to better address the question of whether the signal of sub-annual variability in the end station upper layer transport anomalies is an artefact of the limited data set or a robust feature of the baroclinic circulation.

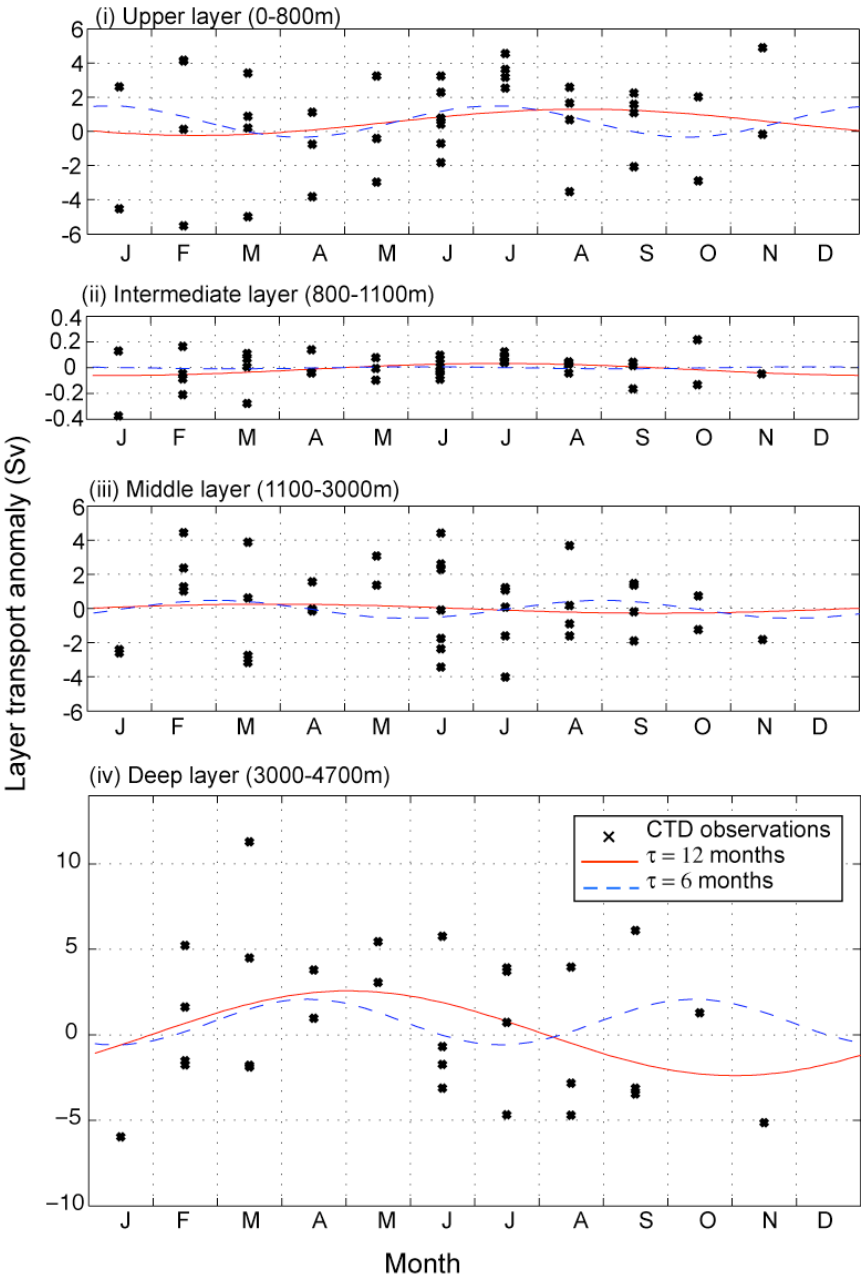

Figure 7.14 *Regression of upper (i), intermediate (ii), middle (iii) and deep (iv) layer transport anomalies to the sinusoidal semi-annual and annual cycles (equation 7.3 with* τ *of 6 or 12 months). Legend of (iv) applies to all plots.*

Layer	τ (months)	A (Sv)	B (Sv)	C (Sv)	Amplitude (Sv)	Month(s) of peak(s)	p-value
0-800m	6	0.87	0.29	0.58	0.9	Jan, Jul	0.4
	12	-0.48	-0.59	0.53	0.8	Aug	0.5
800-1100m	6	0.01	-0.01	0	0.0	Jun, Dec	0.9
	12	-0.05	-0.01	-0.01	0.0	Jul	0.2
1100-3000m	6	-0.26	0.45	-0.06	0.5	Feb, Aug	0.7
	12	0.02	0.27	-0.01	0.3	Apr	0.9
3000-4700m	6	-1.21	-0.56	0.74	1.3	Apr, Oct	0.5
	12	-1.28	2.11	0.09	2.5	May	0.2

Table 7.7 *Coefficients of least squares regression of western boundary end station transport anomalies to time following equation 7.3. Months of peaks correspond to the fitted transport rather than the observed anomalies, and the p-value is of the regression.*

In the intermediate layer, any sub-annual cycle is smaller than ±0.1 Sv (Figure 7.14(ii), Table 7.7). Although the yearly period regression is significant at the 20% confidence level (Table 7.7), it is associated with such a small transport range so as to be insignificant given the estimated errors for this layer (0.2 Sv).

Similarly there is no evidence for robust year to year sub-annual variability in the middle (UNADW) layer. The regressions have amplitudes less than 1 Sv (Table 7.7) which is both well within the bounds of observational uncertainty (Table 7.6), and significantly less than other variability contributions as indicated by p values larger than 0.6 for both the semi-annual and annual cycle fits (Table 7.7).

Resolution of sub-annual variability in the LNADW layer is inhibited by only having 3 data points during the months of October to January inclusive (Table 5.6). For this reason neither of the sub-annual regressions are judged significant (Table 7.7 and Figure 7.14(iv)). Although the p value of the annual cycle is 0.2 (small relative to regressions of other layers), it suggests maximum southward transport in October/November for which data points are as likely to represent interannual as sub-annual variability (only one observation per month). We therefore consider it to be a coincidence that the regression's peak DWBC transport of LNADW is in agreement with Lee et al. (1996)'s October maximum southward transport below 800 m, which we do not expect to see in end station observations since it represents a barotropic response to remote wind forcing (Lee et al., 1996). Again, it is anticipated that the moored dynamic height time series will help resolve this issue (Section 7.5.2).

From the end stations alone, it is apparent that there is too much noise in, and not enough observations of, layer transport anomalies to detect sub-annual cycles in any of the layers (none of the regressions are significant even at a 20% level, Table 7.7). The sinusoidal sub-annual cycle regressions of the upper three layer transport anomalies suggest variability on this timescale to be smaller than ±1 Sv (Table 7.7). Although that of the LNADW layer is larger at ± 2-3 Sv (Table 7.7, Figure 7.14(iv)) this is likely an artefact of the heavily summer biased dataset. To minimise the possible effects of any such sub-annual variability when considering interannual timescale changes (Section 7.5.1.3), averaging of transport anomalies over at least a year will be performed.

7.5.1.3 Interannual flow variability

Here we address the question of whether a long term trend or interannual oscillations may be detected in the western boundary end station layer transport anomalies. In Figure 7.15 we plot for each layer, all data points and their linear regression over time (coefficients in Table 7.8). Two and five year mean anomalies with error bars spanning ± one standard deviation of the constituent observations are also added (the method errors of Table 7.6 are not included). In the absence of resolvable seasonal variability (Section 7.5.1.2), Figure 7.15 illustrates interannual variability in the mid-ocean baroclinic layer transports originating at the western boundary of 26.5ºN between 1980 and 2005 derived from careful selection of high quality hydrographic stations (Section 5.3.1) with quantified errors (Table 5.7). It is immediately apparent that variability is large on annual periods. Trends over the 25 year period in the water masses comprising the upper and lower limbs of the MOC are consistent towards a reduction in strength over time. Interpretation of Figure 7.15 follows for consecutive layers.

Layer	A (Sv per day $x10^{-4}$)	B (Sv)	P value	R^2	25 year range (Sv)
Upper	-0.52 ± 3.65	0.9 ± 1.9	0.8	0.2	-0.5
Intermediate	0.04 ± 0.16	0.0 ± 0.1	0.6	0.6	0.0
Middle	1.41 ± 3.32	-0.7 ± 1.8	0.4	2.0	1.3
Deep	2.64 ± 6.36	-0.7 ± 3.7	0.4	2.6	2.4

Table 7.8 *Linear regression of layer transport anomalies according to* $\Delta tr = A$(day number after 1st January 1980) $+ B$ *with 95% confidence limits for A and B. The 25 year range is the transport change in 25 years according to the regression coefficients*

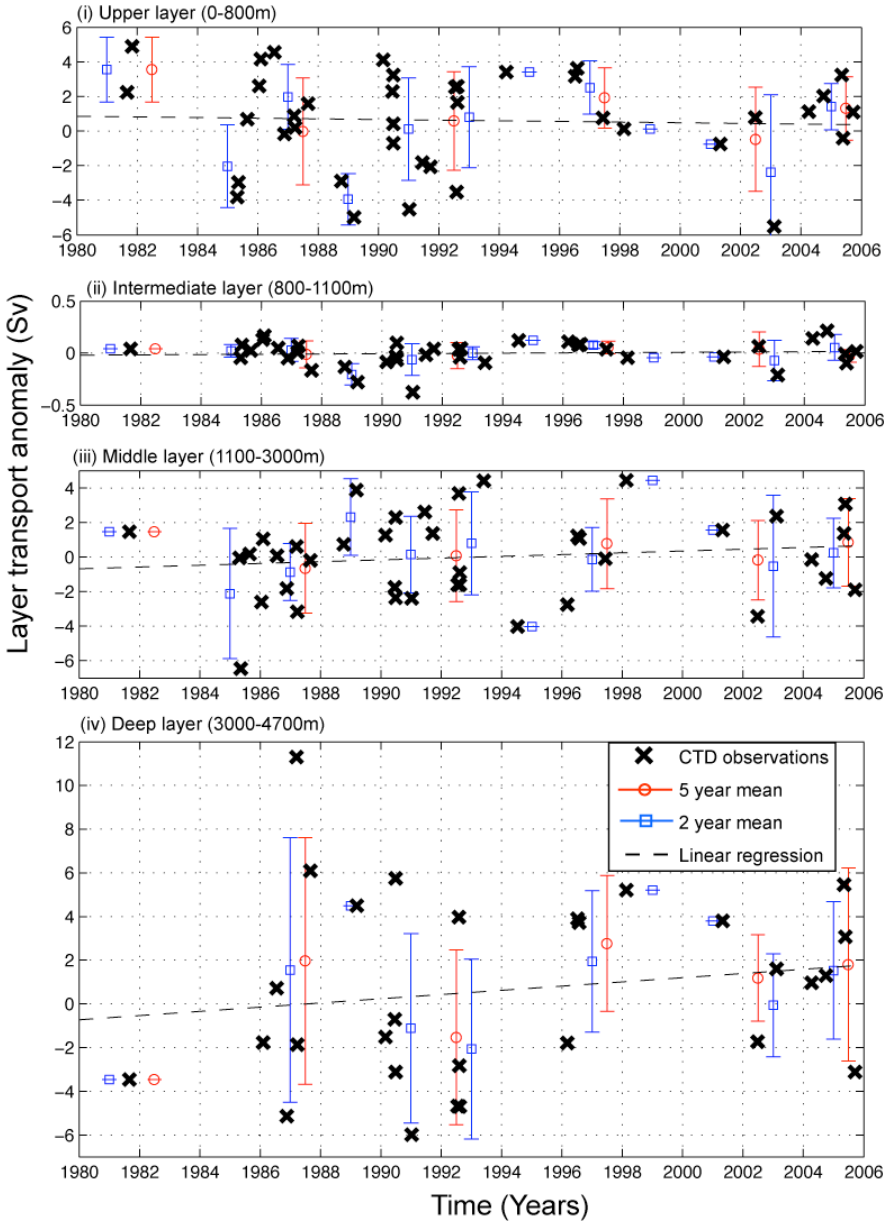

Figure 7.15 *Interannual variability of the upper, intermediate, middle and deep layer transport anomalies at the western boundary. Individual data points are plotted (**x**) along with their 5 year mean (o) and 2 year mean (□) with error bars of ± one standard deviation. For the 5 year means the last group is actually 2005-2006. Dashed lines are the linear regression of individual data points to time, coefficients in Table 7.8.*

The upper layer end stations show a trend towards increased southward transport of the 0-800m waters amounting to a 0.5 Sv change between 1980 and 2005 (Table 7.8). This is small in comparison with the variability observed within two and five year periods (Figure 7.15(i)). The two year mean anomalies are sensitive to data coverage since end stations are concentrated in the late 1980's to early 1990's. We therefore do not attribute any significance to differences in the bi-annual mean anomalies such as between 1988-1990 and 1996-1998. Any possible interannual oscillations in upper layer transport cannot therefore be commented upon from the end stations. In contrast none of the five

year mean anomalies are significantly different given the error bars plotted (Figure 7.15(i)). Identification of any decadal trend in southward transport of thermocline waters at the western boundary from end stations therefore has to contend with the order ± 2-3 Sv interannual variability, to which the ± 2 Sv method error is likely a large contributor.

Interannual variability of the intermediate waters originating at the western boundary is, as at the east, negligible (Figure 7.15(ii)). Linear regression shows any trend to amount to a transport change of less than 0.1 Sv from 1980 to 2005, while the range of 5 year mean transport anomalies, including limits of ± one standard deviation, is less than 0.2 Sv. This is equal to the end station error for this layer.

Transport anomalies of both NADW layers show small insignificant (Table 7.8) trends towards decreased southward flow of the DWBC, amounting to reductions of 1.3 and 2.4 Sv in the upper and lower deep water layers respectively over the 25 years. This is broadly consistent with the freshening of LNADW at this boundary (by 0.009 in 25 years), to which the end stations have been calibrated (Section 5.3.2). Applying a salinity offset of –0.005 results in positive transport anomalies of 1.2 Sv and 2.8 Sv for UNADW and LNADW respectively (Table 5.7). The observed trends due to this freshening are therefore smaller than expected, a likely a result of the substantial interannual variability against which these trends are occurring, reflected in the two and five year transport anomaly means (Figure 7.15(iii) and (iv)).

We conclude that it is difficult to detect interannnual variability with amplitude smaller than 3 Sv (Figure 7.15) due to possible sub annual variability and the end station method error. It is because of the difficulty of separating the observed interannual variability of end station layer transport anomalies from the error contribution that analysis of moored dynamic height profiles (Section 7.5.2) should complement this data set. This is because layer transport anomaly errors are dominated by the allowance made for variable offshore distance of CTD stations (Section 5.3.3.3). Although temporal variability remains to be quantified for mooring observations at a fixed location, dependence on spatial variability of the flow field is constant in time, and should improve our ability to constrain layer transport anomalies at the western boundary.

7.5.2 Moorings

7.5.2.1 Overview

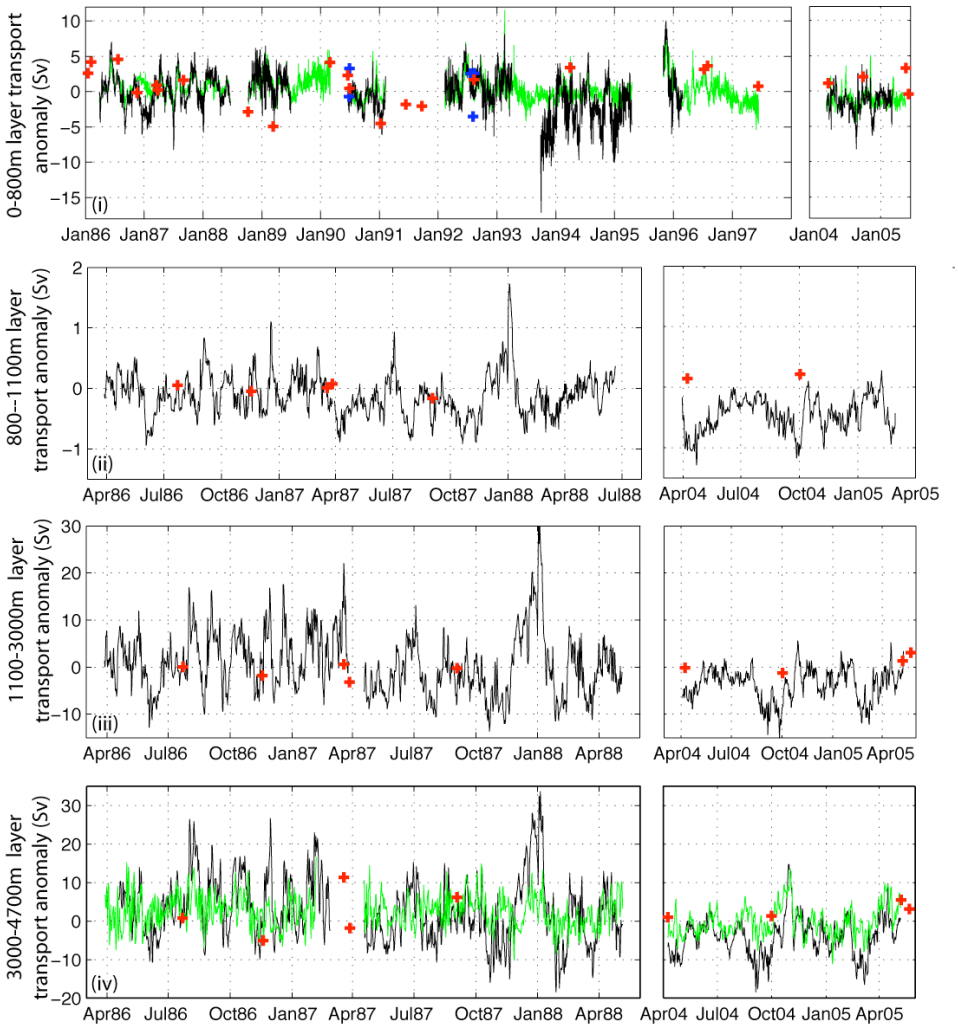

Figure 7.16 *The western boundary upper (i), intermediate (ii), middle (iii) and deep (iv) layer transport anomaly time series from mooring derived dynamic height profiles (black lines), and transport anomalies from either the T_{400} or T_{3000} proxy according to equation (6.8) (green). End station transport anomalies from CTD casts north (+) or south (+) of 26°N also shown. All mooring observations are at 12 hour resolution.*

The layer transport anomalies from mooring dynamic height measurements are in good agreement with discrete end station observations (Figure 7.16). Note that Figure 7.16 shows the full mooring transport anomaly time series of each layer, but only the parts of the end station data set that are coincident in time.

Due to propagating features in the western boundary region (e.g. Lee et al., 1996) we do not expect perfect agreement between simultaneous mooring and end station observations since they differ in location. To assess mooring transport anomaly performance, minimum transport differences between the two data sets within ± 5, ± 8,

± 8 or ± 14 day windows for the upper, intermediate, middle and deep layers respectively are computed. The differences have maximum values of 2, 0.6, 4 and 7 Sv for the respective layers (only using casts north of 26ºN). These are within the estimated errors of all mooring transport anomalies except of the Rapid array deep and middle layers (Table 6.8b), the latter are biased low relative to the CTD anomalies, with mean offsets of –4.3 and –3.6 Sv respectively. This is consistent with DSOW freshening of 0.008 over 25 years in the CTD stations but not incorporated into the θ-S reference curves, equating to a transport range of approximately 3 Sv (Slater 2003).

7.5.2.2 Sub-annual variability

Here we first address the question of sub-annual cycles in layer transport anomalies using the mooring observations, in light of the deficiencies of the end station data set for this purpose. We then compute the sub-annual variability in each layer transport anomaly at the western boundary to estimate the uncertainty of annual mean transport anomalies computed from moorings.

(a) Sub-annual cycles

Possible existence of any sub-annual cycle is assessed using monthly mean mooring layer transport anomalies (Figure 7.17). Monthly means are computed for each layer (Figure 7.17), from the whole time series after removal of each deployment's mean anomaly to prevent biases due, for example, to mooring configuration. 95% confidence limits for the mean are estimated from the transport variance during each month (after removal of the deployment means) and the number of independent observations per month (the record length in days divided by the integral timescales which range from 8 to 53 days but for the most part are 10-20 days (Table 7.9).

Despite upper layer transport anomaly time series amounting to more than 8 years of observations there is little support for seasonal or semi annual cycles in Figure 7.17(i). The summer northward peak in monthly mean dynamic height transport anomaly, also seen in end station observations (Section 7.5.1.2), is not found in the T_{400} observations. Of the alternative mooring products, we place more confidence in the latter due to the longer data set and smaller estimated error (Sections 6.3.7 and 6.3.8). None of the monthly mean anomalies are significantly different from zero at the 95% confidence

level, and have a range of only 2 Sv (dynamic height) or 1.5 Sv (T_{400} proxy). Based on 8 years of data therefore, seasonal cycles in upper layer transport anomalies are less than 2 Sv and not significant.

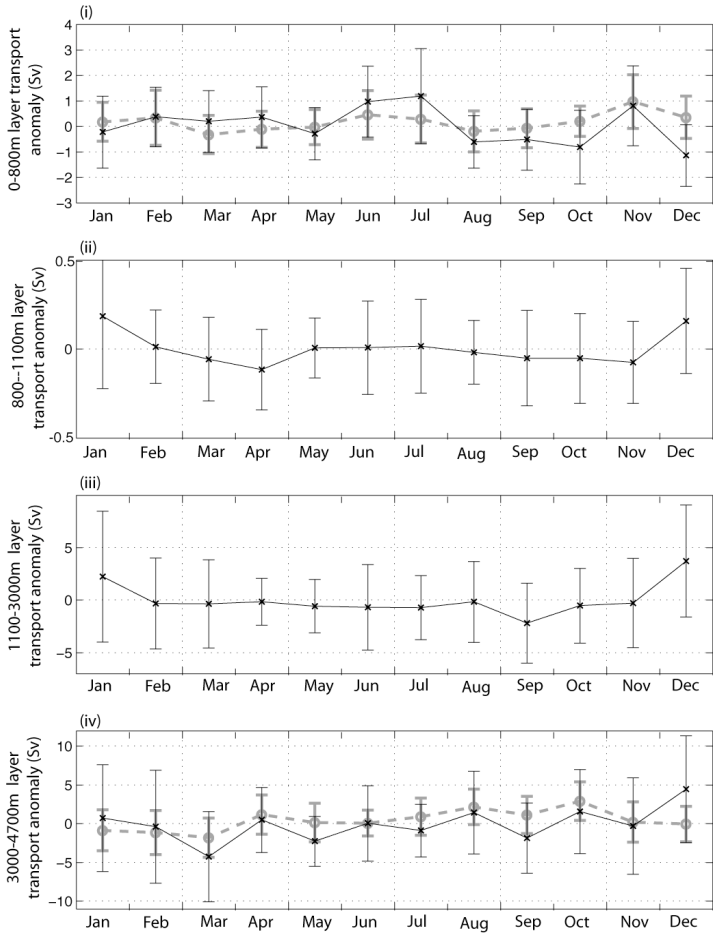

Figure 7.17 *Monthly mean transport anomalies of the upper (i), intermediate (ii), middle (iii) and deep (iv) layers from mooring dynamic height observations (black thin lines) and the T_{400} or T_{3000} proxies from equation (6.8) for the upper and deep layers only. Each continuous record period of Figure 7.16 has had the long term mean removed before computation of monthly means. Error bars are ± 2√(monthly variance/N*) where the monthly variance in computed after removal of each period's mean and N* is the number of independent samples per month.*

For the intermediate, middle and deep layers, time series amount to less than 4 years and are not long enough to identify any sub-annual cycles with confidence. This is illustrated by the strongest positive monthly mean anomaly occurring in December or January for each layer (Figure 7.17(ii-iv)), which is due mainly to the strong northward flow event in all layers of Winter 1987/88 (Figure 7.16). Accordingly, interannual signals are at least as important as that of the sub-annual component in determining the monthly means plotted, and seasonal cycles are not well resolved. Although monthly means of the T_{3000} transport anomaly proxy suggest maximum southward transport in

winter and minimum in late summer, the range of 4.7 Sv is equal to its error (Section 6.3.8), and is not significant at the 95% confidence level. Since no robust cycles have been detected none are removed from the mooring layer transport anomaly time series when examining interannual changes.

	Upper		Intermediate	Middle	Deep	
Period	Transport T* (N)	T_{400} T* (N)	T* (N)	T* (N)	Transport T* (N)	T_{3000} T* (N)
I	44 (364)	31 (364)	9 (364)	8 (364)	9 (314)	8 (364)
II	17 (448)	15 (448)	18 (448)	20 (384)	19 (384)	10 (384)
III	11 (263)	22 (508)				
IV	14 (236)	20 (236)				
V	15 (417)					
VI	22 (565)	40 (1161)				
VII	23 (119)	53 (590)				
VIII	11 (335)	8 (405)	21 (335)	22 (401)	19 (394)	13 (394)

Table 7.9 *Integral timescales (T*) in days, for transport anomaly time series of all deployments as well as the T_{400} and T_{3000} records. N is the record length (also in days).*

(b) Annual mean error estimates

Ultimately we may wish to infer annual mean layer transport anomalies from the mooring time series. The uncertainty of such annual means due to temporal variability (rather than method error) is estimated (Table 7.10) from the standard error of a yearly mean transport anomaly; √(transport variance/N*), where N* is the number of independent observations during the year (see Table 7.9).

For the upper layer, standard errors of annual transport anomalies range from 0.4 to 1.4 Sv, and of the 11 yearly periods, 8 are smaller than 1.0 Sv (Table 7.10). Annual mean 400 dbar temperatures have standard errors of mainly 0.06 to 0.08ºC (Table 7.10), which is equivalent to 0.3 to 0.5 Sv of transport variability following equation (6.8a). Equivalent treatment of the intermediate, middle and deep layers (Table 7.10) yields uncertainties of annual mean transports due to temporal variability of 0.1, 1-2 and 1-2 Sv for the respective layers (for the deep layer we exclude the 3.6 Sv s_ε since it is based on only two independent observations in the year from April 1989). The deep layer 3000 dbar transport anomaly proxy standard error of 0.9 Sv (Table 7.10 and equation 6.8b) is broadly consistent. These standard errors of annual mean layer transport anomalies computed from moorings are discussed in the context of detection of MOC changes in Chapter 8.

Upper layer		Δtr, T* = 20 days				T_{400}, T* = 20 days			
Year start	Year end	N (days)	N*	s_ε (Sv)	Mean (Sv)	N (days)	N*	s_ε (ºC)	Mean (ºC)
Apr-87	Apr-88	362	18	0.6	-0.4	363	18	0.06	17.44
Apr-88	Apr-89	366	18	0.5	0.7	366	18	0.06	17.46
Apr-89	Apr-90	225	13	0.5	0.9	255	13	0.08	17.43
Apr-90	Apr-91	90	4	0.8	1.3	334	17	0.08	17.33
Apr-91	Apr-92	236	12	0.5	-1.3	236	12	0.08	17.70
Apr-92	Apr-93	49	2	1.0	0.7	49	2	0.17	17.62
Apr-93	Apr-94	365	18	0.5	1.0	365	18	0.09	17.41
Apr-94	Apr-95	188	9	1.2	-3.2	365	18	0.06	17.70
Apr-95	Apr-96	365	18	0.7	-2.3	365	18	0.05	17.66
Apr-96	Apr-97	136	7	1.4	1.1	171	9	0.18	17.38
Apr-97	Apr-98					365	18	0.08	17.62
Apr-98	Apr-99					73	4	0.11	17.94
Apr-05	Apr-06	334	17	0.4	-1.5	365	18	0.06	17.86

Intermediate layer		Δtr, T* = 16 days			
Year start	Year end	N (days)	N*	s_ε (Sv)	Mean (Sv)
Apr-87	Apr-88	362	23	0.1	0.0
Apr-88	Apr-89	366	23	0.1	-0.2
Apr-89	Apr-90	81	5	0.1	0.0
Apr-05	Apr-06	334	21	0.1	-0.5

Middle layer		Δtr, T* = 17 days			
Year start	Year end	N (days)	N*	s_ε (Sv)	Mean (Sv)
Apr-87	Apr-88	361	21	1.2	2.1
Apr-88	Apr-89	350	21	1.6	-0.8
Apr-89	Apr-90	35	2	2.3	0.3
Apr-05	Apr-06	362	21	0.8	-3.8

Deep layer		Δtr, T* = 16 days				T_{3000}, T* = 10 days			
Year start	Year end	N (days)	N*	s_ε (Sv)	Mean (Sv)	N (days)	N*	s_ε (ºC)	Mean (ºC)
Apr-87	Apr-88	314	20	1.7	4.8	361	36	0.02	2.86
Apr-88	Apr-89	350	22	1.9	0.9	350	35	0.02	2.78
Apr-89	Apr-90	35	2	3.6	2.2	35	3	0.06	2.83
Apr-05	Apr-06	357	22	1.1	-4.7	357	36	0.02	2.78

Table 7.10 *Statistics of mooring dynamic height derived layer transport anomalies in 1 year periods (starting on April 1st of each year). N is the number of days of observations during any year, and N* is the number of independent observations per year based on integral timescales, T*, stated in table headers.* S_ε *is* $\sqrt{}$*(transport variance/N*) for each year. The equivalent parameters are given for temperature transport anomaly proxies of the upper and deep layers.*

7.5.2.3 Interannual variability

Having established that there are no robust sub-annual cycles in any of the layer transport anomaly time series, we now assess possible interannual signals at the western boundary. This is only possible for the upper and deep layers using the temperature transport anomaly proxies since errors of dynamic height layer transport anomalies are sensitive to mooring configuration which changes between deployments, preventing cross-comparison. The 400 and 3000 dbar temperature record errors do not change

significantly between deployments, facilitating objective assessment of long term changes.

(a) The upper layer

There is general good agreement between the upper layer transport anomalies from dynamic height or the 400 dbar temperature proxy, after low pass filtering for clarity (Figure 7.18). Before filtering, the 3 day gap between periods I and II in the geostrophic transport anomaly time series is filled by cubic spline interpolation using observations from 2.5 days at the end of the adjoining periods to limit data loss when filtering. All other gaps exceed 50 days and no interpolation is performed. Fluctuations of both records are in phase (Figure 7.18), with best agreement in magnitude seen for mooring deployments with nominal instrument depths at 100, 400 and 800m (e.g. mooring 250 in 1989, 268 in 1990 and 296 in 1992) and mooring wb1 with four instruments above 800m. The 3 Sv offset between the records of 1994/95 is assumed to be due to the 3 Sv estimated error in mooring dynamic height transports due to extrapolation below 650m (Table 6.8), rather than to a problem in the 400 dbar temperature record. It also appears that interpolation between instruments at 400 and 1150m on mooring 224 may result in overestimation of the magnitude of short timescale transport fluctuations (Figure 7.18).

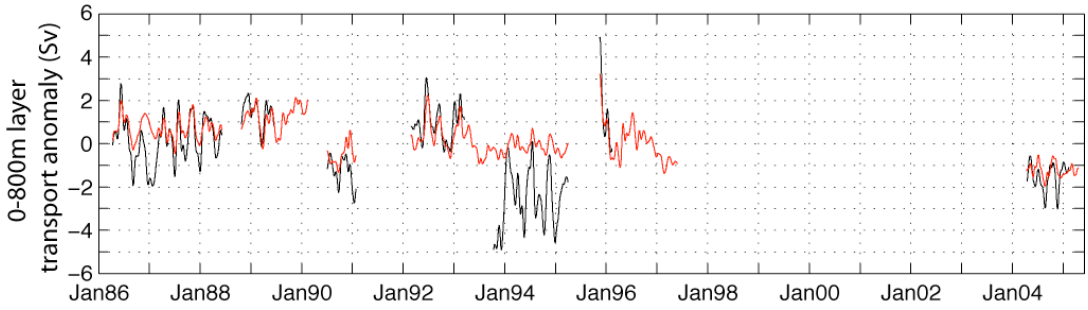

Figure 7.18 *Upper layer transport anomaly time series low pass filtered with a 90 day Lanczos-cosine filter from the mooring dynamic height observations (black) and the T_{400} transport proxy (red),* $\Delta tr_{0-800} = -4.75 * (T_{400} - 17.60) + 0.00$

For the above reasons the 400 dbar temperature transport anomaly proxy is judged more reliable for detection of long term changes in the upper layer transport anomaly. This record also benefits from increased data coverage (relative to the dynamic height observations) with its estimated method error (1.3 Sv, Section 6.3.8) comparable to or smaller than that of the dynamic height derived anomalies (Table 6.8).

Interannual variability of the 400 dbar temperature record and its transport equivalent are presented as 6 month running means (a compromise between smoothing and data loss) in Figure 7.19 along with the 95% confidence limits. The smoothed 400 dbar temperature is approximately 0.4ºC warmer in 2004/05 than in the late 1980's. This is significant at the 95% confidence level (Figure 7.19(i)), and remains significant when accounting for the 0.07ºC uncertainty in 400 dbar temperature (Section 6.3.8). If the eastern boundary conditions were constant over this time, the western boundary warming implies an increase in the net mid-ocean thermocline slope and accordingly, basinwide southward transport of the 0-800m layer. This is seen in Figure 7.19(ii), which shows the 400 dbar temperature transport proxy, also with 6-month running mean smoothing. The 0.4ºC warming equates to a strengthening of the mid-ocean southward transport by approximately 2 Sv.

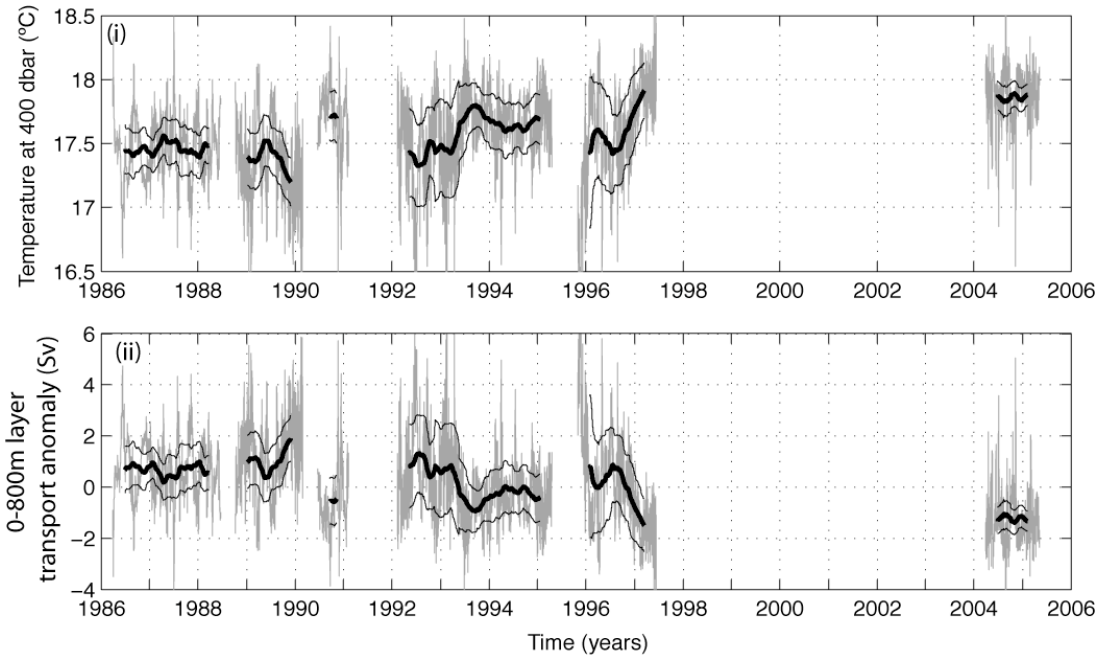

Figure 7.19 *(i) Temperature at 400 dbar and (ii) upper layer T_{400} transport anomaly proxy at 12 hour resolution in grey and overlaid by 6 month running mean (heavy black). 95% confidence limits (thin black) are ± 2 standard errors, equal to √((6 month variance)/N*) where N* is the number of independent samples in the yearly mean using integral timescales of Table 7.9.*

It is unfortunate that the data gap between 1998 and 2004 prevents assessment of whether western boundary conditions in 1998 and 2004/05 are representative of a new state with strengthened southward upper layer flow across the mid-ocean as observed in the transatlantic hydrographic sections (Chapter 3), or are simply interannual fluctuations. The late 1991 warming of similar magnitude (although based on

measurements from a short deployment), suggests that linear trends may not be the most appropriate tool for interpretation of western boundary layer transport anomalies. Nonetheless the warming towards the end of the Abaco records in late 1997 and the continuing high temperatures during RAPID 2004-05 are remarkable. Figure 7.19 clearly demonstrates the value of continuous monitoring over discrete snapshots of western boundary conditions. Although daily temperature excursions in some cases exceeding 1ºC are seen, the long term running means computed permit assessment of interannual changes in western boundary conditions not possible from end stations.

(b) The lower layer

Due to deep water freshening over time we are restricted to the temperature record at 3000 dbar to assess long term variability in the LNADW transports at the western boundary. Figure 7.20 compares the alternative (dynamic height and temperature derived) transport time series of this layer, after smoothing with a low pass 30 day Lanczos-cosine filter. Fluctuations are for the most part in phase, although the amplitude is smaller in the temperature transport proxy than in the dynamic height observations. Except for the RAPID array (2004/05), the estimated error of the temperature transport proxy (4.4 Sv) is smaller than that associated with the dynamic height transport (10.7, 6.1 or 3.4 Sv, Table 6.8b), and the combined errors account for the differences between the time series (remembering that the Rapid dynamic height observations are biased low due to unaccounted for deep water freshening). We therefore proceed with the 3000 dbar temperature transport proxy, judging it to be the best variable for assessment of interannual variability, noting that only moorings A_1 or wb2 are used for this measurement. They lie within 3 km of each other and therefore there should be no bias in the mean isotherm depth at either location.

Temperatures smoothed with a 6 month running mean (a compromise between data loss and the required filtering of high frequency noise) suggest significant interannual fluctuations in LNADW transport at this boundary (Figure 7.21) but should not be interpreted in the context of long term trends. The 3000 dbar temperatures in 1986 are significantly higher (at the 95% confidence level) than in early 1988, and possibly mid 2004 (Figure 7.21). The temperature range between these periods is 0.14ºC (with method error ± 0.01ºC), amounting to 6 Sv (equation 6.8b) between the minimum southward LNADW transport in 1986 and its maximum in 1988. A warm anomaly at

3000 dbar (as in 1986) causes a negative dynamic height anomaly in the LNADW layer (integrating dynamic height downwards from the reference level at 800 dbar), which following equation (4.4), gives a positive transport anomaly or weaker southward flow. The dashed line of Figure 7.21 indicates the zero flow anomaly temperature (2.787ºC), illustrating weaker LNADW flow in 1986 that recovers through 1987 to a maximum, and is also not significantly different from zero in 2004/05. If this were to be interpreted as a trend, it would be towards strengthened LNADW transport over time, in opposition to that derived from the end stations. This is discussed in greater depth in Chapter 8, but we argue that it is not appropriate to fit a linear trend to the 6-monthly smoothed temperature observations, due to sensitivity of such a regression to end points when there is no data between 1989 and 2003.

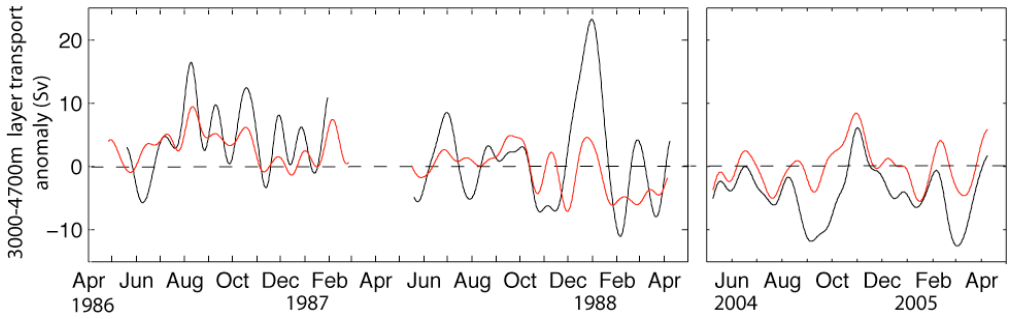

Figure 7.20 *30-day low pass filtered LNADW transport anomaly time series at the western boundary from dynamic height moorings (black) and the 3000 dbar temperature transport proxy (red). Note the break in x-axis time between 1989 and 2003.*

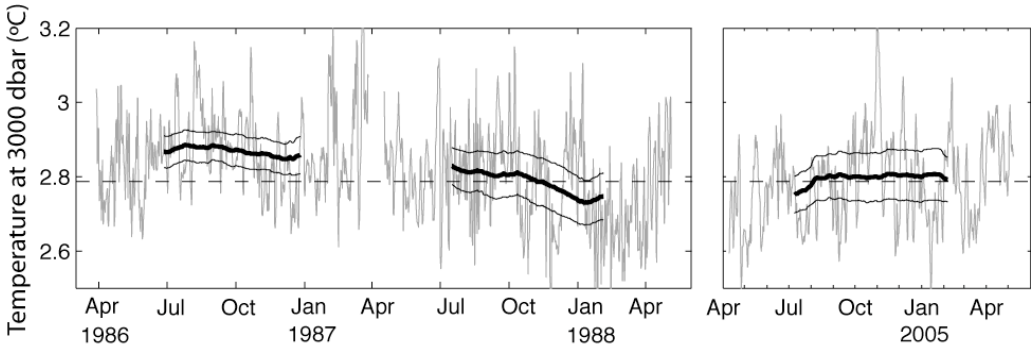

Figure 7.21 *Western boundary mooring 3000 dbar temperature time series at 12 hour resolution (grey) and after smoothing with a 6 month running mean (heavy black) with 95% confidence limits (thin black) of ± 2 standard errors (√(6 month variance)/N*) where N* is the record length divided by the integral timescales of Table 7.9). The dashed line is 2.787ºC, equal to a zero transport anomaly according to equation (6.8b). Note that the data gap between 1989 and 2004.*

The 6 Sv range of 6-month smoothed LNADW transport variability originating at the western boundary as computed from the 3000 dbar temperature record (and larger than the estimated error of the 3000 dbar LNADW transport anomaly proxy of 4.4 Sv) is around 50% of the mean transport of this layer. It is therefore interesting to see such large fluctuations on interannual timescales, even though the 3000 dbar temperature record is not sufficient to resolve any long term trends in transport of this layer that may be present.

7.6 SUMMARY

Results of decomposition of the Atlantic MOC into the components of Chapter 4 have yielded well constrained Ekman and Florida Straits transport time series between 1980 and 2005. The former has been constant during this time at 3.1 ± 1.2 Sv while the latter has ± 2 Sv decadal timescale fluctuations in response to the NAO (Baringer and Larsen, 2001) around its long term mean transport of 32.1 Sv. Neither shows any evidence for long term transport trends over the last 25 years. Variability of mid-ocean geostrophic transport anomalies from boundary dynamic height observations is more complex to interpret.

End station observations of the MOC's lower limb transports (intermediate, UNADW and LNADW) show the eastern boundary not to be a significant source of variability. NADW dominates the deep southward flow of the MOC at this latitude, and the observed eastern boundary fluctuations of both layers (upper and lower) are argued to be noise (± 3 and ± 1 Sv respectively). This is consistent with almost all the southward transport variability occurring in the DWBC (Chapter 3). At the east, trends between 1980 and 2005 of all lower layer transport anomalies are not significant, amount to less than 1 Sv and are not supported by any additional observations. Therefore changes in deep water transports due to eastern boundary variability are interpreted as insignificant for long term variability at 26.5ºN over 1980 to 2005 and insufficient data exists to allow speculation about interannual fluctuations. As such we conclude that the eastern boundary contribution can be neglected when computing transport variability of the deep southward flowing limb of the MOC at 25ºN.

Upper layer transport variability at the eastern boundary computed from end stations is ± 4 Sv but likely includes an unresolved temporal and spatially variable upwelling signal. Resolution of such a signal is limited by only 10 observations in 25 years. We note that the Kiel-276 long term temperature records at 400 dbar have discounted Stramma and Siedler's (1988) hypothesis of a seasonal cycle in the shape of the subtropical gyre, which would add a positive bias to summer transport anomalies with increased southward recirculation inshore of the end stations.

The Kiel-276 upper layer transport anomaly time series suggests an upper limit for variability of the eastern basin subtropical gyre recirculation of ± 3 Sv between 1980 and 2000. Additionally we have quantified the previously suggested weakening of this flow between 1996 and 1998 (Brachet et al. 2004; Volkov 2005), to be of the order 5 Sv. Aside from this event, the interannual transport anomalies computed are unfortunately contaminated by position shifts of the Azores Front. This means that it is not possible to verify (or otherwise) the eastern boundary's upper layer end station trend towards increased southward transport amounting to a 1.2 Sv change in 25 years. The smaller interannual variability at Kiel-276 does however confirm our suspicion that the upper layer variability estimate from eastern boundary end stations of ± 4 Sv is high due to uncertainty in its unresolved seasonal component.

At the western boundary we compute a possible 2 Sv strengthening in southward transport of the upper layer between the 1980's and 2005 particularly from temperature records at 400 dbar. Both the end stations and mooring observations (the latter totalling more than 10 years) show seasonal cycles in transport of this layer to be smaller than ± 1 Sv, and not statistically significant in any dataset. This permits analysis of interannual variability without concern for biasing by significant seasonal transport signals. The end stations show a small trend (approximately 0.02 Sv per year) towards increased southward transport above 800m, which is not statistically significant, but is supported in sign by the moored temperature record at 400 dbar. Western boundary temperatures at this depth were 0.4ºC warmer in 2005 than the 1980's (6 month running mean), corresponding to deeper isotherms by 40m and approximately 2 Sv more southward flow in this layer in later years. The 400 dbar temperature changes are significant at the 95% confidence level and avoid any uncertainties associated with variable positions of end stations.

Accompanying the mid-ocean's upper layer increase of southward transport in later years, western boundary end station observations show southward transport of NADW to have reduced over time. Deep water transport has a (not significant) long term trend towards decreased southward flow, amounting changes of just over 1 and 2 Sv in the UNADW and LNADW layers respectively between 1980 and 2005 (intermediate layer changes are negligible). We argue that such trends are driven by the clear freshening signal of these waters observed and incorporated into the analysis. Resolution of sub-annual transport anomaly signals is not possible with end stations due to a summer biased dataset. The mooring time series, although resolving this problem, only cover 4 years resulting in monthly mean transports dominated by a strong transport anomaly in 1987. Accordingly any baroclinic seasonal transport cycle in the lower waters of the MOC cannot be determined here, although we do not expect such a signal to be present.

The western boundary 3000 dbar temperature proxy for LNADW transport suggests order 6 Sv fluctuations on interannual timescales. Temperature at this depth is important in setting the vertical velocity shear anomalies in the LNADW layer, and the 6 month smoothed record shows a range of 0.14ºC; high in 1986 and low late in 1988, significant above both high frequency variability and method errors. Unfortunately observations are restricted to 1986-1988 and 2004-2005 due to mooring locations in the intervening Abaco arrays, and we are reluctant to compute 25 year trends from observations with a data gap exceeding 10 years. The temperature transport proxy record does not however suggest weaker southward LNADW transport in 2004/05. Thus from this proxy dataset, we cannot confirm the western boundary trend towards weakened southward DWBC transport by 2-3 Sv in the last 25 years, but we can say larger oscillations have occurred on interannual timescales.

The above observations are discussed in the next Chapter.

CHAPTER 8: **Discussion and Conclusions**

In this chapter we first review the data available, and evaluate the methods employed to constrain the last 25 years of Atlantic MOC variability at 26.5ºN (Section 8.1). Observed interannual variability is then interpreted within the context of other studies (Section 8.2). Section 8.3 provides the conclusions of this study, with suggestions for future work in Section 8.4.

8.1 DATA AND METHOD EVALUATION

We have supplemented the transatlantic hydrographic section datasets traditionally used to determine the strength of the Atlantic MOC (e.g. Hall and Bryden, 1982; Lavín et al., 1998) with transport time series of the Ekman, Florida Straits, and mid-ocean geostrophic components of the MOC at 26.5ºN for 1980 to 2005. Availability of monthly mean wind stress from the NOC climatology and cable-derived daily transports of the Florida Current have made variability of the former two components relatively straightforward to observe. The same cannot be said of the mid-ocean geostrophic transport however, for which the dataset and methods are best able to resolve the upper layer, particularly the western boundary's contribution to its variability. The issues in historical data availability and method limitations have been discussed throughout this thesis and are summarised in the following paragraphs.

The end station approach has two potential downfalls for resolution of strength changes of the MOC's lower limb. Firstly the transport of AABW is not measured. Since AABW is found on the western flank of the Mid-Atlantic Ridge (MAR) (Bryden et al., 1996) the steep topography dictates that transport occurs predominantly in bottom triangles which are not resolved by end stations. Although AABW is a small component of the MOC (Chapter 3), its absence is a shortfall for assessing deep water transport

fluctuations. Secondly the topography of the MAR intersects the depth layer of LNADW, this formally invalidates the computation of this water mass's transport anomalies from eastern and western boundary end stations. Under the caveat of negligible LNADW transports in the eastern basin (Figure 3.18 and Section 7.6) to estimate variability of western basin LNADW transports we require "end stations" crawling down the western side of the MAR as in the RAPID mooring array (Rayner and Cunningham, 2005). Historical data availability however precludes this. Preliminary analysis of the 2004-05 RAPID array measurements suggests that fluctuations of deep dynamic height at the western boundary dominate those at the MAR (Bryden, personal communication, 2006). We therefore believe the LNADW transport anomalies computed at the western boundary to be representative of the basinwide layer transport anomalies. The lack of AABW transport estimates over the last 25 years aside from those of the transatlantic hydrographic sections, remains unresolved.

Our analysis of end stations at the east established that this boundary does not make a significant contribution to transport variability of either the intermediate water, UNADW or LNADW. To assess variability of the lower limb of the MOC at 26.5ºN therefore, it is the western boundary's contribution which must be resolved and is interpreted as representative of the basinwide signal. For this, between 29 and 39 end stations over the last 25 years are analysed but they are unfortunately biased towards the summer months. The main limitation however is the lack of suitable moored temperature and pressure time series, with less than 4 years of data for each layer (1986 to 1988 and 2004 - 2005). Mooring time series permit temporal averaging, and thus smaller uncertainties of annual average transport. The three additional annual mean transport anomalies obtained from moorings do not therefore substantially improve the transatlantic hydrographic section dataset significantly. Although the Abaco array had moorings in the western boundary at 26.5ºN between 1988 and 1998, the innermost deep mooring was B which lies close to the core of the DWBC. While mooring B is well placed for monitoring DWBC transport in combination with the offshore moorings to account for meanders, it is too far from the boundary to act as a useful end station. Therein lies one of the challenges of historical analysis based on datasets not designed for a specific task, and is also true of the resolution of the upper layer transport anomalies at the eastern boundary discussed below.

For the upper layer, the primary limitation of the eastern boundary dataset is its contamination by possible seasonal signals. In order to be confident of the interannual variability estimates, we must either compute annual averages of the layer transport anomalies or extract any seasonal signal – requiring first its characterisation. The 10 upper layer end stations at this boundary are expected to be subject to a seasonally varying upwelling regime, broadly supported by the monthly dependence observed in their 400 dbar temperatures. Such temperature changes in the thermocline waters have an imprint on the layer transport anomalies computed, consistent with Kohl (2005)'s findings. We therefore do not consider the individual eastern boundary upper layer end stations to be representative of annual mean transport anomalies and believe their ± 4 Sv variability is an overestimate of that on interannual timescales.

The only dataset that permits higher than annual temporal resolution of the subtropical eastern basin upper layer flows is that of the Kiel-276 mooring, from which approximately 16 years of transport anomaly time series have been obtained. While variability of one year running mean smoothed transport anomalies at Kiel-276 is ± 3 Sv, supporting the assumption that the end station variability of ± 4 Sv is an overestimate, the Kiel-276 observations are also likely biased due the contribution of Azores Front meanders (e.g. Tychensky et al., 1998) as well as subtropical gyre strength changes which we aimed to resolve. A continuous temperature record at mid-depth in the thermocline on the eastern boundary slope region would be most useful for addressing the unresolved questions of upper layer transport changes originating at this boundary, of a seasonal upwelling signal and of possible long term trends. Unfortunately such temperature time series are not available, nor are those from the Argo program a useful substitute since few floats have ventured close enough to the African coast near 25ºN (Fraser, 2006). The end stations and Kiel-276 time series therefore are the only suitable hydrographic datasets with which to address this problem. Through their analysis we believe this study has made as much progress as is possible in determining variability in transport changes due to eastern boundary stations.

Upper layer seasonal variability at the west, in contrast to at the east, has been constrained to be less than ± 1 Sv, in turn constraining the end station upper layer

transport anomaly uncertainty at this boundary due to seasonal fluctuations. An annual cycle in the baroclinic transport less than ± 1 Sv is based on analysis of the approximately 10 year long moored 400 dbar temperature time series, in combination with mooring derived dynamic height observations. Our results are not contradictory to Lee et al. (1996)'s findings of significant seasonal signals in both the Antilles Current and DWBC transports since they were primarily a barotropic response to seasonal wind forcing (Lee et al., 1996). We point out that 10 years should be a sufficiently long time series to resolve a seasonal signal, since 6 years sufficed for Lee et al. (1996) in this region while 4 years was not long enough (Lee et al., 1990). The western boundary mooring dataset is a very valuable resource for upper layer transport anomalies, notably due to its long duration and fixed location. Along with 39 hydrographic end stations in 25 years, these transport anomaly estimates make the western boundary upper layer flow variability the best resolved of the mid-ocean geostrophic components.

We now discuss the relative merits of alternative observations with which to compute boundary transport anomalies of the mid-ocean geostrophic flow. We find the mooring derived fixed depth temperature time series proxy to be the preferred measurement, at least for the upper layer. The primary advantage of transport anomalies from moored temperature and pressure observations is the ability to compute annual means. Consider upper layer transport anomalies at the western boundary. Even though we have constrained any seasonal signal to be less than ± 1 Sv, high frequency variability of ± 4 Sv is seen on weekly timescales (Figure 7.19). It is therefore possible that any single end station observation is contaminated by the magnitude of high frequency variability which results from propagating features in the boundary region (Lee et al., 1996). In contrast, the standard error of an annual mean transport anomaly computed from a year long time series is estimated to be less than 0.5 or 1 Sv for temperature or dynamic height derived transport anomalies respectively (Section 7.5.2.2(b)) due to averaging out the high frequency variability. Even incorporating the uncertainties due to measurement accuracy and data processing of 0.3 Sv (Table 5.7), 1.3 Sv (Section 6.3.8) or 2-3 Sv (Table 6.8) for end stations, the temperature transport proxy or mooring dynamic height observations respectively, the uncertainty of the annual mean transport anomaly from the 400 dbar temperature record (1.4 Sv) remains much lower than that of an end station (4 Sv). Following this evaluation we suggest that detection of interannual changes in the western boundary upper layer transport anomaly larger than ± 1.8 Sv (±

2.7 Sv) can be detected with 80% (95%) confidence from a 400 dbar temperature record adjacent to the boundary. In contrast, to detect an interannual change with 95% confidence from end stations it would have to amount to almost 16 Sv. The end station uncertainty is in closer agreement with Ganachaud (2003)'s ± 6 Sv uncertainty of layer transport changes from hydrographic sections. This clearly illustrates the advantages of continuous monitoring.

To summarise, given the value of continuous time series for estimation of interannual variability, it follows that the datasets available are best suited to resolving anomalies of the upper limb of the MOC at 26.5ºN, i.e. net northward transport above 800m. This includes the Florida Straits and Ekman components as well as the baroclinic mid-ocean geostrophic transports. The weakness in this is that the eastern boundary contribution is not well resolved, and has an uncertainty of ± 3 Sv. This however, is smaller than the uncertainties associated with lower layer end station transport anomalies due to high frequency signals, of the order ± 7 and ± 10 Sv for the upper and lower NADW transports respectively (Figure 7.16). While annual averages may be computed from the mooring derived anomalies of the lower limb transports, thus decreasing the uncertainty due to high frequency signals, these only span 4 years and have method errors of approximately 6-11 Sv for UNADW and LNADW from the Abaco arrays with relatively poor vertical resolution in the deep water. In contrast, estimation of the upper layer baroclinic mid-ocean transport anomaly time series benefits from a long duration of satisfactory mooring observations– totalling a decade or more at the west and east respectively – as well as smaller processing errors when transport anomalies are computed from the 400 dbar temperature record. It is unfortunate that dataset limitations prevent computation of the barotropic component of the mid-ocean geostrophic transport by mass balance constraints, since upper and lower limb, and east and west transport anomalies are not coincident in time. We are not the first to estimate only the baroclinic component of water mass transport variability (e.g. Bacon, 1998; Kieke and Rhein, 2006) and argue that it remains a useful and interesting approach. The following discussion (Section 8.2) of interannual variability in the Atlantic MOC at 26.5ºN reflects the differing values of the transport anomaly time series components imposed by the historical datasets.

8.2 INTERANNUAL VARIABILITY

The following discussion has two main aims. One is to discuss whether or not our observations support the suggestion of the transatlantic hydrographic sections that the MOC at 26.5ºN is evolving towards a new state with reduced strength. The other is to synthesise the results of Chapter 7 to constrain the possible magnitude of interannual timescale fluctuations of MOC transport over the last 25 years at this latitude.

We argue that the best interpretation of interannual variability of the computed Atlantic MOC components at 26.5ºN as a long term trend, is of a 2 Sv reduction in strength between 1980 and 2005. Historical end station observations of the lower limb MOC transports suggest a trend towards weakened southward DWBC transport in both UNADW and LNADW, by 1 and 2 Sv respectively, over the 25 years. This is from western boundary layer transport anomalies, assuming no contribution from the eastern boundary (justified in Section 8.1). Alone these trends are not significant and could be due to noise in the dataset. If it were not for the underlying deep water freshening, which we believe to be the source of the decreasing NADW transport observed, and the changes in the MOC's upper limb which also suggesting a weakening in overturning of 2-3 Sv over the 25 years, noise might well be our conclusion. The western boundary moored 400 dbar temperature time series identifies a 0.4ºC warming of thermocline waters after 1997 relative to the 1980's, significant over the sub-annual variability. With no change at the east this amounts to a 2 Sv increase in net southward mid-ocean geostrophic transport due to the steeper basinwide thermocline slope. Although eastern boundary upper layer signals are less well defined due to unresolved seasonal variability, the end stations also show a trend towards increased southward transport by 1.2 Sv over the 25 years. We have argued that this is unlikely a seasonal artefact (Section 7.4.1.3(a)) and therefore there is no reason to suppose that the eastern boundary upper layer transport anomalies cancel out those at the west. Due to discrepancies over this time between trends in wind stress curl of the NOC and NCEP wind stress climatologies, whether the mid-ocean upper layer circulation changes are indicative of changes in Sverdrup transport or in the non-linear western boundary regime, remains unresolved. There is no evidence for a long term change in either Ekman or Florida Straits transports between 1980 and 2005, therefore combined with the identified mid-ocean baroclinic circulation trends, the observations all point towards a reduction in strength of the Atlantic MOC at 26.5ºN of 2 -3 Sv from 1980 to 2005.

If such a reduction in the net northward transport of upper warm waters at 26.5ºN is indeed occurring, could we observe a corresponding change in the meridional heat transport? The 4-5 Sv reduction in strength of the MOC in 2004 as computed from the transatlantic hydrographic section had an associated 0.3 PW reduction in northward heat transport (Section 3.3.3). A 2 Sv change in the overturning strength would not therefore be expected to cause a detectable change in the meridional heat transport, since its error is approximately 0.3 PW when measured from hydrographic sections (Lavín et al., 1998). We also note that some modelling studies (e.g. Drijfhout and Hazeleger, 2006) suggest that anthropogenically forced weakening of the MOC is largely compensated by changes in gyre northward heat transport. The resulting net change in oceanic heat transport with a weakening MOC is small. A drawback of the end station method is that we cannot compute changes in meridional heat transport mechanisms through decomposition into overturning, gyre and eddy components (e.g. Lavín et al., 2003) due to a lack of zonal resolution, and therefore cannot assess whether or not such compensation appears in our historical dataset. Drijfhout and Hazeleger (2006) do however observe a western boundary warming of the upper waters associated with their compensation mechanism, similar to our own observations. Until any long term trend in the MOC amounts to a larger reduction in strength than the 2-3 Sv estimated here, possible changes in magnitude and mechanisms of oceanic meridional heat transport will remain unresolved by observations at this latitude.

The observed warming of western boundary thermocline waters underpinning the reduction in MOC strength, and freshening of LNADW are qualitatively in agreement with the water mass property changes identified from the five transatlantic hydrographic sections at this latitude and are consistent with a weakened MOC (Cunningham and Alderson, 2006, manuscript in preparation). This analysis however benefits from an extended dataset. 522 CTD stations in the western boundary between 1980 and 2005 identify the LNADW freshening as a significant long term trend with a salinity reduction of 0.003 per decade on potential temperature surfaces. Although further north the DSOW freshening trend has been found to be interrupted by warm saline anomalies (Stramma et al., 2004), we suggest that such anomalies are negligible at 26.5ºN due to exponential decay of their amplitude with distance from the source region (Waugh and Hall, 2005). Additionally we can see (Figure 7.18) that the western boundary

thermocline warming seen in the 1998 and 2004 hydrographic sections (Figure 3.15 and Cunningham and Alderson, 2006, manuscript in preparation) were representative of the annual mean states (possibly longer term) and are not seasonal effects.

Despite the increased temporal resolution afforded by end station and mooring derived estimates of mid-ocean geostrophic transports relative to those of hydrographic sections, reconciliation of the observed layer transport changes with high latitude observations, or indeed forcing mechanisms, remains elusive. For UNADW causal relationships are confused by the different water masses which make up the 1100-3000m layer. The zonal resolution of full sections permitted transports to be computed in temperature classes, enabling identification of possible trends in both LSW and ISOW. The former strengthened over time by approximately 3 Sv and the latter possibly weakened, but remained uncertain due to NAIW contamination. Our end station observations show a 1 Sv weakening trend over time for the UNADW layer, but this combines both LSW and ISOW transports. Since the 1 Sv trend is smaller than the estimated error and not significant, and the LSW trend computed from the five section snapshots is consistent with high latitude observations of increased deep convection in the Labrador Sea (Dickson et al., 1996), we do not revise the Chapter 3 conclusion of strengthened LSW transport over the last 25 years at 26.5ºN. A trend towards increasing LSW transport since the 1980's is also suggested by Latif et al. (2006) as a lagged response to the NAO, the difference being that they found this to be larger than changes in LNADW transport resulting in a strengthening MOC. Caution should however be employed in comparison of their study with this one since the relationship between sea surface temperature anomaly patterns and MOC strength used by Latif et al. (2006) is only valid on multi-decadal timescales, and our assessment of interannual variability only spans three decades.

Also the end station derived transport anomalies of LNADW do not allow us to confidently trace the changes at 26.5ºN back to the subpolar north Atlantic. Noting that we have only one end station data point for this layer at the west prior to 1986, the trend towards decreased southward transport over time is primarily representative of 1986 to 2005. Based on a 6-7 year transit time from Cape Farewell to 26.5ºN (see Section 3.4) this is consistent with LNADW transport peaking in the early 1980's and decreasing to the early 2000's (Bacon, 1998; Kieke and Rhein, 2006). Extension of the time series

backwards in time to the 1970's, when LNADW transport is expected to be weak in the subtropics based on the Cape Farewell observations of the 1950's and 1960's, is required to ascertain whether the trends of this layer transport over the last 25 years are representative of a longer term slowing of the MOC or are part of a decadal timescale oscillation as the high latitude observations suggest (Bacon, 1998; Kieke and Rhein, 2006).

Whether the MOC is suggested to be strengthening or weakening may be strongly dependent on the timeframe of observations. Our observations permit constraint of the estimated magnitude of interannual fluctuations of the MOC over the last 25 years at ± 6 Sv. Time series of annual mean Florida Straits and Ekman transports show variability of ± 1 and ± 2 Sv respectively. The western boundary 400 dbar temperature transport anomaly proxy (Figure 7.18(ii)) does not show any 6 month running mean transport anomalies larger than ± 2 Sv. This is in good agreement with the Kiel-276 temperature transport proxy which constrains interannual changes in the eastern basin subtropical gyre recirculation strength at ± 3 Sv (Figure 7.12). Combining variability of the MOC upper layer components at 26.5ºN we suggest that interannual changes have been smaller than ± 6 Sv between 1980 and 2005. We also note that the 3000 dbar western boundary temperature record suggested approximately 6 Sv interannual fluctuations in LNADW transport in the late 1980's. Such fluctuations against a long term mean MOC at 26.5ºN of 16-18 Sv are large and easily encompass the 2004 transatlantic section overturn of 13 Sv. The time series in addition to the transatlantic hydrographic section analyses therefore suggest that fluctuations on interannual timescales over the last 25 years have been at least as important, if not more so, than the long term 2-3 Sv trend towards decreasing MOC strength.

8.3 CONCLUSIONS

We started this thesis with a historical review of understanding of Atlantic MOC strength. The 16-18 Sv mid to low latitude overturning has been the accepted view since transition from the 6-8 Sv MOC picture that persisted from the early application of the dynamic method to Atlantic circulation up to 1957. 1957 saw Stommel's insightful deep water circulation scheme, the first direct observations of the DWBC and the first transatlantic hydrographic section at 25ºN from which the first modern estimates of the

overturning strength were obtained and its important role in meridional heat transport quantified. We now suggest that it was partly coincidental that the analyses of zonal hydrographic sections since 1980 all yielded such a consistent MOC strength of 16-18 Sv up until the 2004 section, since variability up to ± 6 Sv may have occurred in annual average overturning strengths over the last 25 years.

The 13 Sv overturn computed from the 2004 hydrographic section resulted predominantly from a 7 Sv reduction in southward transport of LNADW, and a corresponding increase in southward transport of the mid-ocean thermocline waters. These changes also characterised the 1998 hydrographic section but that year were compensated by strong Florida Straits and Ekman transports, resulting in a 17 Sv overturning strength consistent with the earlier sections. Decomposition of the Atlantic MOC at 26.5ºN into Ekman, Florida Straits and mid-ocean geostrophic transport time series has been performed to facilitate resolution of the questions raised by the 25% weaker 2004 overturning strength. Interannual variability of the former two components is well constrained, but historical datasets have made estimation of the mid-ocean geostrophic component more challenging, and only the baroclinic component of flow could be assessed.

Our best interpretation of interannual variability of the transport anomaly time series obtained, if modelled by a long term trend, amounts to a 2 – 3 Sv weakening of the Atlantic MOC at 26.5ºN between 1980 and 2005. There is evidence for persistent warming in the thermocline at the western boundary since the late 1990's, which may signify either increased southward recirculation in the mid-ocean thermocline or reduced northward Antilles Current transport. Either way this increases net southward transport above 800m across the mid-ocean section, consistent in sign with, but weaker than, the 1998 and 2004 hydrographic section transport changes relative to the 1981/1992 baseline state. Similarly end station observations of LNADW transport anomalies at the western boundary show a trend towards reduced southward transport of the DWBC over time.

Superimposed on the 2 - 3 Sv reduction in strength of the overturning at 26.5ºN over the last 25 years, there is also evidence for interannual fluctuations in water mass transports of order 6 Sv. Changes of this size are seen in LNADW transport in the late 1980's, and

in the eastern basin subtropical recirculation in the 1990's. Combining interannual variability of the MOC's upper limb components estimated we obtain a constraint of ± 6 Sv for year to year changes in the annual averaged overturning strength at this latitude. In this context the 2004 section overturning of 13 Sv is not unusual and we should instead be surprised that the earlier sections yielded such consistent transports.

This analysis has clearly demonstrated the value of a high temporal resolution moored time series for observing a system with the range of variability timescales exhibited by the Atlantic MOC. The most useful historical observation has been the western boundary 400 dbar temperature time series, derived from the Abaco array, with which interannual changes in the western boundary's contribution to upper layer flow of ± 2.7 Sv can be detected with 95% confidence. This is a marked improvement on the ± 6 Sv associated with one time hydrographic section layer transports, and even more so relative to the end station upper layer transport anomaly 95% confidence interval of ± 7.8 Sv. The drawback of such boundary observations is their lack of zonal resolution, required to assess possible changes in meridional heat transport mechanisms.

The aim of this thesis was to constrain the magnitude of interannual variability of the Atlantic MOC at 26.5ºN from 1980 to 2005 from historical observations to complement results of the RAPID monitoring array and we conclude that this has been achieved within the limitations of the available dataset.

8.4 FUTURE WORK

We have exhausted high quality hydrographic observational data records at 26.5ºN from the last 25 years for assessment of MOC changes, and do not believe any more can be learnt about its interannual variability for this period at the present time. It might however be beneficial to return to the issue after resolution of the eastern boundary upwelling's seasonal influence on upper layer transport anomalies. This should be possible with a few years of RAPID mooring array observations, and would enable extraction of any interannual signal from the eastern boundary end station 0-800m layer transport anomalies. It will of course be interesting to see whether the RAPID array with a sufficiently long time series continues to observe the trend towards decreased overturning strength we have seen since 1980.

Additionally there is a current interest in whether zonal density observations alone provide the best indicator of MOC change. This has motivated a number of modelling studies aiming to assess whether additional observations can reduce the uncertainty associated with detecting trends from MOC time series at one latitude (e.g. Vellinga and Wood, 2004, review in Baehr et al., 2006). It would be interesting and possibly beneficial to see if any of these additional observations suggested to improve detection capabilities of a MOC monitoring array are linked with the variability we observe in the historical observations at 26.5ºN.

Most importantly, the RAPID monitoring programme is currently operational and into the third year of obtaining measurements of the strength of the Atlantic MOC at 26.5ºN. It follows the same underlying method for monitoring the overturning strength as employed in this thesis but mid-ocean geostrophic transports are obtained from a specifically designed array of moorings at the western and eastern boundaries as well as over the mid-Atlantic ridge. Dynamic height profiles computed from these moorings benefit from improved vertical resolution relative to the Abaco or Kiel-276 moorings, conductivity sensors for salinity, bottom pressure sensors to provide the barotropic component of the flow and are at fixed locations well within the boundary study regions employed here, eliminating the spatial complexity of the historical dataset. The RAPID monitoring programme is thus providing the first multi-year time series of the Atlantic MOC that also resolves high frequency variability, without the large uncertainties of the analysis presented in this study.

References

Amos, A. F., A. L. Gordon and E. D. Schneider, 1971: Water masses and circulation patterns in the region of the Blake-Bahama Outer Ridge. *Deep-Sea Research,* **18**, 145-165.

Arhan, M., A. Colin de Veriere, and L. Mémery, 1994: The Eastern Boundary of the Subtropical North Atlantic. *Journal of Physical Oceanography*, **24,** 1295-1316.

Armi, L. and W. Zenk., 1984: Large lenses of highly saline Mediterranean Water. *Journal of Physical Oceanography,* **14**, 1560-1576.

Bacon, S., 1998: Decadal variability in the outflow from the Nordic seas to the deep Atlantic Ocean. *Nature,* **394**, 871-874.

Bacon, S., H. M. Snaith and M. J. Yelland, 2000: An evaluation of some recent batches of IAPSO standard seawater. *Journal of Atmospheric and Oceanic Technology,* **17**, 854-861.

Baehr, J. H. Haak, S. Alderson, S. A. Cunningham, J. H. Jungclaus and J. Marotzke, 2006: Timely detection of changes in the meridional overturning circulation at 26ºN in the Atlantic. *Manuscript submitted to Journal of Climate.*

Baringer, M. O. N. and R. L. Molinari, 1999: Atlantic Ocean baroclinic heat flux at 24 to 26ºN. *Geophysical Research Letters*, **26,** 353-356.

Baringer, M. O. N. and J. C. Larsen, 2001: Sixteen years of Florida Current transport at 27ºN. *Geophysical Research Letters*, **28,** 3179-3182.

Brachet, S., P. Y. Le Traon and C. Le Provost, 2004: Mesoscale variability from a high-resolution model and from altimeter data in the North Atlantic Ocean. *Journal of Geophysical Research,* **109**, C12025, doi:10.1029/2004JC002360

Broecker, W. S., D. M. Peteet and D. Rind, 1985: Does the ocean-atmosphere system have more than one stable mode of operation? *Nature,* **315** 21-26

Broecker, W. S., 1991: The Great Ocean Conveyor. *Oceanography*, **4,** 79-89.

Broecker, W. S., T. Takashi and Y. H. Li, 1976: Hydrography of the central Atlantic – I. The two-degree discontinuity. *Deep-Sea Research,* **23**, 1083-1104.

de Boer, A. M. and H. L. Johnson, 2007: Inferring the zonal distribution of measured changes in the meridional overturning circulation. *Ocean Science*, **3**, 55-57.

Bryan, K., 1962: Measurements of meridional heat transport by ocean currents. *Journal of Marine Research*, **67,** 3403-3413.

Bryden, H. L., 1974: Geostrophic comparisons using measurements from a moored current and temperature meter. *Nature*, **251,** 409-410.

Bryden, H. L., 1977: Geostrophic comparisons from moored measurements of current and temperature during the Mid-Ocean Dynamics Experiment. *Deep-Sea Research*, **24,** 667-681.

Bryden, H. L., 1993: Ocean Heat Transport across 24ºN latitude. *Interactions Between Global Climate Subsystems: The Legacy of Hann*, G. A. McBean and M. Hantel, Eds., American Geophysical Union, 65-75.

Bryden, H. L., et al., 2003: *RRS* Charles Darwin *Cruise 139, 01 Mar-15 Apr 2002. Trans Indian Hydographic Section across 32ºS.* Southampton Oceanography Centre Cruise Report No. 45, Southampton, United Kingdom. 122pp.

Bryden, H. L. and M. M. Hall, 1980: Heat transport by currents across 25ºN latitude in the Atlantic Ocean. *Science*, **207,** 884-886.

Bryden, H. L., W. E. Johns, and P. M. Saunders, 2005a: Deep western boundary current east of Abaco: Mean structure and Transport. *Journal of Marine Research*, **63,** 35-57.

Bryden, H. L., H. R. Longworth, and S. Cunningham, 2005b: Slowing of the Atlantic meridional overturning circulation at 25ºN. *Nature*, **438,** 655-657.

Bryden, H. L., M. J. Griffiths, A. Lavín, R. C. Millard, G. Parrilla, and W. M. J. Smethie, 1996: Decadal Changes in Water Mass Characteristics at 24ºN in the Subtropical North Atlantic Ocean. *Journal of Climate*, **12**, 3162-3186.

Chave, A. D., D. S. Luther, and J. H. Filloux, 1997: Observations of the boundary current system at 26.5ºN in the subtropical North Atlantic Ocean. *Journal of Physical Oceanography*, **27,** 1827-1848.

Cipollini, P., D. Cromwell, M. S. Jones, G. D. Quartley and P. G. Challenor, 1997: Concurrent altimeter and infrared observations of Rossby wave propagation near 34ºN in the Northeast Atlantic. *Geophysical Research Letters,* **24(8)**, 889-892.

Coachmann, L. K. and A. Aagaard, 1988: Transports through Bering Strait: Annual and interannual variability. *Journal of Geophysical Research,* **93**, 15535-15539.

Cubasch, U., G. A. Meehl, G. J. Boer, R. J. Stouffer, M. Dix, A. Noda, C. A. Senior, S. Raper, and K. S. Yap, 2001: Projections of future climate change. *Climate Change 2001: The Scientific Basis. Contribution of Working Group I to the Third Assessment Report of the Intergovernmental Panel on Climate Change*, J. T. Houghton, Y. Ding, D. J. Griggs, M. Noguer, P. J. v. d. Linden, X. Dai, K. Maskell, and C. A. Johnson, Eds., Cambridge University Press, 525-582.

Cunningham, S. A. and S. Alderson, 2006: Transatlantic temperature and salinity changes at 24.5ºN from 1957 to 2004. *Draft manuscript to be submitted to Geophysical Research Letters.*

Cunningham, S. A., T. Kanzow, D. Rayner, M. O. Baringer, W. E. Johns, J. Marotzke, H. R. Longworth, E. M. Grant, J. J. M. Hirschi, L. M. Beal, C. S. Meinen and H. L. Bryden, 2007: Temporal variability of the Atlantic Meridional Overturning Circulation at 26.5ºN. *Manuscript submitted for publication in Science, February 2007.*

Cunningham, S. A., D. Rayner, et al., 2005: *RRS* Charles Darwin *Cruise CD170 and RV* Knorr *Cruise KN182-2. RAPID mooring cruise report April-May 2005.* National Oceanography Centre Southampton Cruise Report No. 2. Southampton, United Kingdom. 148pp.

Curry, R. G. and M. S. McCartney, 2001: Ocean gyre circulation changes associated with the North Atlantic Oscillation. *Journal of Physical Oceanography*, **31,** 3374-3400.

Deacon, M., 1971: *Scientists and the Sea 1650-1900. A study of marine science.* Academic Press, London.

Deacon, M. D., 1985: An early theory of ocean circulation: J. S. von Waitz and his explanation of the currents in the Strait of Gibraltar. *Progress in Oceanography*, **14**, 89-101.

Defant, A., 1941: Quantitative Untersuchungen zur Statik und Dynamik des Atlantischen Ozeans. Die relative Topographie Einzelner Druckflachen im Atlantischen Ozean (The Realtive Topography of individual pressure surfaces of the Atlantic Ocean). *Wissenschaftliche Ergebnisse der Deutschen Atlantischen Expedition auf dem Forschungs und Vermessungsschiff "Meteor" 1925-1927.* 6: 2nd Part.

Dickson, B., I. Yashayaev, J. Meincke, B. Turrell, S. Dye, and J. Holfort, 2002: Rapid freshening of the deep North Atlantic Ocean over the past four decades. *Nature*, **416,** 832-837.

Dickson, R. R., R. Curry, and I. Yashayaev, 2003: Recent changes in the North Atlantic. *Philosophical Transactions of the Royal Society of London A*, **361,** 1917-1934.

Dickson, R. R., J. R. N. Lazier, J. Meincke, P. Rhines, and J. Swift, 1996: Long-term coordinated changes in the convective activity of the North Atlantic. *Progress in Oceanography*, **38,** 241-295.

Doney, S. C. and J. L. Bullister, 1992: A chlorofluorocarbon section in the eastern North Atlantic. *Deep Sea Research A,* **39(11/12)**, 1857-1883.

Drijfhout, S. S. and W. Hazeleger, 2006: Changes in MOC and gyre-induced Atlantic Ocean heat transport. *Geophysical Research Letters*, **33**, L07707, doi: 10.1029/2006GL025807.

Eden, C. and J. Willebrand, 2001: Mechanism of interannual to decadal variability of the North Atlantic circulation. *Journal of Climate*, **14**, 2266-2280.

Emery, W. J., 1975: Dynamic height from temperature profiles. *Journal of Physical Oceanography*, **5,** 369-375.

Emery, W. J. and R. T. Wert, 1976: Temperature-Salinity Curves in the Pacific and their Application to Dynamic Height Computation. *Journal of Physical Oceanography*, **6,** 613-617.

Emery, W. J. and R. E. Thomson, 2001: *Data analysis methods in physical oceanography*. Elsevier Science, Amsterdam, 637pp.

Fiekas, V., J. Elken, T. J. Muller, A. Aitsam and W. Zenk, 1992: A view of the Canary Basin thermocline circulation in winter. *Journal of Geophysical Research,* **97(C8)**, 12495-12510.

Fine, R. M., 1995: Tracers, time scales, and the thermohaline circulation: The lower limb in the North Atlantic Ocean. *Reviews of Geophysics*, **33,** 1353-1365.

Fine, R. M. and R. Molinari, 1988: A continuous deep western boundary current between Abaco (26.5ºN) and Barbados (13ºN). *Deep Sea Research*, **35,** 1441-1450.

Fomin, L. M., 1964: *The Dynamic Method in Oceanography*. Elsevier Publishing Company, 47-72.

Fraile-Nuez, E. and A. Hernández-Guerra, 2006: Wind-driven circulation for the eastern North Atlantic Subtropical Gyre from Argo data. *Geophysical Research Letters,* **33**, L03601, doi:10.1029/2005GL025122

Fraser, K., 2006: *Using Argo profiles to monitor the variability of the eastern boundary across 26.5ºN*. MSc Thesis, School of Ocean and Earth Science, University of Southampton. Southampton. United Kingdom. 64pp.

Fuglister, F. C., 1960: *Atlantic Ocean Atlas of Temperature and Salinity Profiles and Data from the International Geophysical Year of 1957-1958*. Vol. 1, *Woods Hole Oceanographic Institution Atlas Series*, WHOI, Woods Hole, Massachusetts.

Ganachaud, A., 2003: Error budget of inverse box models: The North Atlantic. *Journal of Atmospheric and Oceanic Technology*, **20,** 1641-1655.

Ganachaud, A. and C. Wunsch, 2000: Improved estimates of global ocean circulation, heat transport and mixing from hydrographic data. *Nature*, **408,** 453-456.

Gill, A. E., 1982: *Atmosphere-Ocean Dynamics*. Vol. 30, International Geophysical Series, Academic Press.

Gill., A. E. and P. Niiler, 1973: The theory of seasonal variability in the deep ocean. *Deep Sea Research,* **20**, 141-177.

Girton, J. B., T. B. Sanford, and R. H. Käse, 2001: Synoptic sections of the Denmark Strait Overflow. *Geophyscal Research Letters,* **28**, 1619-1622.

Gordon, A. L., R. F. Weiss, W. M. J. Smethie, and M. J. Warner, 1992: Thermocline and Intermediate Water communication between the South Atlantic and Indian Oceans. *Journal of Geophysical Research*, **97,** 7223-7240.

Hall, M. M. and H. L. Bryden, 1982: Direct estimates and mechanisms of ocean heat transport. *Deep-Sea Research*, **29,** 339-359.

Hamilton, P., J. C. Larsen, K. D. Leaman, T. N. Lee and E. Waddell, 2005: Transports through the Straits of Florida. *Journal of Physical Oceanography,* **35(3)**, 308-322.

Hansen, B., W. R. Turrell, and S. Østerhus, 2001: Decreasing overflow from the Nordic seas into the Atlantic Ocean through the Faroe Bank channel since 1950. *Nature*, **411,** 927-930.

Hendry, R. M., 1993: Canadian Technical Report of Hydrography and Ocean Sciences, Bedford Institute of Oceanography CTD Trials. BIO, Dartmouth, Nova Scotia. 97 pp.

Hernández-Guerra, A. and L. Nykjaer, 1997: Sea surface temperature variability off north-west Africa 1981-1989. *International Journal of Remote Sensing*, **18,** 2539-2558.

Hernández-Guerra, A., E. Fraile-Nuez, R. Borges, F. López-Laatzen, P. Véllez-Belchi, G. Parilla, and T. Müller, 2003: Transport variability in the Lanzarote passage (eastern boundary current of the North Atlantic Subtropical Gyre). *Deep Sea Research I*, **50,** 189-200.

Hernández-Guerra, A., E. Fraile-Nuez, F. López-Laatzen, a. Martínez, G. Parrilla and P. Vélez-Belchi, 2005: Canary Current and North Equatorial Current from an inverse box model. *Journal of Geophysical Research,* **110**, C12019, doi:10.1029/2005JC003032.

Hernández-Guerra, A., F. Machín, A. Antoranz, J. Cisneros-Aguirre, C. Gordo, A. Marrerro-Díaz, A. Martínez, A. W. Ratismandresey, A. Rodríguez-Santana, P. Sangría, F. López-Laazen, G. Parilla, and J. L. Pelegrí, 2002: Temporal variability of mass transport in the Canary Current. *Deep Sea Research II*, **49,** 3415-3426.

Hirschi, J., J. Baeher, J. Marotzke, J. Stark, S. Cunningham, and J. –O. Beismann, 2003: A monitoring design for the Atlantic meridional overturning circulation. *Geophysical Research Letters,* **30(7)**, 1413 doi:10.1029/2003GL016776

Hurrell, J. W., Y. Kushnir, and M. Visbeck, 2001: The North Atlantic Oscillation. *Science*, **291,** 603-605.

Jayne, S. R. and J. Marotzke, 2001: The Dynamics of Ocean Heat Transport Variability. *Reviews of Geophysics*, **39,** 385-411.

Johns, E., R. M. Fine, and R. Molinari, 1997: Deep flow along the western boundary south of the Blake Bahama Outer Ridge. *Journal of Physical Oceanography*, **27,** 2187 - 2208.

Johns, W. E., T. N. Lee, D. Zhang, R. Zantopp, C. T. Liu, and Y. Yang, 2001: The Kuroshio east of Taiwan: moored transport observations from the WOCE PCM-1 array. *Journal of Physical Oceanography,* **31**, 1031-1053.

Johns, W. E., T. Kanzow, and R. J. Zantopp, 2005: Estimating ocean transports with dynamic height moorings: An application in the Atlantic Deep Western Boundary Current at 26ºN. *Deep Sea Research I*, **52**, 1542-1567.

Josey, S. A., E. C. Kent, and P. K. Taylor, 1998: *The Southampton Oceanography Centre (SOC) ocean-atmosphere heat, momentum and freshwater flux atlas*. Southampton Oceanography Centre Report 6, Southampton, United Kingdom, 30 pp.

Josey, S. A., E. C. Kent, and P. K. Taylor 2002: Wind Stress Forcing of the Ocean in the SOC Climatology: Comparisons with the NCEP-NCAR, ECMWF, UWM/COADS, and Hellerman and Rosenstein Datasets. *Journal of Physical Oceanography*, **32,** 1994-2019.

Jung, G. H., 1952: Note on the meridional transport of energy by the oceans. *Journal of Marine Research*, **11,** 139-146.

Jung, G. H., 1955: *Heat Transport in the North Atlantic Ocean*. Ref 53-54T, Department of Oceanography, A and M College of Texas, Texas, U.S.A.

Kanzow, T., U. Send, W. Zenk, A. D. Chave, and M. Rhein, 2006: Monitoring the integrated deep meridional flow in the tropical North Atlantic: Long-term performance of a geostrophic array. *Deep-Sea Research,* **53**, 528-546.

Käse, R. H. and W. Krauss, 1996: The Gulf Stream, the North Atlantic Current, and the origin of the Azores Current. *The Warmwatersphere of the North Atlantic Ocean*, W. Krauss, Ed., Gebrüder Borntraeger, 291-337.

Kerr, R. A., 2005: The Atlantic conveyor may have slowed, but don't panic yet. *Science*, **310**, 1403-1404.

Kieke, D. and M. Rhein, 2006: Variability of the overflow water transport in the western subpolar North Atlantic, 1950-97. *Journal of Physical Oceanography,***36**, 435-456.

Klein, B. and G. Siedler, 1989: On the Origin of the Azores Current. *Journal of Geophysical Research*, **94,** 6159-6168.

Kohl, A., 2005: Anomalies of meridional overturning: Mechanisms in the North Atlantic. *Journal of Physical Oceanography,* **35**, 1455-1472.

Koltermann, K. P., A. V. Sokov, V. P. Tereschenkov, S. A. Dobroliubov, K. Lorbacher, and A. Sy, 1999: Decadal changes in the thermohaline circulation of the North Atlantic. *Deep-Sea Research II*, **46,** 109-138.

Larsen, J. C., 1992: Transport and heat flux of the Florida Current at 27ºN derived from cross-stream voltages and profiling data: theory and observations. *Philosophical Transactions of the Royal Society of London A*, **338,** 169-236.

Latif, M., C. Böning, J. Willebrand, A. Biastoch, J. Dengg, N. Keenlyside, U. Schweckendiek and G. Madec, 2006: Is the thermohaline circulation changing? *Journal of Climate*, **19**, 4631-4637.

Lavín, A., H. L. Bryden, and G. Parrilla, 1998: Meridional transport and heat flux variations in the subtopical North Atlantic. *The Global Atmosphere and Ocean System*, **6,** 269-293.

Lavín, A. M., H. L. Bryden, and G. Parrilla, 2003: Mechanisms of heat, freshwater, oxygen and nutrient transports and budgets at 24.5ºN in the subtropical North Atlantic. *Deep-Sea Research I*, **50,** 1099-1128.

Le Traon, P. –Y, and P. De Mey, 1994: The eddy field associated with the Azores Front east of the Mid-Atlantic Ridge as observed by the Geosat altimeter. *Journal of Geophysical Research,* **99(C5)**, 9907-9923.

Leaman, K. D. and J. E. Harris, 1990: On the average absolute transport of the deep western boundary currents east of Abaco Island, the Bahamas. *Journal of Physical Oceanography,* 20, 467-475.

Leaman, K. D., R. L. Molinari, and P. S. Vertes, 1987: Structure and variability of the Florida Current at 27ºN : April 1982-July 1984. *Journal of Physical Oceanography*, **17,** 565-583.

Leaman, K. D., P. S. Vertes, L. P. Atkinson, T. N. Lee, P. Hamilton and E. Waddell, 1995: Transport, potential vorticity, and current/temperature structure across Northwest Providence and Santaren Channels and the Florida Current off Cay Sal Bank. *Journal of Geophysical Research,* **100(C5)**, 8561-8569.

Lee, T. L., W. E. Johns, F. Schott, and R. J. Zantopp, 1990: Western Boundary Current Structure and Variability East of Abaco, Bahamas at 26.5ºN. *Journal of Physical Oceanography*, **20,** 446-466.

Lee, T. N., W. E. Johns, R. J. Zantopp, and E. R. Fillenbaum, 1996: Moored observations of Western Boundary Current variability and Thermohaline Circulation at 26.5ºN in the Subtropical North Atlantic. *Journal of Physical Oceanography*, **26,** 962-983.

Levi, B. G., 2006: Is there a slowing in the Atlantic Ocean's overturning circulation? *Physics Today*, **59,** 26-28.

Lynch-Stieglitz, J., 2001: Using ocean margin density to constrain ocean circulation and surface wind strength in the past. *Geochemistry, Geophysics, Geosystems*, **2,** Paper number 2001GC000208.

Macdonald, A., 1998: The global ocean circulation: a hydrographic estimate and regional analysis. *Progress in Oceanography*, **41,** 281-382.

Macdonald, A., M. O. N. Baringer, R. Wanninkhof, K. Lee, and D. W. R. Wallace, 2003: A 1998-1992 comparison of inorganic carbon transport across 24.5ºN in the Atlantic. *Deep Sea Research II*, **50,** 3041-3064.

Macdonald, A. M. and C. Wunsch, 1996: An estimate of global ocean circulation and heat fluxes. *Nature*, **382,** 436-439.

Macrander, A., U. Send, H. Valdimarsson, S. Jónsson, and R. H. Käse, 2005: Interannual changes in the overflow from the Nordic Seas into the Atlantic Ocean through the Denmark Strait. *Geophysical Research Letters,* **32**, L06606, doi:10.1029/2004GL021463.

Manabe, S. and R. J. Stouffer, 1988: Two stable modes of a coupled ocean-atmosphere model. *Journal of Climate,* **1**, 841-866.

Mantyla, A. W., 1994: The treatment of inconsistencies in Atlantic deep water salinity data. *Deep Sea Research I*, **41,** 1387-1405.

Marotzke, J., 2000: Abrupt climate change and thermohaline circulation: Mechanisms and predictability. *Proceedings of the National Academy of Sciences of the United States of America*, **97(4)**, 1347-1350.

Marotzke, J. and J. R. Scott, 1999: Convective mixing and the thermohaline circulation. *Journal of Physical Oceanography*, **29,** 2962-2970.

Marotzke, J., R. Giering, K. Q. Zhang, D. Stammer, C. Hill, and T. Lee, 1999: Construction of the adjoint MIT ocean general circulation model and application to Atlantic heat transport sensitivity. *Journal of Geophysical Research*, **104,** 29529-29547.

McCartney, M. S. and L. D. Talley, 1984: Warm-to-cold water conversion in the northern North Atlantic Ocean. *Journal of Physical Oceanography*, **14,** 922-935.

Meinen, C. S., S. L. Garzoli, W. E. Johns, and M. Baringer, 2004: Transport variability of the Deep Western Boundary Current and the Antilles Current off Abcao Island, Bahamas. *Deep Sea Research I*, **51,** 1397-1415.

Mills, E. L., 2005: From *Discovery* to discovery: the hydrology of the Southern Ocean, 1885-1937. *Archives of Natural History*, **32,** 246-264.

Mittelstaedt, E., 1991: The ocean boundary along the northwest African Coast: Circulation and oceanographic properties at the sea surface. *Progress in Oceanography,* **26**, 307-355.

Molinari, R. L., R. A. Fine, W. D. Wilson, R. G. Curry, J. Abell, and M. S. McCartney, 1998: The arrival of recently formed Labrador Sea Water in the Deep Western Boundary Current at 26.5ºN. *Geophysical Research Letters,* **25**, 2249-2252.

Molinari, R. L., E. Johns, and J. F. Festa, 1990: The annual cycle of meridional heat flux in the Atlantic Ocean at 26.5ºN. *Journal of Physical Oceanography*, **20,** 476-482.

Müller, T. J. and G. Siedler, 1992: Multi-year current time series in the eastern North Atlantic Ocean. *Journal of Marine Research,* **50**, 63-98.

Niiler, P. P. and W. S. Richardson, 1973: Seasonal Variability of the Florida Current. *Journal of Marine Research*, **31,** 144-167.

Olson, D., B., F. A. Schott, R. J. Zantopp, and K. D. Leaman, 1984: The mean circulation east of the Bahamas as determined from a recent measurement program and historical XBT data. *Journal of Physical Oceanography*, **14,** 1470-1487.

Palmer, M. D., H. L. Bryden, and J. Marotzke, 2004: Observed changes in the South Indian Ocean gyre circulation, 1987-2002. *Geophysical Research Letters*, **31**, L15303, doi:10.1029/2004GL020506.

Parilla, G., A. Lavín, H. Bryden, M. Garcia, and R. Millard, 1994: Rising temperatures in the subtropical North Atlantic Ocean over the past 35 years. *Nature*, **369,** 48-51.

Pingree, R., 2002: Ocean structure and climate (Eastern North Atlantic) *in situ* measurement and remote sensing (altimeter). *Journal of the Marine Biological Association of the U.K.,* **82**, 681-707.

Pond, S. and G. L. Pickard, 1983: *Introductory Dynamical Oceanography*, 2nd Edition ed. Butterworth-Heinemann, 329pp.

Rayner, D. and S. A. Cunningham, 2005: RRS *Discovery* Cruises D277/D278, RAPID mooring cruise report, February-March 2004. *Southampton Ocenography Cruise Report,* **53**, 103pp.

Reid, J. L., 1981: On the mid-depth circulation of the World Ocean. *Evolution of Physical Oceanography*, B. A. Warren and C. Wunsch, Eds., Massachusetts Institute of Technology, 70-111.

Richardson, P. L., 1977: On the crossover between the Gulf Stream and the Western Boundary Undercurrent. *Deep-Sea Research,* **24**, 139-159.

Richardson, W. S. and J. R. Finlen, 1967: The transport of Northwest Providence Channel. *Deep Sea Research*, ***14, 361-367.***

Richardson, P. L. and A. Tychensky, 1998: Meddy trajectories in the Canary Basin measured during the SEMAPHORE experiment, 1993-1995. *Journal of Geophysical Research,* **103(C11)**, 25029-25045.

Riley, G. A., 1951: Oxygen, phosphate and nitrate in the Atlantic Ocean. *Bulletin of the Bingham Oceanographic Collection*, **13,** 1-126.

Rintoul, S. R., 1991: South Atlantic interbasin exchange. *Journal of Geophysical Research*, **96,** 2675-2692.

Roach, A. T., K. Aagaard, C. H. Pease, S. A. Salo, T. Weingartner, V. Pavlov, and M. Kulakov, 1995: Direct measurements of transport and water properties through the Bering Strait. *Journal of Geophysical Research,* **100**, 18443-18457.

Roemmich, D., 1980: Estimation of meridional heat flux in the North Atlantic by inverse Methods. *Journal of Physical Oceanography*, **10,** 1972-1983.

Roemmich, D. and C. Wunsch, 1985: Two transatlantic sections: meridional circulation and heat flux in the subtropical North Atlantic Ocean. *Deep Sea Research*, **32,** 619-664.

Saunders, P. M., 1982: Circulation in the eastern North Atlantic. *Journal of Marine Research*, **40**, 641-657.

Saunders, P. M., 1986: The accuracy of measurements of salinity oxygen, and temperature in the deep ocean. *Journal of Physical Oceanography*, **16,** 189-195.

Schmitz, W. J. and P. L. Richardson, 1991: On the sources of the Florida Current. *Deep Sea Research*, **38,** S379-S409.

Schmitz, W. J. Jr. and M. S. McCartney, 1993: On the North Atlantic Circulation. *Reviews of Geophysics*, **31,** 29-49.

Sena Martins, C., M. Hamann and A. F. G. Fiúza, 2002: Surface circulation in the eastern North Atlantic, from drifters and altimetry. *Journal of Geophysical Research*, **107(C12)**, 3217, doi:10.1029/2000JV000345.

Shoosmith, D. R., M. O. Baringer and W. E. Johns, 2005: A continuous record of Florida Current temperature transport at 27ºN. *Geophysical Research Letters,* **32**, L23603, doi:10.1029/2005GL024075.

Siedler, G. and L. Stramma, 1983: The applicability of the T/S method to geopotential anomaly computations in the Northeast Atlantic. *Oceanologica Acta*, **6,** 167-172.

Siedler, G. and R. Onken, 1996: Eastern Recirculation. *The Warmwatersphere of the North Atlantic Ocean*, W. Krauss, Ed., Gebrüder Borntraeger, 339-364.

Siedler, G., L. Armi, and T. Müller, 2005: Meddies and decadal changes at the Azores Front from 1980 to 2000. *Deep Sea Research II*, **52,** 583-604.

Siedler, G., W. Zenk and W. J. Emery, 1985: Strong-current events related to a subtropical front in the Northeast Atlantic. *Journal of Physical Oceanography,* **15**, 885-897.

Slater, D. R., 2003: *The Transport of Mediterranean Water in the North Atlantic Ocean*. PhD Thesis, School of Ocean and Earth Science, University of Southampton, Southampton, United Kingdom.

Spall, M. A., 1996: Dynamics of the Gulf Stream/Deep Western Boundary Current Crossover. Part I: Entrainment and recirculation. *Journal of Physical Oceanography,* **26**, 2152-2168.

Spall, M. A. and R. S. Pickart, 2001: Where does dense water sink? A subpolar gyre example. *Journal of Physical Oceanography*, **31,** 810-826.

Srokosz, M. A., 2003: Rapid climate change: scientific challenges and the new NERC programme. *Philosophical Transactions of the Royal Society London A,* **361**, 2061-2078.

Stammer, D. and C. W. Böning, 1996: Generation and distribution of Mesoscale eddies in the North Atlantic Ocean. *The Warmwatersphere of the North Atlantic Ocean*, W. Krauss, Ed., Gebrüder Borntraeger, 159-193.

Stommel, H., 1947: Note on the use of the T-S correlation for dynamic height anomaly computations. *Journal of Marine Research*, **2,** 85-92.

Stommel, H., 1957: A survey of ocean current theory. *Deep Sea Research,* **4**, 149-184.

Stommel, H., 1958: *The Gulf Stream*. Cambridge University Press, 153-172 pp.

Stommel, H. and A. B. Arons, 1960a: On the abyssal circulation of the world ocean-I. Stationary planetary flow patterns on a sphere. *Deep-Sea Research*, **6,** 140-154.

Stommel, H. and A. B. Arons, 1960b: On the abyssal circulation of the world ocean-II. An idealized model of the abyssal circulation pattern and amplitude in oceanic basins. *Deep-Sea Research*, **6,** 217-233.

Stommel, H., A. B. Arons, and A. J. Faller, 1958: Some examples of stationary planetary flow patterns in bounded basins. *Tellus*, **2,** 179-187.

Stouffer, R. J., J. Yin, J. M. Gregory, K. W. Dixon, M. J. Spelman, W. Hurlin, A. J. Weaver, M. Eby, G. M. Flato, H. Hasumi, A. Hu, J. H. Jungclaus, I. V. Kamenkovich, A. Levermann, M. Montoya, S. Murakami, S. Nawrath, A. Oka, W. R. Peltier, D. Y. Robitaille, A. Sokolov, G. Vettoretti, and S. L. Weber, 2006: Investigating the causes of the response of the thermohaline circulation to past and future climate changes. *Journal of Climate,* **19(8)**, 1365-1387.

Stramma, L., 1984: Geostrophic transport in the Warm Water Sphere of the eastern subtropical North Atlantic. *Journal of Marine Research,* **42**, 537-558.

Stramma, L., D. Kieke, M. Rhein, F. Schott, I. Yashayaev, and K. P. Koltermann, 2004: Deep water changes at the western boundary of the subpolar North Atlantic during 1996 to 2001. *Deep-Sea Research I*, **51,** 1033-1056.

Stramma, L. and G. Siedler, 1988: Seasonal Changes in the North Atlantic Subtropical Gyre. *Journal of Geophysical Research*, **93,** 811-8188.

Sverdrup, H. U., M. W. Johnson, and R. H. Fleming, 1942: *The Oceans: their physics, chemistry and general biology*, H. U. Sverdrup, M. W. Johnson, and R. H. Fleming, Eds., Prentice-Hall

Swallow, J. C. and L. V. Worthington, 1957: Measurements of deep currents in the western North Atlantic. *Nature*, **179**, 1183-1184.

Swallow, J. C. and L. V. Worthington, 1961: An observation of a deep countercurrent in the western North Atlantic. *Deep Sea Research,* **8**, 1-19.

Talley, L. D., J. L. Reid and P. E. Robbins, 2003: Data-based meridional overturning streamfunctions for the Global Ocean. *Journal of Climate*, **16,** 3213-3226.

Thompson, D. W. J. and S. Solomon, 2002: Interpretation of recent Southern Hemisphere climate change. *Science,* **296**, 895-899.

Togweiller, J. R. and B. Samuels, 1995: Effect of Drake Passage on the global thermohaline circulation. *Deep-Sea Research I*, **42(4)**, 477-500.

Tsuchiya, M., 1989: Circulation of the Antarctic Intermediate Water in the North Atlantic Ocean. *Journal of Marine Research*, **47,** 747-755.

Tsuchiya, M., L. D. Talley and M. S. McCartney, 1992: An eastern Atlantic section from Iceland southward across the equator. *Deep Sea Research A,* **39(11/12)**, 1885-1917.

Tychensky, A., P. –Y. Le Traon, F. Hernández-Guerra and D. Jourdan, 1998: Large structures and temporal change in the Azores Front during the SEMAPHORE experiment. *Journal of Geophysical Research,* **103**, 25009-25027.

Vaughan, S. L. and R. L. Molinari, 1997: Temperature and salinity variability in the Deep Western Boundary Current. *Journal of Physical Oceanography*, **27,** 749-761.

Vellinga, M. and R. A. Wood, 2002: Global climate impacts of a collapse of the Atlantic thermohaline circulation. *Climatic Change,* **54**, 251-267.

Vellinga, M. and R. A. Wood, 2004: Timely detection of anthropogenic change in the Atlantic meridional overturning circulation. *Geophyical Research Letters,* **31**, L14203, doi:10.1029/2004GL020306.

Volkov, D. L., 2005: Interannual variability of the altimetry-derived eddy field and surface circulation in the extratropical north Atlantic Ocean in 1993-2001. *Journal of Physical Oceanography*, **35**, 405-426.

Wacongne, S. and L. Crosnier, 2002: Seasonal variation of baroclinic geostrophic heat transport: is it resolved by existing climatologies of the Atlantic Ocean? *Journal of Physical Oceanography*, **32,** 278-294.

Warren, B. A., 1981: Deep circulation of the World Ocean. *Evolution of Physical Oceanography*, B. A. Warren and C. Wunsch, Eds., Massachusetts Institute of Technology, 6-41.

Waugh, D. W. and T. M. Hall, 2005: Propagation of tracer signals in boundary currents. *Journal of Physical Oceanography*, **35**, 1538-1552.

Weijer, W., W. P. M. de Ruijter, H. A. Dijkstra, and P. J. van Leeuwen, 1999: Impact of Interbasin Exchange on the Atlantic Overturning Circulation. *Journal of Physical Oceanography*, **29,** 2266-2284.

Whitworth, T., 1983: Monitoring the transport of the Antartic Circumpolar Current at Drake Passage. *Journal of Physical Oceanography,* **13**, 2045-2057.

Wijffels, S. E., E. Firing, and H. L. Bryden, 1994: Direct observations of the Ekman balance at 10ºN in the Pacific. *Journal of Physical Oceanography*, **24,** 1666-1679.

Woodgate, R. A., K. Aagaard and T. J. Weingartner, 2005: Monthly temperature, salinity, and transport variability of the Bering Strait through flow. *Geophysical Research Letters*, **32,** L04601, doi:10.1029/2004GL021880

Worthington, L. V., 1958: Oceanographic data from the RRS Discovery II during the Internation Geophysical Year, *Woods Hole Oceanographic Institution Technical Report* **58-30**, Woods Hole MA, 58p.

Worthington, L. V., 1976: *On the North Atlantic circulation*. Vol. 6, *The John Hopkins Oceanographic Studies*, The John Hopkins University Press, 110 pp.

Wunsch, C., 1977: Determining the general circulation of the oceans: A preliminary discussion. *Science*, **196,** 871-875.

Wunsch, C., 1978: The North Atlantic General Circulation West of 50ºW Determined by Inverse Methods. *Reviews of Geophysics and Space Physics*, **16,** 583-620.

Wunsch, C., 1980: Meridional heat flux of the North Atlantic Ocean. *Proceedings of the National Academy of Sciences, USA,* **77(9)**, 5043-5047.

Wunsch, C., 2000: Moon, tides and climate. *Nature*, **405**, 743-744.

Wunsch, C., 2002: What is the thermohaline circulation? *Science*, **298**, 1179-1180.

Wunsch, C. and R. Ferrari, 2004: Vertical mixing, energy and the general circulation of the oceans. *Annual Reviews of Fluid Mechanics*, **36**, 281-314.

Wüst, G., 1935: Schichtung und Zirkulation des Atlantischen Ozeans, Die Stratosphäre. *Wissenschaftliche Ergebnisse der Deutschen Atlantischen Expedition auf dem forschuungs und Vermessungsschiff "Meteor" 1925-1927.* 6: 1st Part. 180pp (*The stratosphere of the Atlantic Ocean*, WJ Emery (ed), 1978, Amerind, New Delhi, 112pp).

Wüst, G., 1955: Stromgeschwindigkeiten im Tiefen- und Bodenwasser des Atlantischen Ozeans auf Grund dynamischer Berechnung der *Meteor*-Profile Deutschen Atlantischen Epedition 1925/27. *Deep Sea Research,* **3 (Supplement)**, 373-395.

Zantopp, R., J. and K. D. Leaman, 1984: The feasibility of dynamic height determination from moored temperature sensors. *Journal of Physical Oceanography*, **14,** 1399-1406.

Zantopp, R. J., T. N. Lee, and W. E. Johns, 1989a: Moored current meter observations east of Abcao, Bahamas at 26.5ºN (STACS-7 Array) 89-002, 4 pp.

Zantopp, R. J., T. N. Lee, W. E. Johns, 1989b: Moored current meter observations east of Abcao, Bahamas at 26.5ºN (STACS-8 Array) 89-001, 6 pp.

Zantopp, R. J., T. N. Lee, and W. E. Johns, 1990: Moored current meter observations east of Abcao, the Bahamas at 26.5ºN (STACS-10 Array) 90-002, 10 pp.

Zantopp, R. J., T. N. Lee, and W. E. Johns, 1993: Moored current meter observations east of Abcao, the Bahamas (WATTS Array) 93-006, 77 pp.

Zantopp, R. J., T. N. Lee, and W. E. Johns, 1996: Moored current meter observations east of Abcao, the Bahamas (ACCP-1 Array) 96-001, 80 pp.

Zantopp, R. J., T. N. Lee, and W. E. Johns, 1998a: Moored current meter observations east of Abcao, the Bahamas (ACCP-2 Array) 98-005, 80 pp.

Zantopp, R. J., T. N. Lee, and W. E. Johns, 1998b: Moored current meter observations east of Abcao, the Bahamas (ACCP-3 Array) 98-006, 80 pp.

Zenk, W. and T. J. Müller, 1988: Seven-year current meter record in the eastern North Atlantic. *Deep-Sea Research,* **35**, 1259-1268.